cadangan sistem *fuzzy inference.* Sistem diagnosis yang dicadangkan itu dapat disahkan oleh lima puluh rekod ECG dan keputusan pengesahan mencapai seratus peratus (100%) bagi sensitiviti, kejituan, dan ketepatan manakala ketepatan mendiagnosis terbaik yang boleh dicapai dengan menggunakan kriteria diagnostik tradisional tidak melebihi 90%.

A New Fuzzy Based Diagnosing System for Instantaneous Processing 12 Lead ECG Signal

ABSTRACT

The Electrocardiogram (ECG) signal reflects the performance of the human heart as an electrical signal. It consists of three main waves (P, QRS complex, and T), and is recorded by an ECG machine in the form of 12 leads which include valuable information about the functional activities of the human heart and cardiovascular system. It is annotated manually by a cardiologist to diagnose cardiac disease, but for a long time ECG recordings were performed to get an effective measure of heart rate variability. The generated ECG data is huge and the probability of wrong analysis or misreading by manual annotation is increased. Therefore, many computerized based techniques have been proposed in literature for analyzing and detecting ECG waves, and at a lower rate for diagnosing cardiac diseases. In this thesis, a new robust intelligent system has been proposed to perform an accurate diagnosis of a high risk cardiac disease named left ventricular hypertrophy (LVH). Four approaches are developed within the proposed ECG system to improve the performance of processing the ECG signal with respect to the existing methods and to discover new system for diagnosing cardiac disease based on the computerized intelligence technique. The first proposed approach is a digital recovery system which addresses the limitation of digital 12 lead ECG data by reconstructing it from the colour scanned image of the ECG printed chart. This approach is implemented by four image processing steps and captures raw ECG data with respect to the baseline which is detected by the same approach. Furthermore, it is reliable for different ECG morphologies and printout charts. The reconstructed data is evaluated qualitatively and quantitatively using some predefined standard features. The analytic results demonstrate the consistency and robustness of this approach to generate 12 lead ECG data with high precision (98%). The second and third approaches are proposed to detect ECG waves and then delineate all time characteristics of these waves. In contrast to the existing methods, both approaches are based on straightforward algorithms that perform instantaneous processing for the ECG signal. As a result, detection operation is executed in a high speed which reaches (4.5s per 650,000 beats) for QRS complex and (2.7s per 225,000 beats) for P&T waves. The based technique in both detection approaches has the advantage of rising falling edge mutation as a base rule for delineating subject. This technique reduces undetected beats and provides accurate detection results exceeding ones in up to date existing methods. The fourth proposed approach is a diagnostic system for LVH cardiac disease based on proposed diagnostic criterion. In contrast to the conventional LVH diagnostic criteria, the decision in the proposed criterion is computed by three logical expressions; two of which are determined by a combination of classic criteria, whereas the third is obtained by eight ECG voltages and takes two different levels for each gender. These expressions are represented by the membership functions in the proposed design of the fuzzy inference system. The proposed diagnosing system is validated by fifty ECG records, in which the validation results score were perfect (100%) in terms of sensitivity, specificity, and accuracy, while the best diagnosing accuracy achieved by traditional diagnostic criteria does not exceed 90%.

CHAPTER 1

INTRODUCTION

1.1 Background

The electrocardiogram (ECG) represents the electrical activity of the human heart (HH), as well as showing the systematic contraction and relaxation of the HH muscle. Electrocardiography is a significant tool in diagnosing the state of HH (Güler, 2005). Moreover, it provides precise information to doctors about the functional aspects of the HH and the cardiovascular system which can help them to make a correct heart diagnosis (Ghongade & Ghatol, 2007; Mariano Llamedo & Martínez, 2011; Maglaveras, Stamkopoulos, Diamantaras, Pappas, & Strintzis, 1998; Mehta & Lingayat, 2008). The early detection of cardiac diseases/abnormalities can prolong human life and enhance the quality of life through appropriate treatment. On the other hand, it is very difficult and time consuming for doctors to make an accurate analysis for long time ECG recordings, if we take into account that the possibility of misreading (or the wrong analysis) in manual diagnosis of the enormous volume of ECG data is high. Therefore computerized based techniques for ECG signal analysis and beat classification can be very helpful in diagnosing different cardiac diseases (Addison et al., 2000; Dokur & Ölmez, 2001; Güler, 2005; Kundu, Nasipuri, & Kumar Basu, 2000; Özbay & Tezel, 2010; Rajendra Acharya, Subbanna Bhat, Iyengar, Rao, & Dua, 2003; Sternickel, 2002). Many methods with computerized based techniques have been proposed in literature for this subject. The main concepts of such methods are based on different adopted

techniques of pattern recognition. (Korürek & Doğan, 2010; Mehta & Lingayat, 2008). The general block diagram of ECG signal processing is shown in Figure 1.1. In this figure, the time characteristic information that is delineated by the QRS complex detector can be fed to the data compression and noise filtering operations (marked with gray arrows) to enhance their performance. In addition, the time characteristics of the QRS complex are mainly used to delineate related temporal information of other ECG waves (P and T waves) including boundaries (onset and end) and peak time locations (Sörnmo & Laguna, 2006). According the valuable information which is extracted from dynamic processing of the ECG signal, this represents one of the most significant applications in the signal processing field.

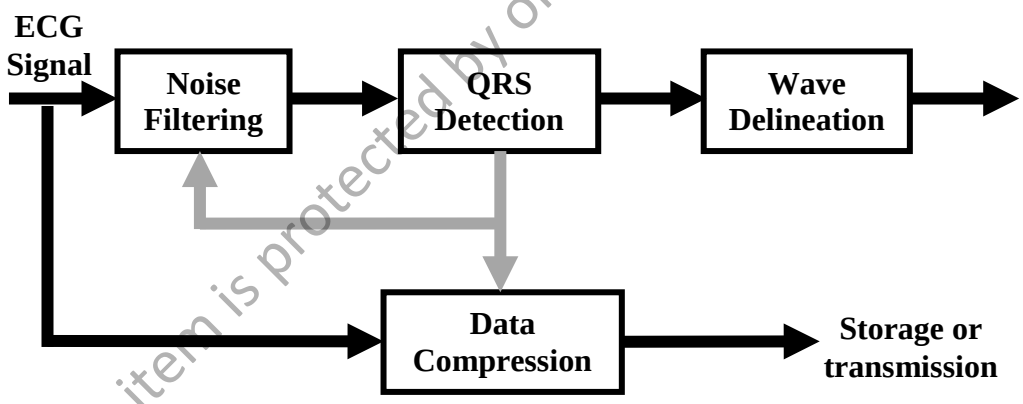

Figure 1.1: General Block Diagram of ECG Processing Signal (Sörnmo & Laguna, 2006).

Various methodologies with computerized based techniques have been proposed in literature for the purpose of automated ECG diagnosis (Addison et al., 2000; Chang, Lin, Hsieh, & Weng, 2012; Doğan & Korürek, 2012; Rai, Trivedi, & Shukla, 2013). However, the entire ECG diagnosis process can generally be partitioned into a number of disjoint processing steps: ECG beat detection, diagnostic features/parameters extraction or selection, and classification as shown in Figure 1.2.

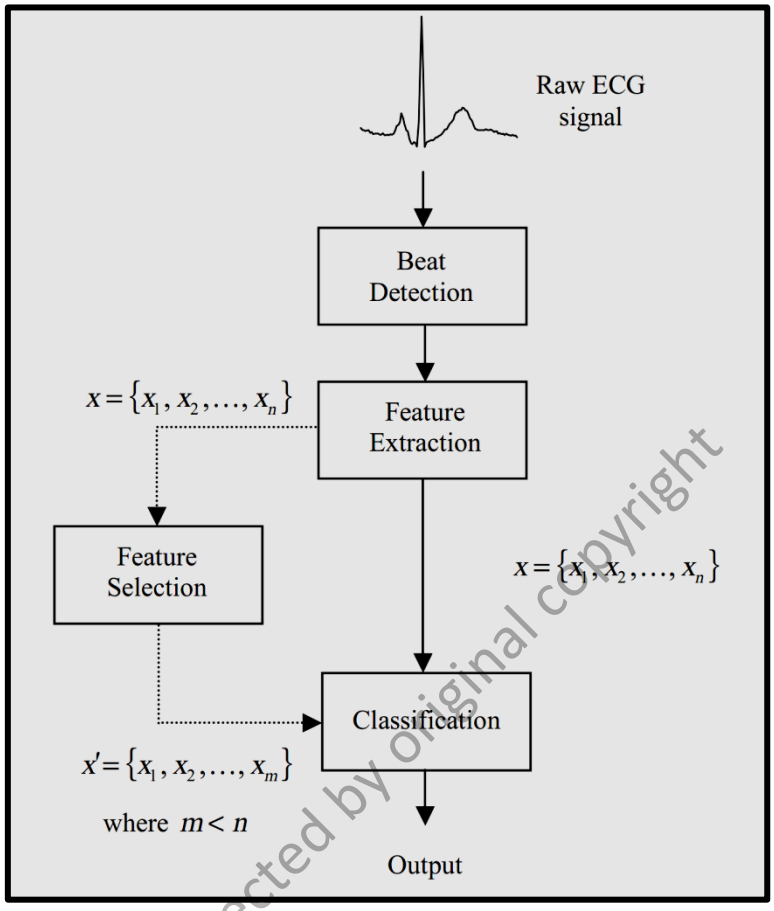

Figure 1.2: General Block Diagram of Classifying/ Diagnosing ECG Signal using Computerized Based Technique (Güler, 2005).

Most computerized based techniques developed for analyzing the ECG signal to detect electrocardiographic changes use autocorrelation function, frequency domain features, time frequency analysis, and wavelet transform (WT) to transform the ECG signal to a more objective quantitative for extracting diagnostic features (Kundu et al., 2000; Nugent, Webb, Black, Wright, & McIntyre, 1999; Sternickel, 2002). The reported results in related methods proposed in literature demonstrate that WT is the most trustworthy transformation to extract valuable features from ECG signals (Addison et al., 2000; Dokur & Ölmez, 2001; Güler, 2005). The greatest WT efficiency comes from the capability of wavelet coefficients which are used as feature vectors to identify further ECG characteristics that are not apparent inside the original ECG signal in the

time domain, as well as its capability to address the problem of non-stationary ECG signals (Daubechies, 1990; Unser & Aldroubi, 1996). Additionally, the multi-resolution that is generated from WT allows the decomposition of the ECG signal a number of scales, each of which can be represented as a particular feature of the ECG signal under test (Choi, 2008; Kutlu & Kuntalp, 2012).

1.2 Problem Statements

Many studies found in literature deal with processing and analyzing the 12 lead ECG signal to detect ECG waves (P, QRS complex, and T) waves and then delineate the time characteristics of these waves, which are most significant to compute many diagnostic criteria that are mainly used in ECG beat classification and diagnosing different cardiac diseases. Most of the studies are validated with different ECG records that are collected from free online ECG databases while several studies have used private ECG data which is collected from clinical centres. The online ECG databases present single or multi-lead ECG data with different morphologies moreover, most of these databases are annotated manually by cardiologists with significant information about heart status and time location events of the ECG waves, which are mostly used to evaluate the findings obtained by the ECG approaches. Finally, it should be noted that most of the current ECG detectors are applied to ECG data after transforming them using certain frequency or time transformations like (WT, Walsh Transform, etc). As a result more time is needed to process ECG data.

On the other hand, very few studies of computerized based techniques found in literature for the purpose of diagnosing general cardiac diseases exist. However, for high risk diseases that cause sudden cardiac death for many people at a young age (under 40 years old) no more systems with computerized based techniques have been

adopted for this subject. Two main reasons can be given for the limitation in this field of research. First, it is related to the limited amount of 12 lead ECG data in digital form for people who suffer from certain cardiac diseases. The second reason is related to clinical subjects, that many cardiac diseases must be diagnosed by cardiologist after doing additional heart tests like (stress tests, echocardiography, etc) due the difficulty in fixing certain ECG parameters or diagnostic criteria to perform accurate diagnosis with high percent of accuracy.

Regarding the previous presentation, some problems can be seen as follows:

1- The limited amount of digital 12 lead ECG data suitable for the computerized processing technique which is originally recorded from patients who suffer from certain high risk cardiac diseases.

2- The incompatibility of most of adopted ECG waves detection methods for real time applications because their based technique is applied on transformed versions of the ECG signal not on the original signal itself. In addition, because some other techniques are applied through the series of mathematical estimation operations with complicated calculations, more processing time is spent.

3- Systems coupled with computerized intelligent based techniques are not found in literature for the purpose of diagnosing high risk cardiac diseases with high precision based on 12 lead ECG signal analysis.

1.3 Research Objectives

In this thesis, a new ECG system is proposed for processing the ECG signal, detecting entire ECG waves (P, QRS complex, and T waves) and delineating their time characteristics, and diagnosing specific high risk cardiac disease based on the

diagnostic features/parameters which computed from the delineated time characteristics of the detected ECG waves. Thus, three objectives are considered in the proposed ECG system which can be summarized as follows:

1- To propose a new approach for the digital recovery of 12 lead raw ECG data by reconstructing it from scanned images of the ECG printed chart, thus an open bank of 12 lead ECG data in digital form is generated from the ECG paper printout recording that can be collected from expert hospitals or clinical centres.

2- To propose new high speed algorithms for detecting ECG waves (P, QRS complex, and T), and the ability to delineate their time locations with high precision. The proposed detection and delineation algorithms take a straightforward flow with instantaneous processing techniques on the ECG input signal itself without the need for any mathematical transformation or estimation process.

3- To design a diagnosis system of computerized intelligent techniques for specific high risk cardiac diseases with high levels of sensitivity, specificity, and accuracy for both genders based on the proposed diagnostic criteria that is computed by analyzing the 12 lead ECG signal.

1.4 Scope of Research

The aim of this thesis is to propose a new system for processing the 12 lead ECG signal to detect all ECG waves P, QRS complex and T wave, to delineate their time characteristics, and to diagnose specific high risk cardiac diseases. The implementation of these aims will be performed through four proposed approaches inside the proposed ECG system. In each of these approaches, a completely new algorithm of processing ECG signals is proposed to improve the entire performance of each approach in term of

the processing time considerations, the capability of processing different ECG morphologies, and the precision of final outcomes in comparison with the adopted works. Moreover, different evaluation scenarios are conducted for each approach using standard sets of evaluation metrics to compute precision levels of final outcomes. The proposed approaches are validated with different categories of ECG data in order to prove the capability of these approaches in adapting with various ECG morphologies.

The first approach is proposed to address the limitation in digital 12 lead ECG data especially for some high risk cardiac diseases. However, huge amount of this data is available as paper printout in specialist hospitals and general clinical centres around the world and become more beneficial if they are converted to digital version. The proposed approach applies a sequence of image processing operations on the scanned image of the printed ECG chart to reconstruct the digital raw ECG data that is ready to be used by different computerized based techniques of processing and analyzing the ECG signal.

A second approach is proposed to delineate the time characteristics of the QRS complex using a proposed straightforward algorithm of instantaneous processing for ECG input signal (beat by beat) without the need for any mathematical transformation or estimation operations. According to this type of processing, the whole QRS complex detection operation is performed at high speed, thus considering this approach for real time clinical applications becomes more realistic.

Similarly, the third approach is proposed to delineate P and T time characteristics (boundaries and peak time locations) based on pre detected time locations of the QRS complex using proposed algorithms which apply conditional scanning operations in both sides of the QRS complex, but in the same processing type used in the QRS complex algorithm.

The fourth approach is proposed for accurate diagnosis of one particular high risk cardiac disease called left ventricular hypertrophy. This diagnosing approach is based on proposed criterion expressed by the voltage parameters of eight ECG leads to maximize the probability of detecting the abnormality within the 12 lead ECG. The proposed diagnostic criterion is designed to get different decision levels for each gender. The overall diagnosis approach is implemented using one of the computerized intelligent systems named "fuzzy inference system". Therefore, this approach can be integrated as a portable hardware unit added to the ECG machine as a diagnosis module.

1.5 Summary of Main Contributions

The main contributions of this research can be summarized as follows:

1- To propose a new digital recovery approach to reconstruct raw ECG data from scanned colour image of ECG paper printout recording. This approach is designed to reconstruct all 12 leads of the ECG signal and detect the ECG baseline to ensure the final plotting of reconstructed ECG data with the correct reference level. Additionally, the proposed digital recovery approach is capable of processing ECG paper printout with different paper size, different printing colours, and different pen size of the printed ECG chart. Finally, different evaluation scenarios are performed to prove the robustness of the proposed digital recovery approach to produce raw ECG data with high precision

2- To propose a new approach for QRS complex detection with high processing speed. This approach is designed to delineate all time characteristics of QRS complex including boundaries and peak time locations of Q, R, and S waves that are formed by this complex using a straightforward algorithm with instantaneous processing techniques without the need to use additional transform or mathematical

estimations. The proposed detection approach is validated with standard online ECG records with different ECG morphologies to evaluate the overall performance of this approach with respect to the adopted methods. A property of high processing speed in this approach proves the usefulness of considering this approach in future real time applications of ECG signal processing.

3- To propose a new approach for P and T wave detection with high processing speed. This approach is designed to delineate all time characteristics of P and T waves including boundaries and peaks time locations of these waves based on pre detected time locations of the QRS complex. Moreover, it includes two proposed algorithms (one for each wave) with the same processing type followed in the proposed QRS complex detector. The proposed detection approach is validated with standard online ECG records from different ECG categories to prove the ability of this approach to perform accurate delineation of all time characteristics for different shapes of P and T waves.

4- To design a new system for diagnosing specific high risk cardiac disease called left ventricular hypertrophy (LVH) using a computerized intelligent technique. A new diagnostic criterion for LVH cardiac disease is proposed in this system, which includes eight parameters that are extracted from analyzing 12 lead ECG data. The final decision to diagnose LVH cardiac disease is prepared according to proposed diagnostic criterion and two traditional criteria to increase the sensitivity and specificity of the final diagnosed results. The proposed system is designed to perform accurate diagnosis of LVH cardiac disease based on analyzing 12 lead data from both genders. In addition, it is validated by 50 ECG records from both genders. Only 42% of this data is from LVH patients, while other data is from other cardiac diseases and some normal patients. This selection is made to prove the

robustness of the proposed diagnostic system to overcome any interference in diagnosing between different cardiac diseases. Additionally, some evaluation scenarios are performed to compute the accuracy of the diagnosed results.

1.6 Thesis Outline

Chapter 1 introduces an overview of processing the ECG signal using a computerized system and extracting significant features and time characteristics events of ECG waves to interpret and describe the heart status and diagnosing cardiac diseases. Additionally, it provides the problem statement, the objectives of thesis, a summary of main contribution, and thesis outline.

Chapter 2 introduces the basic concepts of the ECG signal through the brief descriptions of cardiac conduction system, ECG components, and types of ECG lead. Additionally, all resources of 12 lead ECG data are reported. The second part of this chapter provides a literature review of well-known published works related to the main contributions that are presented in this thesis in terms of four subjects (digital recovery of raw ECG data, QRS complex detection, P and T wave detection, and diagnosing high risk cardiac diseases).

Chapter 3 introduces the general block diagram of the proposed system for pre-processing the 12 lead ECG signal, detecting (P, QRS complex, and T) waves and delineating their time characteristic events, and diagnosing one particular high risk cardiac disease. Additionally, four proposed approaches corresponding to the four contributions in this thesis are presented in this chapter. The methodology of each proposed approach is discussed in more detail through the description of the basic idea,

the applied algorithms, the block diagrams, and the mathematical definitions which are related to each approach.

Chapter 4 introduces the results that are obtained by each proposed approach, as well as the scenarios that are considered to evaluate the performance of these approaches with the mathematical definitions of all evaluation metrics used in each evaluation scenario. Additionally, the validation of the obtained results with respect to another that are reported by well-known published works in literature if found is performed also in this chapter.

Chapter 5 introduces the general discussion for all proposed approaches and new findings through their originality, the ability to address the present problem and their activity to perform designated objectives. Additionally, significant topics and suggestions for future work are presented in this chapter.

CHAPTER 2

LITERATURE REVIEW

2.1 Introduction

The development of a computerized intelligent system in medical applications is a significant challenge faced by physicians, engineers and computer scientists. The ability to process medical signals by such expert systems is combined mainly with the availability of medical data in a digital form, also with a sufficient amount of different morphologies.

One of the most popular medical signals that can be recorded for both genders in all ages, even the fetus, is an ECG signal. As a part of periodic medical tests, many cardiologists advise healthy people to have this test every six or twelve months, especially for the people over forty. The ECG signal is a graphical registration of the electrical signal generated by the HH against time (Gacek & Pedrycz, 2012; Suri & Spaan, 2007). The ECG is used to interpret some types of abnormal heart cases like conduction disturbances, arrhythmias and heart morphology (e.g., hypertrophy, and evolving myocardial ischemia or infarction). The clinical practices show that some cardiac diseases can be diagnosed accurately, depending on ECG test, while other diseases are estimated with an acceptable probability (Malmivuo & Plonsey, 1995). The ECG diagram is also helpful when assessing the performance of portable pacemaker devices to control abnormal heart rhythms. For example, in the United States more than 50% of hundred-million ECGs recorded annually are identified and diagnosed by computer systems (Drazen, Mann, Borun, Laks, & Bersen, 1988).

2.2 The Basic Concepts of ECG signal

Simply, the HH is a muscle that works continuously to pump the blood throughout the different parts of the human body. The HH is partitioned into right and left units segregated by a septum. It consists of four chambers (right/left atrium and ventricle, respectively), and four valves to manage the flow of blood between the chambers of the heart to/from arteries (Hampton, 2008). All parts of the HH are marked clearly in Figure. 2.1.

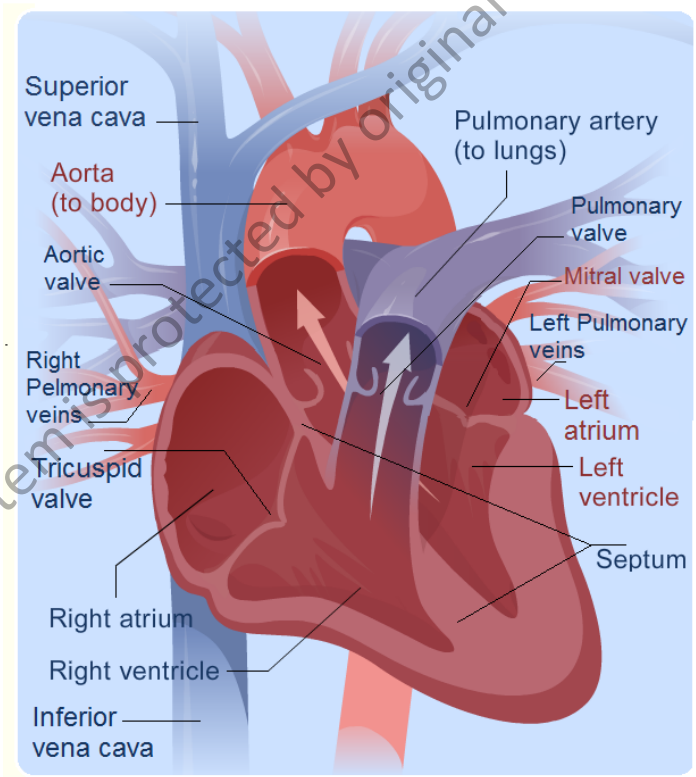

Figure 2.1: Structure of the Human Heart.

2.2.1 The Cardiac Conduction System

The cardiac conduction system shown in Figure 2.2 controls all activities performed when the HH pumps the blood. Thus this system is termed as the electrical

control system of the HH, as well as the provider of its repeated rhythmic beat. These electrical activities are recorded by the machine as a signal variation against time, this signal is called ECG or EKG (this abbreviation is used in some countries (Hampton, 2008)), which is printed onto grid paper or viewed on the monitor.

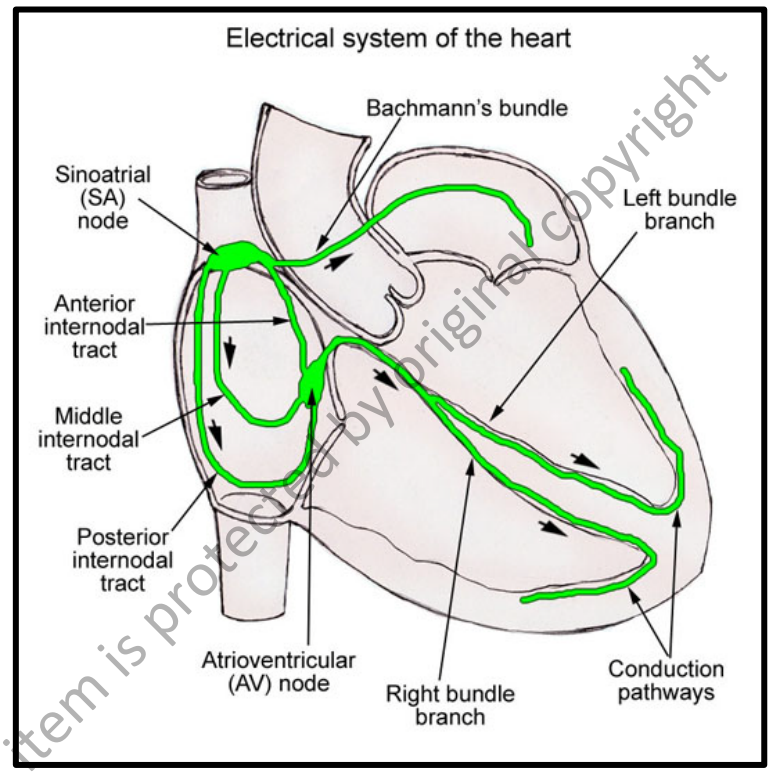

Figure 2.2: Cardiac Conduction of the HH (Assadi et al., 2011).

The first event in the cardiac conduction system starts when the sinoatrial node (SA) node generates an impulse (when the right atrium is full of blood) and then circulates as a depolarization over the cells of the right and left atria until it arrives the atrioventricular (AV) node (Foster, 2007) as shown in Figure 2.3.a. The upper right corner of this figure contains a diagram which simulates one complete cycle of the ECG

signal. A position of the circle remark indicates the start of the cardiac conduction system (first beat in the ECG cycle).

It should be noted that the AV node is the unique pathway for conducting the electrical impulse from the right and left atrium to the right and left ventricle, respectively (Foster, 2007). The next step in the cardiac conduction cycle is started when the first impulse generated by the SA node reaches the AV node and spreads across the atria to contract it. The contraction of the atria pumps the blood through release valves (the tricuspid and mitral valve in the right and the left side of the HH, respectively) into corresponding ventricles; this contraction is expressed in the ECG by the P wave as shown in Figure 2.3.b. When the blood passes to ventricles, there is a period time needed to fill both ventricles with blood. This time interval is represented on the ECG by the PQ segment (limited between P and Q wave) as shown in Figure 2.3.c.

In the next step of the cardiac conduction system, the electrical signal is moved to the bundle of His (which is discovered by German cardiologist Wilhelm His (1836-1934)) and separated to the right and the left bundle branch through the septum of the HH. This progress is represented in the ECG by the Q wave as shown in Figure 2.3.d. The electrical signal then leaves the right and the left bundle branches and passes through the Purkinje fibers that are diffused around the walls of the ventricles (Foster, 2007). Consequently, the muscles of both ventricles are stimulated by the electrical impulse moving down the Purkinje fibers but not at the same moment (the left ventricle precedes the right ventricle) (Azeem, Vassallo, & Samani, 2005) as shown in Figure 2.3.e. On an ECG, the R wave represents the contraction of the left ventricle, while the S wave represents the contraction of the right ventricle as shown in Figure 2.3.f and g, respectively. It should be noted that the contraction of the right ventricle pumps the

blood to the lungs through the pulmonary valve, while the contraction of the left ventricle pumps the blood to the rest of the human body through the aortic valve. When the electrical signals of these contractions are passed, the walls of both ventricles are relaxed gradually. This process includes a time period where the ventricles do not respond to further electrical catalysts (Azeem et al., 2005), which is represented in the ECG by the ST segment as shown in Figure 2.3.h. this occurs continuously, when the walls of ventricles are reverted completely to its resting state. This process is represented in the ECG by the T wave as shown in Figure 2.3.i.

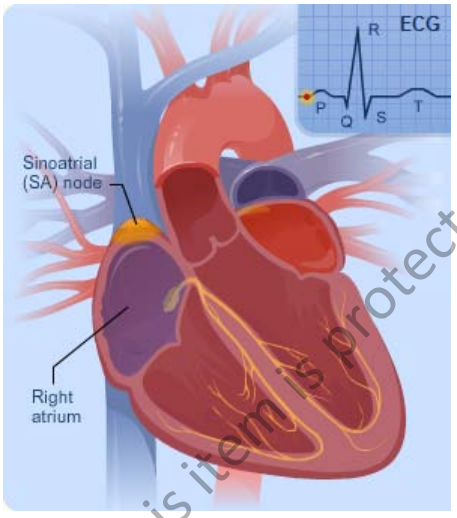

(a)

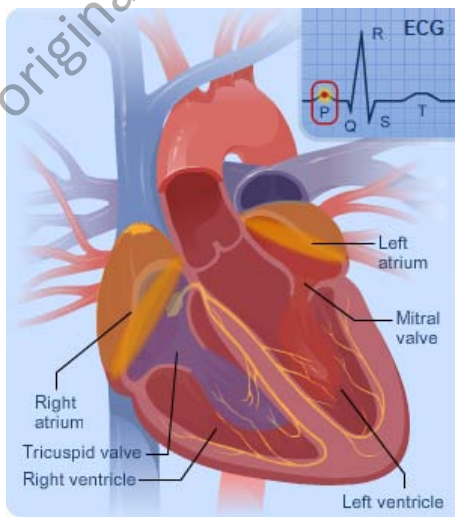

(b)

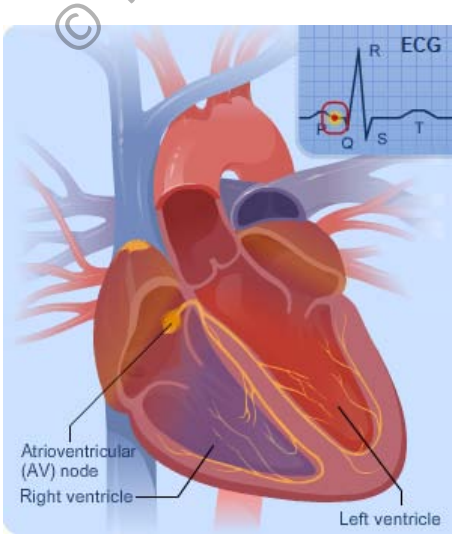

(c)

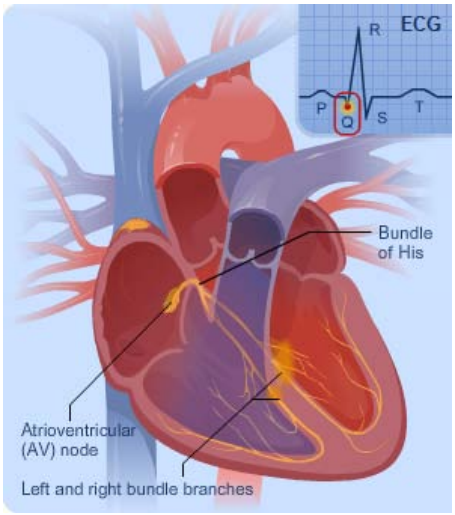

(d)

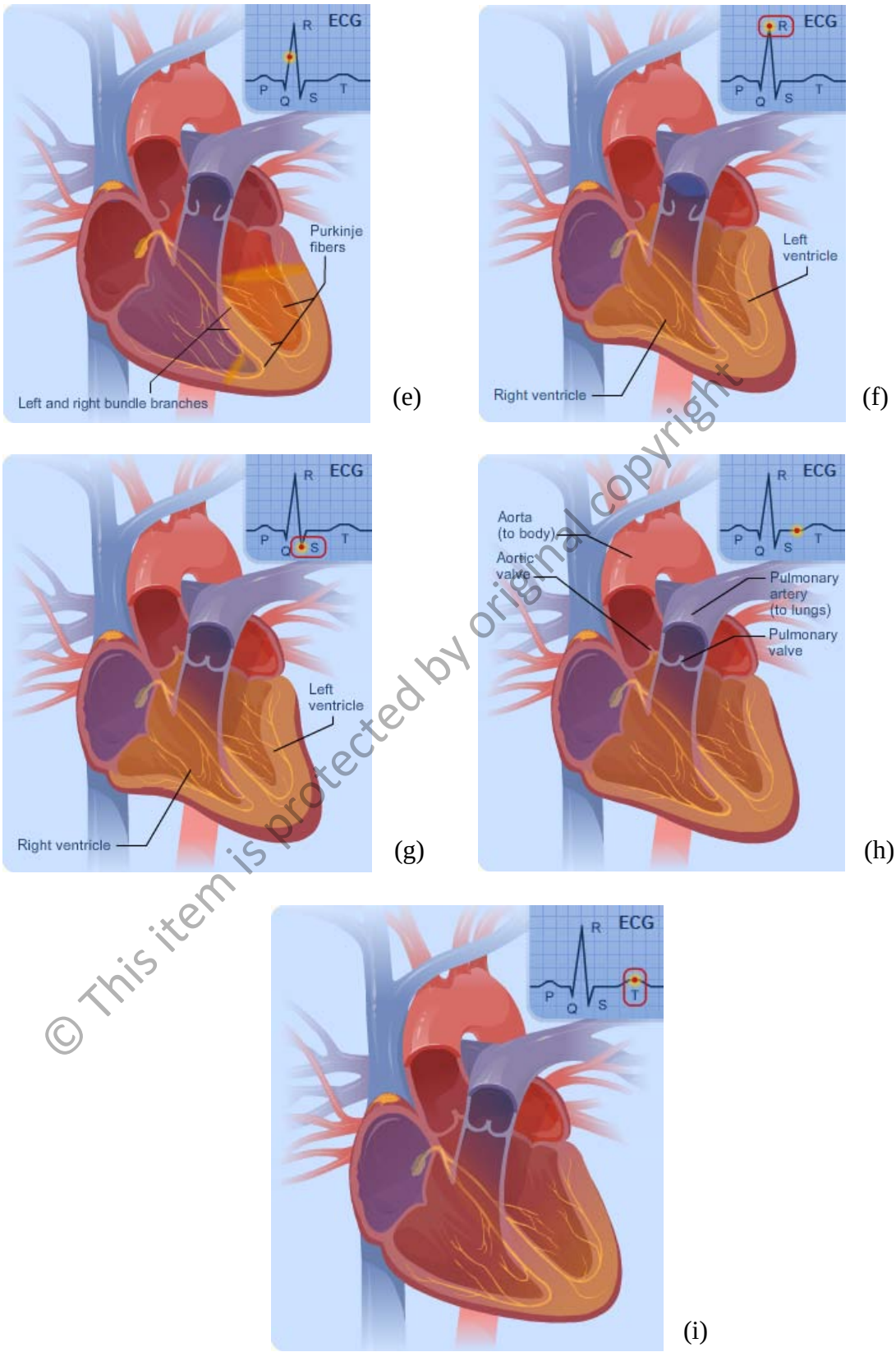

Figure 2.3: Representation the Electrical Conduction System of the HH by the ECG Signal.

2.2.2 The ECG components

A typical ECG recording from a normal patient is shown in Figure 2.4. The ECG signal consists of six waves (P, Q, R, S, T, and U). Three waves (Q, R, and S) are usually expressed as a single composite wave called the QRS-complex (Suri & Spaan, 2007). In addition, between the ECG waves there are two time intervals and one segment. The first time interval is termed the PR interval and is computed from the starting point of the P wave to the starting point of the QRS complex. The second time interval is termed the QT interval and is measured from the starting of the QRS complex to the end of the T wave. However, the standard time segment on the ECG is the ST segment, which is the time portion between the termination of the QRS complex (J-point) and the starting of the T wave.

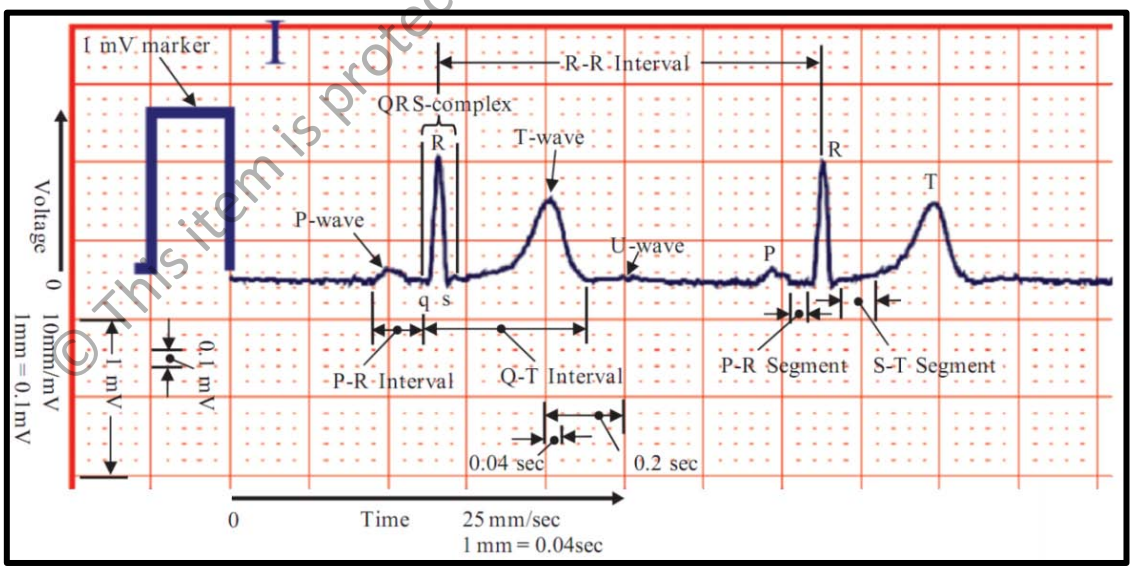

Figure 2.4: The Waves, Intervals, and Segments of Typical ECG Signal (Suri & Spaan, 2007)

In addition to the above intervals and segments, another time interval is considered in the ECG signal and termed the RR interval. This interval is measured

between the peaks of two consecutive R waves. The RR interval represents one complete cardiac cycle and is mainly used to compute the heart rate. What is more, a small time portion, termed as the PR segment, is measured from the end of the P wave until the starting point of the QRS complex. It should be noted that the PR segment does not include the duration of the P wave, while the PR interval includes it (Luthra, 2011).

Another ECG component termed QT_c is measured by the modern ECG machine in addition to the QT interval mentioned above. The QT_c interval represents the corrected value of the original QT interval and is determined by Bazett's formula as defined in Equation (2.1). In this formula the observed QT interval is divided by the square root of $RR_{successive}$ intervals (i.e. the distance variation between the present and the next RR interval) (Azeem et al., 2005; Gacek & Pedrycz, 2012).

$$QT_c = \frac{QT}{\sqrt{RR_{successive}}} \tag{2.1}$$

2.2.3 The 12 Lead ECG

As mentioned previously, the ECG registers the electrical activities of the HH against time. The ECG is recorded by the electrodes that are attached directly to the surface of the human body on the chest and on the limbs. The electrical activities of the HH are sensed by electrodes and are passed through the connecting cables to the ECG machine. In addition, the potential difference between two electrodes (one with positive polarity and other with negative polarity) is expressed by a single ECG lead to assess the average cardiac activity in a specific portion of the HH at a specific time (Aehlert, 2012).

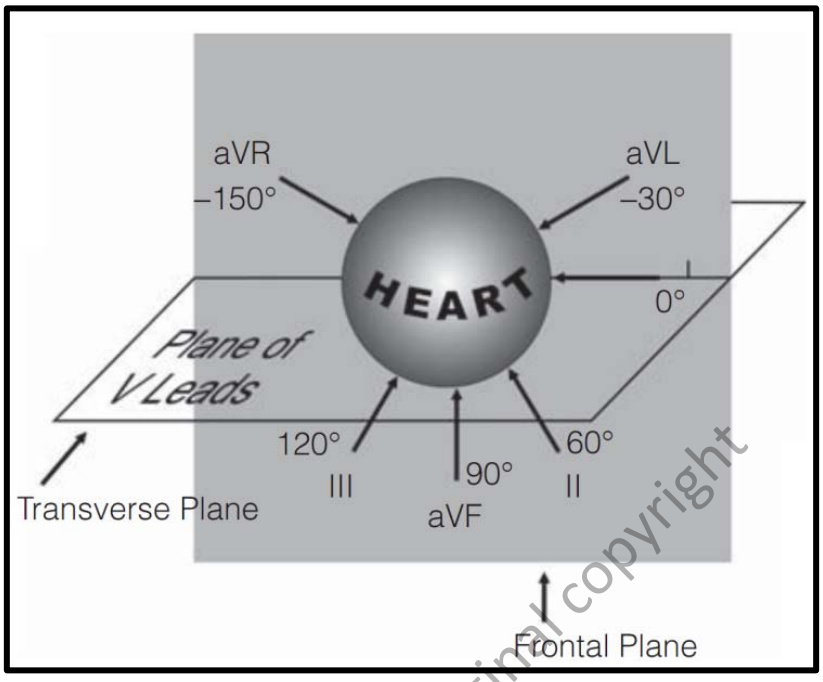

Figure 2.5: The Transverse and Frontal Planes of the 12 Lead ECG (Foster, 2007).

The ECG leads view the electrical activity of the HH in two planes: the horizontal plane (transverse) and the fontal plane (coronal) as shown in Figure 2.5. There are two types of ECG leads: the first are limb leads and the second are chest leads. The standard leads in the ECG are twelve; six of them are the chest leads and the others are the limb leads.

2.2.3.1 The Limb leads

The limb leads sense the electrical activity of the HH in the frontal plane. There are six limb leads which are labeled as: I, II, III, aVR, aVL, and aVF. The electrical connections of these leads with respect to the human body are shown in Figure 2.6. The limb leads are composed of two groups: bipolar leads and augmented (unipolar) leads.

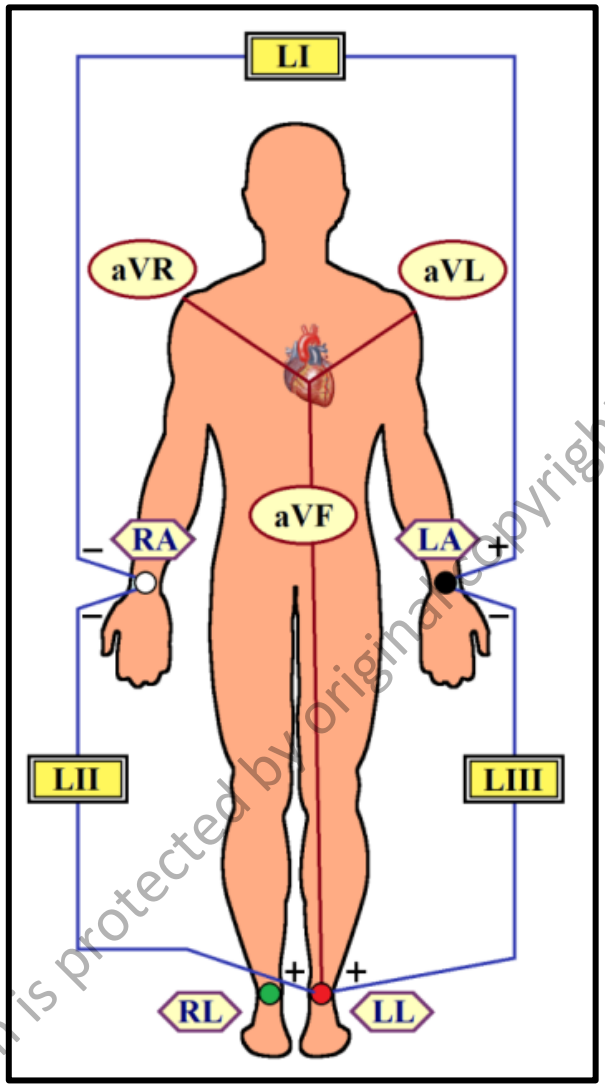

Figure 2.6: The Electrical Connection of the Limb Leads to the Human Body.

2.2.3.1.1 The Bipolar Leads

The ECG leads in this group assess the electrical activity between two electrodes (one acts as a positive and other as a negative polarity) that are connected to the limbs (left arm, right arm, and left leg). As viewed in Figure 2.6, this group includes three ECG leads as follows:

- Lead I is the potential difference between the (positive) left arm (LA) electrode and right arm (RA) electrode.
- Lead II is the potential difference between the (positive) left leg (LL) electrode and the right arm (RA) electrode.
- Lead III is the potential difference between the (positive) left leg (LL) electrode and the left arm (LA) electrode.

2.2.3.1.2 The Augmented (Unipolar) Lead

The second group of limb leads is the augmented leads. The basic concepts of these leads were described firstly by Frank Wilson in 1931. Wilson introduced three leads obtained from the mean of potential difference between any two bipolar leads described above. Moreover, he produced a connection reference point termed as the "Wilson Central Terminal" (WCT) of the limb electrodes (LA, RA, and LL) to obtain an average potential difference across the HH (Bowbrick & Borg, 2006). Additionally, the WCT represents the electrical centre of the HH (Suri & Spaan, 2007). The new produced leads are:

- Lead aVR is the potential difference of the RA with respect to the average of the LA and LL.
- Lead aVL is the potential difference of the LA with respect to the average of the LL and RA.
- Lead aVF is the potential difference of the LL with respect to the average of the LA and RA.

The voltage obtained from Wilson's three leads was very small. Thus, Emmanuel Goldberger in 1942 was able to increase the resultant voltage by 50%. The

names of the new leads were changed slightly to aVR, aVL, and aVF, respectively where (letter "a" refers to augmented). The augmented leads are also termed as unipolar leads because they are determined by a single positive electrode with respect to the combination of the other limb leads. The electrical polarity diagram of the augmented leads incorporated into the Einthoven's triangle is shown in Figure 2.7.a. This figure shows that the limb electrodes (LL, LA, and RA) are the vertices of the Einthoven's triangle. Also, the final representation of bipolar and augmented (unipolar) leads with respect to the central terminal (which are referred virtually to the negative polarity of the augmented leads) is shown in Figure 2.7.b.

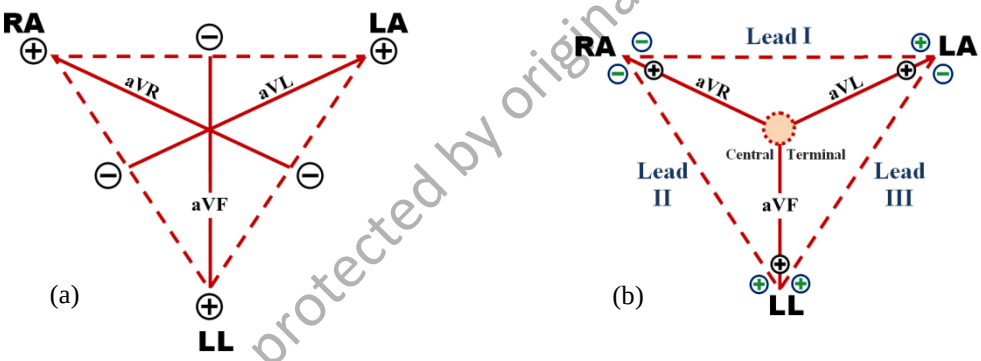

Figure 2.7: (a) Polarity Diagram of the Augmented (Uni-polar) Leads Incorporated into Einthoven's Triangle (Bowbrick & Borg, 2006), (b) View of the Limb Leads with Respect to the Common Central Terminal (Aehlert, 2012).

2.2.3.2 The Chest (Precordial) Leads

In addition to the limb leads that assess the electrical activity of the HH from the frontal plane as shown in Figure 2.5, there are six precordial chest leads named (V1, V2, V3, V4, V5, and V6). Each chest lead is determined by the potential difference between the positive electrode termed as the chest lead and a virtual negative electrode which is represented by WCT. Thus the chest leads are known as the unipolar leads. The placement of the chest leads on the HH is shown in Figure 2.8.a.

The chest leads assess the ECG in the transverse plane as shown in Figure 2.5. Leads V1 and V2 are placed above the anterior wall of the right ventricle. For this reason, they are referred to as right ventricular leads as shown in Figure 2.8.b. When the heart is normally oriented along the long axis, leads V5 and V6 are placed above the lateral wall of the left ventricle, therefore known as the left ventricular leads. The transitional zone between the left and right ventricles (interventricular septum) is found at the level of lead V3 and V4 (equal amplitudes of the R-wave and S-wave) (Gacek & Pedrycz, 2012).

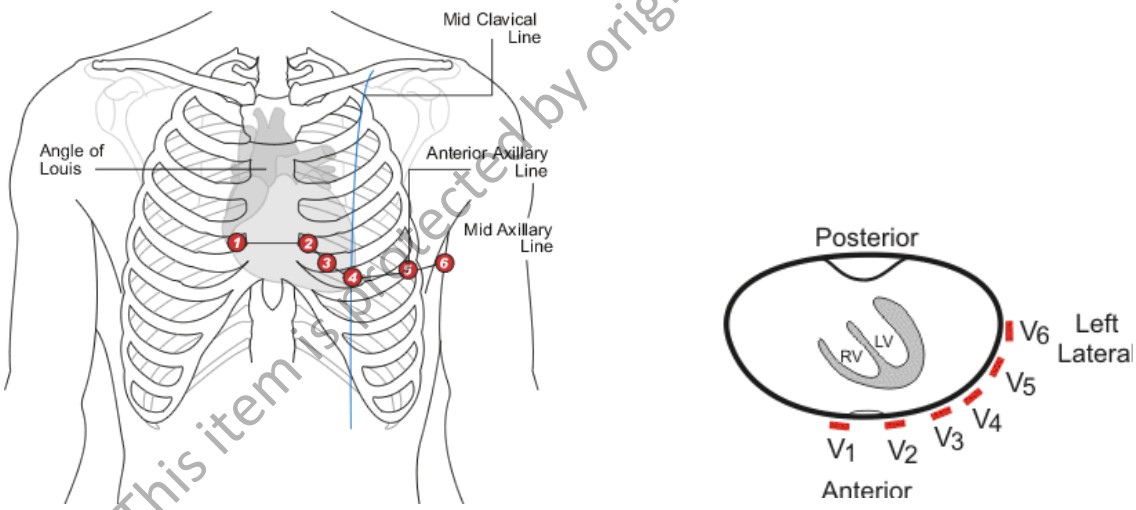

(a) (b)

Figure 2.8: (a) The Placement of ECG Chest Leads in the HH (Bowbrick & Borg, 2006), (b) Top View of the Chest Leads (Aehlert, 2012).

The different placements of the chest leads produce dissimilar patterns in the ECG output diagram. In other words, the ECG waves (P, QRS, and T) have a different amplitude and direction due to the placement of the chest lead in the left, right, or septum side of the HH, Figure. 2.9 shows an ECG diagram of the six chest leads.

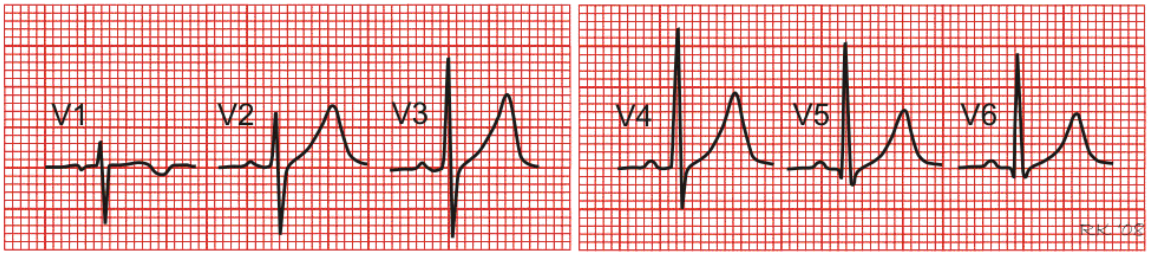

Figure 2.9: The ECG Patterns of the Chest Leads.

2.3 The Data Resources of the 12 lead ECG

A basic investigation and clinical diagnosis of the ECG signal are dependent on the availability of the ECG data with different morphologies. Moreover, can this data be found in a digital raw form? To process it easily by the expert computerized system. The main data resources of the ECG signal are highlighted in the following text.

2.3.1 The ECG machine

The ECG machine assesses and amplifies the small electrical variations on the skin that are caused when the heart muscle is released during each heartbeat. The electrical signal of the HH is detected as a tiny rising and falling voltage between two ECG electrodes placed either side of the HH and displayed as a wavy line either on a screen or on paper. The ECG signal is printed on paper as a graph; its time is represented on the x-axis, while the voltage is represented on the y-axis of the print-out paper.

The ECG machine must be calibrated to represent each 1 mV on the y-axis as 1 cm and each 1 second as 25 mm on the x-axis. What is more, the ECG paper contains a background pattern of a 1mm small square and every 5 mm in both horizontal and vertical directions as a large square. The standard speed of moving paper from the ECG

machine is 25 mm/s. At this speed, one small square on the ECG paper is translated as 40 ms of the ECG signal as shown in Figure 2.10.a. A standard calibration signal of 1 mV is included with the ECG record and must cover vertically 20 small squares (2 large squares) of the ECG paper as shown in Figure 2.10.b (Aehlert, 2012; Azeem et al., 2005).

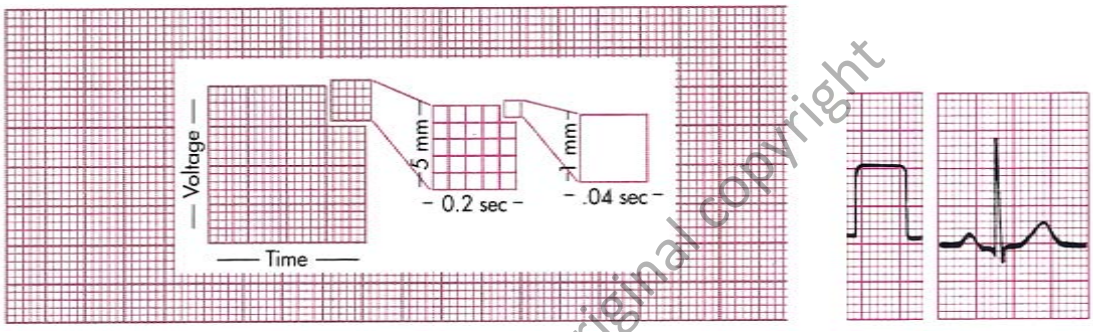

(a) (b)

Figure 2.10: The ECG Grid Paper; (a) The Time Event is Represented by the Horizontal Axis and the Voltage is Represented by the Vertical Axis, (b) In the Calibration of ECG Machine, a 1 mV Electrical Signal of Square Shape Will Produce a Deflection Measuring Exactly 10 mm Height (Aehlert, 2012).

2.3.2 The ECG Database

Most researchers in the field of ECG signal processing need a huge amount of ECG data to validate their work. In addition to the healthy (or normal patients), in some specialists studies, some patients with high risk cardiac diseases are needed to develop different techniques to diagnose these diseases. It is very difficult to collect enough volume of this data from the clinical centres or general hospitals. Therefore, most studies found in literature have validated their works with certain groups of ECG records which were collected from one or more online ECG databases.

The ECG database simply is a list of some ECG signals which are recorded by one or more clinical centres and characterized specifically by certain pathological

conditions or the affiliation of data resources. There are many ECG databases found in specialist clinical interpretation websites. The largest and well-known archive of characterized digital recordings of biomedical signals around the world is the PhysioBank, which was created under the sponsorship of the National Centre for Research Resources of the National Institutes of Health. It contains more than 50 databases of multi-parameter signals from different healthy topics and patients with satisfactory cases that have a significant impact on public health like myocardial infarction movement disorders, congestive heart failure sleep apnea, sudden cardiac death, aging, etc (Goldberger et al., 2000).

In the PhysioBank ECG databases, the raw digital data for each ECG record is stored in a single file. Additionally, one or more sets of annotations about this record like heart rate, RR interval, beat by beat annotations, time locations of the ECG waves, etc are available on the same database in separate files. In addition, in some PhysioBank ECG database, a complete diagnosis of cardiac disease in each record is available as a separate description file. These annotations provide more facilities for researchers to evaluate the analytic performance of new algorithms. Finally, it should be noted that all databases of the PhysioBank are available to the community of scientific researchers via a PhysioNet website (http://www.physionet.org/).

2.3.2.1 The MIT-BIH Arrhythmia Database

The MIT-BIH Arrhythmia Database was created under the auspices of the Massachusetts Institute of Technology (T. Lin & Tian, 2012). It was the first standard dataset available around the world to evaluate the performance of arrhythmia detectors. Additionally, it has been used for basic research into the analysis and diagnosis of the ECG signal at more than 500 sites worldwide since 1980 (G. B. Moody & Mark, 2001).

This database contains 48 ECG recordings which were obtained from 47 subjects and sampled at 360 Hz. Each record contains two ECG leads (limb lead II and one of the chest lead V1, V2, V4, or V5) for 30 minutes duration. The ECG records in this database were annotated by two or more cardiologists. The annotation information include gender, age, R-peak time location, R-R interval, and beat by beat annotations (G. B. Moody & Mark, 1990).

2.3.2.2 The QT ECG database

Another annotated reference ECG database from the PhysioNet is the QT database. This database contains 105 ECG recordings of 15 minutes. They were selected from seven well-known databases in PhysioNet (MIT-BIH arrhythmia, European ST-T, ST change, supraventricular arrhythmia, normal sinus rhythm, sudden death, and long term). Thus, the existing database includes a wide variety of ECG waves in different morphologies. Also, all records were sampled at 250 Hz and annotated by cardiologists with onset, peak, and end time locations of P-wave, QRS complex, and T-wave, while the cardiac disease for all records was not diagnosed (Laguna, Mark, Goldberg, & Moody, 1997).

Through the valuable annotations and variation of ECG morphologies in the QT database, the ECG records of this database can be mostly used by researchers to validate the new techniques of detecting entire ECG waves.

2.3.2.3 The Diagnostic 12-lead ECG Databases

Unlike the ECG databases mentioned in the previous sections, some of the ECG databases in PhysioNet were available with the conventional 12 leads. The cardiac

disease of all records was diagnosed by cardiologists. The first database in this form was the St. Petersburg Institute of Cardiological Technics 12-lead Arrhythmia Database (INCART). It includes 75 ECG recordings of 30 minutes duration and each was sampled at 257 Hz. In addition, each record contains 12 standard leads. The original records were collected from patients undergoing tests for coronary artery disease (most had ventricular ectopic beats). The INCART database contains preferential cardiac diseases whose ECG was consistent with ischemia, coronary artery disease, arrhythmias, and conduction abnormalities. In addition to the valuable diagnosis information, a detail clinical summary (including age, gender, and blood pressure where necessary) was also available for each record (M Llamedo, Khawaja, & Martínez, 2010; G. Moody, 2008).

Another diagnostic ECG database from PhysioNet was the Physikalisch-Technische Bundesanstalt (PTB) database. The PTB database contains 549 recordings selected from 290 subjects. Each single subject was expressed by (1 to 5) ECG records. Only 268 subjects were diagnosed successfully and distributed into 9 diagnostic classes (Myocardial infarction, Cardiomyopathy/Heart failure, Bundle branch block, Dysrhythmia, Myocardial hypertrophy, Valvular heart disease, Myocarditis, Miscellaneous, and Healthy controls) while the diagnostic details of the other (22) subjects were not available (*PTB Diagnostic ECG Database*).

Through the valuable diagnosis information found in the INCART and PTB databases, many studies deal with ECG beat classification and a diagnosis of cardiac diseases were used these datasets as a reference for the quantitative evaluation and validation of final analytic results (J. Martínez, Almeida, Olmos, Rocha, & Laguna, 2006; G. B. Moody, Koch, & Steinhoff, 2006).

2.3.3 Digital Recovery of the Raw ECG Data from Paper Printout Recording

Many techniques for analyzing and diagnosing ECG signals have been proposed. Certainly, they need huge amount of digital ECG data for processing, as well as special kind of data for quantitative evaluation. The ECG data found in the online databases is not sufficient to perform this purpose, especially for ECG data with specific high risk or generic cardiac diseases. At the same time, huge amounts of historical ECG recordings for different ages, ECG morpholgies, cardiac diseases, etc can be collected from old hospital information systems. These recordings are usually stored in paper printouts or in a non-digital format, thus they must be converted into digital format to facilitate their processing by computerized techniques. Generally, this process of converting is called "Digital Recovery". Most methods for the digital recovery of biomedical signals from printout charts follow a four steps structure (Mitra & Mitra, 2003; Sanromán-Junquera et al., 2012):

Step 1: scanning ECG paper printout recording.

Step 2: correcting the orientation of the scanned image.

Step 3: grid line, annotation symbols, and printed text cancellation.

Step 4: sampling drawing signal in a two-dimensional image with actual units.

The process of digital recovery provides an open bank of ECG data and other biomedical signals, which can be used to develop further medical analysis and diagnosis techniques. However, few studies have dealt with digital recovery of biomedical signals in literature. An integral framework based on basic principles of digital image processing techniques was proposed by (Sanromán-Junquera et al., 2012) for biomedical signal digital recovery from binary black and white (BW) chart printout recordings. In this approach, a new algorithm was developed for improving each of the usual four steps. First, the scanned image was complemented for the purpose of easy

interpretation, thus both the biomedical signal and gridlines pixels were foreground. Second, correcting the orientation of the scanned image was performed by a combination of two stages: estimating the tilt angle by decomposing the eigenvectors of the foreground pixels coordinates, and then refining the estimated angle using standard Hough transform (SHT). Third, the grid line cancelation was tackled using binary morphological filters in a horizontal and vertical direction, while the grids in both directions were detected using discrete cosine transform (DCT). Fourth, the final signal waveform was sampled by analyzing all image columns from left to right and using one trace representative pixel per column. The performance of this approach was evaluated using the time synchronization between the original signal in the scanned image and the recovered biomedical signals. The results proved the capability of this approach in terms of automatically reconstructing the biomedical signal from the BW chart printout recording from old hospital information systems. However, this approach was limited for BW paper printout recordings and no technique was proposed for detecting the signal base line. Additionally, all the validated recordings had one lead only, thus there is no evidence that this approach was reliable for recovering multi ECG leads.

Few studies pay attention to the digital recovery for reconstructing the ECG signal from the trace printout recordings. In (Swamy, Jayaraman, & Chandra, 2010), a new algorithm for recovering the digitized ECG time series from the scanned ECG recordings was proposed. In this algorithm, the orientation angle of the scanned image was detected using random transformation based on the maximum variance. An adaptive threshold technique using Otsu's algorithm (Petrou & Petrou, 2010) was then applied to convert the scanned image into binary form. Finally, the sampling process or as termed by this study, envelop detection was performed by scanning the image columns and recording both upper and lower non-zero values. The digitization accuracy

of this approach was evaluated by computing the heart rate for both the original and the recovered data of six single lead ECG records. The resultant accuracy achieved by this approach did not exceed 95%; moreover, no additional technique has been reported to digitize multi-leads in a single scanned image.

An improvement to the ECG digital data recovery was proposed by (Chebil, Al-Nabulsi, & Al-Maitah, 2008) to tune suitable image resolution for the scanning process. Also, the median and neighbourhood techniques were applied for the reconstruction and digitization of the ECG signal. For each image resolution, four measurable features (heart rate, PR interval, QRS duration, and QT interval) were determined for both original and digitized signals. The results show that the highest accuracy for the digitized ECG data was obtained when the image resolution was 2400 dot per inch (dpi). However, this resolution uses a higher rate of computational cost and more processing time.

A software based approach was proposed by (e Silva, de Oliveira, & Lins, 2008) using eight digital signal processing (DSP) steps (digitalizing the paper strip, image binarization, skew correction, salt-and-pepper filtering, axis identification, converting pixel-to-vector, removing the header and trailer of the acquired signal, and splitting the ECG chart and re-assembling it) for digitalizing the ECG printout chart. All steps were developed by MATLAB^{TM} as the software tools without the need for additional dedicated hardware. Some ECG strips were collected from the ECG databank (Jenkins & Gerred, 2009). All records in this databank were stored in low resolution. At the same time, no measured metrics were considered in this study to evaluate the accuracy of the reconstructed ECG waveform. In addition, spatial and frequency techniques were applied separately by (T. Shen & Laio, 2009) for the ECG signal recovery. The performance of both techniques was evaluated by calculating the percentage root mean

square difference (PRD) of 23 ECG charts which were collected from the MIT/BIH Sudden Cardiac Death Holter Database. The PRD was determined for five interpolation functions in each technique. The PRD results show that linear interpolation was the best (45.46% for spatial and 54.33% for frequency technique). However, these results need more improvement in order to minimize dispensable interpolation.

Finally, a simple procedure for digitizing ECG paper printout recordings was proposed by (Paterni, Belardinelli, Benassi, Carpeggiani, & Demi, 2002) using the first order absolute moment (FOAM) as a mathematical rule to locate the ECG trace points. This procedure was validated by 50 ECG printed recordings of 10 seconds from different ECG morphologies. In addition to the classical measure PRD, two mean opinion score (MOS) tests were used to evaluate this procedure. The results of these three tests showed a positive correlation between the original and reconstructed signal. However, this procedure needs further enhancements (as reported in the article) to remove the wrinkles, handwriting, and printed text that were found on the original ECG graph paper.

2.4 ECG Signal Analysis

The ECG signal analysis is a widely used and restful way to interpret different functions of the HH. Amplitudes, time intervals, and ECG wave morphology are used to obtain most of the clinically useful parameters in ECG signals (Petrutiu et al., 2006; Sörnmo & Laguna, 2005). The advancement of robust and precise techniques for ECG wave delineation is a very attractive challenge for cardiologists and biomedical engineers in order to classify ECG arrhythmia types and have a better solution for diagnosing specific ECG phenomenon such as T-wave alternans, atrial fibrillation, and QT-extension (Minhas & Arif, 2008).

2.4.1 ECG Waves Detection

In recent years, the process of analyzing ECGs takes more attention due to its essential role in diagnosing many cardiac diseases. As a result, the development of an efficient and intensive method for ECG wave detection and delineating their time characteristics is a subject of major importance (Zigel, Cohen, & Katz, 2000).

Generally, the process of diagnosing cardiac diseases of the HH based on analyzing the 12-lead ECG signal is performed by computing some features called diagnostic features. There are three main types of diagnostic features: duration, amplitude, and shape features (Zigel et al., 2000). The duration and amplitude features are extracted from certain time location points which are located on boundaries and peak time locations of P, QRS, and T (P-QRS-T) waves; Figure 2.11 shows these time location points, as well as the diagnostic features limited by these points in a single cardiac cycle.

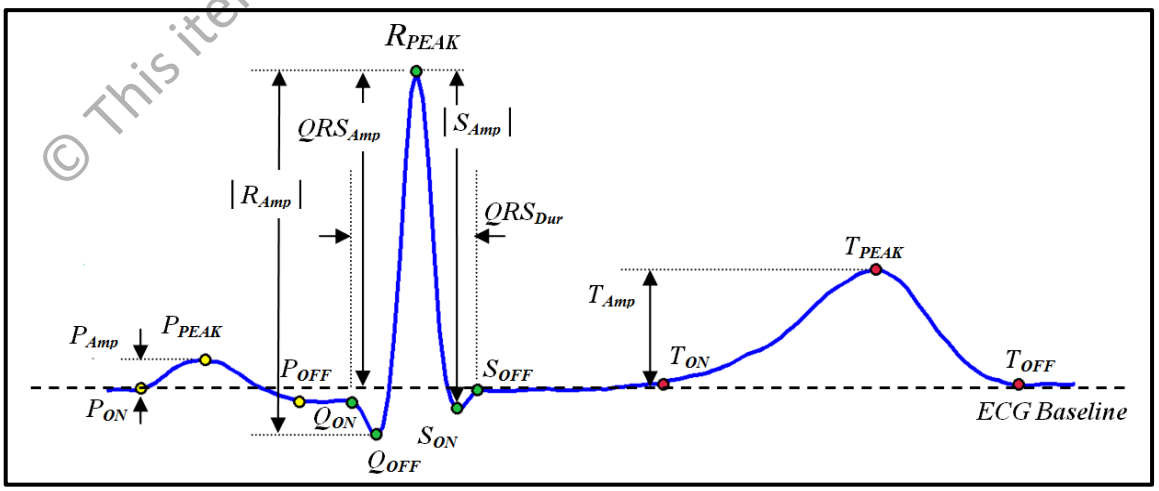

Figure 2.11: The Diagnostic Features Limited by the Time Location Points in a Single ECG Cycle.

Figure 2.4 shows all the intervals and segments which are limited by these locations. Differently, the calculations of shape features depend entirely on the texture of the ECG waves (C. Lin, Mailhes, & Tourneret, 2010; J. P. Martínez, Almeida, Olmos, Rocha, & Laguna, 2004; Mneimneh, Povinelli, & Johnson, 2006; Zigel et al., 2000).

2.4.1.1 QRS Complex Detection

The QRS complex represents heart ventricular depolarization and has the highest frequency component in the ECG signal. Therefore, most significant strategies for detecting ECG waves start by finding time location points of the QRS complex then representing these points as a reference to find other locations for P and T waves (C. Lin et al., 2010). The QRS complex constructed from three sequential (Q, R, and S) waves, and the time location points in these waves are Q_{ON}, Q_{OFF}, $R_{PEAK,}$ $S_{ON,}$ and S_{OFF} (J-point). These time location points are used to obtain duration and amplitude features related to the QRS complex, as well as the segments and intervals of P and T waves like PR, QT interval, and ST segment (Chesnokov, Nerukh, & Glen, 2006; Mneimneh et al., 2006; Wu & Chiu, 2006).

In general, the extracted features from the QRS complex are mainly used to diagnose many high risk cardiac diseases like ventricular hypertrophy, cardiac arrhythmia, myocardial infarction, etc (Hadj Slimane & Naït-Ali, 2010), also as mentioned previously the RR interval obtained by the duration between two consecutive R_{PEAK}s is used to compute heart rate of the HH.

Many studies are found in the literature survey dealing with QRS complex detection. A new method named the difference operation method (DOM) was proposed by (Yeh & Wang, 2008) to detect the QRS complex in the ECG signal. This method was applied using a simple algorithm of two stages. The first stage was to detect R_{PEAK} by means of the difference (differentiation) between the current and previous beat, while the second stage was to detect Q and S waves by applying the search operation for maximum amplitudes at dual intervals to the right and left side of the R_{PEAK} position detected in the first stage. This method does not need complex mathematical computations, thus the time required to process 10 minutes of ECG data does not exceed 30 seconds. The 48 ECG records from MIT-BIH were used to validate the DOM detector. The validation results show that the DOM detector performed in perfect specificity and low sensitivity in comparison with the other two detection methods (Li, Zheng, & Tai, 1995; Pan & Tompkins, 1985). Another approach for QRS complex detection was proposed by (Saini, Singh, & Khosla, 2013) using the K-nearest neighbor (KNN) algorithm. In this approach, the ECG signal was filtered using a digital band pass filter to minimize the false detection generated by power line interference. The gradient of the ECG signal was then used to extract many features which were used by the KNN classifier for QRS complex detection. This detection approach was validated by 48 ECG records from the MIT-BIH arrhythmia database and 125 original 12-lead ECG records from the diagnostic CSE database. The validation results show that the detection rate for CSE database was excellent, while for the MIT-BIH arrhythmia database, it was limited (also less than the DOM detector). Additionally, the time considerations for processing ECG data were not reported in this study.

The empirical mode decomposition (EMD) technique is mostly used for ECG noise reduction (Kabir & Shahnaz, 2012; Kasturiwale & Deshmukh, 2009; Tang & Qin,

2008). The same technique was also used for the purpose of QRS complex detection. In (Hadj Slimane & Naït-Ali, 2010) , a new EMD based algorithm was proposed to detect the QRS complex. The EMD algorithm includes 5 steps to perform subject detection: applying a 5^{th} order high pass Butterworth filter to remove any frequencies within the ECG signal between 0-1 Hz and reducing the influence of the baseline wander, decomposing the filtered ECG signal into a sum of three intrinsic mode functions (IMF) that handle enough information about the slope of the QRS complex, applying nonlinear transform on the resulted IMF, integrating the resulted components, and then applying a 1^{st} order low pass Butterworth filter to compute a unique maximum value for each QRS complex event. The EMD algorithm was validated by 48 ECG records from the MIT-BIH arrhythmia database. The validation results show better performance for the EMD algorithm compared to ones that were determined by the real time QRS complex detection method proposed by (Christov, 2004) and based on comparing the adaptive threshold value with the absolute sum of differentiated ECG signals in one or more leads. A new R_{PEAK} detection method was proposed by (Manikandan & Soman, 2012). This method was applied in four stages: firstly, the QRS complex in the entire ECG signal was emphasized and the noise was removed by three processing steps (band pass filtering, 1^{st} order forward differentiation, and amplitude normalization). In the second stage, the approximate locations of R_{PEAK} in the ECG signal were obtained by applying Shannon energy (SE) estimation and zero-crossing filtering. In the third stage, the local R_{PEAK} was identified by detecting positive zero-crossing points in the Hilbert transform of the SE envelop. Finally, the final true R_{PEAK} time locations were obtained by applying a simple search for the largest amplitude within 25 ECG beats of the candidate R_{PEAK} in the previous stage. The performance of this method was validated with the same set of ECG records used in previous studies. The R_{PEAK} detection results obtained

by this method improve performance compared to ones in (Hadj Slimane & Naït-Ali, 2010) and the other five detection methods.

In general, a WT is widely used by researchers to detect ECG signals due to its flexibility and adaptability. Additionally, the structural design of this transformation addresses the problem of non stationary ECG signals (Güler, 2005). In (Zahia Zidelmal, Amirou, Adnane, & Belouchrani, 2012), a new method of detecting the QRS complex was proposed using the wavelet detail coefficients in fourth and fifth wavelet resolution (d4 and d5) due to the highest QRS energy in these resolutions compared with the first three resolutions (d1..d3). Therefore this energy property was used to distinguish between the false beats and the normal and abnormal true beats. This method was validated with the same set of ECG records as in the previous studies. The detection accuracy was slightly lower than ones that were performed by previous studies.

Lately, a new method of detecting R_{PEAK} time location based on S-transform (ST) and SE has been proposed by (Z Zidelmal, Amirou, Ould-Abdeslam, Moukadem, & Dieterlen, 2014). This method exploits the advantages of ST to extract the QRS complexes in the time-frequency domain. The energy of each local spectrum computed with ST was then determined using SE to localize the R_{PEAK} time location in the time domain. This method was validated with the same set of ECG records used in the previous studies. The obtained results proved the performance in terms of detection accuracy compared with the previous studies. As happened in previous studies (except the DOM detector) (Yeh & Wang, 2008), there is no estimation of the processing time required to compute the SE and ST which were used in this method. As a result, any decision about its validity for real time ECG processing cannot be made clearly. Additionally, this method was validated with 48 ECG records of MIT-BIH arrhythmia

database, while many QRS complex detectors found in literature were tested alongside 2 or 3 other ECG databases to prove the ability of suggested methods to process different morphologies of ECG patterns.

2.4.1.2 P and T waves Detection

As mentioned in the previous section, most strategies of ECG detection start with QRS complex detection, then P and T waves that have lower amplitude than the QRS complex are detected sequentially, depending on the pre-detected time location points of the QRS complex. The time location points of P and T waves can be summarized by the boundary points (onset and end), as well as the peak point, which are labeled as P_{ON}, P_{PEAK}, P_{END}, T_{ON}, T_{PEAK}, and T_{OFF} respectively, as shown in Figure 2.11. These time characteristics are mostly used to obtain many diagnostic criteria related to P and T waves alone, as well as some other criteria correlated with QRS complex characteristics.

The process of detecting P and T waves has been addressed by many studies in literature. A new method for delineating time characteristics of P, QRS, and T waves was proposed by (J. P. Martínez et al., 2004) based on WT. Firstly, the QRS time characteristics were detected by searching for "maximum modulus lines" that exceeded some thresholds at wavelet scales, and then marking the pair limited by positive maximum and negative minimum with respect to the zero crossing of the 1^{st} WT scale as the QRS interval. T wave detection was then performed by looking for local maximum WT coefficients of certain morphologies within a search window that was defined relative to the QRS position and its obtained RR interval. Similarly, the P wave was detected, except that the RR dependent search window was defined on the other side of the QRS position with different morphologies than ones for the T wave. The

performance of this detection system was validated using four ECG databases (MIT-BIH Arrhythmia, QTDB, European ST-T (Taddei et al., 1992), and CSE (Willems et al., 1987)) databases, which were mostly used by other detection techniques according to the manual annotation information inside them. The time characteristics of ECG waves that were obtained by this system were P_{ON}, P_{PEAK}, P_{END}, Q_{ONSET}, $S_{ONSET,}$ T_{PEAK}, and T_{END}. The greatest detection accuracy was found in T_{END}, while the others time characteristics were comparable to those found in the literature.

Another method of detecting ECG waves was proposed in (Ghaffari, Homaeinezhad, Akraminia, Atarod, & Daevaeiha, 2009) using discrete wavelet transform (DWT) to delineate onset, peak, and end time locations of P, QRS complex, and T waves. In this method, a window with a fixed length was slid sample to sample on the fourth wavelet scale then the curve length in each window was multiplied by the area under the curve. Finally, a designated variable thresholding criterion was applied to delineate the time locations of the ECG waves. This method was validated with the same sets of ECG databases used in the previous study. In contrast to the previous WT based detector, the most significant performance was found in the detection results of P wave time locations compared with those in the QRS complex and T wave.

A new method of delineating time locations in P, T, and the QRS complex was proposed by (A. Martínez, Alcaraz, & Rieta, 2010) based on Pahsor transform (PT). In this method, each instantaneous ECG sample was converted to complex form; the real part was represented with a constant value, while the original ECG sample was considered as an imaginary part. The detection of the P and the T wave was performed by considering the instantaneous phase deviation in successive ECG samples of PT. The phase angles caused by P and T waves in the pahsor form are maximized, regardless of their eventually small amplitude in the original ECG signal, thus making the delineation

of their time locations easier. The performance of this method was validated with the same sets of ECG records used in previous studies. The detection results of P and T waves for all time locations were lower or compatible with those computed by similar studies in the literature.

2.5 Diagnosing Cardiac Disease Based on 12-Lead ECG Signal Analysis

The most important objective of ECG signal processing is diagnosing the cardiac disease of the HH based on the diagnostic features which were extracted from analyzing and detecting ECG waves as mentioned in Section 2.4.1. The precision of these features is responsible for the correct diagnosis cardiac diseases. The results of the studies that were proposed in literature for diagnosing cardiac diseases demonstrate that WT is the most promising method to perform feature extraction from 12 lead ECG signals (Addison et al., 2000; Dokur & Ölmez, 2001; Saxena, Kumar, & Hamde, 2002; Sternickel, 2002).

While, there are many cardiac diseases, some of them can be diagnosed extremely accurately based on the extracted diagnostic features from the time characteristics of 12 lead ECG records (Malmivuo & Plonsey, 1995). Also, the ECG test performs estimation with accepted probability compared to other cardiac diseases because they need additional clinical heart tests like Echocardiography (ECHO), which uses sound waves to generate a series of moving pictures that describe the size and shape of the HH and how well its chambers and valves are working.

Additionally, the areas of the HH muscle that do not contract normally and the areas of poor blood flow to the HH can be captured by this test. Other clinical heart tests were recommended by cardiologist to get more valuable information about the status of the HH and can make an accurate diagnosis easily.

2.5.1 Diagnosing High Risk Cardiac Diseases

Among cardiac diseases, there are some which mainly cause sudden cardiac death (SCD), thus these diseases are called high risk cardiac diseases. The simplest accepted interpretation of SCD is death caused by unexpected circulatory arrest due to HH causes that leads to sudden loss of consciousness within 1 hour from the starting of acute symptoms in a person with/without existence of specific cardiac disease (Vasiliadis, Kolovou, Mavrogeni, Nair, & Mikhailidis, 2014). Hypertrophic obstructive cardiomyopathy (HOCM) is the most common cardiac disease that causes SCD in young athletic persons. The pathophysiology of SCD that is caused by HOCM involves complex arrhythmogenic substrate that prepares the person to fatal ventricular fibrillation (Kelly & Galvin, 2010). Additionally, arrhythmogenic right ventricular cardiomyopathy (ARVC), Wolf Parkinson White syndrome (WPW), LVH, long QT corrected syndrome (LQTcS), and brugada syndrome are classified as the high risk cardiac diseases that cause SCD with a lower percentage (low risk) than for HOCM. The risk percentage of SCD for some high risk cardiac diseases were presented in a form of pie chart by (Maron, 2009) according the well known standard guidelines of the American College of Cardiology (Graham et al., 2005) and the European Society of Cardiology (Pelliccia et al., 2005). In this study, the risk percentage that causes SCD for HOCM was 35%, 8%, 4%, and 2% for LVH, ARVC, and WPW, respectively.

Many diagnostic criteria that were found in different well-known cardiology references can be used to perform a diagnosis of high risk cardiac diseases, but with limited accuracy. These criteria were obtained originally by the time characteristics that resulted from analyzing P, QRS, and T waves in 12-lead ECG and the standard ECG intervals limited by these time characteristics. Some diagnostic criteria were based on the shape of the ECG waves themselves. However, most of these criteria take the form

of simple logical conditions or basic mathematical definitions which can be computed easily by computerized systems using programming languages or modern intelligent systems like fuzzy logic, artificial neural network (ANN), etc. In spite of these facilities to design an intelligent diagnosis system using different computerized techniques, most studies found in literature that deal with diagnosing high risk cardiac diseases based on 12-lead ECG signal take the form of statistical medical studies on selected group of patients to develop new diagnostic criterion or to get the detailed medical reports about the most causes of cardiac disease and the correct ways of treatment.

On the other hand, few studies have been proposed in literature for the purpose of diagnosing generic cardiac diseases using successive computerized systems. In (Chang et al., 2012), a new diagnosing system was proposed for myocardial infarction (MI) classification based on multi-lead ECG (V1, V2, V3, and V4). These four leads reflect the MI infection in the anterior and septum wall of HH, therefore they were considered in this system to determine four corresponding sets of ECG features using hidden Markov models (HMMs). These 4 HMMs are used not only to find the ECG segmentations but also to compute the probability value (or likelihood value in HMM). The probability for each heartbeat will be transferred to logarithm, log-likelihood, and adopted as statistical feature data of each heart-beat's ECG complex. These likelihood values are adopted as statistical different features for each heart-beat's ECG complex. Then, the two well-known classification methods, support vector machines (SVMs) and Gaussian mixture models (GMMs) are applied to classify a set of testing data represented by four sets of HMMs feature into myocardial infarction and normal classes. This system was validated with 1129 ECG samples collected from private clinical centres, including 582 MI samples and 547

normal samples. The final diagnosis results of sensitivity, specificity, and accuracy were 85.71%, 79.82%, and 82.50%, respectively.

Additionally, the precise detection and classification of different types of ECG arrhythmias is crucial for the correct medical treatment of cardiac patients, so the detection of the ECG arrhythmia using the ECG signal was the most significant subject (Kutlu & Kuntalp, 2011; Nasiri, Naghibzadeh, Yazdi, & Naghibzadeh, 2009; Özbay & Tezel, 2010). Many computer based approaches have been proposed in literature for the purpose of detecting and classifying various arrhythmia types. An intelligent diagnosis system of adaptive neuro-fuzzy inference systems (ANFIS) was proposed by (Nazmy, El-Messiry, & Al-Bokhity, 2010) to classify ECG beats into six types of arrhythmias; normal sinus rhythm (NSR), ventricular premature contraction (VPC), atrial premature contraction (APC), ventricular tachycardia (VT), ventricular fibrillation (VF), and supraventricular tachycardia (SVT), based on a feature vector that was extracted from independent component analysis ICA, power spectrum, and RR interval. A simple and reliable method named "range overlaps method" was proposed by (Yeh, Wang, & Chiou, 2010) for classifying cardiac arrhythmia into five types; NORM, VPC, APC, and left/right bundle brunch block (LBBB and RBBB), respectively.

2.5.2 Predication of Sudden Cardiac Death using ECG Signal Analysis

However, SCD in young people is rare, but it is a tragedy which threatens all families and communities around the world (Maron, 2009; Maron, Doerer, Haas, Tierney, & Mueller, 2009). The incidence of SCD in any population varies due to many reasons including: nationality, age, gender, ethnic group, clinical techniques to detect SCD, and facilities to obstruct or overcome SCD pharmacologically, surgically, and the use of clinical implantable devices. There are 80 incidences of sudden death (SD)

(fewer than 40 years old) per year in New Zealand; and 427 incidences of SD from 1995 to 2004 in Australia. However, the statistical clinical studies performed by experts estimate that at least eight incidence of SD happen weekly in the United Kingdom (Fishbein, 2010). Additionally, the reported information in (Noseworthy & Newton-Cheh, 2008) shows that there are more than 300,000 incidences of SD in the United States annually. Most of these people (about 80%) suffered from coronary artery diseases; fewer cases (15%-20%) were associated with non-ischemic myopathic processes like HOCM, and approximately 5% were related to a primary defect of cardiac electrophysiology like (LQTcS or brugada syndrome) (Zipes, 2005).

The process of SCD predication using a 12-lead ECG takes in a wide area of research due to the seriousness of this subject. A large number of studies found in literature survey deal with SCD predication as an attempt to get an early warning about this problem and surviving cardiac incidences, then thinking about possible ways to overcome it. Numerous approaches and methods to detect and predict SCD have been proposed in literature. These studies have been based on certain parameters like heart rate turbulence (HRT), heart rate variability (HRV), T wave alternans (TWA), and signal averaged electrocardiogram (SA-ECG), which can be obtained by the same set of time characteristics related to ECG waves that were presented in Section 2.4.1.1 and Section 2.4.1.2.

In (E. Ebrahimzadeh & Pooyan, 2011), a new algorithm was proposed to detect and predict SCD based on HRV and two sets of features were extracted by processing two minutes of ECG beats before SCD. The first set of features was extracted from the ECG signal itself using time and frequency domain, while the second set was extracted by applying a time-frequency transformation on the resultant HRV signal .The decision to classify healthy persons and others who are liable to SD was performed by multilayer

perceptron (MLP) and K-Nearest Neighbour (KNN) with neural networks based on the two sets of features after reducing their dimensions by principle component analysis (PCA). This predication method was evaluated by 35 SCD patients from the MIT-BIH SCD Holter database in PhysioBank. The behaviour of the ECG signal of one patient from this database before two minutes of SCD and few seconds after is shown in Figure 2.12. The resulted prediction accuracy of SCD with this method was 91.42% which was better than the percentage obtained by another method (T.-W. Shen, Shen, Lin, & Ou, 2007). This made a prediction of SCD with 87.5% accuracy by applying ANN on the features of HRV in Lead I from the ECG patients of the same database used in the previous method.

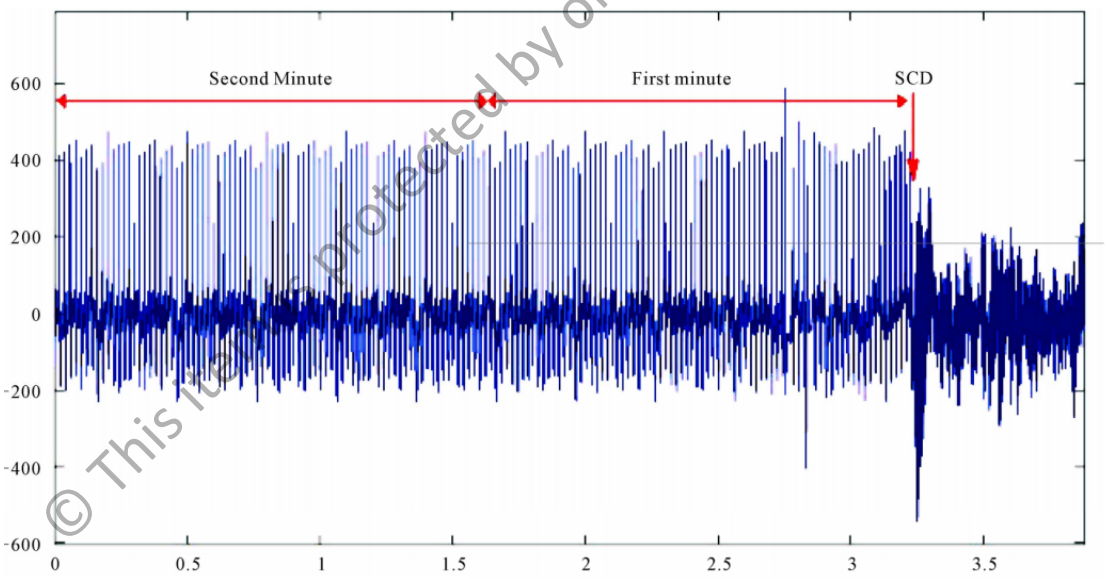

Figure 2.12: The ECG Signal of SCD Patient Before 2 minutes of SCD Event and Several Seconds After that (E. Ebrahimzadeh & Pooyan, 2011).

Finally, a review study was presented by (Murukesan, Murugappan, & Iqbal, 2013) about the methods and techniques based on HRV to detect and predict SCD. Many important recommendations were made in this study. The first was that the

predication accuracy of SCD based on HRV was limited because HRV factors cannot be accurately evaluated in the patients with frequent Premature Ventricular Contractions (PVC) or Atrial Fibrillation (AF). Moreover, these factors were influenced by many parameters like age, gender, and the medicines taken by patients. The second conclusion made by this study was that the HRV factors must be combined with other ECG parameters like HRT and TWA to produce a highly precise SCD predication. The last conclusion made by this study was that statistical tools were a processing way of predicting SCD in comparison with classifier based tools.

2.6 Summary

Chapter two has been divided into two main parts; in the first part, a detailed interpretation of the basic concepts of ECG signal including the cardiac conduction system of HH and its representation in the ECG signal and the standard components of the ECG signal have been presented and discussed. Moreover, the main groups of 12 leads considered in ECG signal and adopted sources of ECG data have been explained.

A literature review of the latest researches and studies that are related to the main contributions of this thesis, which include the methods of digital recovery raw ECG data from printed charts, QRS complex detection methods, P and T wave detection methods, and the methods of diagnosing high risk cardiac diseases were presented in the second part of this chapter.

Table 2.1 summarized all the literature survey related to the main contributions of this research.

Table 2.1: Summary of Literature Review

Reconstructing Digital Raw ECG Data From ECG Paper Printout Recording			
#	**Authors**	**Year**	**Description of based technique**
1	M. Sanroma´n-Junquera	2012	An integral automatic approach for recovering biomedical signals from BW grid paper printouts based on digital image processing principles (Image orientation correction, Pre processing and grid cancellation, Signal waveform extraction, Conversion from the waveform in the image plane to 1D biomedical signal).
2	Prashanth Swamy	2010	an improved methodology to extract the digitized version ECG time series using the Radon transform for de-skewing the scanned images. Even though the conventional Furthermore, a simple and useful way of axis identification is proposed.
3	Jalel Chebil	2008	A new method for converting ECG paper printout recording of into digital form using neighbourhood and median approaches. In addition, the relationship between pixels and time-voltage values is automatically determined.
4	A.R. Gomes e Silva	2008	A new software-based approach using Matlab environment through 8 image processing tools Digitalization of the paper strip, Image binarization, Noise filtering, Axis identification, Pixel-to-vector conversion, Removing the header and trailer of the acquired signal, Splitting the ECG chart and re-assembling it.
5	TW Shen	2009	A new method of recovering ECG signal using spatial and frequency techniques separately.
6	M Paterni	2002	a simple procedure for digitizing ECG paper printout recordings using the FOAM as a mathematical rule to locate the ECG trace points.

Delineating Time Characteristics of The QRS Complex			
#	**Authors**	**Year**	**Description of based technique**
1	Yun-Chi Yeh	2008	A new method named the difference operation method (DOM) which be applied using a simple algorithm of two stages: • Detect R_{PEAK} time location by means of the difference (differentiation) between the current and previous beat • Detect Q and S waves by applying the search operation for maximum amplitudes at dual intervals to the right and left side of the R_{PEAK} position.
2	Indu Saini	2013	A new approach for detecting QRS complex using the K-nearest neighbor (KNN) algorithm. In this approach, the ECG signal was filtered using a digital band pass filter to minimize the false detection generated by power line interference. The gradient of the ECG signal was then used to extract many features which were used by the KNN classifier for QRS complex detection.
3	Zine-Eddine Hadj Slimane	2010	a new EMD based algorithm to detect the QRS complex. This algorithm includes 5 steps to perform subject detection: • Applying a 5^{th} order high pass Butterworth filter. • Decomposing the filtered ECG signal into a sum of three (IMF). • Applying nonlinear transform on the resulted IMF.

			• Integrating the resulted components. • Applying a 1st order low pass Butterworth filter to compute a unique maximum value for each QRS complex event.
4	M.Sabarimalai Manikandan	2012	A new R_{PEAK} detection method based on the SEE estimator and a simple peak-finding logic using the HT and moving average filter to address the problem of detecting unusually shaped QRS complexes and noises.
5	Z. Zidelmal	2012	a new method of detecting the QRS complex using the wavelet detail coefficients in 4th and 5th wavelet resolution (d4 and d5) due to the highest QRS energy in these resolutions compared with the first three resolutions (d1..d3). Therefore this energy property was used to distinguish between the false beats and the normal and abnormal true beats.
6	Z.Zidelmal	2014	A new R_{PEAK} detection method based on ST and SE. This method exploits the advantages of ST to extract the QRS complexes in the time-frequency domain. The energy of each local spectrum computed with ST was then determined using SE to localize the R_{PEAK} time location in the time domain.

Delineating Time Characteristics of P and T Waves			
#	**Authors**	**Year**	**Description of based technique**
1	Juan Pablo	2004	A new method for delineating time characteristics of P, QRS, and T waves based on WT. Firstly, the QRS time characteristics were detected by searching for "maximum modulus lines" at wavelet scales. T wave detection was then performed by looking for local maximum WT coefficients of certain morphologies within a search window that was defined relative to the QRS position and its obtained RR interval. Similarly, the P wave was detected, except that the RR dependent search window was defined on the other side of the QRS position
2	A. Ghaffari	2009	A new method of detecting ECG waves using DWT to delineate onset, peak, and end time locations of P, QRS complex, and T waves. In this method, a window with a fixed length was slid sample to sample on the fourth wavelet scale then the curve length in each window was multiplied by the area under the curve.
3	Arturo Martı´nez	2010	A new method of delineating time locations in P, T, and the QRS complex based on PT. In this method, each instantaneous ECG sample was converted to complex form. The detection of P and T waves were performed by considering the instantaneous phase deviation in successive ECG samples of PT. The phase angles caused by P and T waves in the PT are maximized, regardless of their eventually small amplitude in the original ECG signal

Diagnosing Generic Cardiac Diseases			
#	**Authors**	**Year**	**Description of based technique**
1	Pei-Chann Chang	2012	a new diagnosing system was proposed for MI classification based on 4 sets of ECG features which were extracted from (V1, V2, V3, and V4) leads using HMMs, then the two well-known

			classification methods SVMs and GMMs are applied to classify a set of testing data represented by 4 sets of HMMs feature into myocardial infarction and normal classes.
2	Nazmy El-messiry	2010	An intelligent diagnosis system of ANFIS to classify ECG beats into six types of arrhythmias; NSR, VPC, APC, VT, VF, SVT based on a feature vector that was extracted from ICA, power spectrum, and RR interval.
3	Yeh Wang	2010	A simple and reliable method named "range overlaps method" to classify cardiac arrhythmia into five types; NORM, VPC, APC, LBBB, and RBBB.

CHAPTER 3

RESEARCH METHODOLOGY

3.1 Introduction

Many computerized based techniques have been proposed in literature for the purpose of analyzing, detecting ECG waves, and delineating the time characteristics of these waves to extract many valuable parameters and diagnostic features to interpret different functional activities of the HH. Most of these techniques were validated with the online ECG data that was downloaded from specialist physiological websites like PhysioNet as mentioned in Chapter 2 Section 2.3.2. However, many of these techniques provide acceptable results, but need further improvements to generate perfect outcomes especially the incompatibility of these techniques for real time applications. This is due to the fact that the greatest numbers of these techniques were applied to the transformed version of ECG data (not on the ECG data itself) using certain mathematical transform like DWT, PT, etc or using the series of mathematical estimations like SE. EMD. As a result, more time was spent on arriving of these calculations.

As mentioned in Chapter 2 Section 2.5.1, a limited number of computerized based techniques have been proposed in literature for the purpose of diagnosing cardiac diseases based on diagnostic features that were extracted from analyzing a 12 lead ECG signal. This limitation has many reasons, the first of which is the limitation of digital 12 lead ECG data as it is only persons who suffer from certain cardiac diseases who are suitable to process in a computerized system. Second, many cardiac diseases, especially high risk cardiac diseases, need more specialist cardiac information and more HH tests than that normally reported by cardiologists.

In this chapter, an intelligent system is proposed for analyzing a 12 lead ECG signal and diagnosing LVH high risk cardiac disease. The proposed system includes three main stages: pre-processing the ECG signal, analyzing and detecting ECG waves, and diagnosing LVH high risk cardiac disease. The general block diagram for the proposed ECG system is shown in Figure 3.1.

In the first stage of proposed ECG system, a new digital recovery approach is proposed to address the limitation of digital ECG data by reconstructing it from the scanned image of the ECG paper printout recording.

In the second stage of the proposed ECG system, two approaches are proposed to detect the QRS complex and P, T waves, respectively, and then delineates the boundaries and peak time locations of these waves which are used to compute diagnostic parameters for various cardiac diseases. Both proposed approaches are designed to apply a straightforward algorithm with an instantaneous processing technique on the ECG input signal.

As mentioned in Chapter 2 Section 2.5.1, LVH cardiac is one of the high risk cardiac diseases that cause SCD in young people. In the third stage of the proposed ECG system, a new approach is proposed for diagnosing LVH cardiac disease based on some voltage parameters determined from the previous detection stage and some traditional diagnostic criteria. The proposed diagnosis approach is modelled by the new design of the fuzzy Inference system (FIS), and it is designed to test any 12 lead ECG data and provide an accurate diagnosis of LVH cardiac disease for both genders.

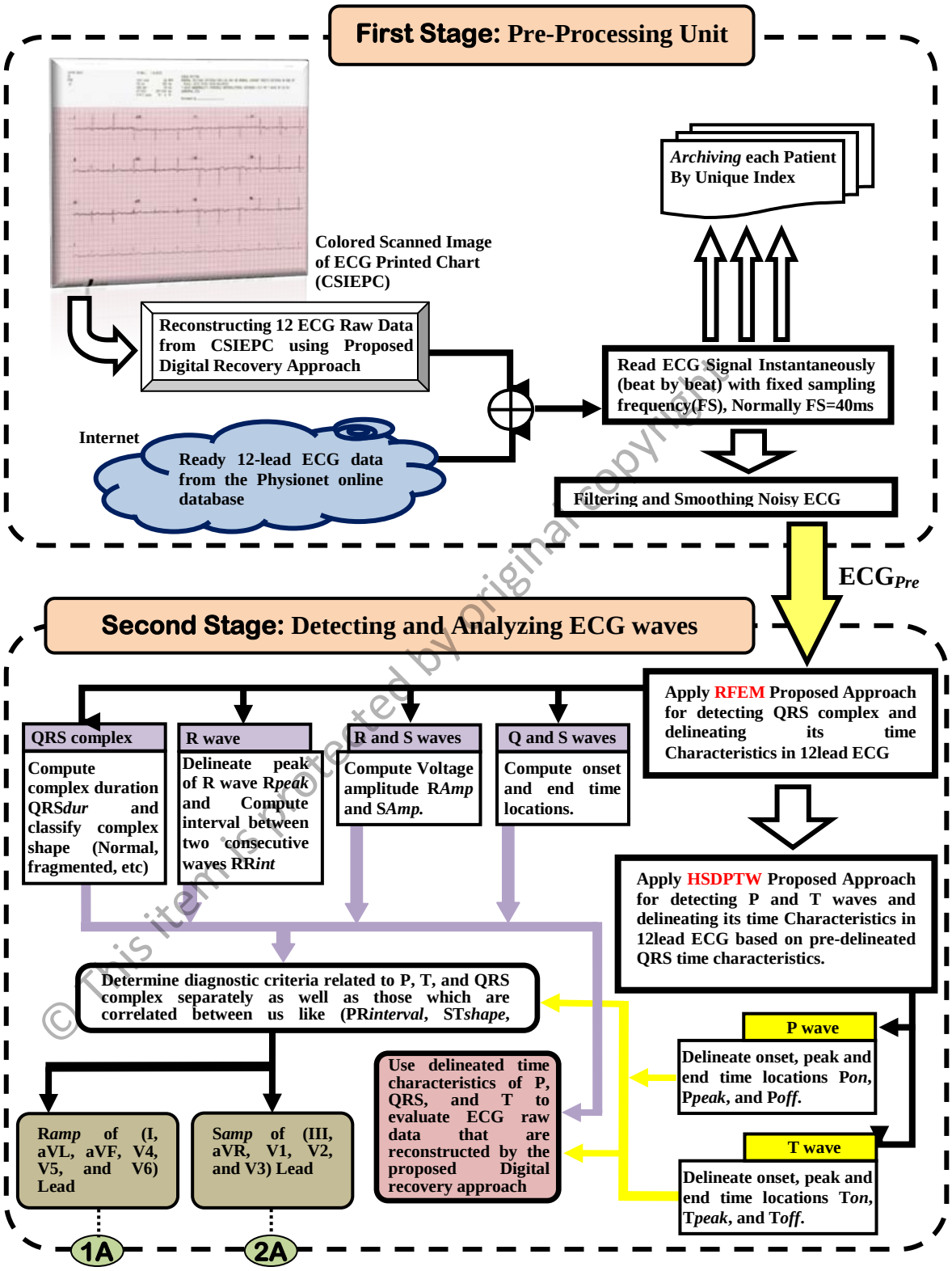

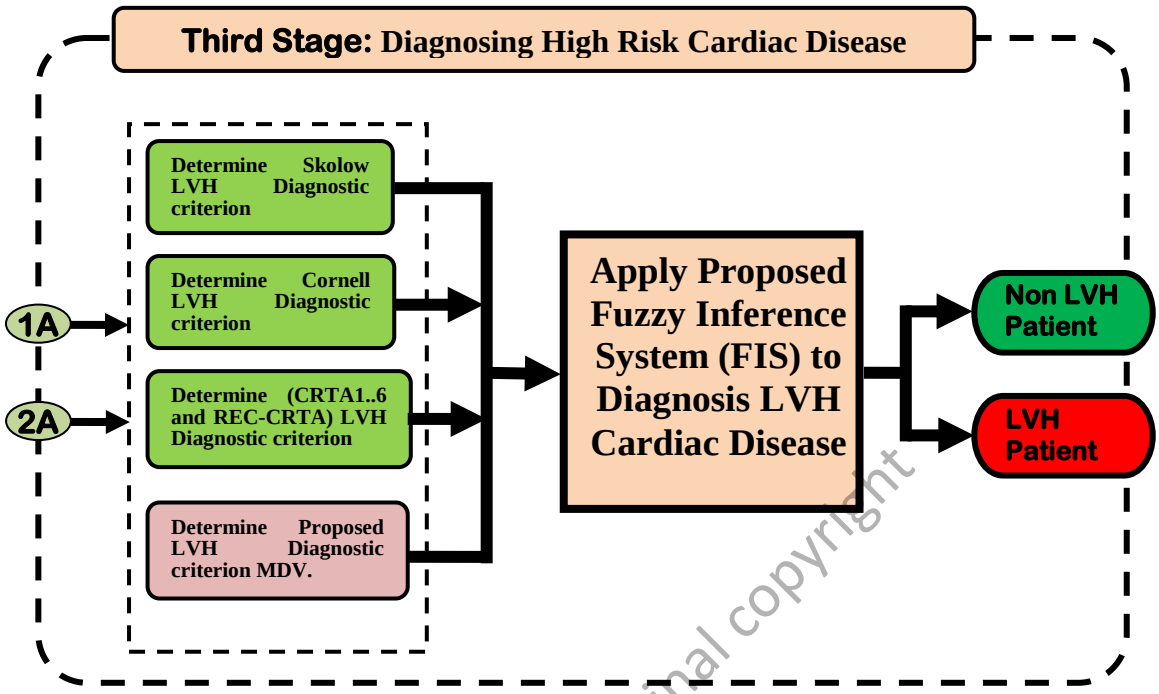

Figure 3.1: General Block Diagram of Proposed System for Analyzing and Diagnosing 12-lead ECG Signal.

3.2 12-Lead ECG Data

As mentioned in Chapter 2 Section 2.1, the ability to interpret any medical data using a computerized system is related mainly to the availability of this data in a digital form with various morphologies. In this section, the resources of ECG data used to validate the proposed approaches for analyzing, detecting and diagnosing are discussed in more detail.

3.2.1 Online ECG Data

Most studies found in the literature survey for analyzing, classifying, and diagnosing ECG signals were validated by ready data that was downloaded from specialist databases on the internet. The online ECG data was arranged as groups of databases with different subjects in a digital form. In addition, the original ECG

recordings for this data were collected from many specialist clinical centres around the world.

As mentioned in Chapter 2 Section 2.3.2, the Physionet website is a great resource for different physiological signals. It contains a huge bank of data called PhysiBank which is organized into more than 50 ECG databases with different numbers of records, and most databases are annotated manually by cardiologists with important analysis information like RR interval, time characteristics of ECG waves, ECG beat classification, etc. Additionally, some ECG databases in this bank include a complete diagnosis of cardiac disease and all data inside this bank is free of charge. Therefore, these databases have become the main resources of ECG data for all studies presented in the literature survey which is concurred with ECG analysis, classification, and diagnosis.

In the second stage of the proposed ECG system shown in Figure 3.1, two approaches have been proposed to detect ECG wave characteristics; one for detecting or delineating the QRS complex and other for P and T waves. Selecting the suitable ECG database to validate any detector depends mainly on the annotated information available in this database. The first detector for the QRS complex is validated with the ECG records in the MIT-BIH database from Physiobank which was discussed in Chapter 2 Section 2.3.2.1. Also, in the same data bank, the ECG records from the QT database discussed in Chapter 2 Section 2.3.2.2 are used to validate the second detector of P and T waves. Additionally, some ECG records from diagnostic 12 lead ECG database INCART discussed in Chapter 2 Section 2.3.2.3 are used to validate the proposed approach for diagnosing LVH cardiac disease in the third stage of the proposed ECG system shown in Figure 3.1. The limited amount of ECG records in these databases which are suitable for diagnosing validation, especially for high risk cardiac diseases

like LVH, opens the way for other ECG record resources like reconstructing 12 lead ECG data from the printed ECG chart.

3.2.2 Digital Recovery of 12-lead ECG data from Paper Printout Recordings

As mentioned in Chapter 2 Section 2.3.3, the digital recovery of ECG data from paper printout recordings has become essential, especially for the ECG data of high risk cardiac diseases. Moreover, it is very difficult to assemble sufficient amounts of this data through online databases. At the same time, unlimited ECG records as the paper printout recordings can be collected from different clinical centres, even if they have been recorded using a traditional ECG machine. Thus, a new approach for the digital recovery of 12 lead ECG data has been proposed to reconstruct this data from the digital image scanned from the ECG paper printout recording (printed ECG chart). The proposed digital recovery approach is based on the basic principles of image processing techniques and is applied in four stages. The general block diagram of this approach and a sample result for each step is shown in Figure 3.2.

3.2.2.1 Proposed Approach for Digital Recovery of 12-Lead ECG from Paper Printout Recordings

The final shape of the ECG chart depends mainly on the ECG machine that has recorded it. Traditional ECG machines use long roll paper to print the ECG. In this machine, the 12 lead ECG is printed one after another in a sequential form, while in modern machines, all 12 lead ECG are printed on single paper.

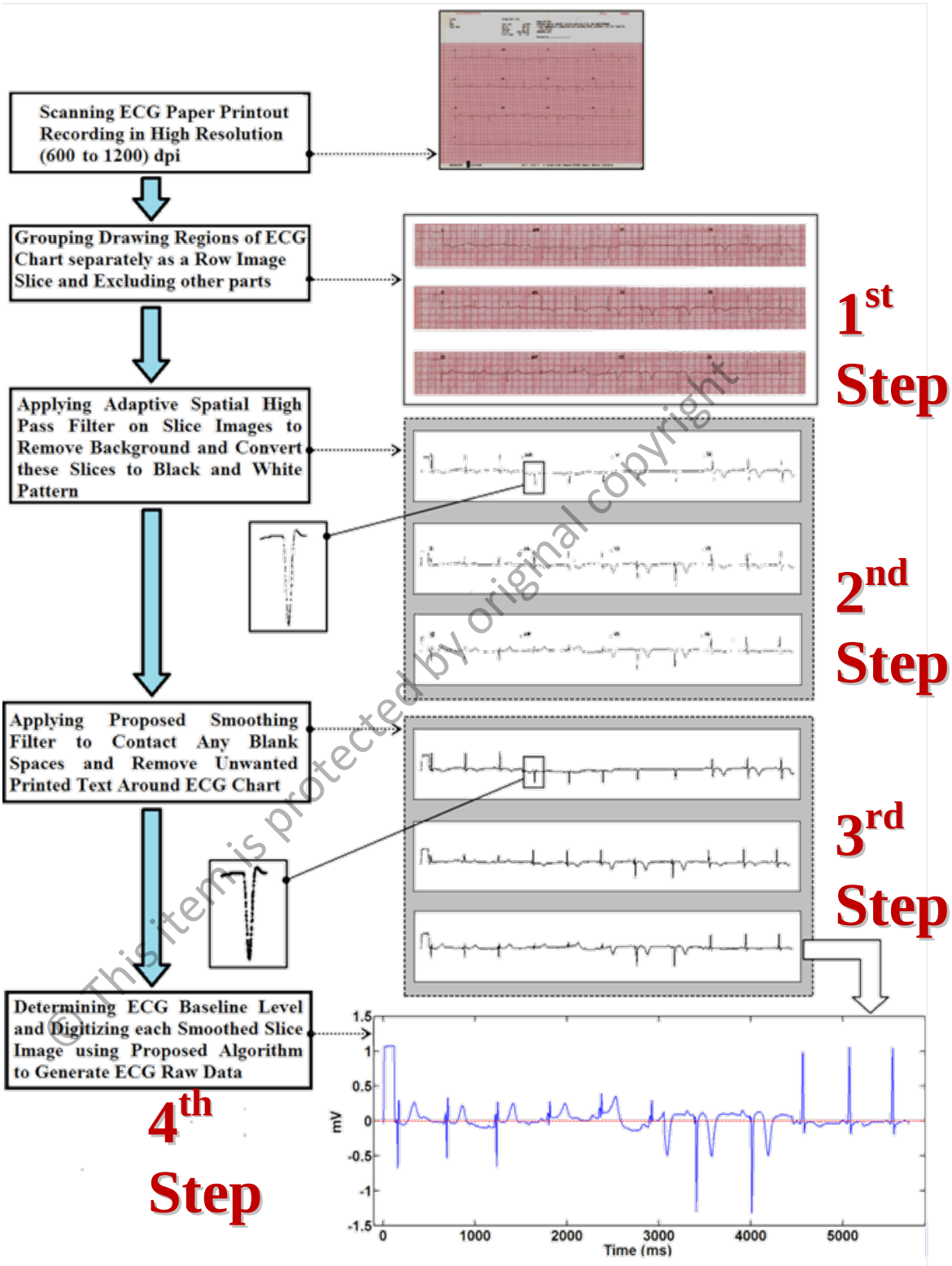

Figure 3.2: General Block Diagram of Proposed Approach for Digital Recovery of 12 lead ECG Data from Colour Scanned Image of ECG Paper Printout Recording.

Additionally, certain types of these machines are programmed to make basic analysis and pre diagnosis for the ECG signal recorded but their accuracy is limited because many parameters in these machines must be adjusted before reuse. One sample of ECG printout recording from a traditional machine is shown in Figure 3.3.a, and two samples of ECG recordings which are recorded by different modern ECG machine models are shown in Figure 3.3.b and c, respectively.

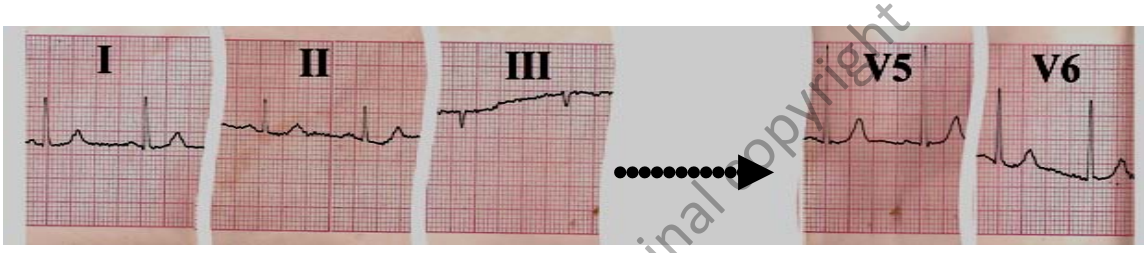

(a)

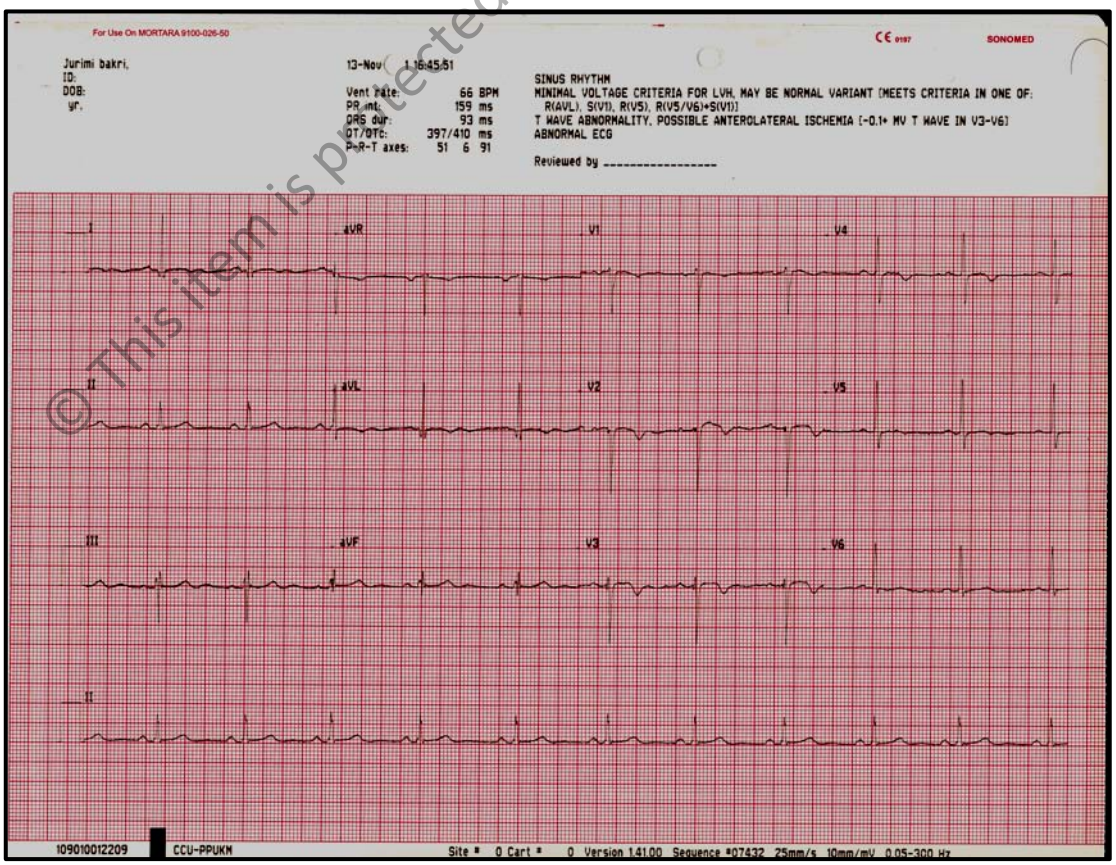

(b)

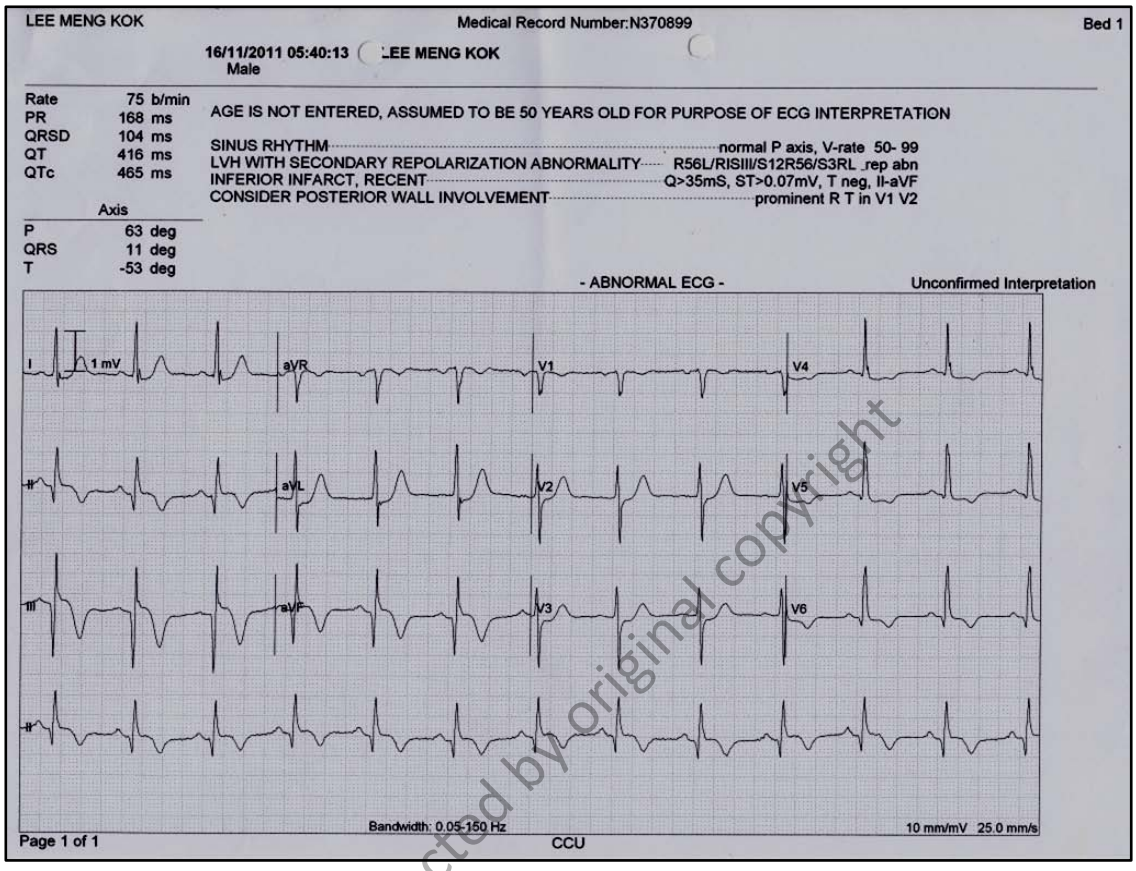

(c)

Figure 3.3: (a) Classical 12-lead Paper Printout Recording, (b), (c) Modern Forms of 12-lead Paper Printout Recordings with Automatic ECG Interpretation.

In the first step of the proposed digital recovery approach, the 12-lead ECG paper printout is scanned with high resolution (600 to 1200 dpi) to maintain the most accurate details of the ECG drawing, which means that the final recovered raw ECG data is very accurate. Next, each row region of the ECG drawing that contains four different leads is grouped separately as an image slice with (WS) width and (HS) height, while the remaining area in the scanned image is excluded from the following calculations as shown in the 1st step of Figure 3.2.

The resulting image slices from the previous step are converted to black and white colour mode by removing background colour which is viewed as small and large

squares. The background colour is usually light (light green, orange, red, or blue). This background colour must be erased and only the dark colour (usually black) of the ECG chart stays (alone) within the image slice. To perform this subject analysis, an adaptive high pass filter is applied on each slice including three colour layers (RGB) for each point. As is known, the value of each (RGB) component is limited between (0 ... 255) and each colour filter applied on this pattern must be fixed exactly with an adaptive threshold value for component for each colour to make a decision to pass or reject (erase) the tested point. The special colour filter is designed to erase all points within the image slice that verify the mathematical rule expressed in Equation (3.1), which at the same time passes all points elsewhere. The threshold values (R_{th}, G_{th}, and B_{th}) must be determined accurately according to the components of the background colour; this is done by applying a simple analysis on the (RGB) components of some points found in small selected segments inside the tested slice, however, the selected segment must be empty (from any drawings).

$$\exists[\text{Erase } X_{ij}]:\ Red(X_{ij}) < R_{th}\ AND\ Green(X_{ij}) < G_{th}\ AND\ Blue(X_{ij}) < B_{th}\ ,$$
$$\forall\ i, = 1, \dots, HS;\quad \forall\ j, = 1, \dots, WS \tag{3.1}$$

The resultant image slices from the previous step contain the ECG chart and some printed text around this chart. The enlarged segment in the 2nd stage of Figure 3.2 shows that some blank spaces are found within the ECG chart. These gaps in the drawing will be considered as missing data in the next steps, which will have an effect on the accuracy of the final recovered data.

The third step in the proposed digital recovery approach overcomes this problem by applying an intelligent technique to track the resulting ECG chart' points and fill any

blank spaces within them. As well as, removing any printed text or lines around ECG chart. The delineation value of the new data added must be computed accurately to remove any distortion which occurs in the final ECG drawing. The new intelligent technique takes four (3 x 3) masks (left, right, up, and down) around the tested point as a base rule to make a decision to contact two neighbouring end points if at least one mask (M) from the four contains more than two black points (pixels) as expressed in Equation (3.2).

$$\exists[Fill\ X_{ij}]: \sum M_{Left} \geq 2\ or \sum M_{Right} \geq 2\ or \sum M_{Up} \geq 2\ or \sum M_{Down} \geq 2 \quad (3.2)$$

The contact decision takes the form of replacing the blank point by a designed (3 x 3) mask, which makes the contact with four possible end points in four directions as shown in Figure 3.4.

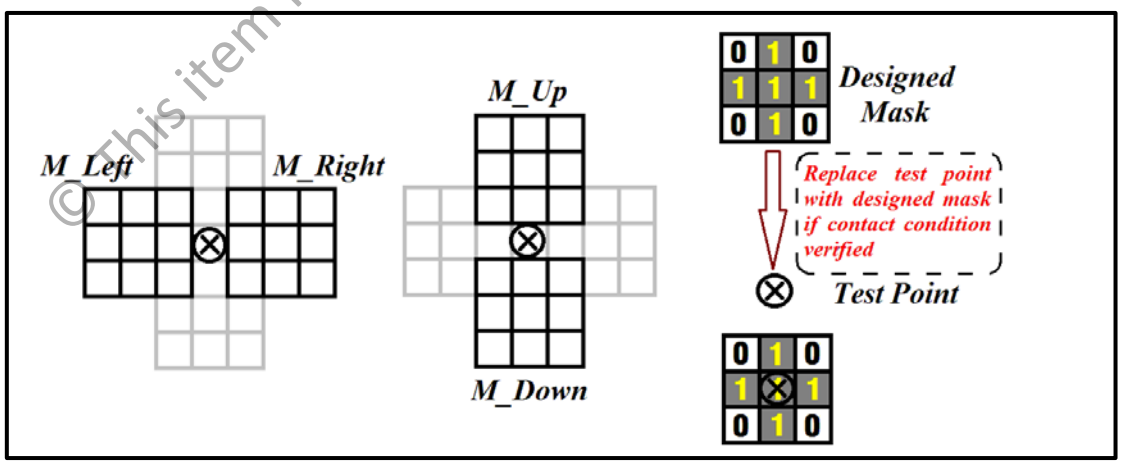

Figure 3.4: A Process of Replacing Test Point with Designed Mask to Fill Blank Spaces between Two Neighbouring Points.

In addition to contacting two end points spaced by a blank space within the ECG chart, other advantages are gained from applying the previous technique. First, the resulting ECG chart takes a smooth form, thus the enlarged segment shown in the 3rd stage of Figure 3.2 is smoother than the resulting ECG chart when the previous intelligent technique was applied. Second, the testing of the blank spaces is limited to the points that fall inside the four tested masks (M_{Up}, M_{Down}, M_{Left}, and M_{Right}). This means that any points outside these masks are not considered in the resulting smoothed image and, as a result the unwanted printed text and the handwritings outside the ECG chart are removed.

The final step in the proposed digital recovery approach is focused on detecting the ECG baseline and reconstructing useful raw ECG data. The proposed technique of computing the level of the ECG baseline is performed by partitioning the complete area of each image slice resulting from the previous step into small horizontal segments with the same heights equal to 5 points (pixels) and the same widths equal to the width of the image slice (WS).

The baseline position is allocated in the centre of the segment that has a maximum number of black points as expressed in Equation (3.3). The baseline detection process is applied once in each image slice (i.e. all four leads in single image slice take same baseline level).

$$\exists! \, [BaseLine \leftarrow i + 2] : MAX\left(\sum^{i} X(i..i+4,\ 1..WS)\right)$$

$$, \forall \ i \ = 1, 6, 11 \ldots, size(HS - 5) \tag{3.3}$$

The second operation which will be applied in this step is the digital recovery of raw ECG data. In general, sampling any continuous signal must be processed with a certain frequency. The output frequency of the ECG signal is related directly to the speed of the ECG device. As standard, this speed is equal to 25 mm/s, thus the time interval for one ECG beat is (40 ms). These basic principles are reported in most cardiology resources (Azeem et al., 2005; Bowbrick & Borg, 2006; Hampton, 2008; Luthra, 2011; Wagner, 2008).

As the time interval of a single ECG beat is represented by a small square in the final ECG paper printout, the sampling process of the ECG chart must be applied to each small square. However, the difference here is that the small square is represented by a number of image pixels, not as a time interval.

The size of a small square in pixels (PS) can be determined easily by computing a number of pixels with the same colour which forms the square shape in any clear region from the original scanned image. The complete area of the image slice is partitioned into vertical segments with the same widths equal to PS pixels and the same heights equal to the height of the image slice (HS). The width of the vertical segments (PS) can be reduced to 50% or more in order to increase the resolution of the final reconstructed data, especially for the low printed quality of the ECG chart.

The sampling or digitizing process is applied according to the proposed algorithm mentioned in Algorithm I. In this algorithm, each vertical segment is scanned from the bottom in an upward direction to find the first column mask of 5 points which has more than 2 black points. When this mask is reached, the scanning process in this segment is terminated and the centre point of this mask is fixed as a digitizing point. This point represents primary voltage amplitude of the raw ECG data in this segment; the final voltage amplitude level is determined by shifting it with the baseline level

computed in the first operation of this step, and then normalizing it by a certain amplitude factor determined by the number of pixels in the two large squares which simulate 1mV in a real ECG signal (Aehlert, 2012; Azeem et al., 2005; Hampton, 2008, 2013; Jenkins & Gerred, 2011; Luthra, 2011).

Algorithm I Proposed Algorithm for Sampling Raw ECG Data from Slice Image

BEGIN

Read *FS_image* = Image Slice (k_i, k_j) ,$\forall k_i$=1, … ,*HS*; $\forall k_j$=1, …. ,*WS*

/ WS, HS are width and height of testing Image Slice */*

PS = **Calculate** (No. of Pixels in each small Square of ECG chart)

Amp_Fact = **Calculate** (Scaling Factor from Total Height HS with respect to PS)

Raw_Data=Zeros (1...WS/ PS) */* Generate an empty matrix of Raw ECG Data */*

for j=1 **to** WS **STEP** PS **do**

for i=3 **to** HS-2 **do**

Sum_Rg= ∑ Fs_image (i-2…i+2, j) */* Calculate No. Of Black Pixels in Mask Column Vector of Five Points that is cantered by tested point (i,j) */*

if *Sum_Rg* ≥ 3 **then**

Raw_Data(j)= i + (*Sum_Rg*/2) */* Store Centre Position of First Verified Column Mask with 5 points That includes more than two Black Pixels into Raw ECG Data Vector */*

Break loop(i);

end if

end for */* end of loop i*/*

end for */* end of loop j*/*

Final_Raw_Data = (*Raw_Data* - Baseline Level) / *Amp_Fact* */* shifting Resulted Raw ECG Date by the baseline level and scaling them with amplitude factor */*

END

3.3 Detection Time Characteristics of ECG Waves

As mentioned in Chapter 2 Section 2.4.2, most approaches for detecting and delineating P, the QRS complex, and T waves were applied using certain mathematical transformation like wavelet, Walsh, cosine, Fourier, etc, adaptive filtering techniques like low pass differentiation, nested median filtering, etc, or intelligent classifier like fuzzy theory, ANN, etc (C. Lin et al., 2010). In these approaches, the detection of ECG waves is performed by processing the ECG data after converting it to another sampling or sequence form that makes the processing of the ECG signal simpler. However, the resulting detection rates which are obtained by these approaches are highly accurate. Nevertheless, the ability to apply them as a real time system becomes more difficult due to the complexity in the mathematical calculations needed for these approaches. On the other hand, the validity of the real time detecting approach becomes more realistic when the based technique tracks the ECG signal beat by beat and performs the entire subject detection by simple mathematical calculations.

According to the last observation of processing the ECG signal instantaneously, two detection approaches have been proposed based on a straightforward algorithm that tracks the ECG signal beat by beat, and then delineates the time location points of P, the QRS complex, and T waves. The first approach is proposed to delineate the time characteristics of the QRS complex. While, the second approach is proposed to delineate the time characteristics of the P and T waves depending on the time location points of the QRS complex that are pre-delineated in the first approach.

3.3.1 Proposed Approach for Detecting QRS Complex

As mentioned in Chapter 2 Section 2.4.2.1, the first step in detecting ECG waves in most detecting techniques found in literature survey is to delineate the time location points of the QRS complex, and then represent these locations as the reference points to delineate other time locations in the P and T waves. Additionally, the obtained diagnostic features from these locations are used to make a diagnosis for different cardiac diseases. Therefore, the detection of the QRS complex can be seen as the core of analyzing and interpreting ECG signals. As a result, developing new approach for detecting and delineating the QRS complex accurately is essential.

In this section, a new approach to delineate the time characteristics of the QRS complex (Q_{ONSET}, Q_{END}, R_{PEAK}, S_{ONSET}, and S_{END}) has been proposed using an instantaneous algorithm applied directly on the ECG signal without the need for any mathematical transform, additional filters, or classification with the intelligent technique. The proposed detection approach takes the advantage of mutation from tall rising to falling edge as the basis for delineating the time location points of the QRS complex. The proposed detection approach includes three steps as shown in Figure 3.5. In the following text, each of these steps is highlighted in more detail to interpret its main function in the final detection process.

In the first stage which can be represented as a pre-processing unit, simple calculations are performed to compute two threshold values (R_{th} and S_{th}), which are used in the next steps to make a decision of considering R and S waves, respectively. These threshold values are determined by computing the maximum positive and negative difference along with the beats of two or three ECG cycles. Next, the largest two sequential sets are extracted as a maximum positive difference Rt and a maximum

negative difference St. Finally, the R_{th} and S_{th} are obtained by Rt and St values after scaling them with a factor (0.85 .. 0.95).

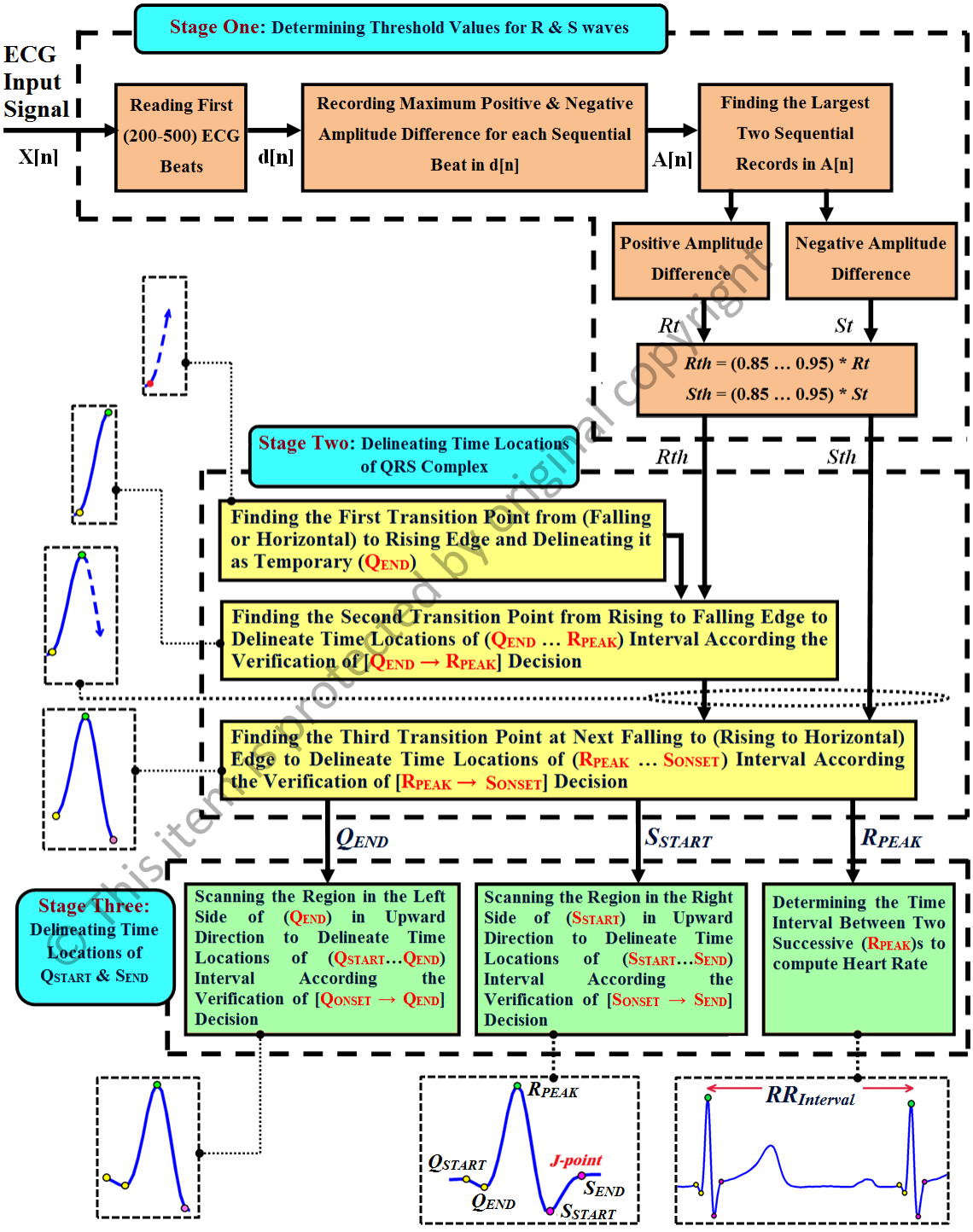

Figure 3.5: General Block Diagram of Proposed RFEM Approach for Detecting Time Characteristics of QRS Complex.

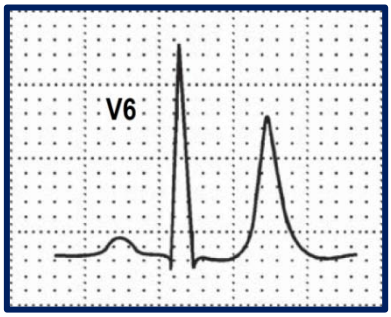

Figure 3.6: Extremely Tall amplitude of T wave (Foster, 2007).

This scaling factor is selected at a high level to make sure that the decision about detection is related to the QRS complex and not for the T wave because in some cardiac diseases, the T wave has a high amplitude level due to hyperkalemia (Foster, 2007) (asymptotic amplitude level of the QRS complex) as shown in Figure 3.6. Another reason for this scaling factor comes from the fact that not all QRS complexes along the same ECG record take the exact same amplitude level.

The second stage of the proposed QRS detection approach represents the first step in the QRS complex detection process by delineating the time location points of (Q_{END}, R_{PEAK}, S_{ONSET}) which are the vertices of a triangle that forms the QRS complex. These locations are delineated using a proposed algorithm named rising falling edge mutation (RFEM). The new algorithm includes two parts. The first starts when the ECG signal is mutated from the horizontal level or falling edge direction to the rising edge direction. This transition can be detected by comparing two voltage differences (AMP_i and AMP_{i-1}) defined in Equation (3.4) and Equation (3.5), which denote the amplitude difference between the next and current beat, and between the current and previous beat, respectively. In this case, the AMP_i has a positive value, while the AMP_{i-1} has a zero or negative value. At this moment the time event of ($Beat_i$) is assumed to be temporary as a Q_{END} time location.

$$AMP_i = \Delta Voltage(Beat_{i+1} - Beat_i) \quad (3.4)$$

$$AMP_{i-1} = \Delta Voltage(Beat_i - Beat_{i-1}) \quad (3.5)$$

Where AMP_i: Amplitude difference between next and current beat, AMP_{i-1}: Amplitude difference between current and previous beat.

The ECG signal within the actual QRS complex must continue in an upward direction until it reaches the R_{PEAK} point. This behaviour can be interpreted with the positive signs of AMP_i and AMP_{i-1} along this period; moreover, the number of beats within this period is determined as (rm). When the ECG signal reaches the peak point of the QRS complex, the direction of the signal is converted from upward to downward. At this moment the time event of ($Beat_i$) is assumed to be temporary as the R_{PEAK} time location and the first part of the proposed delineation algorithm is finished. Finally, the left side of Figure 3.7.b shows a graphical representation of this part of the algorithm in a single ECG cycle which is labelled 1st step. In addition, all instruction sets of this operation illustrated in the first part are marked (*check the occurrence of rising edge*) in Algorithm II. As seen as, the second part of the proposed delineation algorithm is started, the first process performed here is the decision to consider the ECG period limited down by Q_{END} and up by R_{PEAK}, due to the verification of the compound condition expressed in Equation (3.6). This decision condition contains two criteria; first, that the voltage amplitude difference between the R_{PEAK} and Q_{END} is greater than or equal to R_{th} to make sure that this amplitude is related to the QRS complex, which takes the highest amplitude components, while at the same time excluding any amplitudes that are related to the P and T waves. Second, the number of beats in this time period rm is at least two beats.

$$\exists! \, [Q_{END} \rightarrow R_{PEAK}] : (\Delta Voltage(R_{PEAK} - Q_{END}) \geq R_{th} \; and \; rm \geq 2) \quad (3.6)$$

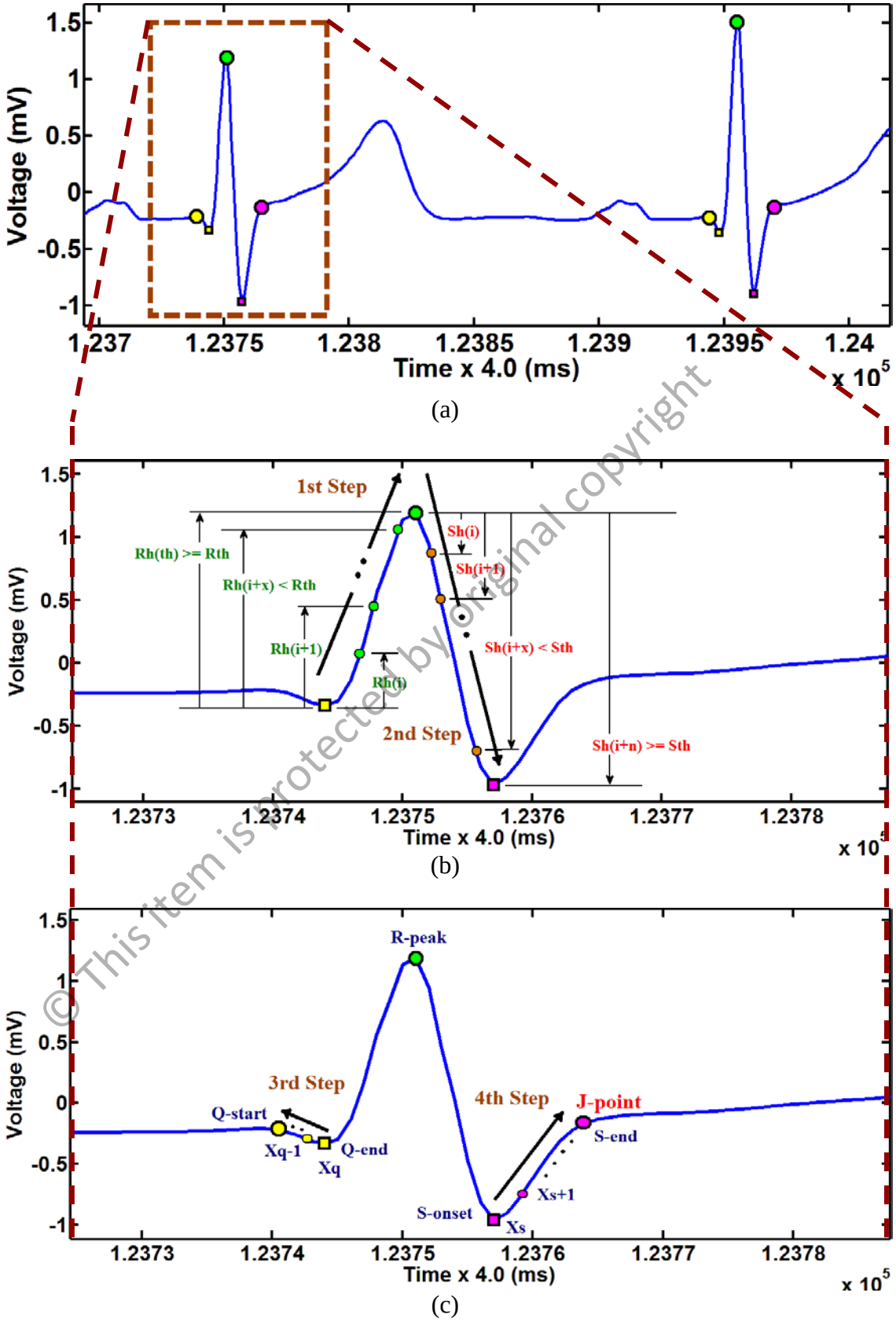

Figure 3.7: Graphical Representation of RFEM Approach, (a) Original ECG Signal [SEL16483 from MIT-BIH Normal Sinus Rhythm], (b) Delineation of Q_{END}, R_{PEAK}, S_{ONSET} Time Location Points (c) Delineation of Q_{ONSET}, S_{END} Time Location Points.

The last criterion is based on the information reported in most cardiology resources that the duration of the QRS complex in normal ECG does not exceed 120 ms (3 ECG beats as a maximum) (Azeem et al., 2005; Bowbrick & Borg, 2006; Gacek & Pedrycz, 2012). Therefore, the R wave which represents the left half of the QRS complex takes a half of this duration.

Beside the decision of ($Q_{END} \rightarrow R_{PEAK}$), this part of the algorithm still determines the continuity of the falling edge which can be interpreted with negative signs of AMP_i and AMP_{i-1} along this period. This sequence continues until the ECG signal reaches the next mutation point; at this moment the time event of ($Beat_i$) is assumed temporary at the S_{ONSET} time location due to the verification of compound condition is expressed in Equation (3.7). The same criteria for the previous decision are used here, except that the threshold value is S_{th} and the number of required beats within this period is (sm). The right side of Figure 3.7.b shows a graphical representation of this part of the algorithm in single ECG cycle which is labelled 2nd step. Moreover, all instruction sets of this operation are illustrated in the second part which is marked (*Check the occurrence of Falling Edge*) in Algorithm II.

$$\exists! \, [R_{PEAK} \rightarrow S_{ONSET}] : \, (\Delta Voltage(R_{PEAK} - S_{ONSET}) \geq S_{th} \; and \; sm \geq 2) \qquad (3.7)$$

The third stage of the proposed approach is performed to delineate a start time location point of the QRS complex Q_{ONSET} and the end time location point S_{END} (J-point) that makes the connection between the QRS complex and T wave in the ECG cycle.

In general, the Q wave in an ECG signal is expressed by a negative deflection that precedes the occurrence of the R wave. This deflection represents the left to right depolarization of the inter-ventricular septum of the HH.

Algorithm II Proposed Algorithm to Delineate Q_{END}, R_{PEAK}, and S_{ONSET} Time Locations

BEGIN

X = [$BEAT_1$,…,$BEAT_i$] , ∀i=1,….,N */* N : total No. of beats in ECG input signal */*

for I =1 **to** N **do**

AMP_{dif} =Δ *Voltage* (X_{i+1} - X_i) */* Determine the voltage difference between current and next beats */*

/ Check the occurrence of Rising Edge */*

if AMP_{dif} > 0 **then**

rm=rm+1 */* rm is the counter of beats in Rising Edge */*

i_{FIRST} = Xi */* store first Rising Edge point in i_{FIRST} */*

if sm > 2 **and** Δ (AMP($X_{R\text{-}PEAK}$) – AMP(X_{i-1})) > Sth **and** R_{flag} =1 **then**

S_{ONSET} =X_{i-1} */* record the existence of S-wave start point */*

Reset R_{flag}=0 */* reset R_{flag} when successive falling edge is detected */*

endif

sm=0

endif

/ Check the occurrence of Falling Edge */*

if AMP_{dif} < 0 **then**

sm=sm+1 */* sm is the counter of beats in Falling Edge */*

if rm > 2 **and** Δ (AMP($X_{R\text{-}PEAK}$) – AMP(X_{i-1})) > Rth **then**

Q_{END} = $X_{i\text{-}FIRST}$ */* Q_{END} point is the first point in successive Rising Edge */*

R_{PEAK} = X_i

Set R_{flag}=1 */* set R_{flag} when successive Rising edge is detected */*

endif

rm=0

endif

endfor

END

The amplitude of the Q-wave is small in left leads (I, aVL, V5, and V6); however, its amplitude becomes deeper (greater than 2mm) in leads (II, III, and aVR). Additionally, the Q wave is not seen in the right side leads (V1, V2, and V3) (Alfaouri

& Daqrouq, 2008; Azeem et al., 2005; Bowbrick & Borg, 2006). According to the variation in the amplitude of the Q wave in different ECG leads, a simple search process is performed from the Q_{END} time location towards the upper left corner. This search process checks the voltage amplitude difference between the Q_{END} point determined in the previous stage and the previous beat ($Beat_{Qend}$-i), as well as the number of beats within this period is determined. The search operation is terminated when one of the conditions expressed in Equation (3.8) is verified. The first condition limits the amplitude difference that does not exceeds 2mm (0.2mV) (the maximum amplitude for a normal Q wave) (Azeem et al., 2005), and the second condition limits the time duration of the detected Q wave less than 2 beats, which limits the duration of the Q wave and is reported in most cardiology references (Aehlert, 2012; Azeem et al., 2005; Bowbrick & Borg, 2006; Hampton, 2008). In the same manner, another search process is performed on the upper right corner of the S_{ONSET} time location point to detect the end time location of the S wave (S_{END}). The same search process which is used in the Q wave is implemented to locate ($S_{ONSET} \rightarrow S_{END}$) time interval, except that the start beat is the (S_{ONSET}) time location point and the assuming threshold for the time duration does not exceeds 3 beats as expressed in Equation (3.9).

$$\exists! \left[Q_{ONSET} \rightarrow Q_{END}\right] : \left(\Delta Amp \left| Bt_{Qe} - Bt_{Qe-i} \right| \leq 2mm \; or \; TDQ_{O \rightarrow E} < 2 \; beats\right) \quad (3.8)$$

$$\exists! \left[S_{ONSET} \rightarrow S_{END}\right] : \left(\Delta Amp | Bt_{So} - Bt_{So+i} | \leq 2mm \; or \; TDS_{O \rightarrow E} < 3 \; beats\right) \quad (3.9)$$

3.3.2 Proposed Approach for Detecting P and T waves

As mentioned in Chapter 2 Section 2.4.2.2, most detector approaches of P and T waves found in the literature survey mainly depend on the time characteristics of the

QRS complex which are pre-detected by another detection approach. In this section a new high speed approach for delineating time characteristics of P and T waves (HSDPTW) has been proposed. The new approach includes two algorithms to delineate time locations (onset, peak, and end) of P and T waves, respectively. Both delineated algorithms scan the target ECG signal within the adaptive interval that can be identified relative to the time characteristics of the QRS complex which are pre-detected by another detector. In the following text, each algorithm is discussed in a single section in order to highlight the details for each algorithm separately.

3.3.2.1 Delineating the Time Characteristics of P wave

The P wave represents the depolarization of the atrial muscle in the HH. According to the small mass of atrial muscle, the P wave is represented as low voltage in the ECG diagram (Foster, 2007). In this section, a new algorithm for detecting the time characteristics of the P wave is proposed. Firstly, this algorithm takes the time characteristics of the QRS complex in the left side as a reference point to delineate the peak time location, and then use this location as a reference point to delineate the onset and the end time locations of the P wave. As, the delineation processes of the peak and the boundaries time locations are performed with a different processing technique, each one is discussed separately in the following sections.

3.3.2.1.1 Delineating the Peak Time location of P wave

The proposed approach to delineate the peak time location of the P wave includes four steps. The first step is a pre-processing unit that involves the process of extracting time characteristics of the QRS complexes using another detector. The

proposed QRS detector RFEM is considered for this issue. The second step allocates a small search segment in the left side of QRS complex in a limited period called the "search period", thus delineating the peak time location of the P wave which is limited within this period only. The start and end time limits of the search period are marked P_{start} and P_{end}, respectively as shown in Figure 3.8.a. However, the most difficult problem is to allocate these limits correctly.

In the P wave detection method, proposed by (Espiritu-Santo-Rincon & Carbajal-Fernandez, 2010), two search periods were suggested; the first was a narrow period and defined as *0.81*RR(i)-7 to Q(i)-18,* the second was the wide period and defined by *0.71*RR(i)-7 to Q(i)-18*. Additionally, another approach (Tan, Chan, & Choi, 2000) suggests a single search period which is limited by 0.1 to 0.3 s back from the QRS complex.

The PR interval, which was discussed in Chapter 2 Section 2.2.2, varies from 0.12 to 0.20 s (Azeem et al., 2005), and the number of ECG beats within the PR interval depends mainly on this time duration, as well as the frequency used in sampling the ECG signal as defined in Equation (3.10). A standard frequency used by most ECG machines to record the ECG signal is 25 Hz, but most ECG databases found online use a higher frequency for sampling to maintain the smallest details in the ECG record, for example the sampling frequency in QTDB is 250 Hz, and in the MIT-BIH arrhythmia database, it is 360 Hz. The proposed detection approach can be applied to any ECG records with a different sampling frequency.

$$No\ of\ ECG_{BEATS} = Time\ Interval\ (s) * Sampling\ Frequency\ (Hz) \qquad (3.10)$$

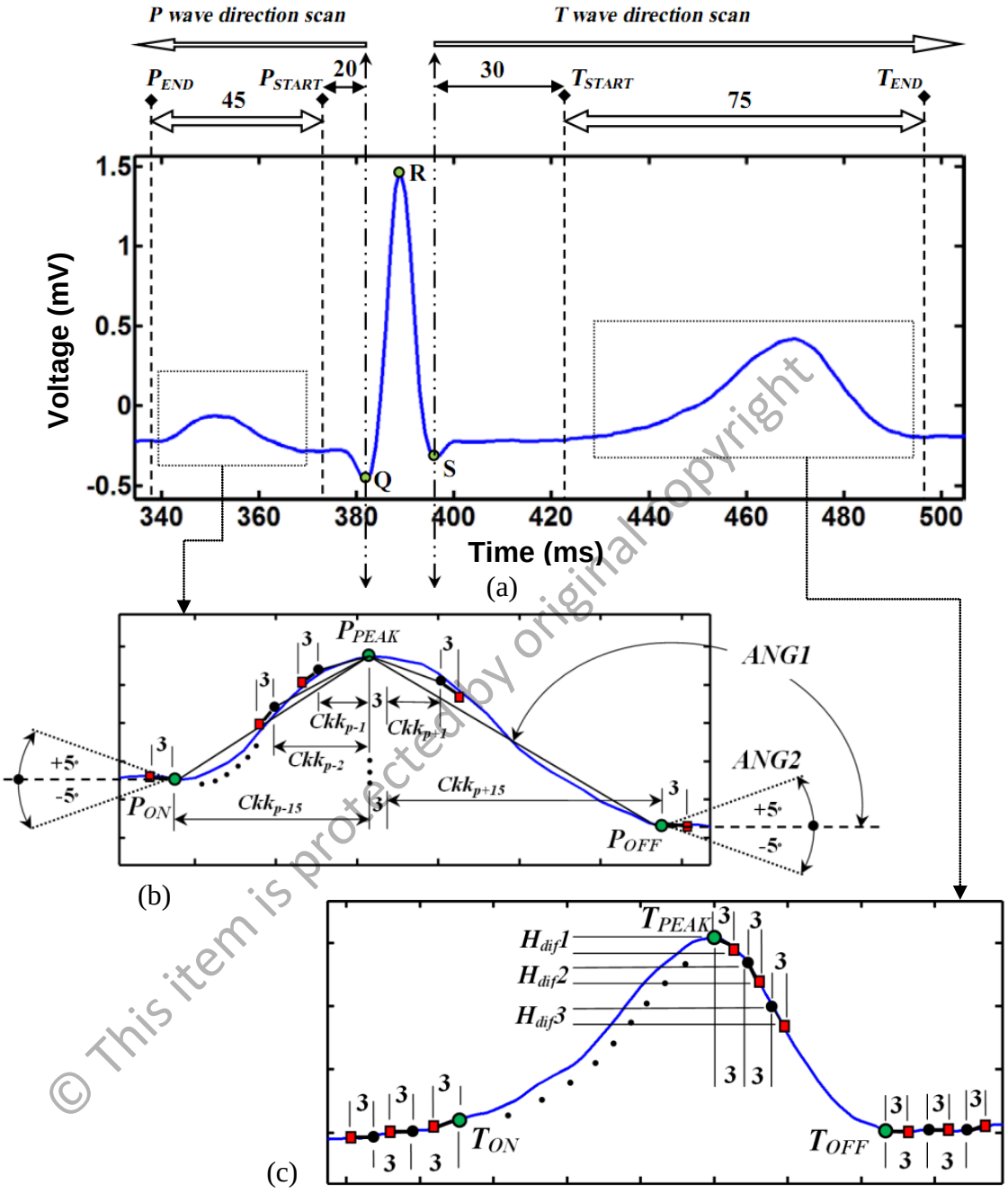

Figure 3.8: Graphical Representation of Proposed Approach for Detecting P and waves, (a) Search Period Limits Utilized by Proposed Algorithm for P and T Peak Delineation in Single ECG Record of Dataset "SEL307" From ST Change Category in QTDB, (b) P-wave Segment Marked with Angles and Intervals Utilized by PWONOFF Subroutine to Extract the Onset and the End time locations of P wave and (c) T-wave Segment Marked with Three Sequential Stairs Utilized by TWONOFF Subroutine to Extract the Onset and the End of T wave (|3| : time interval of three beats, H_{dif} : Height Difference (Δ amplitude) of |3|).

In most well known cardiology references, the normal duration of the P wave does not exceed 0.1 seconds, its amplitude does not exceed 0.25 mV, and its boundaries are 0.1 to 0.2 seconds relative to the QRS complex (Azeem et al., 2005; Gacek & Pedrycz, 2012). According to these parameters, the limits of the search period P_{start} and P_{end} must be 25 and 50 samples back from the beginning of the QRS complex. In the proposed approach, the search period is assumed to be wider as defined in Equation 3.11 and Equation 3.12. Therefore, the duration of this search period is 45 samples and started before 20 samples from the beginning of the QRS complex. The idea of enlarging the search period utilizes the process of detecting the P wave in every position even if any shifting to the right or left occurs due to any instant abnormality in the heart rhythm. As a result, the probability of detecting the P wave within the assumption search period is increased.

$$P_{START} = Q_{END} - 20 \tag{3.11}$$

$$P_{END} = P_{START} - 45 \tag{3.12}$$

The third step of the proposed approach performs the main job of delineating the peak time location of the P wave using a proposed algorithm to process the ECG beats along the search period which was allocated in the previous step. The proposed algorithm allocates peak position at the mutation point between the conditional rising and falling interval sequentially because the search direction of starts from P_{END} towards P_{START}. Algorithm III views all instruction codes for rising and falling conditions as well as the main iteration of the search operation. The peak time location delineated by the previous operation is reported as a primary peak. In some cases, different forms of concavity appear near the actual peak of the P wave in both sides that lead to an

incorrect peak time location point. The final step in this approach overcomes this problem by applying multi-scan iterations on both sides of the primary peak time location. The first iteration Frw_{index} scans a limited interval on the right side of three translation steps allocating the odd beats, while the second iteration Bak_{index} scans a same interval in the reverse direction but passes on the even beats. The graphical representation of the last correction operation is shown in Figure 3.9. Additionally, its instruction codes are mentioned in the second part of algorithm III and labelled (*/*Delineating correct peak time location of P wave */*).

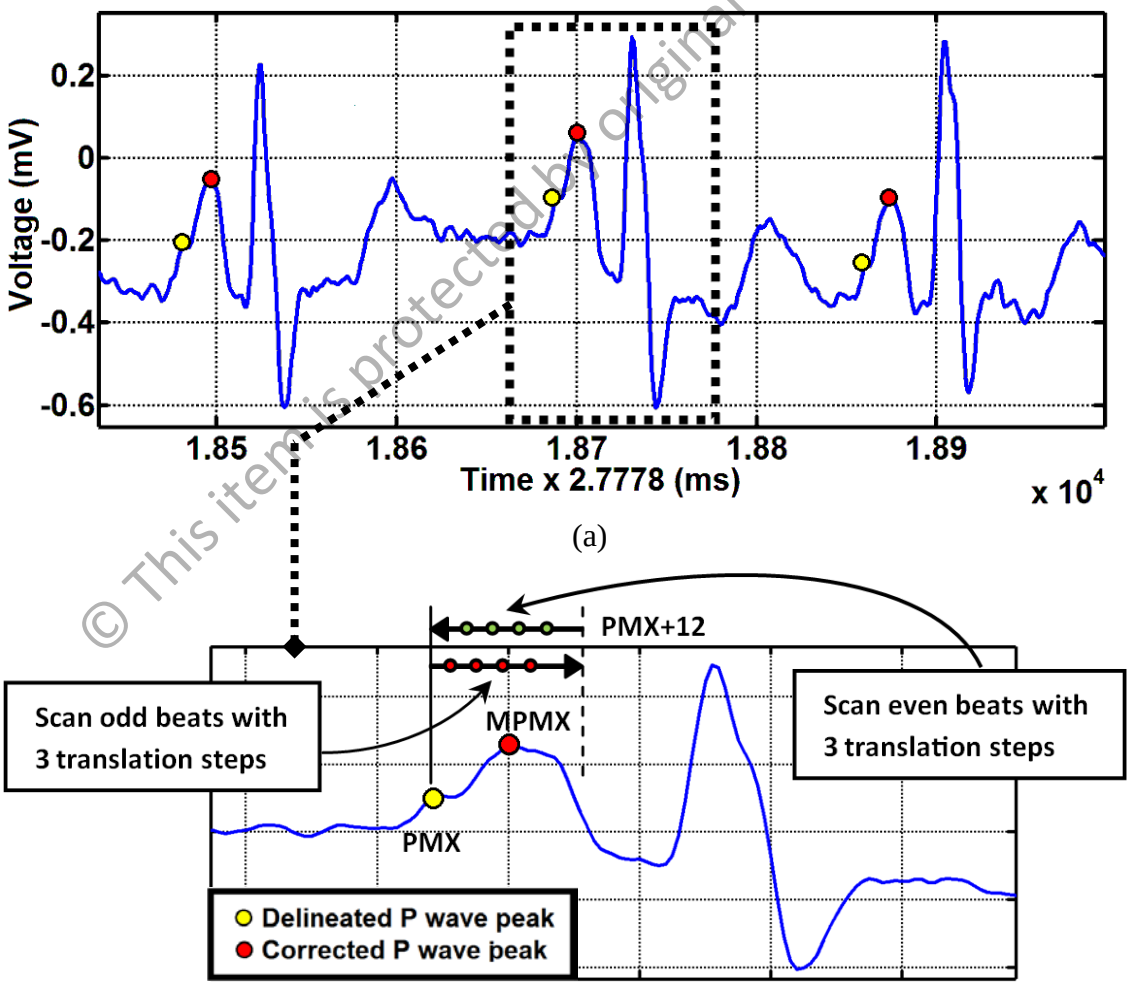

Figure 3.9: The Effect of Correcting the Delineated Primary Peak of the P Wave, (a) Three ECG Cycles of Dataset "SEL39" From the Sudden Death Category in QTDB; (b) Right/Left Scan Iteration.

Algorithm III Proposed Algorithm of Delineating Peak Time Location of P wave

```
BEGIN
  Read QRS=[QRS1,..,QRSN] /* N is total No. of pre-detected QRS complexes by RFEM*/

  for I=1 to N do
   QSTART = time(Q[ I ]); /* QSTART is a pre detected onset time location of Qwave by RFEM*/

   PEND = QSTART - 20 ; PSTART = PEND – 45;  /*PSTART and PEND are the start and end limits
                                               of P wave Peak search period */
   FLP=0;                 /*Status Flag*/
   PUP=0 ; PDW=0    /* PUP, PDW are counting of rising and falling interval in P wave */
   Wf=0;  PMX =0 ;    /*PMX is the primary time location of P-wave Peak*/

    /* Delineating primary peak time location of P wave */

   for KT = PEND to PSTART do
     if Xkt < Xkt-1 then PDW = PDW+ 1; FLP = 1; PUP = 0;
                    else   PUP = PUP + 1;
                      if (FLP equal 1 and PDW ≥ 10 and PUP ≥ 10) then
                                                                  PMX = Wf (Kt-1) ;
                                                                  PDW = 0;
                                                                  FLP  = 0;
                                                                  Break loop (KT);
                      endif
     endif
   end for      /* end of loop KT*/

    /* Delineating correct peak time location of P wave */
   MPMX  = PMX;
   for MP = PMX+2 to PMX+10 STEP +3 do
     if XMPMX ≤ XMP  then  MPMX = MP; endif
   end for

   for MP = MPMX downto MPMX-9 STEP -3 do
     if XMPMX ≤ XMP  then  MPMX = MP; endif
   end for

   PPeak [I] = MPMX;            /* Store corrected Peak time location of P wave (MPMX) in
                                  PPeak Matrix */
  end for /* end of loop I */

  Call PSON~OFF(MPMXi);   /* Call a subroutine for determining start PON and end POFF time
                             location of P-wave*/
END
```


The previous correction operation is the last part of the proposed approach to delineate the peak time location of the P wave. When it is finished, the process of

delineating the onset and end time locations of the P wave is started directly by calling a proposed subroutine named $PS_{ON\sim OFF}$ in the last part of algorithm III.

3.3.2.1.2 Delineating the Onset and the End Time Locations of P wave

In this section, a new algorithm to delineate the onset and end time locations of the P wave has been proposed. The new algorithm takes a form of a subroutine which is called by the main P wave peak delineation algorithm mentioned in the previous section. The new subroutine uses the peak time location of the P wave as a base to delineate the P wave boundaries (onset and end) time locations by applying two scan iterations beginning from the peak time location point towards the boundary points of the P wave period.

The first iteration (BG) scans the interval to the left of the P wave peak beat by beat, and two angles (ANG1 and ANG2) are determined continuously based on Equation (3.13) and Equation (3.14), respectively. This iteration continues until the determined angles match the condition mentioned in the $PS_{ON\sim OFF}$ subroutine. The P wave segment shown in Figure 3.8.b elucidates the based technique used to determine these angles. Both angles represent the convexity degree in the rising interval of the P wave. At the same time, the ANG2 represents the flatness degree at the end points in the same wave. The time location allocated by this iteration represents the onset time location of the P wave and is labelled P_{ON} in Figure 3.8.b.

$$ANG1 = 180^{\circ} - tan^{-1}\left[\frac{X_{BG} - X_{PEAK}}{Ckk}\right] \tag{3.13}$$

$$ANG2 = tan^{-1}\left[\frac{X_{BG} - X_{BG-2}}{3}\right] \tag{3.14}$$

where X_{PEAK}: Amplitude voltage (mV) of the pre-detected P_{PEAK}, X_{BG}, X_{BG-2}: Amplitude voltage (mV) of current and previous beat is separated by 3 time units, respectively, BG: 1st Iteration index of the interval on the left side of P_{PEAK}.

Through the same technique applied in the first iteration (BG), the second iteration (EF) scans the right interval of the P wave peak; however, the ANG1 and ANG2 are determined using different sets of equations, which are defined in Equation (3.15) and Equation (3.16), respectively. The time location allocated by this iteration represents the end time location of the P wave which is labelled with P_{OFF} in Figure 3.8.b. The ANG1 angle represents the angular obliquity between the line segment limited by the peak point (X_{PEAK}) and the test point in both iterations (X_{BG} and X_{EF}) with respect to the horizontal axis. Therefore, the determined ANG1 yields a pure obtuse angle, but it takes a different sign in both iterations because the arctangent angle computed by $(X_{BG}-X_{PEAK})/C_{KK}$ is allocated in the third quadrant and has a positive sign. On the other hand, the corresponding angle in second iteration computed by $(X_{EF}-X_{PEAK+3})/C_{KK}$ is allocated in the fourth quadrant and has a negative sign.

The final decision to delineate the P-wave onset and end time locations depends mainly on the determined ANG1 and ANG2 value in the boundary points of the P-wave. At the same time, it is very difficult to specify certain threshold values for these angles due to the variety of P-wave texture in various ECG categories, but an assumption value can be obtained by analyzing some ECG signals with different P waves' morphologies, and then taking the average limits for two angles on both sides. The overall instruction codes for the previous two iterations and all related calculations of delineating P_{ON} and P_{OFF} are illustrated in Algorithm IV.

$$ANG1 = 180^{\circ} + tan^{-1}\left[\frac{X_{EF} - X_{PEAK+3}}{Ckk}\right] \quad (3.15)$$

$$ANG2 = tan^{-1}\left[\frac{X_{EF+2} - X_{EF}}{3}\right] \quad (3.16)$$

where X_{PEAK+3}: Amplitude voltage (mV) of the ECG beat separated by 3 time units from the right of P_{PEAK}, X_{EF}, X_{EF+2}: Amplitude voltage (mV) of the current and next beat separated by 3 time units, respectively, EF: 2nd Iteration index of the interval in the left side of P_{PEAK}.

Algorithm IV $PS_{ON\sim OFF}$ Subroutine of Delineation Onset and End Time Locations in the P Wave

BEGIN

Ckk = 1; pw = 0; FLKP = 0;

for BG =MPMX **downto** MPMX-15 **do**

/* MPMX is the modified peak location after the correcting operation */

ANG1 = 180^o - $\tan^{-1}[(X_{BG} - X_{MPMX}) / Ckk]$;

ANG2 = $\tan^{-1}[(X_{BG} - X_{BG-2}) / 3]$;

if ANG1 $\leq 120^o$ **and** ANG1 $\geq 100^o$ **then** FLKP = 1; **endif**

if $|$ANG2$|$ $\geq$ 5 **then** pw = pw+1; **endif**

if pw > 3 **and** (FLKP **equal** 1) **then Break** loop(BG); **endif**

Ckk = Ckk+1 ;

end for /* end loop (BG) */

Ckk=1;

for EF =MPMX+3 **to** MPMX+15 **do**

ANG1=180^o + $\tan^{-1}[(X_{EF} - X_{MPMX+3}) / Ckk]$;

ANG2=$\tan^{-1}[(X_{EF+2} - X_{EF}) / 3]$;

if ANG1 $\leq 110^o$ **and** ANG1 $\geq 95^o$ **and** $|$ANG2$|$ $\geq$ 5 **then Break** loop(EF);

endif

Ckk = Ckk+1 ;

end for : */* end loop(EF) */*

P_{ON}[I] = BG; */* Store onset time location of P-wave P_{ON} (BG) Matrix at I index */*

P_{OFF}[I] =EF; */* Store end time location of P-wave P_{OFF} (EF) Matrix at I index */*

RETURN

3.3.2.2 Delineating the Time Characteristics of T wave

The T wave corresponds to ventricular repolarisation of the HH. Normally, it has the same direction as the predominant deflection of the QRS complex (Foster, 2007; Morris, Brady, & Camm, 2009). The normal shape of the T wave is in a positive direction and its amplitude must not exceed half the amplitude of the preceding QRS complex. The abnormalities of the T wave take three shapes, and each of these shapes is caused by certain/many cardiac disease(s) or some general diseases in the human body. The first abnormal shape is flat which is caused by Myocardial Ischemia, Hypothyroidism, and Pericarditis. The tall amplitude of the T wave is the second abnormal shape, which is caused by hyperkalemia as shown in Figure 3.6. Finally, the inverted T wave is the abnormal shape of the T wave which occurs most frequently and is caused by many cardiac diseases like Ventricular Hypertrophy, complete heart block, right bundle brunch block, etc (Azeem et al., 2005; Foster, 2007; Gacek & Pedrycz, 2012). At the same time, the T wave is normally inverted in aVR and V1 lead, and sometimes in III, V2, and V3 leads in some black people (Hampton, 2008).

According to the different shapes of the T wave mentioned above, it is very difficult to detect this wave with a single algorithm (Espiritu-Santo-Rincon & Carbajal-Fernandez, 2010). A new approach for detecting the T wave with different shapes has been proposed in this section. Like the P wave detector which was mentioned in the previous section, the proposed T wave detector includes a main algorithm to delineate peak time location of the T wave, and then calling a small subroutine to delineate boundaries time locations based on the delineated peak time location. Each part of the proposed T wave detector is discussed separately in the following sections in order to highlight each in more detail.

3.3.2.2.1 Delineating the Peak Time Location of T wave

As happen with the P wave detection approach, the first process is delineating the peak time location, which is considered as reference point to delineate other boundaries of the T wave (onset and end). A new approach of delineating the peak time location of the T wave has been proposed in this section based on the same strategy that was used in the P wave peak delineation algorithm mentioned in the previous section, except that the search period is allocated on the right side of the QRS complex.

Through the basic concepts of the ECG signal that are found in most well known cardiology references, the normal period of the QT interval is 0.44 seconds (Azeem et al., 2005; Foster, 2007; Gacek & Pedrycz, 2012; Gupta, Mitra, & Bera, 2013). As a result, the total number of ECG samples obtained by Equation (3.10) along the QT interval is 110 beats, and each T wave must start and end within these beats.

In the proposed algorithm, the T wave search period is assumed to be 75 ECG beats according to Equation (3.17) and (3.18).

$$T_{START} = S_{START} + 30 \tag{3.17}$$

$$T_{END} = T_{START} + 75 \tag{3.18}$$

The T_{START} and T_{END} represent the lower and the upper limits of the search period, respectively. It is different from that of the S wave which has 30 ECG samples as shown in Figure 3.8.a. Therefore, the entire search period takes 105 ECG samples in addition to the normal duration of the QRS complex defined in most cardiology references (20 - 25 ECG samples).

According to the previous calculation, the assumed QT interval from the onset of the QRS complex to the end of the search period is 125 to 130 ECG samples, which is wider than the normal QT interval by 15 to 20 ECG samples. This wider range of the QT interval utilizes the ability to detect the T wave period, even those with a long duration and those that shift to the right or left due to any disturbance in the performance of the HH.

The same pre-processing step of detecting QRS time characteristics in P wave peak delineation approach is applied in the proposed approach to delineate the peak time location in the T wave. Moreover, the second step focuses on determining the lower limit T_{START} and upper limit T_{END} of the search period according the definition in Equation (3.17) and (3.18) based on the S wave time characteristics that are predefined in the pre-processing step. The third and final step in this approach performs the delineating of the peak time location of the T wave using a new algorithm that allocates peak time location when the ECG signal within the search period is mutated from the falling edge to the rising edge for negative T wave or vice versa for the positive T wave. The number of ECG samples within the first interval in both cases is determined by separate counters termed C_{UP} and C_{DOWN}, respectively. The decision about the peak event occurs when the counter value C_{UP} or C_{DOWN} exceeds 15 ECG samples (less than the half of the search period limited by T_{START} and T_{END}) to consider the tipping event as a peak time location in the T wave which is labelled T_{PEAK}.

The instruction codes for the previous three steps are illustrated in Algorithm V. As another decision about the direction of T wave is computed in this algorithm, the total number of normal and inverted T waves along the ECG signal can be easily determined.

Algorithm V Proposed Algorithm of Delineating Peak Time Location of T wave

BEGIN

Read QRS = [$Q_1R_1S_1$,…,$Q_NR_NS_N$] */* N is total No. of QRS complexes which are pre-detected by RFEM */*

for I=1 **to** N **do**

S_{END} = time (S[I]); */* S_{END} is the end time location of S wave pre- detected by RFEM */*

T_{START}= S_{END} + 30; T_{END}= T_{START} + 75; */*T_{START} and T_{END} are the start and stop time of T wave peak search period*/*

FLT=0; */*Status Flag of interval direction1 for rising, 2 for falling*/*

C_{UP}=0 ; C_{DW}=0 */* C_{UP} , C_{DW} are counting of rising and falling interval in T wave */*

TUP=0; TDW=0; */* TUP,TDW are event counting of Up and Down direction in T- wave */*

TMX = 0 ; */* TMX is the time location of T-wave Peak */*

/ Delineating peak time location of T wave */*

for KT = T_{START} **to** T_{END} **do**

if $X_{kt} \geq X_{kt-1}$ **then** C_{UP}= C_{UP} + 1;

if ((FLT **equal** 2) **and** C_{DW}>15**) then** TMX = kt; TDW=TDW+1;

Break loop(KT);

end if

FLT = 1; C_{DW} = 0;

else

C_{DW}=C_{DW}+1;

if ((FLT **equal** 1) **and** C_{UP}>15**) then** TMX = kt; TUP = TUP+1;

Break loop(KT);

end if

FLT = 2; C_{UP} = 0;

end if

end for */* end of loop KT*/*

T_{PEAK}[I] ← TMX; */* Store Peak time location of T-wave (TMX) in T_{PEAK} Matrix */*

Call $TS_{ON\sim OFF}$(TMX_i) */* Call $TS_{ON\sim OFF}$ subroutine for determining onset T_{ON} and end T_{OFF} time location of T-wave*/*

END

3.3.2.2.2 Delineating the Onset and the End Time Locations of T wave

In addition to the peak time location of the T wave delineated in the previous section, there are two time characteristics which are represented by the boundaries (onset and end) time locations of the same wave. The T wave has taller amplitude and a wider duration compared with the P wave in most ECG signal categories.

In this section, a new approach to delineate the onset and the end time locations of the T wave has been proposed. The new approach maximizes the fact that the T wave constructs a semi-orthogonal angle with the ECG baseline at the end events of the T wave. The new approach considers this fact as the main criterion to delineate the boundaries time locations of the T wave.

The new algorithm takes the form of a subroutine termed $TS_{ON\sim OFF}$, which is called by the main T wave peak delineation algorithm mentioned in the previous section. As in the P wave algorithm, the $TS_{ON\sim OFF}$ subroutine uses the T_{PEAK} time location as a base point to delineate the boundaries of the T wave (onset and end) time locations by applying two scan iterations (TN and TD) starting from the T_{PEAK} time location point to the endpoints of the T wave period as shown in categories of the T wave segment in Figure 3.8.c. Each of these iterations is repeated up to 30 ECG samples. Therefore, the maximum duration for the detected T wave which is limited between the onset and the end time locations is 60 from 75 ECG samples, which is assumed to be the period for the T wave. Only one amplitude segment named H_{dif} is determined in both iterations as the difference between two successive ECG beats isolated by three time locations. The delineation decision of the onset and the end time locations is taken according the occurrence of three sequential segments with the smallest H_{dif}, which demonstrates the behaviour of the ECG signal at the endpoints of the T wave. This decision is more effective in delineating the end time location of the T

wave but not as effective in delineating the onset time location, especially when the starting segment of the T wave is merged with the previous S wave (i.e. takes the same slope). All instruction codes for the proposed subroutine to delineate the onset and end time locations of the T wave are illustrated in Algorithm VI. In addition, the resulting onset and end time locations of the T wave are labelled T_{ON} and T_{OFF}, respectively in the T wave segment shown in Figure 3.8.c.

Algorithm VI $TS_{ON\sim OFF}$ Subroutine of Delineation Onset and End Time Locations in the T wave

```
BEGIN

  Ckk = 1;
  for TN =TMX+3 to TMX+30: STEP 3  do
    Hdif =Δamplitude( XTN+2 -  XTN);  /* Amplitude difference between current beat XTN and
                                         next beat spaced by three  time units XTN+2  */
    if │ Hdif │< 0.001 then  Ckk  =  Ckk+1;
                        if Ckk ≥ 3  then Break loop(TN);   /* Decision for TOFF when
                                                              three continuous semi flat segment are verified */
                        endif
    endif
  end for  /* end loop (TN) */

  Ckk=1;
  for TD =TMX-3 to TMX-30: STEP -3  do
    Hdif =Δamplitude( XTD-2 -  XTD);   /* amplitude difference between previous beat spaced
                                          by three time units XTD-2  and  current beat XTD */
    if │ Hdif │< 0.015 then  Ckk  =  Ckk+1;
                        if  Ckk  ≥ 3  then Break loop (TD);  /* Decision for TON when
                                                                three continuous semi flat segment verified */
                        endif
    endif
  end for  /* end loop (TD) */

  TON[ I ] = TD+9;   /* Store time location of T-wave ON (TD+9) in TON Matrix */
  TOFF[ I ] = TN-9;   /* Store time of T-wave OFF (TN-9) in TOFF Matrix */

RETURN
```

In the previous sections, two approaches have been proposed to delineate time characteristics (onset, peak, and end) time locations of P and T waves in the ECG signal. The general block diagram of these approaches is shown in Figure 3.10.

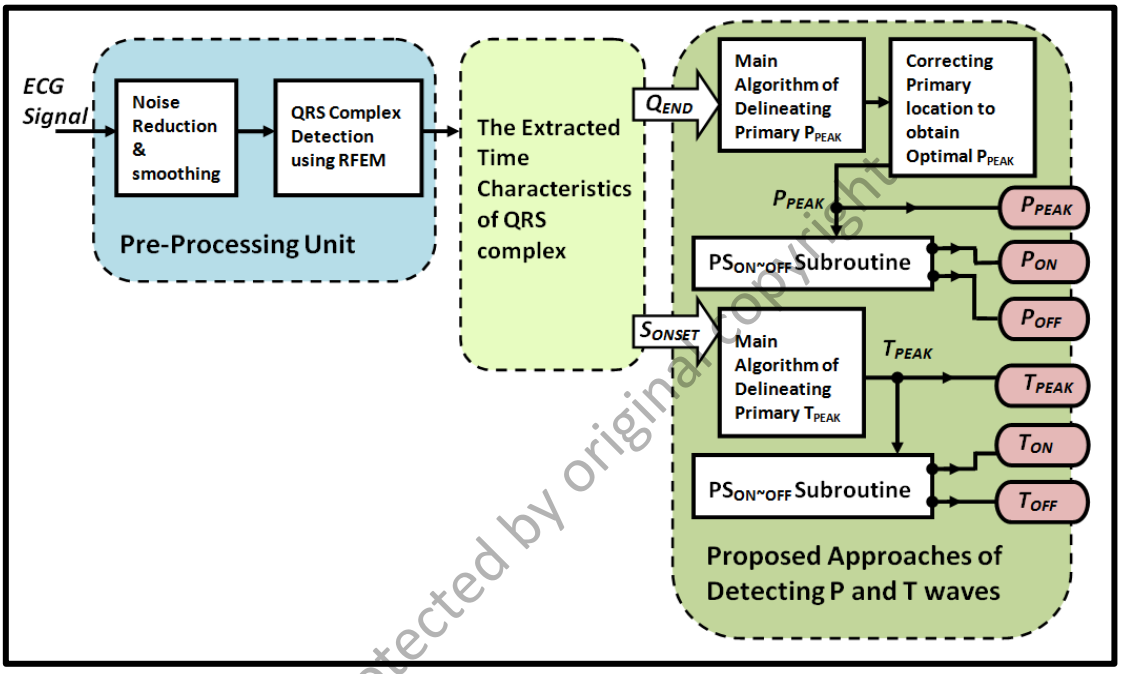

Figure 3.10: General Block Diagram of Proposed Approaches to Delineate the Onset, Peak, and End Time Locations of P and T Waves in the ECG Signal.

3.4 Diagnosing High Risk Cardiac Diseases

As mentioned in Chapter 2 Section 2.5, most studies found in literature that deal with the diagnosis of high risk cardiac diseases take the form of statistical studies. On the other hand, several methods proposed in literature use the computerized system tools for the purpose of diagnosing cardiac diseases based on a 12 lead ECG signal (A. Ebrahimzadeh, Shakiba, & Khazaee, 2014). In the following text, the standard diagnostic criteria for diagnosing LVH cardiac disease are highlighted in more detail,

and an intelligent computerized system of diagnosing LVH cardiac disease based on new diagnostic criterion is proposed.

3.4.1 Diagnosing Left Ventricular Hypotrophy

As mentioned in Chapter 2 Section 2.5.1, LVH cardiac disease is one of the high risk cardiac diseases that causes SCD, and electrocardiographic evidence of LVH is a major indicator of cardiovascular morbidity and transience around the world (Levy et al., 1990). In LVH cardiac disease, the muscle mass of the left ventricle increases. This leads the main vector of ventricular depolarization more toward the left ventricle and enlarges its magnitude. As a result, the R wave in the lateral precordial leads (V5 and V6) becomes longer, the S wave in V1 becomes deeper, and the amplitude of the R wave in Lead (I or aVL). Figure 3.11 shows the 12 lead ECG record of a man with longstanding severe hypertension and LVH (Foster, 2007).

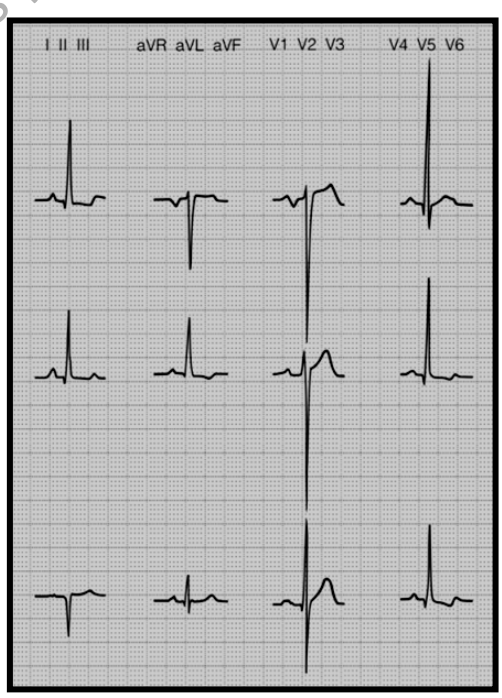

Figure 3.11: A 12-lead ECG Record of a 38-year-old Man with Long-Standing Severe Hypertension and LVH (Foster, 2007).

Preparing an accurate and early diagnosis of LVH is a significant issue in the care of patients with hypertension (Pewsner et al., 2007). The process of diagnosing LVH from a 12-lead ECG depends mainly on several voltage and duration criteria related to each single lead with respect to another. The standard diagnostic criteria for diagnosing LVH cardiac disease based on ECG parameters are highlighted in more detail in the next section.

3.4.1.1 Standard Diagnostic Criteria for LVH Cardiac Disease

In general, the diagnostic criteria of LVH can be classified as either voltage or non-voltage criteria (Morris et al., 2009). Many criteria for diagnosing LVH have been proposed in literature. These diagnostic criteria are obtained by certain parameters in a 12-lead ECG signal, many of them have remained anecdotal (Pewsner et al., 2007). On the other hand, there are some criteria that are commonly used to diagnose LVH, which are more suitable for computerized ECG (Casale, Devereux, Alonso, Campo, & Kligfield, 1987). Typically, high specifications are verified by these criteria (greater than 90%), while the sensitivities are low (20%-60%) (Devereux, Casale, Eisenberg, Miller, & Kligfield, 1984; Reichek & Devereux, 1981).

The first standard criterion for diagnosing LVH was proposed in an early study and is usually referenced as "Sokolow-Lyon". This criterion uses the uni-polar limb and precordial leads to detect the atypical and early patterns of LVH (Sokolow & Lyon, 1949). Another criterion used for diagnosing LVH was the "Cornell voltage" (Casale et al., 1985). This criterion takes two different forms of conditions to detect LVH in men and women, respectively. In (Molloy, Okin, Devereux, & Kligfield, 1992), a modified criterion based on the Cornell voltage product was developed and analyzed. Another

diagnostic criterion was proposed in an old study (GUBNER & UNGERLEIDER, 1943) termed the "Gubner criteria". A different approach is called "Romhilt-Estes scores" and diagnoses LVH using a point score system of multi-criteria (Romhilt & Estes Jr, 1968). The descriptions of the standard criteria for diagnosing LVH cardiac disease are illustrated in Table 3.1. Most of these criteria are considered in proposed diagnostic criterion for diagnosing LVH cardiac disease which is discussed in the next section.

Table 3.1: Standard Diagnostic Criteria of LVH Cardiac Disease (M:Male, F:Female)

#	Criterion Name	Description		Gender
1	Sokolow-Lyon	S(V1) + R(V5 or V6) > 3.5 mV		M and F
2	Cornell voltage	R(aVL) + S(V3) > 2.8 mV		M
		R(aVL) + S(V3) > 2.0 mV		F
3	Cornell product	(S(V3) + R(aVL)) × QRS duration ≥ 2440 ms		M
		(SV3+(RaVL+8 mV)) × QRS duration>2440 ms		F
4	Gubner	RI+SIII≥25 mV		M and F
5	Romhilt-Estes scores	Max(R or S (Limb Leads)) ≥ 20	3	M and F
		S(V1) or S(V2) ≥ 30	3	
		R(V5) or R(V6) ≥ 30	3	
		ST and T wave changes opposite to mean QRS	3	
		ST and T wave changes opposite to mean QRS	3	
		Left atrial involvement	3	

In addition to the standard diagnostic criteria mentioned above, other diagnostic criteria for LVH cardiac disease have been reported by various well known clinical websites. Most of these criteria show the limited accuracy of diagnosing LVH cardiac disease. This low rate of accuracy comes from the wrong diagnosis of LVH cardiac disease, especially in young people (aged <40 years), where the tall R wave and deep S wave are present in ECG leads in the absence of LVH cardiac disease. The additional criteria for diagnosing LVH cardiac disease are illustrated in Table 3.2.

Table 3.2 : Additional Diagnostic Criteria of LVH Cardiac Disease

#	Abbreviation	Description
1	CRTA1	R(aVL)>13mm
2	CRTA2	R(I)+S(III)>25mm
3	CRTA3	R(aVF)>20mm
4	CRTA4	S(aVR)>14mm
5	CRTA5	R(V4 or V5 or V6)>25mm
6	CRTA6	S(V1 or V2) + R(V5 or V6) >35mm
7	Recommended Criterion (REC-CRTA)	S(III) + Max(R,S(V1-V6)) >30 or R(aVL) >13mm

3.4.1.2 Proposed Criterion for Diagnosing LVH Cardiac Disease

In this section, a new criterion of diagnosing LVH cardiac disease has been proposed. The new criterion addresses the problems of previous diagnostic criteria in making an accurate diagnosis in terms of sensitivity and specificity. In contrast to the present diagnostic criteria found in literature, the new criterion considers eight voltages from eight ECG leads to compute the final diagnosis of LVH cardiac disease. The voltage parameters considered in new criterion are split into two groups; the first group includes the R wave amplitude in leads V4, V5, V6, and aVF. The second group includes the S wave amplitude in leads V1, V2, V3, and III. The idea of selecting eight ECG voltage parameters comes from maximizing the area to detect irregularities in all ECG categories (limb [standard, augmented] and precordial) leads. In the new diagnostic criterion, there is a polynomial equation defined in Equation (3.19) which is proposed to compute the main decision value (MDV) for diagnosing LVH cardiac disease. With respect to the chest leads in this equation, the left ventricular leads are most common due to their location on the left of the transitional zone in the HH to assess hypotrophy in the left ventricle (Gacek & Pedrycz, 2012). Thus, only left ventricular leads V5 - V6 (which are placed above the lateral wall of the left ventricle) are considered to have full voltage (weight=1) in the MDV equation, whereas the right

ventricular leads V1 - V2 and V3 - V4 (which are placed between the ventricles and the anterior wall of the left ventricle) are considered to have half voltage (weight=0.5) in the MDV equation. In addition to the chest leads, two of the limb leads (III and aVL) are considered in the same equation because these leads are mostly used in traditional LVH diagnostic criteria. The computed MDV values for the LVH patients are high compared with the normal or non-LVH patients; however, in a few cases, the computed MDV value is high in the absence of LVH cardiac disease. This drawback is solved logically in the final decision of the proposed criterion by successive logical expressions with some traditional diagnostic criteria.

$$MDV = 0.5R(V4) + R(V5) + R(V6) + 0.5R(aVF) + 0.5S(V1) + 0.5S(V2) + 0.5S(V3) + S(III) \quad (3.19)$$

In addition to the MDV equation, the proposed criterion for diagnosing LVH cardiac disease includes three logical expressions. The first expression (Expr1) defined in Equation (3.20) is true according to the verification of either the Cornell or the recommended criterion (REC-CRTA), whereas the second expression (Expr2) defined in Equation (3.21) is verified when the *Sokolow* and the *Cornell* criteria are true and at least five of six criteria (CRTA1...6) are true. The last expression defined in Equation (3.22) represents the main decision for diagnosing LVH cardiac disease based on MDV, Expr1, and Expr2, which were obtained previously.

$$\exists[Expr1]: Cornell\ is\ true\ \boldsymbol{OR}\ REC-CRTA\ is\ true \quad (3.20)$$

$$\exists[Expr2]: \left(Cornell\ \ \textbf{AND}\ Skolow\ \textbf{AND}\ \sum_{i=1}^{6} TRUE(CRTA_i) \geq 5\right) \quad (3.21)$$

$$\exists! \, [LVH_{C.D}]: \left(([MDV_F > 75 \textbf{ OR } MDV_M \geq 105] \textbf{ AND } Expr1) \textbf{ OR } Expr2 \right) \qquad (3.22)$$

In the main expression defined in Equation (3.22), there are two different threshold levels of MDV for each gender. The threshold levels are computed statistically by analyzing a 12-lead ECG record of some patients who suffered from LVH and others with other cardiac diseases. A few normal patients are also considered for this test. The statistical results show that the suitable limit of MDV is 75 for females and 105 for males. However, some results satisfied the MDV limits in the absence of the LVH cardiac disease which leads to an incorrect diagnosis. Therefore Expr1 and Expr2 are added in the main diagnostic expression to overcome this drawback and to perform an accurate diagnosis of LVH cardiac disease.

3.4.1.3 ECG Voltage Parameters for Proposed Diagnostic Criterion

The overall voltage parameters required for the proposed criterion are eleven voltages which are obtained from the 12-lead ECG signal. The voltage parameters include the R wave amplitudes of I, aVL, aVF, V4, V5, and V6 leads and the S wave amplitudes of III, aVR, V1, V2, and V3 leads. These voltages are determined directly using the time characteristics of the QRS complex. The proposed detection approach termed "RFEM" for QRS complex detection mentioned in Section 3.4.1 is considered to determine these characteristics. Because the RFEM approach, like other QRS detectors, works with ECG data in digital form, any ECG record available as a paper printout recording must be converted first. The other proposed approach for digital recovery mentioned in Section 3.2.2.1 is considered to reconstruct raw 12 lead ECG data from the printed ECG chart.

3.4.1.4 Proposed FIS for Diagnosing LVH Cardiac Disease

In general, fuzzy inference is the process of formulating the mapping from a given input to an output using fuzzy logic. The mapping then provides a basis from which decisions can be made, or patterns discerned (Sumathi & Paneerselvam, 2010). The FISs are recently more familiar tools for solving engineering problems because of their unique features in computing complex phenomena. A fuzzy system is a non-linear mapping between inputs and outputs, in which the mapping of inputs to outputs is in part characterized by a set of ‘‘IF-THEN’’ rules. A typical fuzzy logic-based approach involves three main units: fuzzification unit, inference engine, and defuzzification unit as shown in Figure 3.12.

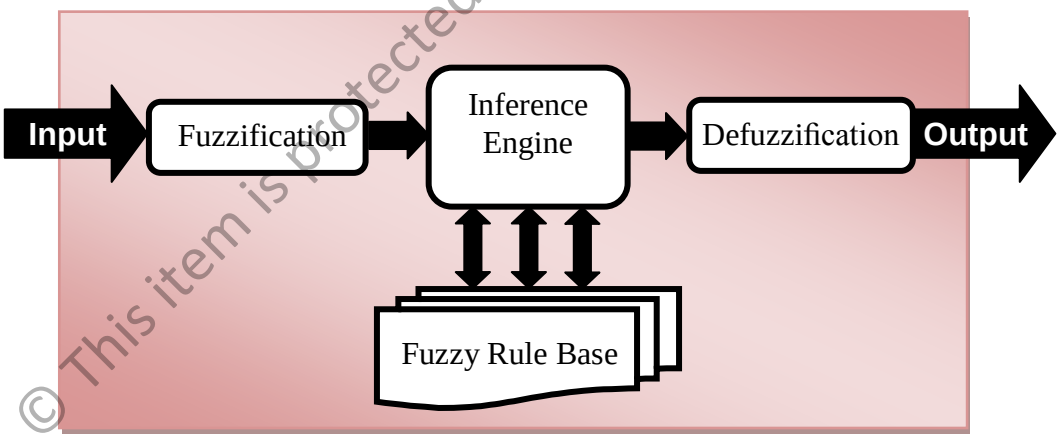

Figure 3.12: Expert FIS System Model (Sivanandam et al., 2007; Sumathi & Paneerselvam, 2010).

As with most traditional criteria used for diagnosing LVH cardiac disease, the computational equation of the proposed diagnostic criterion takes a conditional form. In reality, the final decision about diagnosing LVH is verified according the logical value of four conditions which are defined in Equation (3.22). Therefore, this logical structure

can be represented easily with a FIS according to the basic concepts of mapping rules used in FIS.

In this section, a new FIS for diagnosing LVH cardiac disease has been proposed. The proposed FIS is constructed using fuzzy Mamdani method; in addition, it has seven input membership functions (MFs) which are determined mathematically by analyzing the logical expressions of diagnostic criteria that are defined in Equation (3.19), Equation (3.20), and Equation (3.21) to convert them into simple conditioning statements that can be easily expressed by FIS as the MFs. These MFs are used by 6 fuzzy rules to obtain the decision values of three output MFs (Expr1, Expr2, and MDV) that construct the main parameters in the final diagnosis of LVH cardiac disease defined in Equation (3.22). The general diagram of the proposed FIS is shown in Figure 3.13 as it is viewed by MATLAB environments. Four input MFs are designed to simulate Sokolow-Lyon, Cornell voltage, CRTA1, and REC-CRTA diagnostic criteria. Additionally, the true occurrence of CRTA1 to CRTA6 diagnostic criteria is expressed by another input MF. The graphical diagrams of these MFs are shown in Figure 3.14.a-e, respectively. The sixth input MF is designed to evaluate the MDV value defined in Equation (3.22). This MF is composed internally of two sub-MFs. The first MF is termed MDV-Female to compute the MDV criterion for females with respect to the designated threshold of the LVH diagnosis (75). The second MF is termed MDV-Male to compute the same criterion for males with respect to a determined threshold of the LVH diagnosing (105). The graphical diagram of the two sub-MFs is shown in Figure 3.14.f. The last input criterion is termed Gender-CRT to specify the gender of the tested patient as shown in Figure 3.14.g.

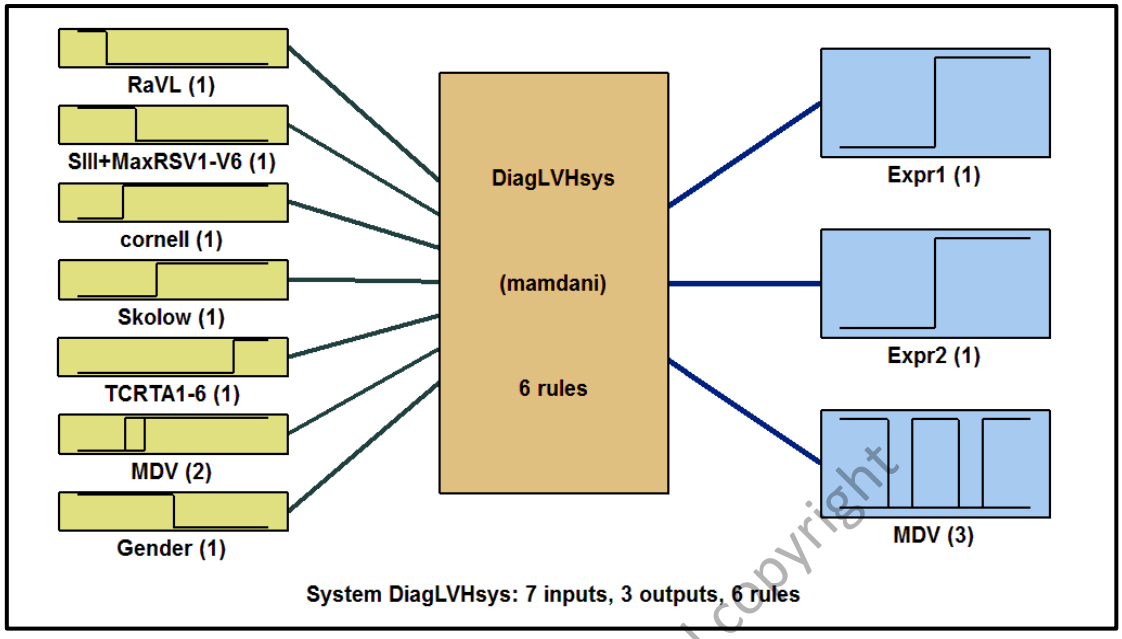

Figure 3.13: The Proposed FIS for Diagnosing LVH Cardiac Disease.

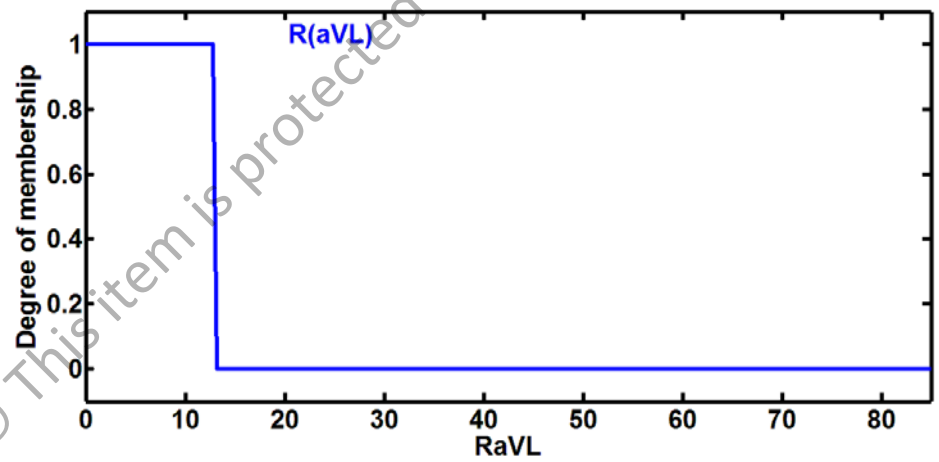

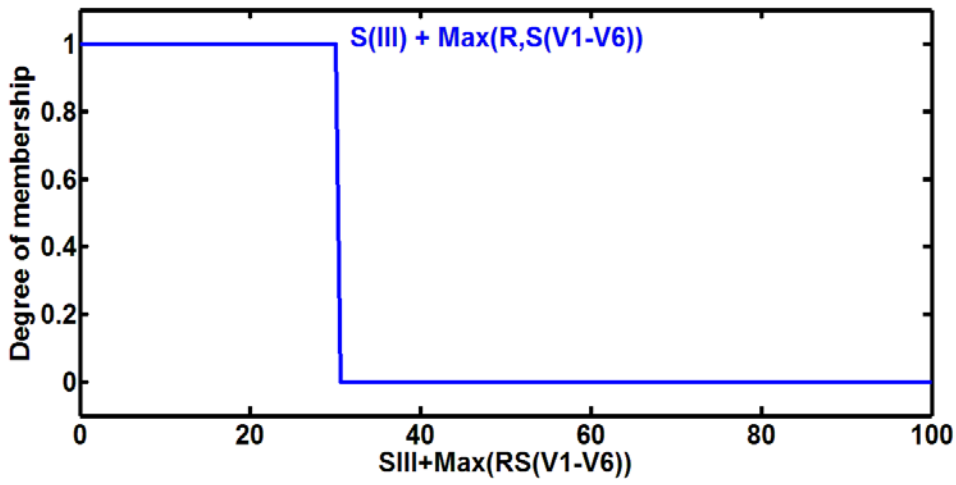

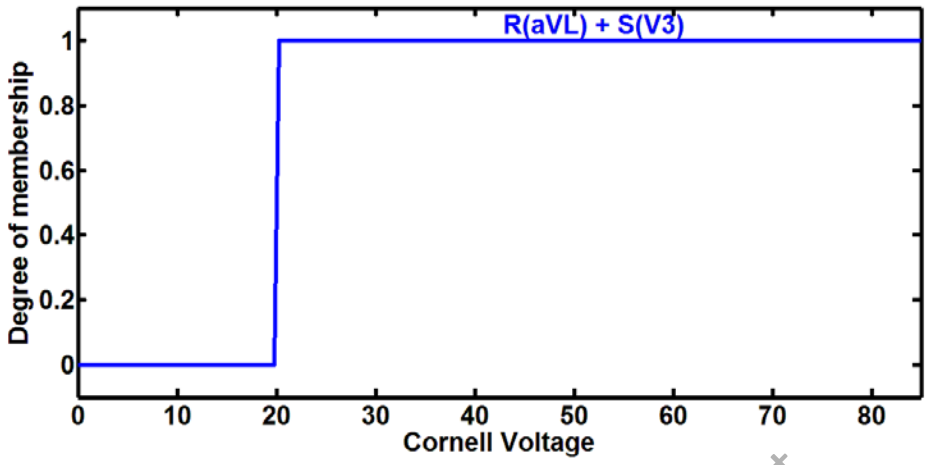

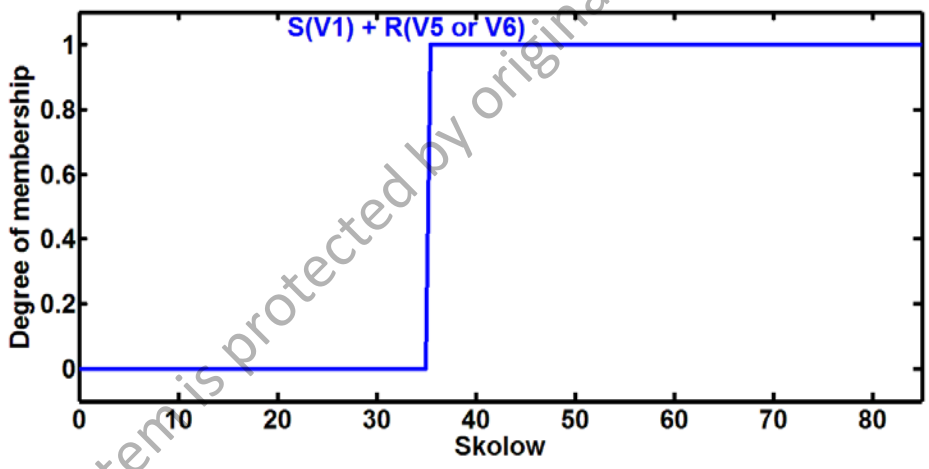

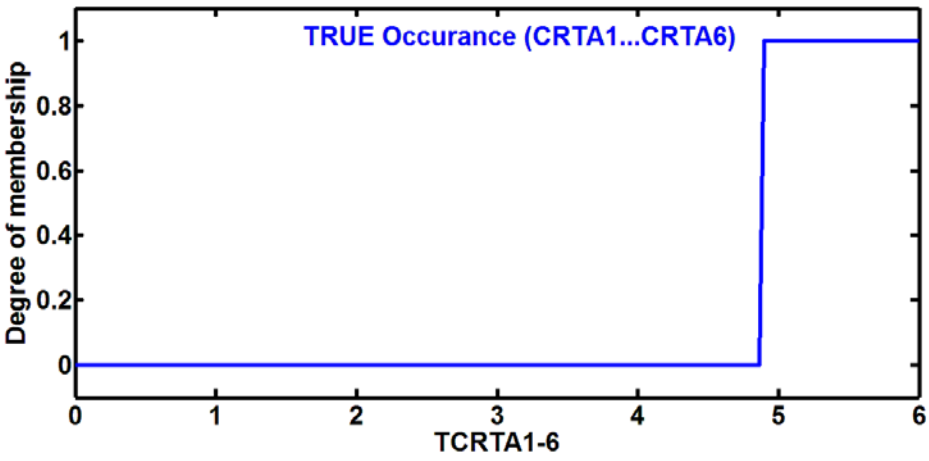

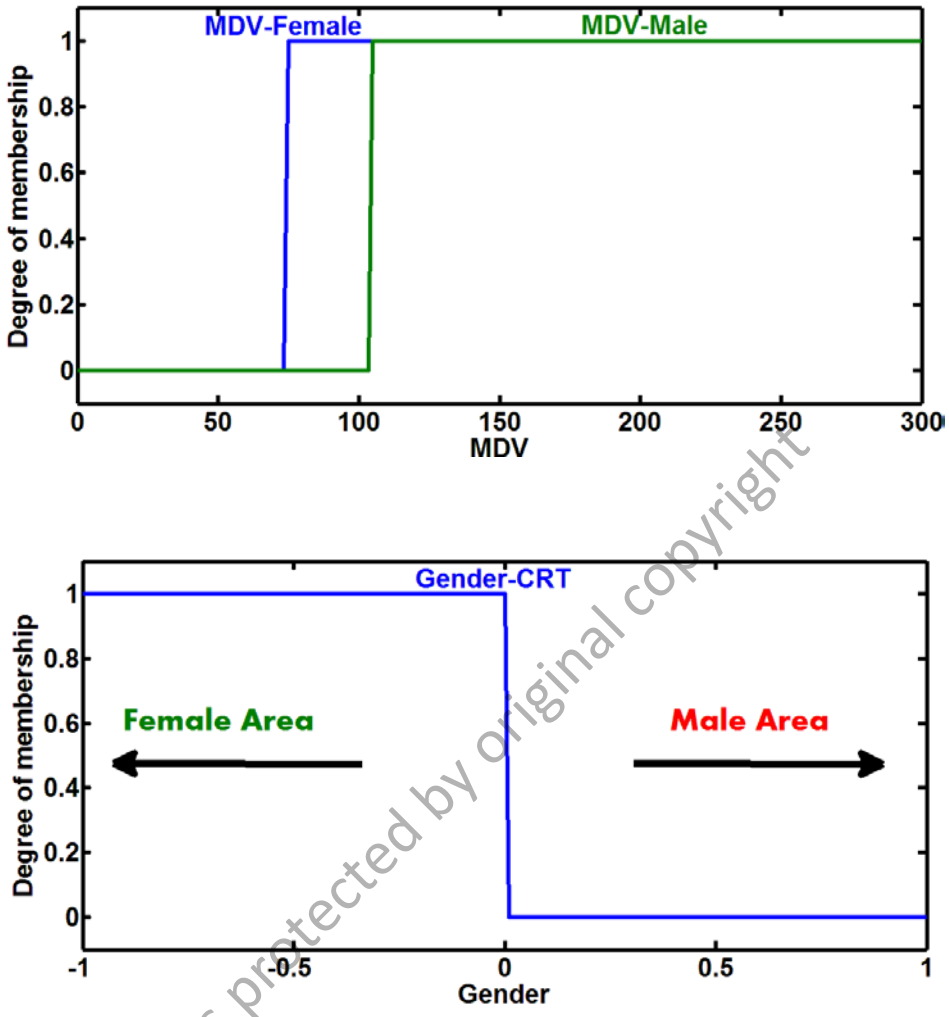

Figure 3.14: Graphical Diagrams of the Input MFs in Proposed FIS.

In general, fuzzification is the process of changing a real scalar value into a fuzzy value. This is performed with three types of fuzzifiers (Gaussian, singleton, and trapezoidal or triangular). All mathematical statements in the proposed diagnostic criterion defined in Equation (3.22) take the form of a single logical condition (greater than or less than the fixed threshold). The trapezoidal fuzzifier includes four scalar parameters (a, b, c, and d) (Hanss, 2005; Sumathi & Paneerselvam, 2010). The membership definition for a trapezoidal fuzzifier is defined in Equation (3.23). From this definition, there are five classification regions, while the logical condition requires

two classification regions. Thus, a small change must be applied on the original trapezoidal fuzzifier to convert it to handle two classification regions instead of five. To do this, a and b parameters are assigned to the fixed threshold level, while c and d take the upper limit for the input parameter. Consequentially, all logical statements in proposed diagnostic criterion are expressed with input MF using a modified trapezoidal fuzzifier.

$$F(x) = \begin{cases} 0, & if\ x \leq a \\ \frac{x-a}{b-a}, & if\ x \in [a,b] \\ 1, & if\ x \in [b,c] \\ \frac{d-x}{d-c}, & if\ x \in [c,d] \\ 0, & if\ x \geq d \end{cases} \quad (3.23)$$

The final decision of LVH cardiac disease diagnosis in the proposed FIS is made by three MFs. These MFs compute the value of Expr1, Expr2, and MDV which are defined in Equation (3.20), (3.21), and (3.22), respectively. The output MFs are obtained by six fuzzy rules in such a manner that each MF is verified when the diagnostic criteria found in the input MF within its rule are true. The first and second output MFs include single sub-MF as shown in Figure 3.15.a-b, respectively. The third output MF handles three sub-MFs. The first is termed MDV-Fe-LVH and verifies when the input MF MDV-Female is true and the value of Gender-CRT is in the female area. Similarly, the second sub-MF is termed as (MDV-Ma-LVH) and verifies when the MF MDV-Male is true, and Gender-CRT is in the male area, while the third sub-MF is termed MDV-Normal and verifies when the first MFs are false. The graphical diagram of the third output MF is shown in Figure 3.15.c.

In general, the defuzzification process represents the final step in each fuzzy system which is performed by aggregating the resulting value for all output MFs. In

proposed FIS, the final decision about LVH cardiac disease diagnosis represents the deffuzfication process by aggregating a resultant value for the three output MFs (Expr1, Expr2, and MDV) using the fuzzy rules related to each one. The defuzzification method used is centroid, which computes the defuzzified value at a very fast rate, as well as being able to produce very accurate results (Sumathi & Paneerselvam, 2010). The centroid method returns the centre of area under the curve. The active interval in Expr1 and Expr2 is [0, 1] as shown in Figure 3.15.a-b, respectively, thus the aggregated value using the centroid defuzzification method is 0.5. However, in MDV there are two active intervals [0, 1] and [3, 4], and the aggregated value using the same defuzzification method is 0.5 or 3.5, respectively.

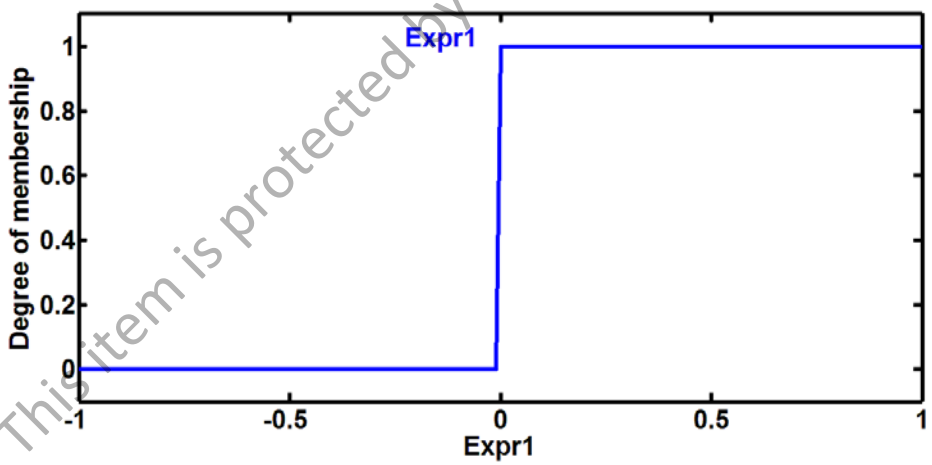

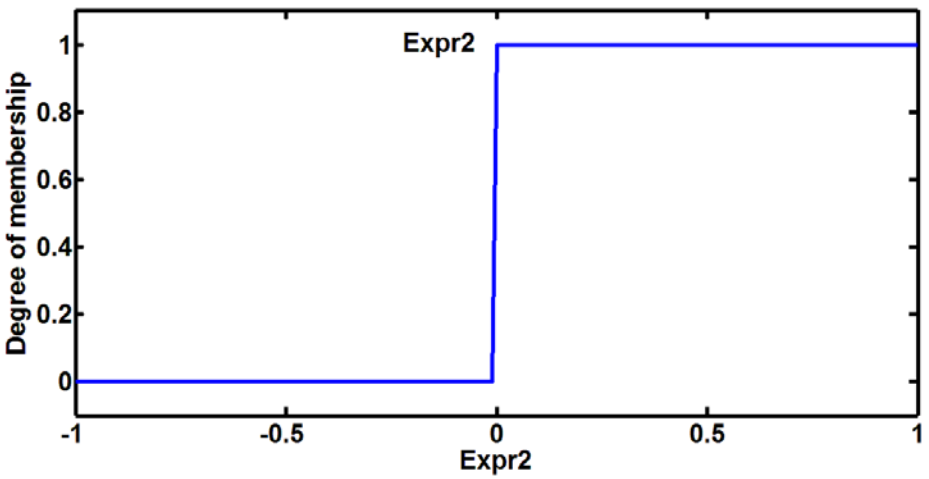

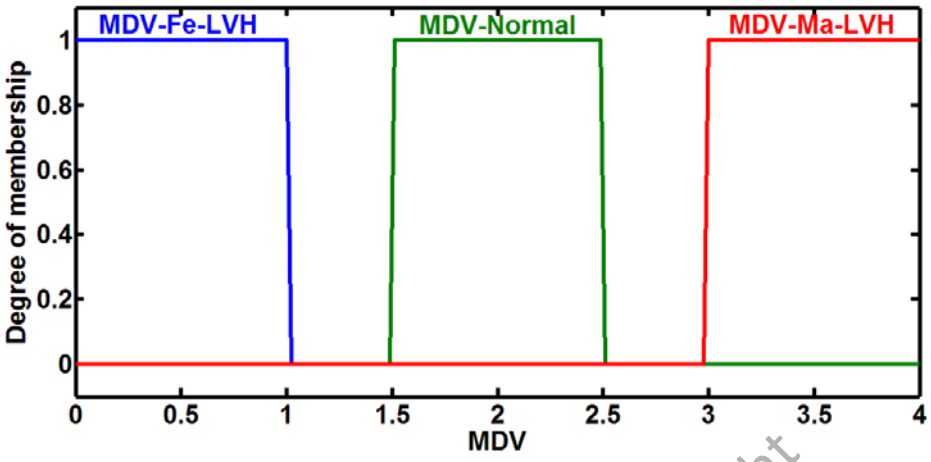

Figure 3.15: Graphical Diagrams of the Output MFs in Proposed FIS.

3.5 Summary

In this chapter, a new system of computerized based technique has been proposed for diagnosing LVH cardiac disease based on processing and analyzing a 12 lead ECG signal. The new proposed system includes three main stages called: pre-processing ECG signal, detecting and analyzing ECG waves, and diagnosing LVH high risk cardiac disease. The descriptions of these stages and their detailed operations were integrated in single graphical block diagram at the first part of this chapter.

Through the first stage of the proposed ECG system that handles all pre-processing operations of reading, smoothing or filtering (if needed), and archiving ECG data. A new system called the digital recovery approach has been proposed to generate 12 lead raw ECG data by reconstructing it from a scanned image (24-bit Bitmap) of the printed ECG chart. This approach includes four image processing steps to provide final 12 lead ECG data in digital form. These steps were integrated in a single graphical block diagram in Section 3.2.2 Figure 3.2, and the theoretical concepts for each step were interpreted separately with related demonstrative diagrams and mathematical

definitions. The 4th step of this approach is the detection of the ECG baseline and reconstructing raw ECG data from the image pixels using the proposed sampling process. The instructions of this process were presented in detail in Algorithm I. The proposed digital recovery approach was designed to process various types of the printed ECG charts.

The second stage of the proposed ECG system was focused on detecting ECG waves (the P wave, the QRS complex, and the T wave), and then delineating time characteristics of these waves which leads to the computing of more diagnostic features/criteria for different cardiac diseases. Two approaches were proposed in this stage. The first approach is named RFEM which performs the process of detecting the QRS complex in different ECG morphologies/ rhythms. The RFEM approach mentioned in Section 3.3.1 was applied by a straightforward algorithm using an instantaneous processing technique on the ECG signal (beat by beat), as a result, the overall processing speed becomes very high. In addition, it takes rising to falling edge mutation as a base rule to accomplish the QRS complex subject detection. All steps of applying RFEM approach on the ECG signal were presented in a single graphical diagram as illustrated in Section 3.3.1 Figure 3.5. The theoretical basis for each step was then interpreted in more detail with related demonstrative diagrams and mathematical definitions. Moreover, the based technique for delineating time characteristic of the QRS complex in the RFEM approach was represented by set of instructions in Algorithm II with quite interpretation for each instruction.

The second proposed detection approach in the same stage of the proposed ECG system named HSDPTW, focused on detecting P and T waves to delineate the boundaries and peak time locations of these waves. The HSDPTW approach mentioned in Section 3.2.2.2 was applied by allocating two limited intervals in the left and right

sides of the QRS complex. Allocating the limits of both intervals was mainly based on the time characteristics of the QRS complex which were pre detected by the RFEM approach. At each interval, a main search algorithm was implemented to delineate the peak time location of the P and T waves based on conditional rising to falling edge mutation within the limits of the search interval. When the peak time location was allocated by the main algorithm, the process of delineating boundary time locations was started directly by another algorithm in a subroutine form called by the main algorithm. This subroutine takes the delineated peak time location as a base point to apply two search iterations towards the boundaries of the P and T waves to delineate the onset and end time locations of these waves. All instructions of the main algorithm and calling subroutine were presented with quite interpretation in Algorithm III, IV for P wave, and Algorithm V, VI for the T wave, respectively.

Through the third stage of the proposed ECG system which was focused on diagnosing high risk cardiac diseases. A new approach to diagnose LVH cardiac disease has been proposed using a proposed FIS design. This system is based on eight voltage parameters which were obtained by the time characteristics of the ECG waves, and two criteria (Skolow, Cornell) which were adopted for diagnosing LVH cardiac disease. The traditional and proposed diagnostic parameters were represented by seven input MFs, while the final diagnosis decision was represented by three MFs in the proposed FIS using the fuzzy Mamdani method.

CHAPTER 4

RESULTS AND DISCUSSION

4.1 Introduction

The general block diagram of the proposed system for analyzing a 12 lead ECG signal, detecting ECG waves and delineating their time characteristics, and diagnosing high risk cardiac diseases was presented in Chapter 3 Section 3.1 Figure 3.1. In each step of this system, there is one approach or more which have been proposed.

In this chapter, each approach in the proposed ECG system is validated with some ECG records which are collected from one or more standard online databases or by the raw ECG data which is reconstructed from ECG paper printout recordings using the proposed approach of digital recovery. The findings from (digital recovery, detecting ECG waves, delineating their time characteristics, and diagnosing a specific high risk cardiac disease called LVH) approaches take different forms, thus many scenarios are suggested to evaluate the overall performance of these approaches. At the same time, these evaluation scenarios are compatible with those that were considered by well known published works in literature in order to facilitate the validation of the obtained results with ones found in existing works.

4.2 Performance Evaluation of proposed Digital Recovery Approach

In Chapter 3 Section 3.2.2.1, a new approach for digital recovery of 12 ECG data from the colour scanned image of ECG paper printout recording (printed ECG

chart) has been proposed. Two simulations are conducted to validate the performance of this approach. The first scenario is a graphical evaluation of the 12-lead raw ECG data that is reconstructed from the printed chart after scanning it with a high resolution (600 dpi), and then saving the resulting image as 24-bit BMP standard format as shown in Figure 4.1. The second evaluation is performed analytically by validating some standard ECG parameters like heart rate, QT interval, QTc, etc which are computed automatically by the modern ECG machine and the corresponding values for these parameters that are obtained by the reconstructed ECG data.

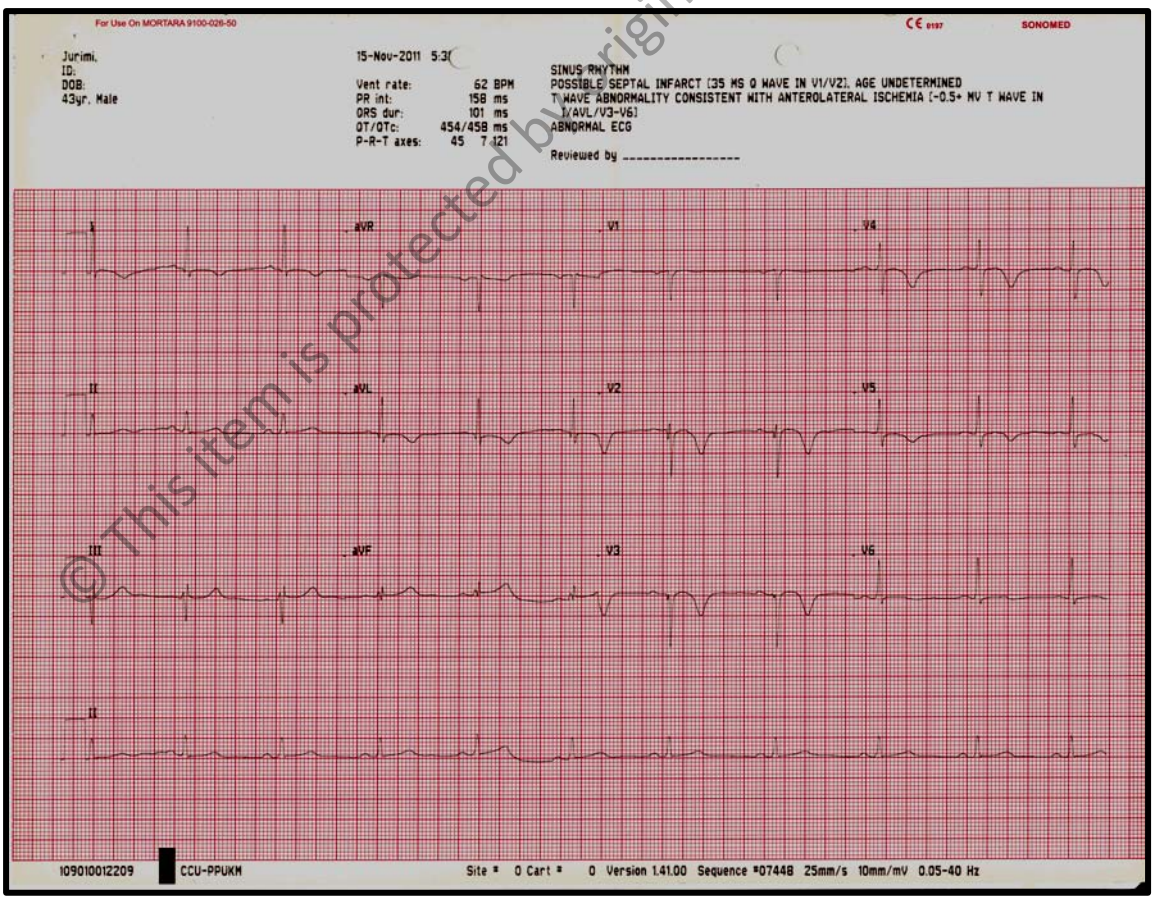

Figure 4.1: The Scanned Image of ECG Printed Chart Using 600 dpi.

4.2.1 Graphical Evaluation of the 12-lead ECG Data

The graphical evaluation of the proposed digital recovery approach is performed by re-plotting the reconstructed 12-lead raw ECG data with respect to the baseline, which was pre detected by the same approach. All steps illustrated in the main block diagram of the proposed digital recovery approach shown in Chapter 3 Section 3.2.2 Figure 3.2 are applied on the scanned ECG image shown in Figure 4.1 (the 1st ECG record from the validation data). The findings from the first step of the proposed digital recovery approach are three slices of rectangular image, each of these slices compounds four ECG leads. In the second step, these slices are digitized using the sampling algorithm presented in Chapter 3 Section 3.2.2.1 Algorithm I to generate twelve signals. These signals represent the reconstructed 12 lead ECG data.

Each one of the reconstructed 12 lead ECG is plotted separately in a single graph with respect to the detected baseline as shown in Figure 4.2.a-l, respectively. In these graphs, the detected baseline level is labelled with a dashed red line. In addition, the y-axis scale of all graphs is limited to (-1.5 mV - +1.5mV) or totally 3mV because the original drawing of ECG signal shown in Figure 4.1 varies to 6 large squares in all three row areas of the printed chart, and each large square represents an amplitude voltage of 0.5mV as discussed in Chapter 2 Section 2.3.1.

(a)

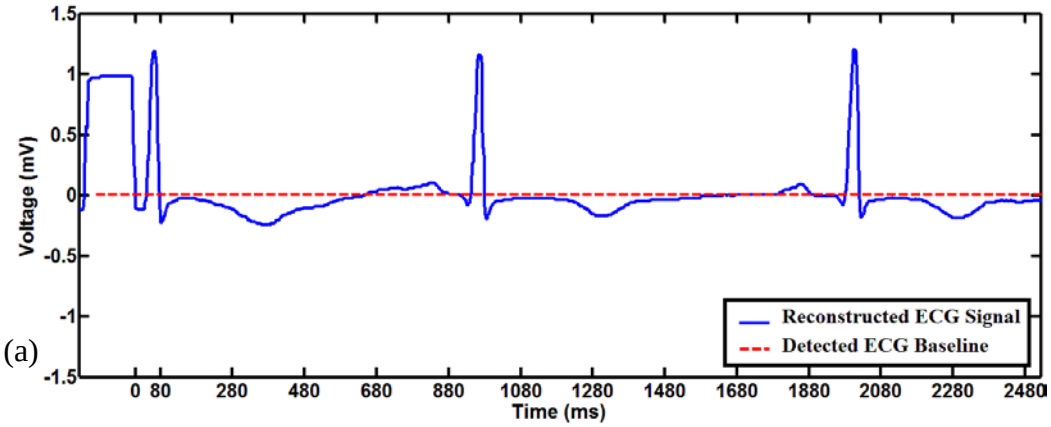

(b)

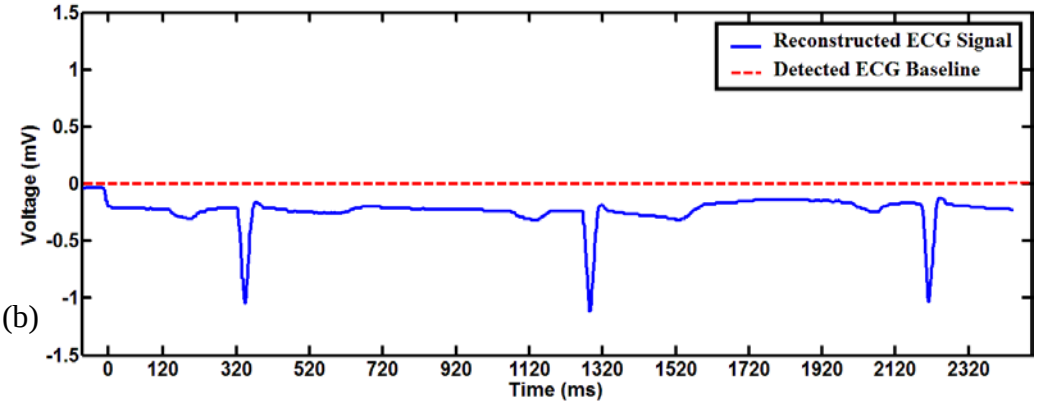

(c)

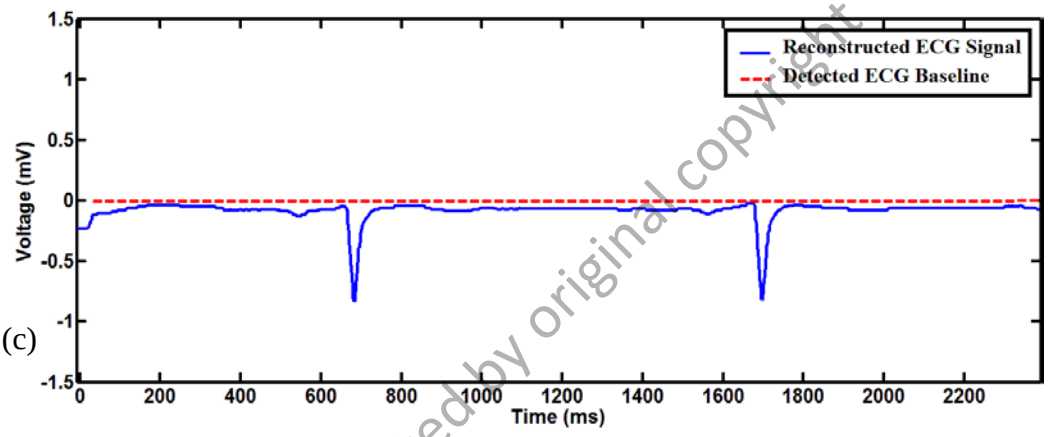

(d)

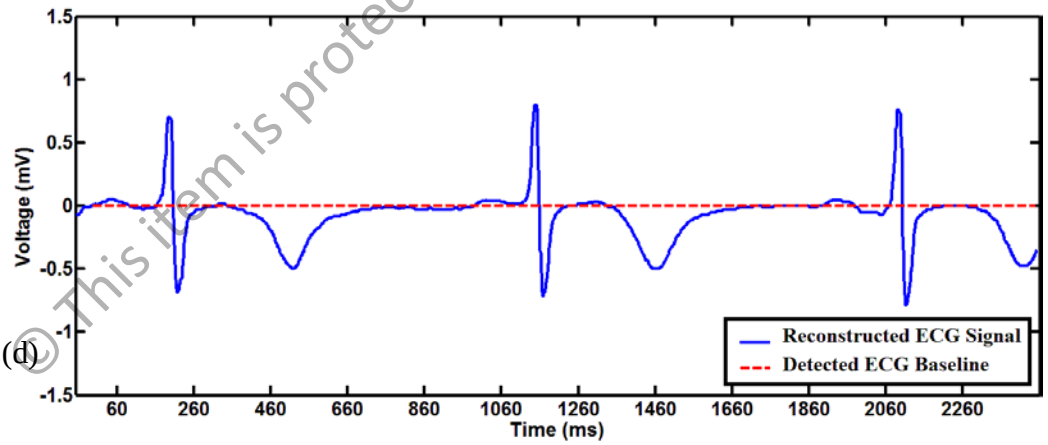

(e)

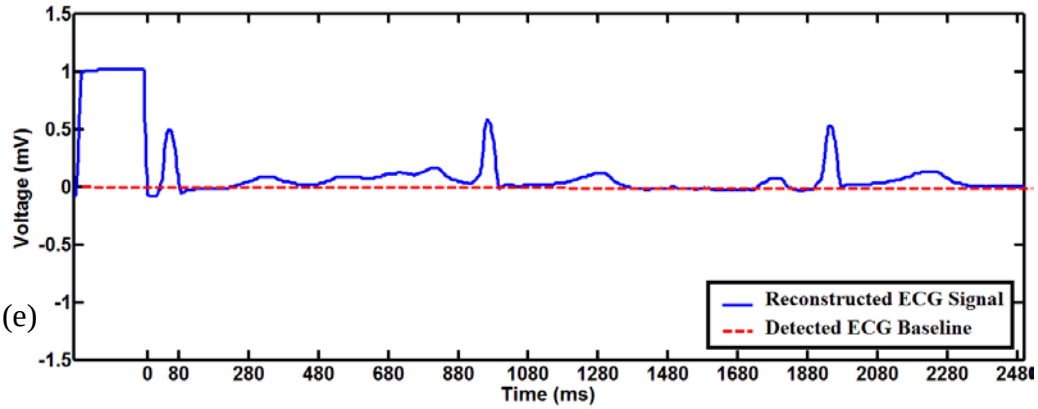

(f)

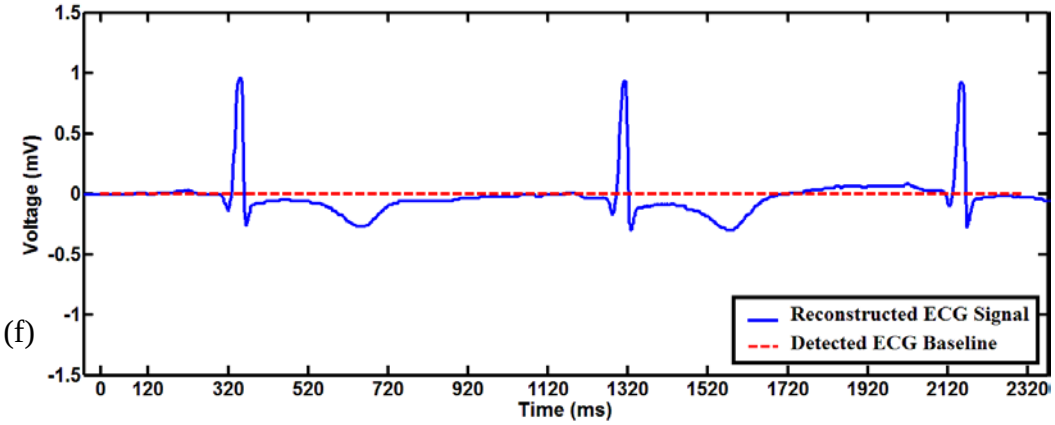

(g)

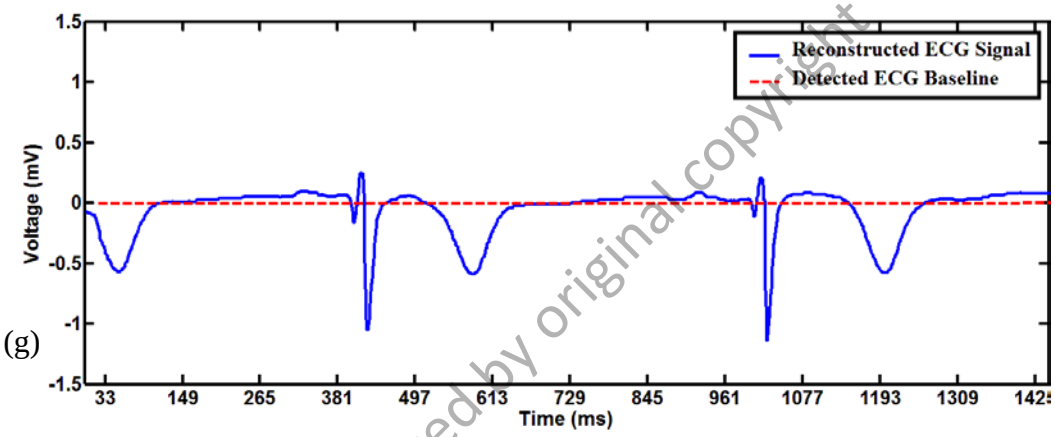

(h)

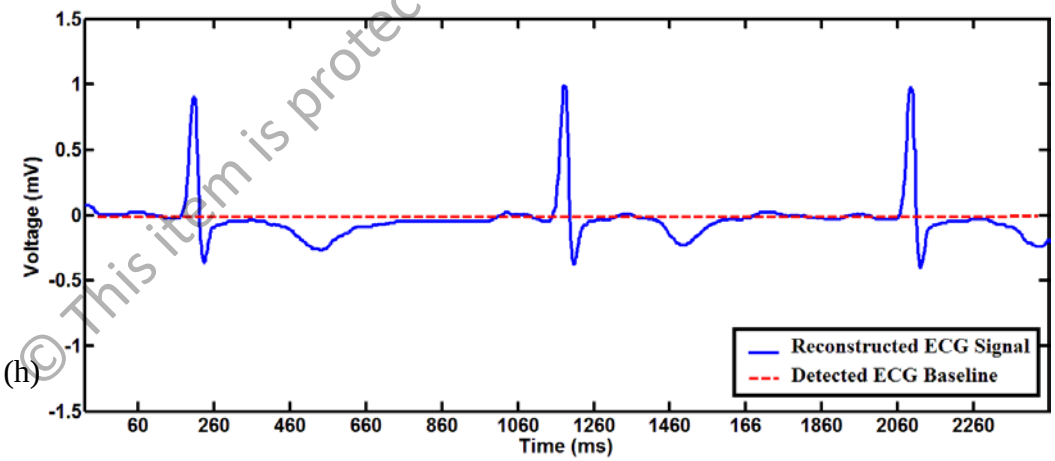

(i)

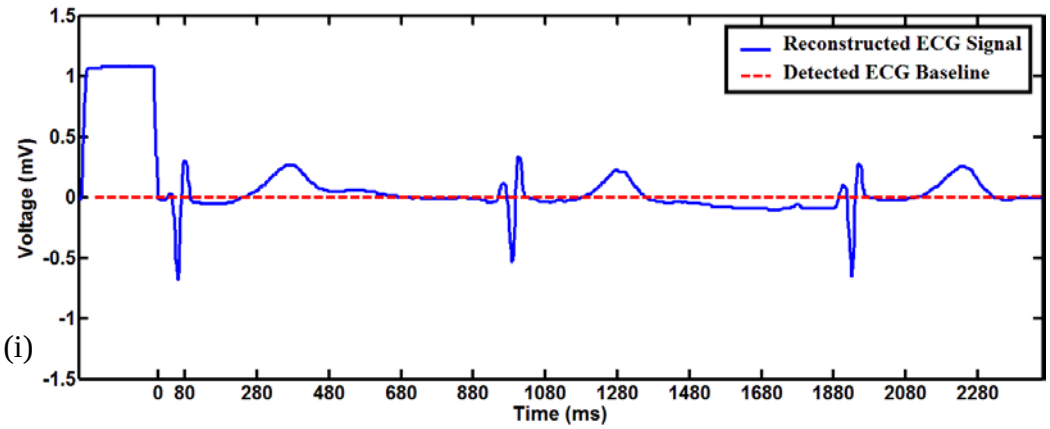

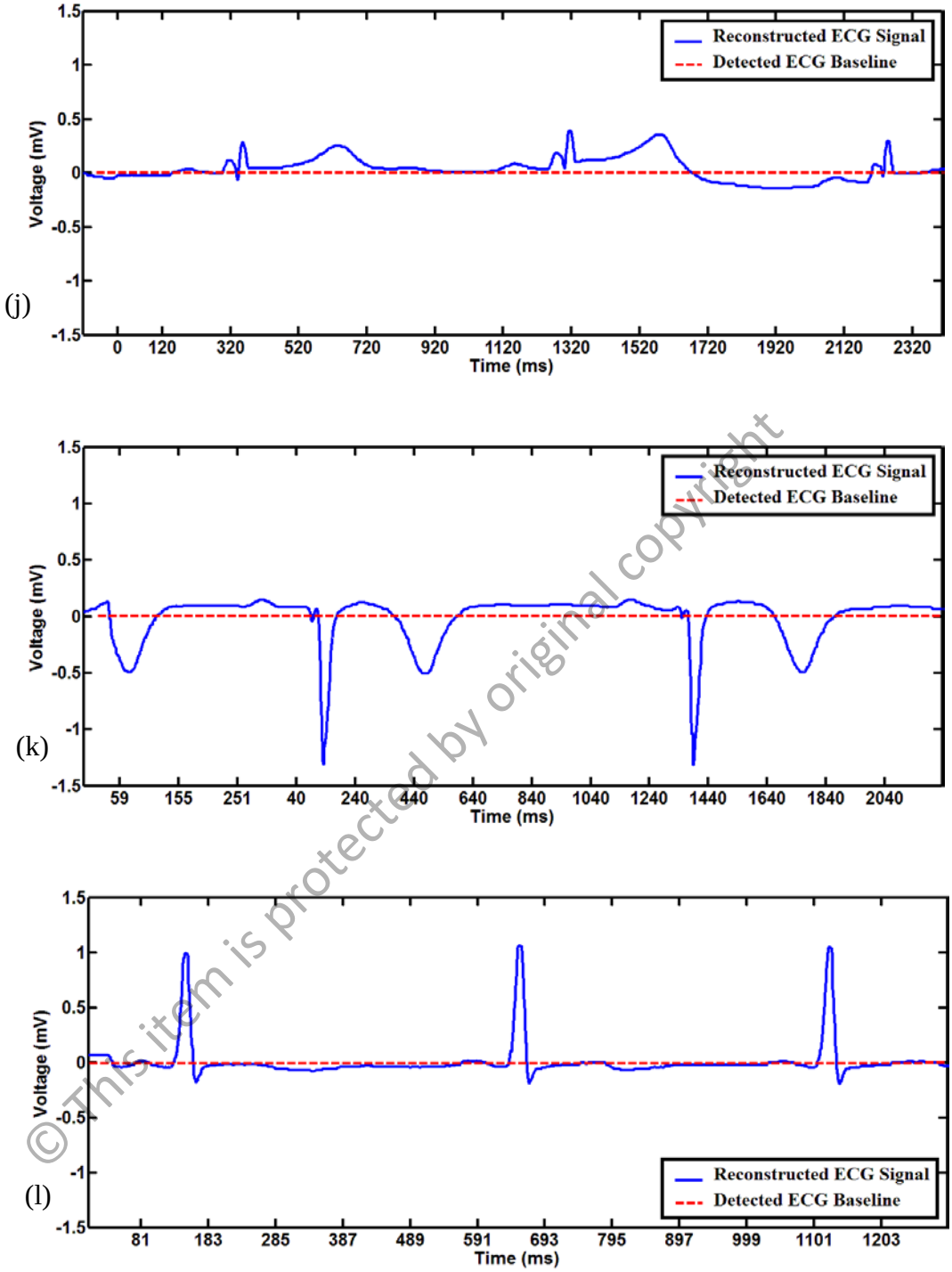

Figure 4.2: Graphical Evaluation of Reconstructed 12 lead Raw ECG Data Resulted from Applying Proposed Digital Recovery Approach on Digital Scanned Image of Printed ECG Chart, Lead (a) I, (b) aVR, (c) V1, (d) V4, (e) II, (f) aVL, (g) V2, (h) V5, (i) III, (j) aVF, (k) V3, and (l) V6.

Finally, to prove the ability of the proposed digital recovery approach to process various types of ECG printed chart, this evaluation is repeated for another ECG record

with a different shape of printout paper, the original ECG record, as well as the drawings of the reconstructed 12 lead ECG data with respect to the ECG baseline detected are illustrated in Appendix A.

As in all continuous signals, the reconstructed raw ECG data obtained by the proposed digital recovery approach is not adopted without true time considerations. The most significant challenge is how to convert graphical data that is represented by sets of pixels to a continuous signal with fixed sampling frequency. This problem has been addressed successfully by computing a number of pixels that are restricted within a small square NP in the scanned image. These pixels correspond to the standard representation of each small square in the ECG recording. As a standard, each small square in the ECG recording represents 0.1 mV as voltage amplitude and 40 ms as a time period (Azeem et al., 2005; Bowbrick & Borg, 2006; Hampton, 2013).

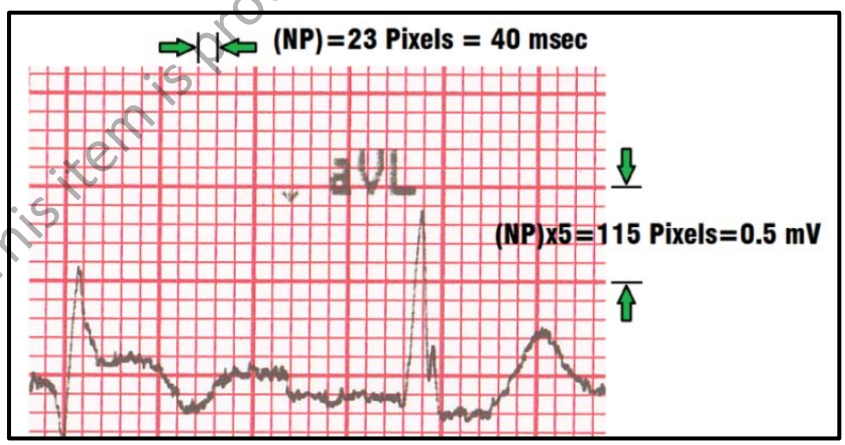

Figure 4.3: Scaling Factors of Time and Voltage Amplitude which are Represented by Number of Pixels in One Small Square of ECG Printed Chart.

The previous presentation proves that the reconstructed ECG data must be scaled with time and voltage amplitude proportionate to the scaling factors that are

determined from the number of pixels in a small square inside a scanned image for the purpose of adopting this data as a true ECG signal. The image slice in Figure 4.3 shows the scaling factors of time and voltage amplitude that is corresponded to one small square within the scanned image.

4.2.2 Analytical Evaluation of Single ECG Lead

In general, the main idea behind a digital recovery approach is to reconstruct digitally raw data from other media like a paper printout recording to facilitate the use of this data for modern archiving applications or for making an accurate analysis and diagnosis by expert computerized systems (Sanromán-Junquera et al., 2012). The process of digital recovery is extremely important if the reconstructed data has similar behaviour to the original ECG chart along the entire recording time of the ECG signal. Thus, the reconstructed raw ECG data must be evaluated accurately to know the ability of adopting this data in later application and processing issues. Two types of analytic evaluation are presented in the following sections to compute the precision of the reconstructed raw ECG data.

4.2.2.1 Qualitative evaluation

This type of evaluation aims to prove the quality of the reconstructed ECG data with respect to the original data represented by the printed chart. In this evaluation, the reconstructed raw ECG data is plotted in the same graph that contains the original ECG chart after scaling it in time and voltage amplitude. The printed chart of lead II in three ECG records is used as the testing data in this evaluation; the combined drawings for the tested ECG records are shown in Figure 4.4.a, b, and c, respectively. The visual

inspection comparison between the original ECG chart and another that was plotted using the reconstructed raw ECG data proves the highest degree of congruence between the reconstructed and original ECG signal in both voltage amplitude and time. This congruence covers all parts of the ECG signal, even those with high chattering variation. As a result, the significant congruence in graphical behaviour between the reconstructed raw ECG data and the original ECG signal gives great trusting to consider digital raw ECG data for future works of detecting ECG waves and diagnosing different cardiac diseases

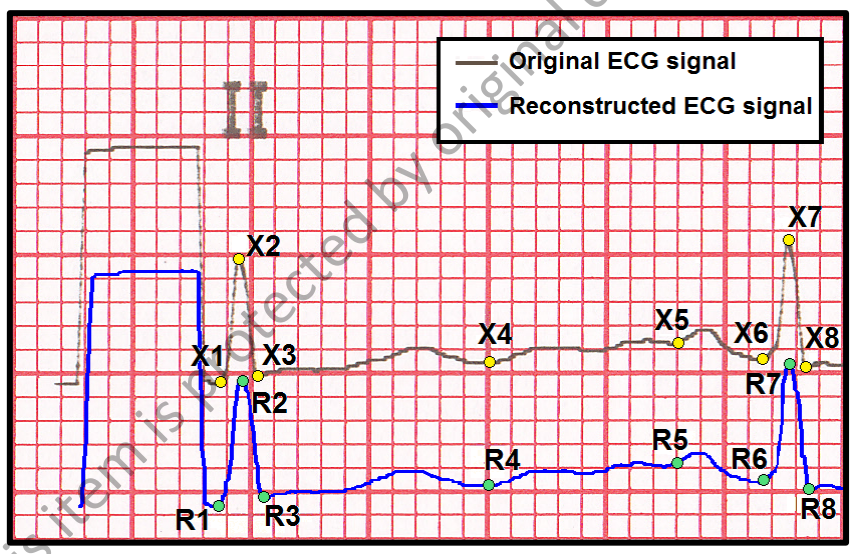

(a)

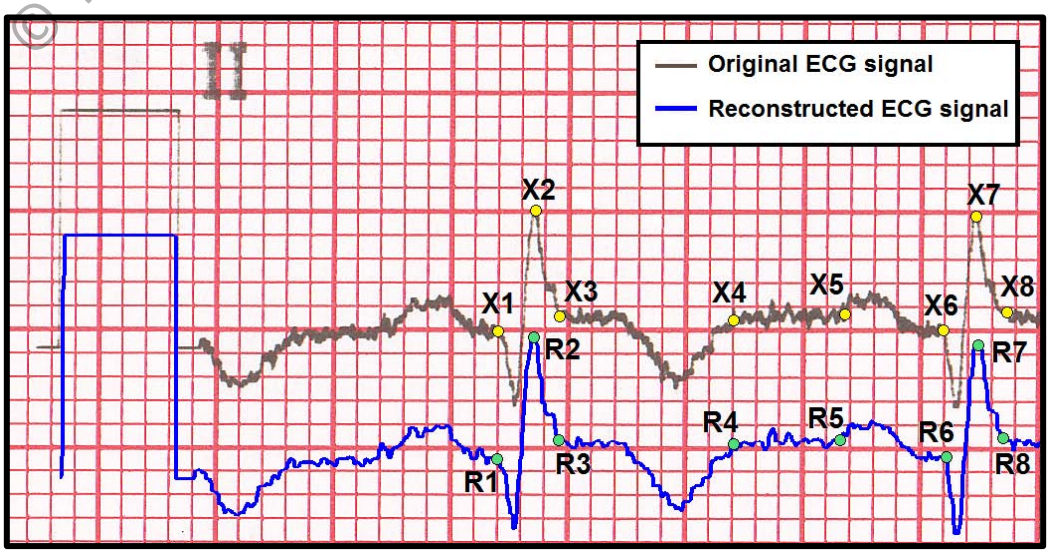

(b)

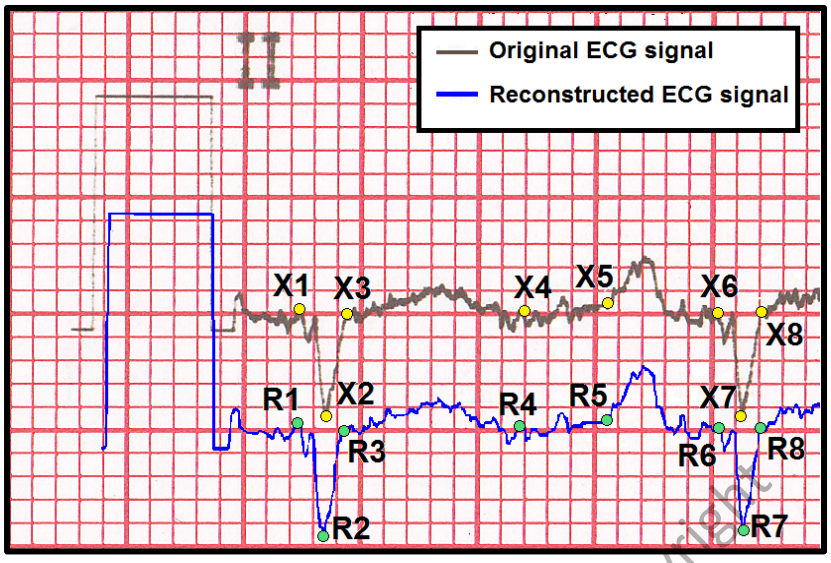

(c)

Figure 4.4: Combined Drawing of Original and Reconstructed ECG Signal with Identical Distribution of Validation Points in Lead II Signals (a) 1st Patient, (b) 2nd Patient, and (c) 3rd Patient.

4.2.2.2 Quantitative Evaluation

The header partition of the 12 lead ECG record shown in Figure 4.1 contains little information which are obtained automatically by the ECG machine itself. In this information, there are five significant parameters (Ventricular Rate, PR interval, QRS duration, QT interval, and QTc interval), which are mostly used for analyzing and diagnosing the ECG signal (C. Lin et al., 2010; Yeh et al., 2010; Zigel et al., 2000).

Another type of analytical evaluation named "quantitative evaluation" is performed by recalculating these parameters using the reconstructed raw ECG data, and then comparing them with the corresponding values which were calculated automatically by the ECG machine. The 1st parameter is the ventricular rate or the heart rate, which is determined by computing a number of small squares between two consecutive QRS complexes then dividing them by 1500 (Azeem et al., 2005; Bowbrick & Borg, 2006; Foster, 2007). The reconstructed raw ECG data must be scaled first by

NP in order to maintain a similar sampling time of the standard ECG signal before the ECG rate is computed as defined in Equation (4.1).

$$Vent_{Rate} = \frac{1500}{Distance\ of\ two\ consecutive\ R_{Peaks}/NP} = \frac{1500}{(R_7 - R_2)/NP} \quad (4.1)$$

The 2nd parameter is the PR interval, which represents the interval that is limited from the beginning of the P wave to the beginning of the QRS complex (end of the Q-wave). This interval can be determined with the reconstructed data by scaling the number of pixels which are limited within this interval by the NP value as defined in Equation (4.2).

$$PR_{Interval} = \frac{Distance(Q_{End},\ P_{Start})}{NP} = \frac{(R_6 - R_5)}{NP} \quad (4.2)$$

Another interval named the QRS duration which represents the width of this complex and is determined in the same manner as the PR interval, except that this duration is limited between the two ends of the QRS complex (start and end) of the Q and the S waves, respectively, as defined in Equation (4.3).

$$QRS_{Duration} = \frac{Distance(QRS_{Start},\ QRS_{End})}{NP} = \frac{(R_8 - R_6)}{NP} \quad (4.3)$$

The last parameters reported are QT and QTc (corrected) interval. The QT interval represents the total electrical duration of the ventricles. It is limited from the beginning of the QRS complex to the end of the T-wave as defined in Equation (4.4). The corrected QT interval (QTc) interval can be arrived at using Bassett's formula (Bazett, 1997) defined in Equation (4.5) to obtain the corrected value of the QT interval.

$$QT_{Interval} = \frac{Distance(QRS\ complex_{\ Start}, T_{End})}{NP} = \frac{(R_4 - R_1)}{NP} \quad (4.4)$$

$$QTc_{Interval} = \frac{QT_{Interval}}{\sqrt{RR_{Interval}\,(sec)}} = \frac{(R_4 - R_1)}{\sqrt{R_7 - R_2}} \quad (4.5)$$

Table 4.1: Validation Results and Accuracy of Five Standard ECG parameters obtained in Lead II of Three Patients ; 1 small square (SS) = 0.04 s (Standard Sampling Time of ECG signal)

Patient	Tested Lead	Parameter Name	Original Data		Recovered Data		Accuracy
			Parameter Value	Referenced Period / Estimated No. of SS	Parameter Value	Referenced Period / Scaled No. of SS	
P1	Lead II	*Ventricular Rate*	62 RPM	X2↔ X7 / 24.2	61.5 RPM	R2↔ R7 / 24.4	99.19%
		PR Interval	158 ms	X5↔X6 / 3.95	160 ms	R5↔R6 / 4	98.73%
		QRS duration	101 ms	X6↔X8 / 2.525	98 ms	R6↔R8 / 2.45	97.02%
		QT , QTc Interval	454 ms , 458 ms	X1↔X4 / 11.35	460 ms , 465 ms	R1↔R4 / 11.5	98.67%
P2	Lead II	*Ventricular Rate*	79 RPM	X2↔ X7 / 18.95	77.72 RPM	R2↔ R7 / 19.3	98.38%
		PR Interval	171 ms	X5↔X6 / 4.275	172.4 ms	R5↔R6 / 4.31	99.18%
		QRS duration	110 ms	X6↔X8 / 2.75	112.4 ms	R6↔R8 / 2.82	97.81%
		QT , QTc Interval	389 ms , 423 ms	X1↔X4 / 9.725	392 ms , 445 ms	R1↔R4 / 9.8	99.20%
P3	Lead II	*Ventricular Rate*	84 RPM	X2, X7 / 17.85	85.22 RPM	R2↔ R7 / 17.60	98.54%
		PR Interval	190 ms	X5↔X6 / 4.75	186.4 ms	R5↔R6 / 4.66	98.10%
		QRS duration	89 ms	X6↔X8 / 2.225	85.6 ms	R6↔R8 / 2.14	96.18%
		QT , QTc Interval	378 ms , 419 ms	X1↔X4 / 9.45	373.2 ms , 449.63	R1↔R4 / 9.33	98.73%
Average Accuracy						98.31%	

The results of computing theses parameters in the original and the reconstructed ECG data for the same ECG records that are used in qualitative evaluation are

illustrated in Table 4.1. The analytic results illustrated in this table show that the average accuracy exceeds 98% which demonstrates the consistency and robustness of proposed digital recovery approach to generate accurate digital 12 lead ECG data. In addition, the scanned images of these records are presented in Appendix B including header information and details for the 12 lead ECG chart.

4.3 Performance Evaluation of Proposed Approaches for Detecting ECG waves

In this section, the performance of the proposed approach RFEM mentioned in Chapter 3 Section 3.3.1 for detecting the QRS complex and HSDPTW mentioned in Chapter 3 Section 3.3.2 for detecting P and T waves are evaluated by applying these approaches on some ECG samples which were collected from standard ECG databases such as MIT-BIH, QT, etc databases. A selection of suitable ECG databases for each detection approach depends mainly on the detailed annotated information in this database as mentioned in Chapter 2 Section 2.3.2.

4.3.1 Performance Analysis of Proposed RFEM Approach

In this section, two simulations were conducted to evaluate the performance of the proposed RFEM approach to delineate the time characteristics of the QRS complex in an ECG signal. The first simulation is performed to evaluate the delineation of R_{PEAK} time location in the QRS complex, while the second simulation is performed to evaluate the delineation of other time characteristics in the QRS complex Q_{ONSET}, Q_{END}, S_{ONSET}, and S_{END}. The obtained results in both simulations are compared with other QRS complex detection methods proposed in literature to prove the robustness of the proposed approaches in the QRS complex detection subject.

4.3.1.1 Graphical Evaluation of R_{PEAK} time locations

In this section, the proposed RFEM approach for detecting the QRS complex is applied on the ECG records from MIT-BIH arrhythmia database (G. B. Moody & Mark, 1990) to validate the delineation of R_{PEAK} time location in the QRS complex. The selection of the ECG records in this database comes from the annotation information inside them, where each ECG record was annotated manually by cardiologists with the R_{PEAK} time locations along the ECG recording time (G. B. Moody & Mark, 2001) as mentioned in Chapter 2 Section 2.3.2.1. Therefore, it is easily to validate the R_{PEAK} time locations by comparing the obtained results with the manual annotations.

The graphical evaluation of R_{PEAK} time location is performed by applying the proposed RFEM approach on eight ECG records (100, 107, 111, 118, 122, 210, 232, and 234) from MIT-BIH. These ECG records were selected with different ECG morphologies to prove the ability of the proposed approach to delineate the R_{PEAK} time location in various ECG signal rhythm changes. The delineation results of the R_{PEAK} time locations obtained by the RFEM approach and the corresponding manual annotation time locations recorded in MIT-BIH of eight ECG records are shown in Figure 4.5.a to h, respectively. The closest match between the delineated R_{PEAK} time locations marked with the green circular markers and the manual annotation time locations marked with the vertical dashed lines in Figure 4.5 prove the robustness of the proposed RFEM approach to give the correct position of the peak time locations in various ECG rhythms and obvious amplitude variations.

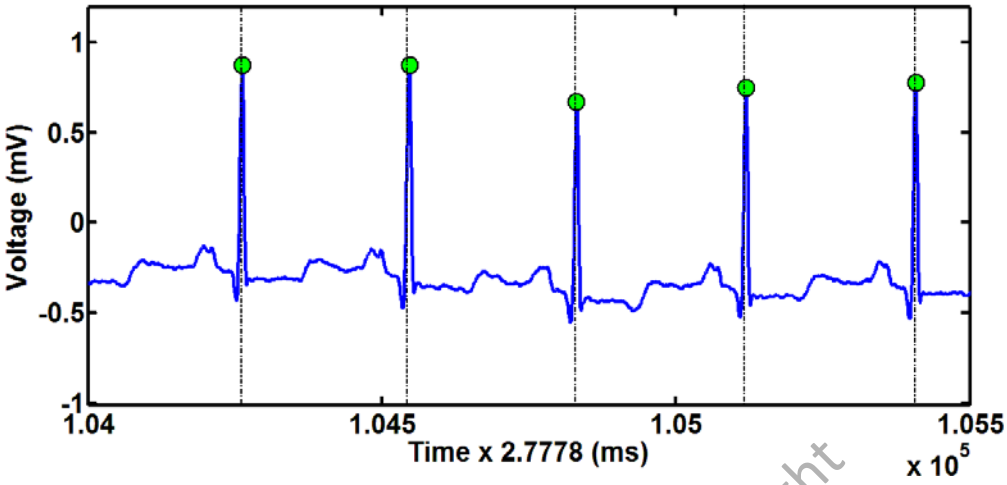

(a)

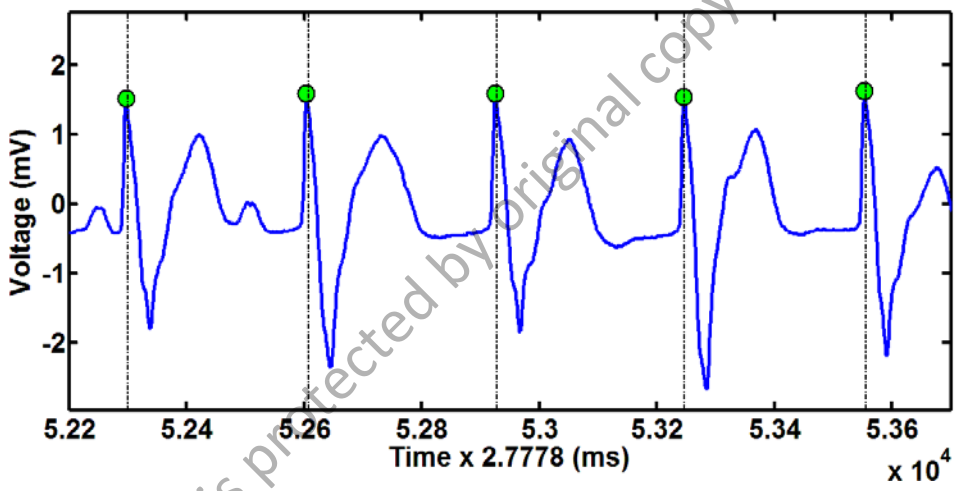

(b)

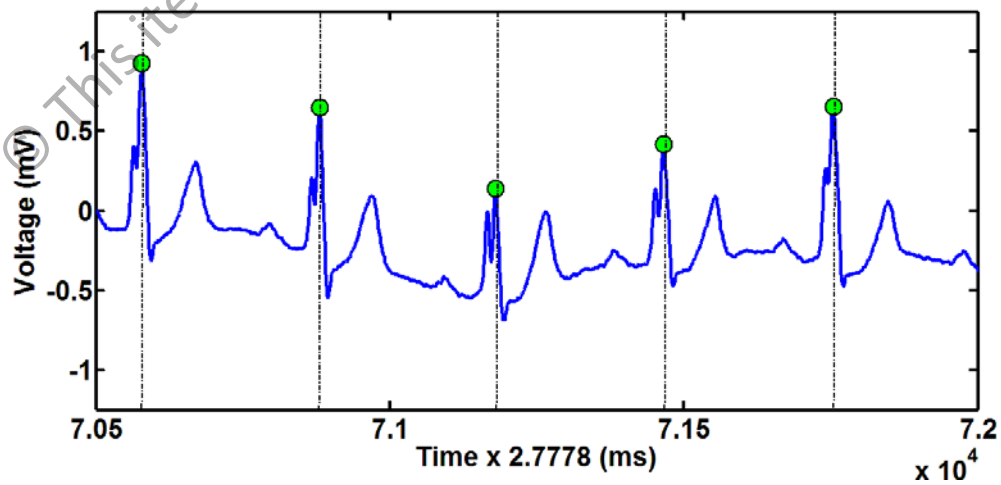

(c)

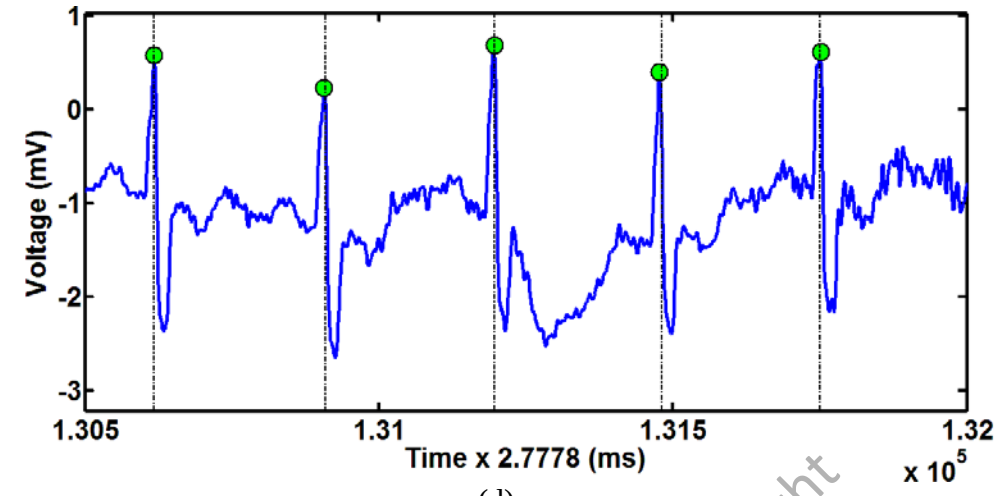

(d)

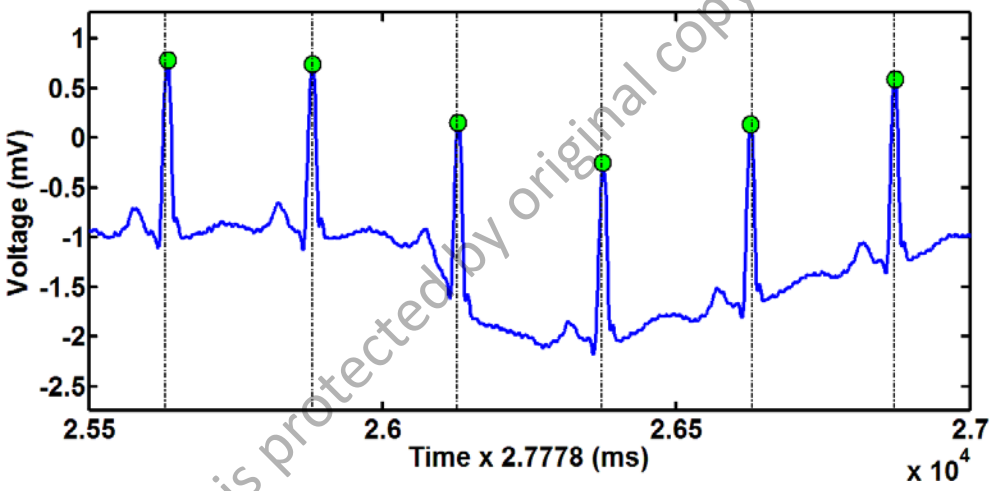

(e)

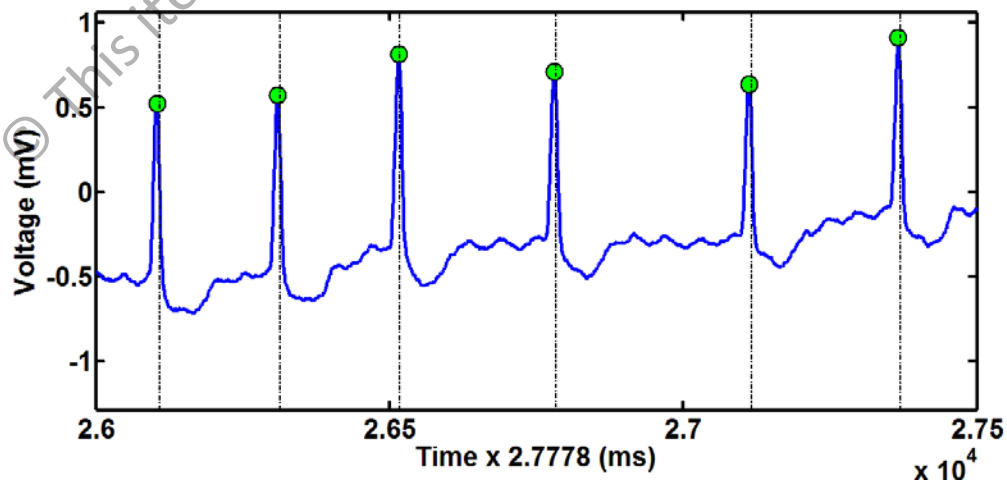

(f)

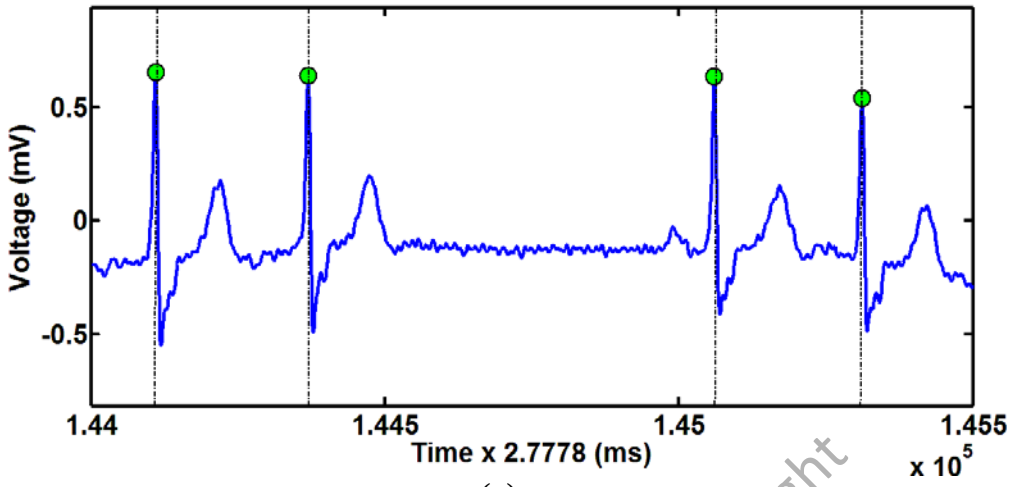

(g)

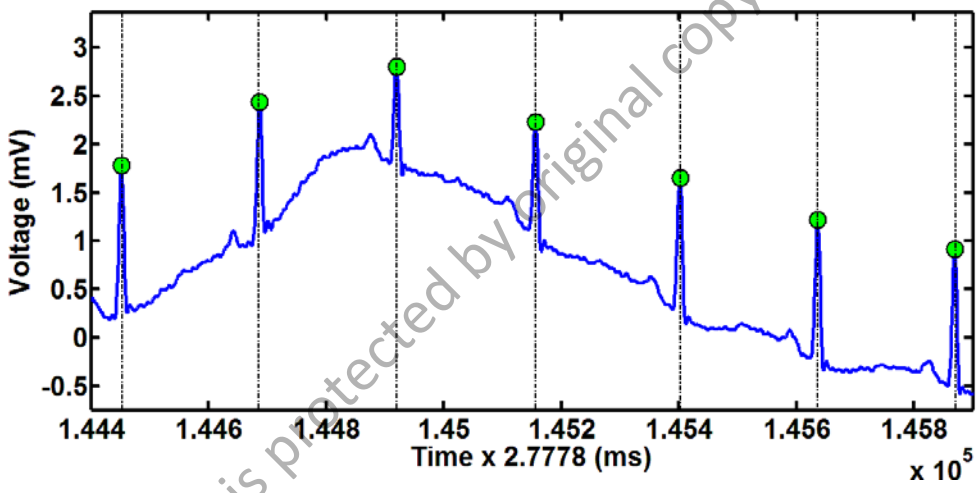

(h)

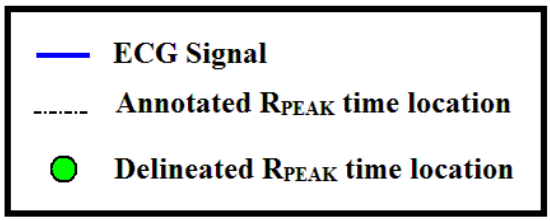

Figure 4.5: Delineation Results of R_{PEAK} Time Locations in Eight ECG Records from MIT-BIH Arrhythmia Database, (a) Record100, (b) Record107, (c) Record111, (d) Record118, (e) Record122, (f) Record210, (g) Record232, and (h) Record234.

4.3.1.2 Graphical Evaluation of QRS time characteristics

In this section, another graphical evaluation is provided to evaluate the delineation results of QRS complex time characteristics (Q_{ONSET}, Q_{END}, R_{PEAK}, S_{ONSET}, and S_{END}). This evaluation is performed by applying the proposed RFEM approach on some ECG records which were collected from QTDB. As mentioned in Chapter 2 Section 2.3.2.2, each ECG record in QTDB (Laguna et al., 1997) was annotated with Q_{ONSET}, R_{PEAK}, and S_{ONSET} time location, which meant that it is easily to validate the time characteristics of the QRS complex obtained by the proposed approach with those annotated inside QTDB. Five ECG records from five categories in QTDB were selected as the validation data for this evaluation. The delineation results of (Q_{ONSET}, Q_{END}, R_{PEAK}, S_{ONSET}, and S_{END}) for these records are shown in Figure 4.6.a to f. All ECG charts in this figure are marked with the corresponding manual annotation by cardiologists, the peak time locations are marked with the vertical dash-dotted lines and the boundaries time locations are marked with vertical dotted lines.

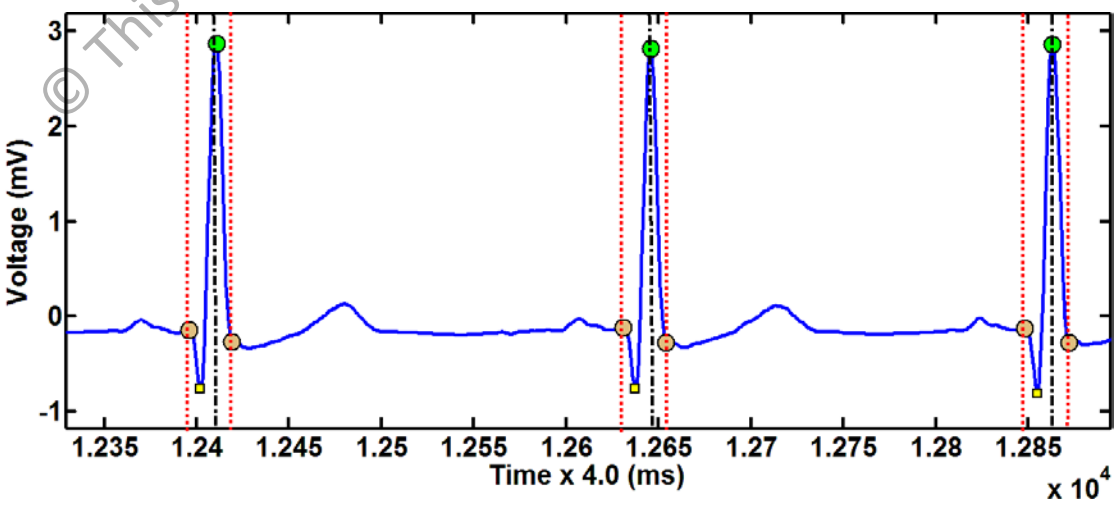

(a)

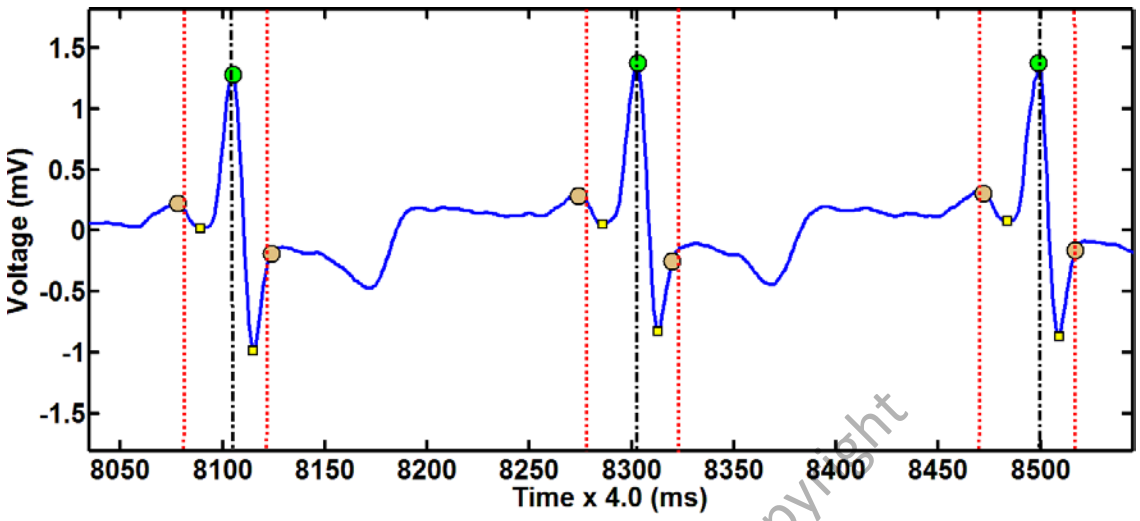

(b)

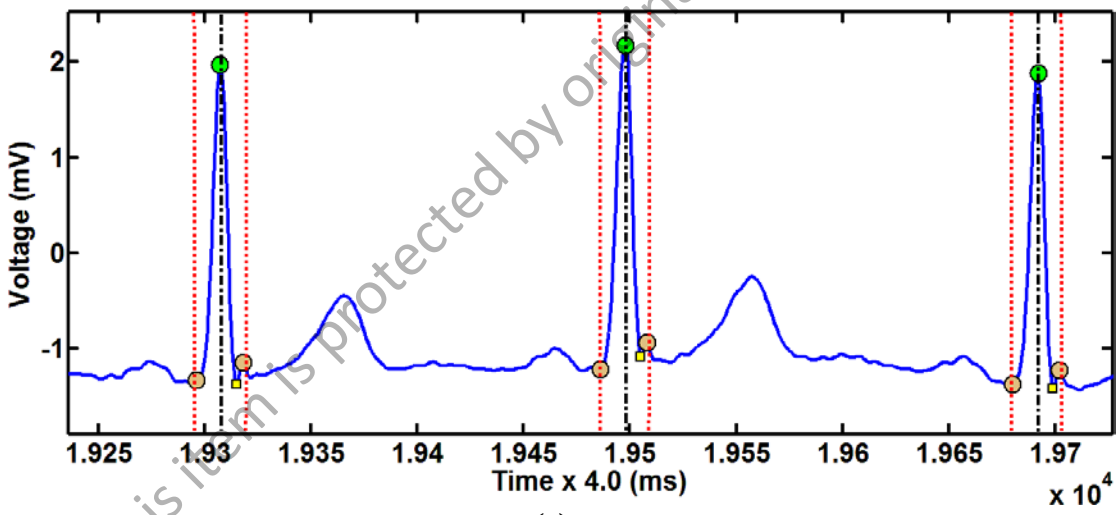

(c)

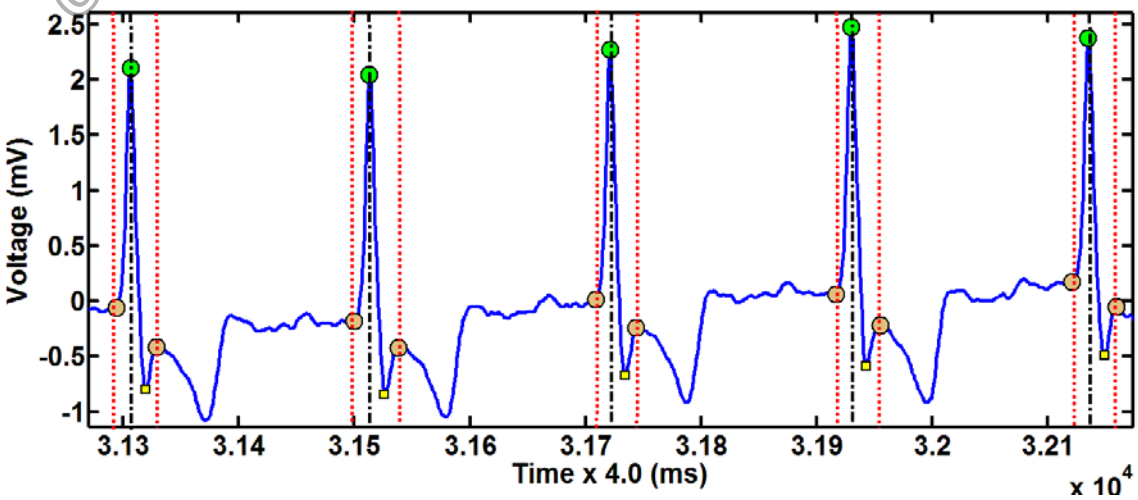

(d)

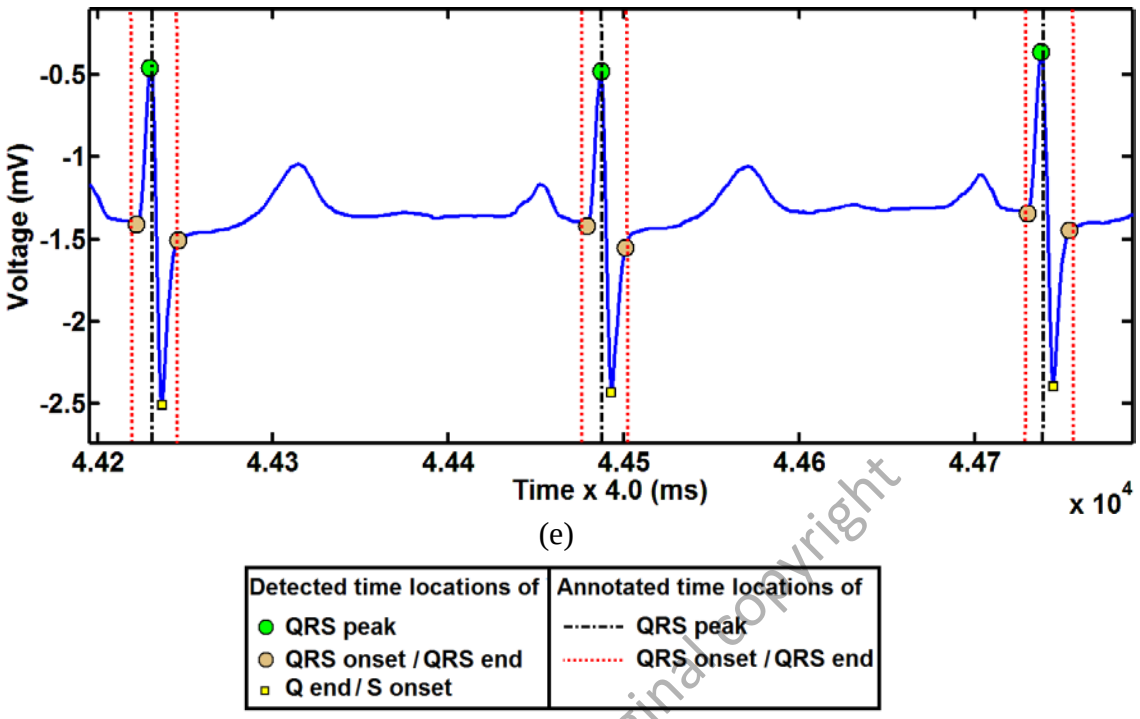

Figure 4.6: The Manual Annotations by Cardiologists and Delineation Results of QRS Time Characteristics for Processing QTDB Records: (a) "SEL16256" Normal Sinus Rhythm DB, (b) "SEL853" Super Ventricular DB, (c) "SEL116" Arrhythmia DB, (d) "SEL14157" Long-Term DB, and (e) "SEL106" European ST-T DB.

The significant congruence between the annotated time locations represented by vertical lines and the delineated time locations represented by small markers in Figure 4.6 proves the capability of RFEM to track the ECG signals with different rhythm and wave morphologies, as well as delineating all time characteristics of QRS complex with highest accuracy. In addition, an evaluation of delineation accuracy in proposed approach can be performed by calculating the time deviation (TDV) between the manual annotation readings and the delineation results obtained by the proposed RFEM approach as defined in Equation 4.6.

$$TDV\left[QRS_{t\_limits}\right] = Annotated\left[QRS_{t\_limits}\right] - Delineated\left[QRS_{t\_limits}\right] \qquad (4.6)$$

The histograms in Figure 4.7.a, b, and c show the distribution of (Q_{ONSET}, R_{PEAK}, and S_{ONSET}) time deviations for all delineated time characteristics in the five ECG

records used in this evaluation. A total of 99.45%, 100%, and 99.30% of time deviations for Q_{ONSET}, R_{PEAK}, and S_{ONSET}, respectively are located within $\pm$ 4 ms of time deviations (marked with red dashed lines) which represent $\pm$ 1 ECG sample as a time deviation error between the annotated and the delineated time characteristics. This is due to the fact that the sampling frequency of all ECG records in QTDB is 250 Hz. Therefore, the time duration for a single ECG beat is 4 ms as mentioned in Chapter 2 Section 2.3.2.2. The lowest percentage time deviation error for (Q_{ONSET}, R_{PEAK}, and S_{ONSET}) gives another indication of the ability of the proposed RFEM approach to provide accurate delineations for all QRS time characteristics.

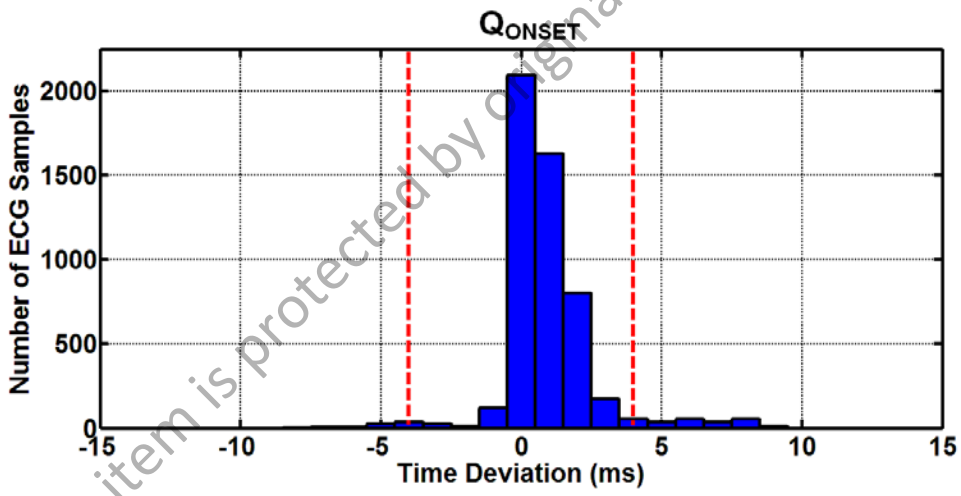

(a)

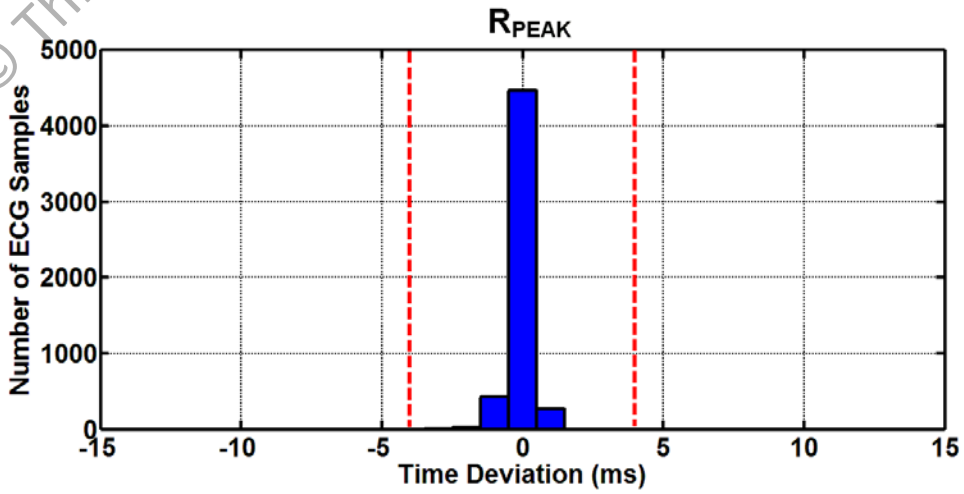

(b)

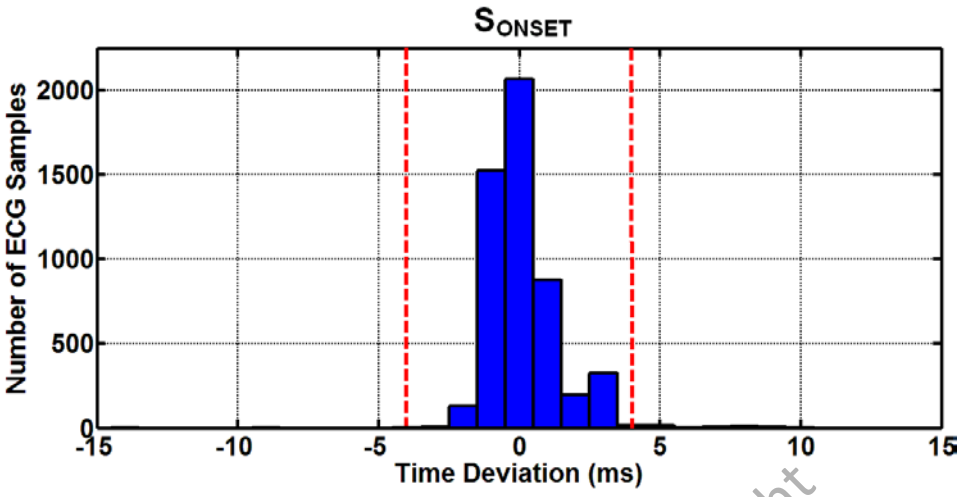

(c)

Figure 4.7: Histogram of Time Deviations Between the Delineation Results of Proposed RFEM Approach and the Manual Annotation Results of Five ECG Records From QTDB for QRS Time Characteristics: (a) Onset of Q wave, (b) Peak of R wave, and (c) Onset of S wave.

4.3.1.3 Validation of RFEM Proposed Approach

As mentioned in Chapter 2 Section 2.4.1.1, many methods have been proposed in literature for the purpose of QRS detection. Most of these methods have been validated with standard 48 ECG records from MIT-BIH, which are described in Chapter 2 Section 2.3.2.1, by calculating three statistical metrics. The first is sensitivity (Se) which is used to evaluate the ability of the applied detection method to detect true ECG beats according to the false negative beats FN (the QRS complex was present but was not detected) with respect to the total true positive beats TP (the correctly detected QRS complexes) as defined in Equation 4.7. The second metric is positive predictivity or (specificity) P^{+}, which is used to evaluate the ability of the applied detection method to differentiate between true and false beats according the false positive beats FP (the QRS complex was not present but was detected) with respect to the total true positive beats TP as defined in Equation 4.8. The third metric is the percent of failure detection (Fd) percentage, which is used to evaluate the detection accuracy of the applied detection

method according to the summation of false positive and negative beats (FP and FN) with respect to the overall analyzed beats TB as defined in Equation 4.9 (Ghaffari et al., 2009; C. Lin et al., 2010; J. P. Martínez et al., 2004; Z Zidelmal et al., 2014).

$$Se = \frac{TP}{TP + FN} \times 100\% \tag{4.7}$$

$$P^{+} = \frac{TP}{TP + FP} \times 100\% \tag{4.8}$$

$$F_d = \frac{FP + FN}{TB} \times 100\% \tag{4.9}$$

The simulation results of (Se, P^{+}, and Fd) obtained by applying the proposed RFEM approach on 48 ECG records from MIT-BIH DB are illustrated in Table 4.2.

Table 4.2: Simulation Results of Statistical Metrics of Applying Proposed RFEM Approach on 48 ECG Records from MIT-BIH DB.

Record	TB	TP	FP	FN	Se(%)	P^{+}(%)	Fd(%)
100	2273	2273	0	0	100.00	100.00	0.00
101	1865	1865	0	0	100.00	100.00	0.00
102	2187	2187	0	0	100.00	100.00	0.00
103	2084	2084	0	0	100.00	100.00	0.00
104	2229	2226	3	0	100.00	99.87	0.13
105	2572	2561	2	9	99.65	99.92	0.43
106	2027	2023	2	2	99.90	99.90	0.20
107	2137	2133	0	4	99.81	100.00	0.19
108	1763	1733	5	25	98.58	99.71	1.70
109	2532	2524	0	8	99.68	100.00	0.32
111	2124	2123	0	1	99.95	100.00	0.05
112	2539	2539	0	0	100.00	100.00	0.00
113	1795	1793	2	0	100.00	99.89	0.11
114	1879	1879	0	0	100.00	100.00	0.00
115	1953	1953	0	0	100.00	100.00	0.00
116	2412	2406	0	6	99.75	100.00	0.25
117	1535	1535	0	0	100.00	100.00	0.00
118	2278	2278	0	0	100.00	100.00	0.00

Table 4.2: (Continued)

Record	TB	TP	FP	FN	Se(%)	P^+(%)	Fd(%)
119	1987	1987	0	0	100.00	100.00	0.00
121	1863	1863	0	0	100.00	100.00	0.00
122	2476	2476	0	0	100.00	100.00	0.00
123	1518	1518	0	0	100.00	100.00	0.00
124	1619	1619	0	0	100.00	100.00	0.00
200	2601	2572	17	12	99.54	99.34	1.11
201	1963	1953	3	7	99.64	99.85	0.51
202	2136	2133	1	2	99.91	99.95	0.14
203	2980	2944	11	25	99.16	99.63	1.21
205	2656	2650	0	6	99.77	100.00	0.23
207	1862	1847	3	12	99.35	99.84	0.81
208	2955	2944	4	7	99.76	99.86	0.37
209	3005	3005	0	0	100.00	100.00	0.00
210	2650	2632	3	15	99.43	99.89	0.68
212	2748	2748	0	0	100.00	100.00	0.00
213	3251	3251	0	0	100.00	100.00	0.00
214	2262	2259	1	2	99.91	99.96	0.13
215	3363	3355	0	8	99.76	100.00	0.24
217	2208	2204	1	3	99.86	99.95	0.18
219	2154	2154	0	0	100.00	100.00	0.00
220	2048	2048	0	0	100.00	100.00	0.00
221	2427	2422	2	3	99.88	99.92	0.21
222	2483	2483	0	0	100.00	100.00	0.00
223	2605	2602	3	0	100.00	99.88	0.12
228	2053	2050	0	3	99.85	100.00	0.15
230	2256	2256	0	0	100.00	100.00	0.00
231	1571	1571	0	0	100.00	100.00	0.00
232	1780	1769	4	7	99.61	99.77	0.62
233	3079	3075	0	4	99.87	100.00	0.13
234	2753	2753	0	0	100.00	100.00	0.00
Total	**109496**	**109258**	**67**	**171**	**99.85**	**99.94**	**0.21**
	Sum						

Moreover, the obtained statistical metrics (Se, P+, and Fd) are used by most well known ECG waves detection methods proposed in literature as the base rules to prove the robustness of these methods to provide accurate detection by comparing them with the corresponding metric values obtained by other detection methods using the same set of ECG records. The simulation results of (Se, P+, and Fd) obtained by applying the

proposed RFEM approach on 48 ECG records from MIT-BIH DB and eight other QRS detection methods are illustrated in Table 4.3. The validation results in this table show that the RFEM approach has the lowest Fd percentage: according to the minimum number of FN and FP beats obtained which proves the delineation accuracy provided by this approach. Moreover, the highest percentage of P^+ was performed by the RFEM approach, which reflects the ability of this approach to minimize false positive beats, while the Se percentage obtained by the RFEM approach was compatible (with slightly improvement) to those in other methods proposed in literature for QRS complex detection.

Table 4.3: Simulation Results of Statistical Metrics (Se, P^+, and Fd) obtained by Proposed RFEM Approach and Other Eight QRS Detection Methods.

Method		TB	TP	FP	FN	Fd(%)	Se(%)	P^+(%)
RFEM (Proposed Approach)		109496	109258	67	171	0.21	99.85	99.94
Wavelet-Based ECG Delineator (J. P. Martínez et al., 2004)		109428	109208	153	220	0.34	99.80	99.88
Automatic Detection of ECG waves by PT (A. Martínez et al., 2010)		109428	109111	35	317	0.32	99.71	99.97
QRS Detection using EMD (Hadj Slimane & Naït-Ali, 2010)		110050	109792	84	174	0.24	99.84	99.92
QRS detection using combined adaptive threshold (Christov, 2004)	Algo.1	110050	109548	215	294	0.42	99.69	99.66
	Algo.2	110050	109616	239	240	0.44	99.74	99.65
KNN algorithm (Saini et al., 2013)		109966	109608	151	207	0.33	99.81	99.86
QRS Detection using S-Transform & Shannon Energy (Z Zidelmal et al., 2014)		108494	108323	97	171	0.25	99.84	99.91
Wavelet Coefficients based QRS Detection (Zahia Zidelmal et al., 2012)		109494	109101	193	393	0.54	99.64	99.82

Finally, as mentioned in Chapter 3 Section 3.3.1, the RFEM approach was designed to track the ECG signal and delineates time characteristics of the QRS complex using a straightforward instantaneous processing algorithm, thus processing the ECG signal becomes faster. The average processing time required to delineate the QRS time characteristics of each ECG record of 10 minutes is about 1.0 to 1.5 seconds. The processing time performed by the RFEM approach is much faster than the times of QRS complex detection methods as illustrated in Table 4.4.

Table 4.4: Comparison of Average Required Time of Processing ECG Signal Using Proposed RFEM Approach and Other Three QRS Complex Detection Methods.

#	Method	Validation ECG Data	Based Technique	Processing time of 10 min ECG signal
1	RFEM (Proposed Approach)	48 records from MIT-BIH Arrhythmia Database	New straight forward algorithm	1 – 1.5 s
2	DOM (Yeh & Wang, 2008)		Difference equation operation between current and previous ECG beat	30 s
3	Detection of ECG characteristics points using WT (Li et al., 1995)		Multi-scale feature extraction of WT	60 s
4	R_{PEAK} Detection by Shannon energy envelope (SEE) (Manikandan & Soman, 2012)		SEE estimator	2.24 s

4.3.2 Performance Analysis of Proposed HSDPTW Approach

Two simulations were conducted to validate the performance of the proposed HSDPTW approach. Both simulations are applied on the ECG records from QTDB. The ECG records in QTDB were selected from seven existing ECG databases; also each ECG record was annotated with onset, peak, and end time locations for P and T waves

as mentioned in Chapter 2 Section 2.3.2.2. The first simulation is performed to evaluate the delineation results of P and T waves graphically using seven ECG records selected randomly from the QTDB in different categories. The second simulation includes the analytic results of the boundaries and the peak time locations in P and T waves which are delineated by HSDPTW using twenty eight ECG records (four ECG records from each category). Finally, the delineation results obtained by HSDPTW is compared with similar results that were obtained by some well known P and T detection methods proposed in literature using the same ECG records to prove the robustness of HSDPTW to delineate accurate time characteristics of P and T waves in comparison with existing methods.

4.3.2.1 Evaluation metrics of P and T waves delineation

The performance evaluation of the proposed HSDPTW approach can be performed by determining four statistical metrics (Se, P^{+}, mean (m), and standard deviation (s)). These four metrics were mostly used by other P and T wave detection methods (Ghaffari et al., 2009; C. Lin et al., 2010; Madeiro et al., 2013; A. Martínez et al., 2010; J. P. Martínez et al., 2004) to evaluate their delineations results. The first two metrics are the same as in the evaluation of the proposed QRS detection approach as mentioned in Section 4.3.1.3.

Other statistical metrics (m and s) are used to determine the time deviation between delineated and annotated time locations of peak and boundaries in P and T waves as defined in Equation 4.10 and 11, respectively. The average values of (m and s) give a clear indication of the accuracy of the proposed detection approach due to its ability to perform peak and boundary time locations closest to the annotation time locations prepared by cardiologists.

$$m = \frac{1}{TP}\sum_{i=1}^{TP}(Xi_{det} - Xi_{ant}) \tag{4.10}$$

$$s = \sqrt{\frac{\sum_{i=1}^{TP}(Xi_{det} - m)^2}{TP}} \tag{4.11}$$

where *Xi* indicates time locations of onset, peak and end time locations in the P and T wave and *TP* is the total number of true detected waves (either P or T waves).

4.3.2.2 Graphical Evaluation of P and T wave Delineation in Various Categories

In this section, a graphical evaluation of onset, peak, and end time locations of both P and T waves has been performed by applying the proposed HSDPTW approach on seven ECG records selected randomly from QTDB (one record from each category). The delineation results of the P and T wave time characteristics for these records are shown in Figure 4.8. All ECG charts in this figure are marked with the corresponding manual annotation time characteristics by cardiologists, the peak time locations are marked with vertical dash-dotted line, while the boundary time locations are marked with the vertical dotted lines. The significant match between the annotated time locations, which are marked by vertical line, and delineated time locations which are represented by small markers in Figure 4.8, prove the ability of the proposed HSDPTW approach to perform accurate time locations of boundaries and peak for P and T waves.

From the selection of ECG records used in this evaluation from different ECG categories, it can be seen the P and T waves in these records have variant shape, amplitude, and wave duration. In addition, the T wave may be inverted in some ECG records. The P wave has tall amplitude in ECG records shown in Figure 4.8.c, e and f,

but normal amplitude in other ECG records except for the ECG record shown in Figure 4.8.f which has low amplitude of the P wave. With respect to the T wave, the ECG records shown in Figure 4.8.a, b, d, and f have tall amplitudes. Additionally, the ECG records shown in Figure 4.8.a, b, d, and f have a wide T wave interval, while the T waves in the ECG records shown in Figure 4.8.g, were inverted. In spite of the previous variation in the different P and T wave parameters, the proposed HSDPTW approach tracks the ECG signal and provides accurate delineation of the boundaries and peak time locations for different ECG P and T wave morphologies.

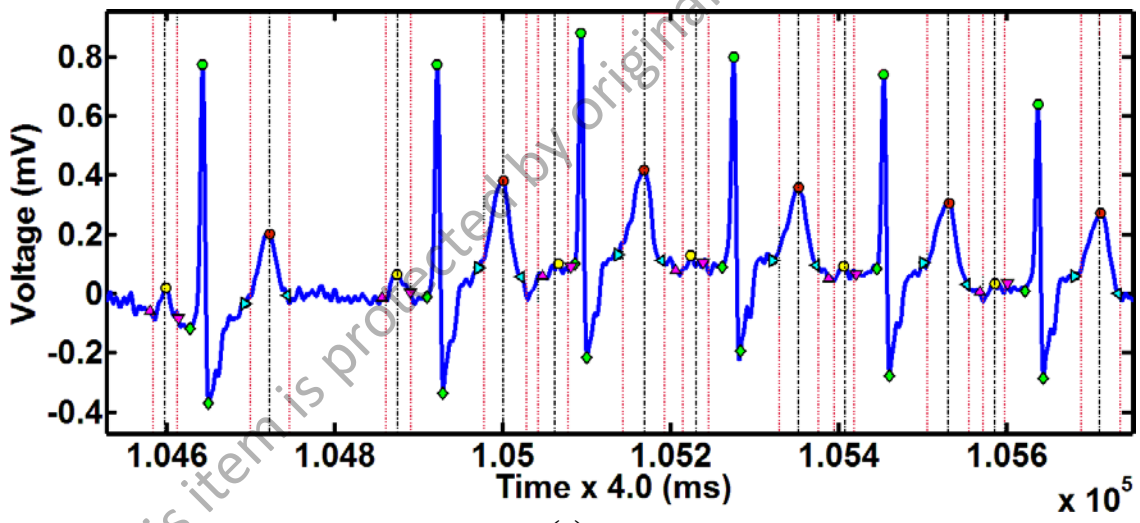

(a)

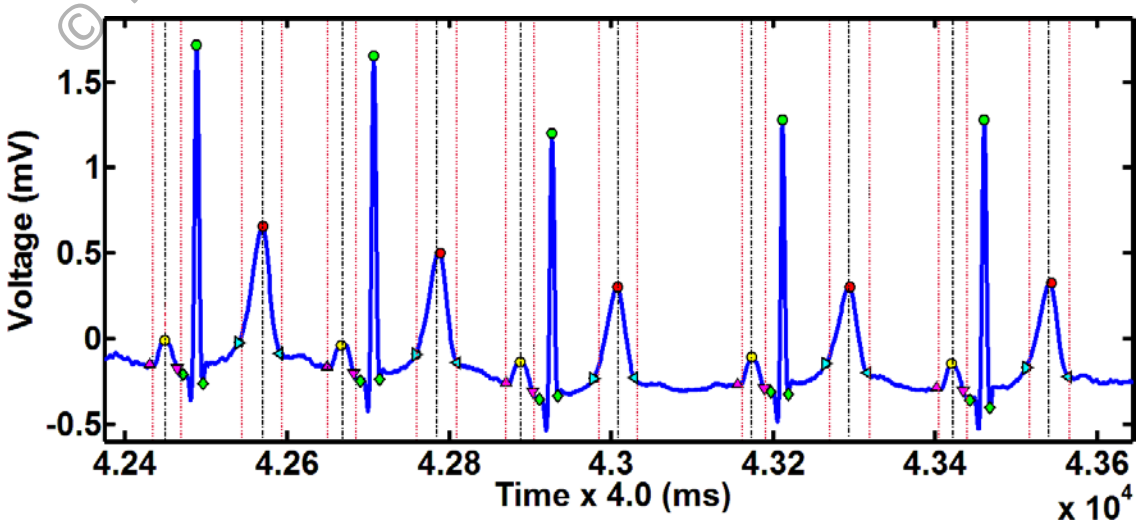

(b)

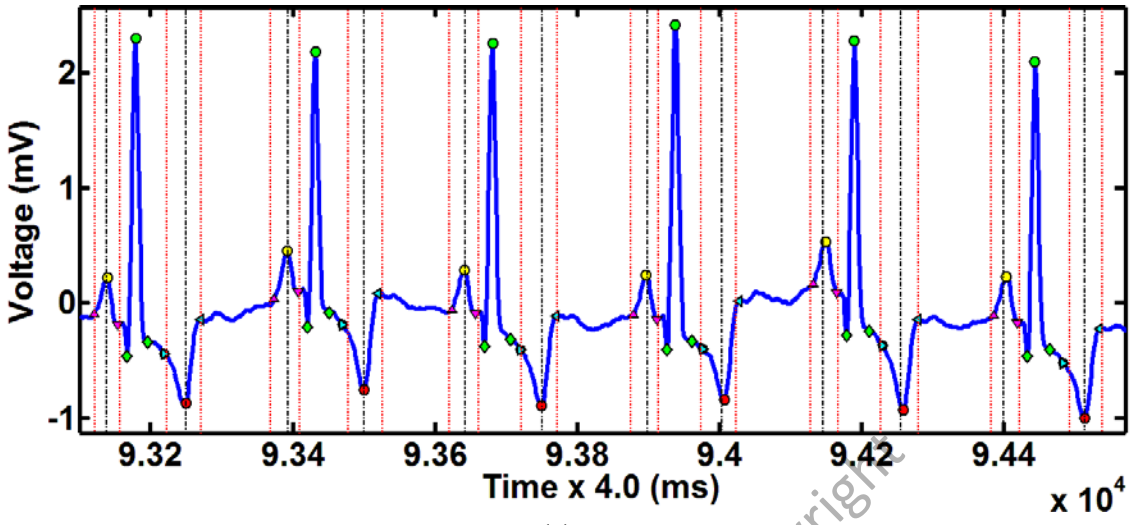

(c)

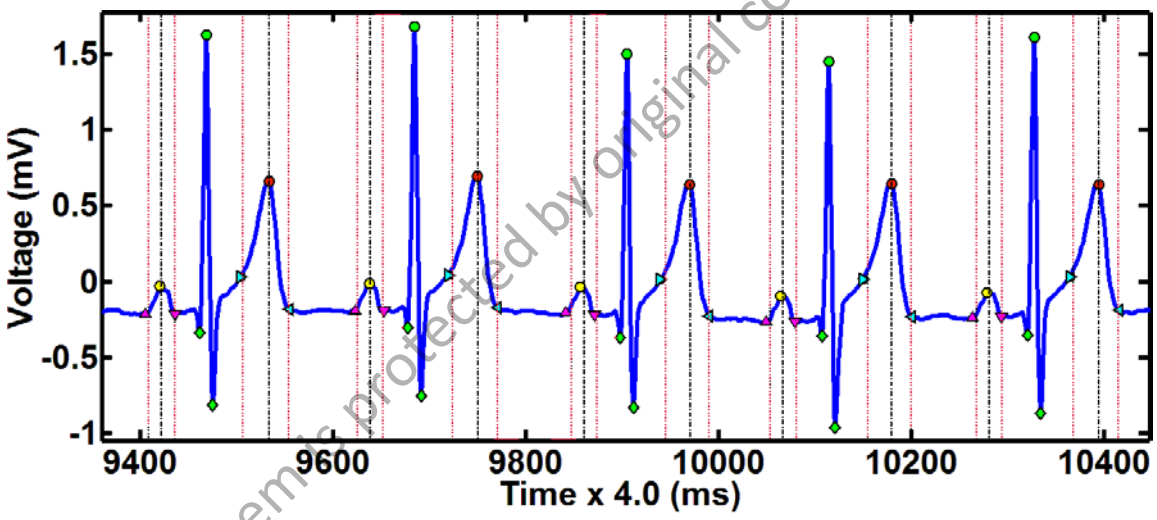

(d)

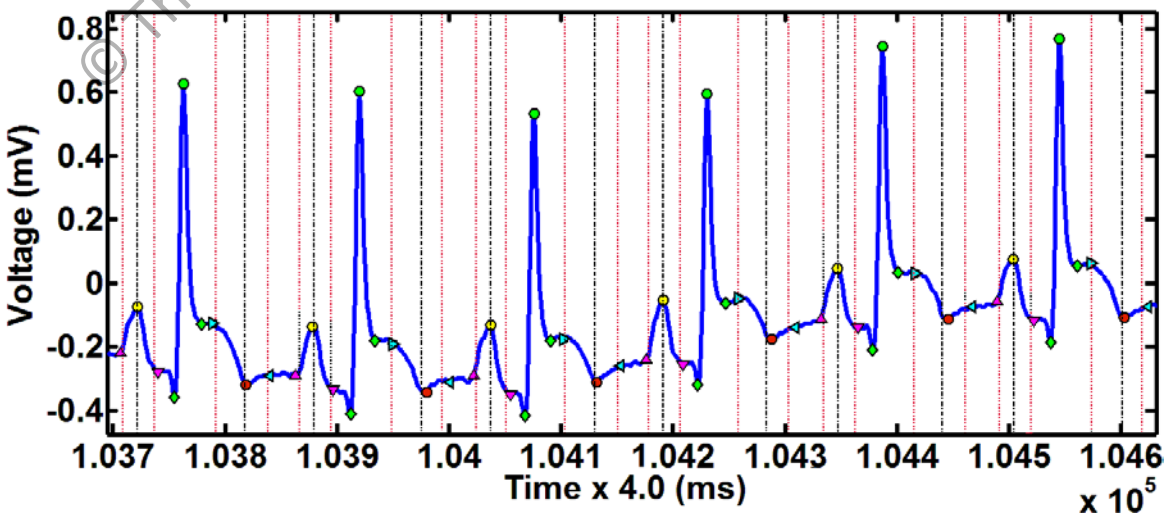

(e)

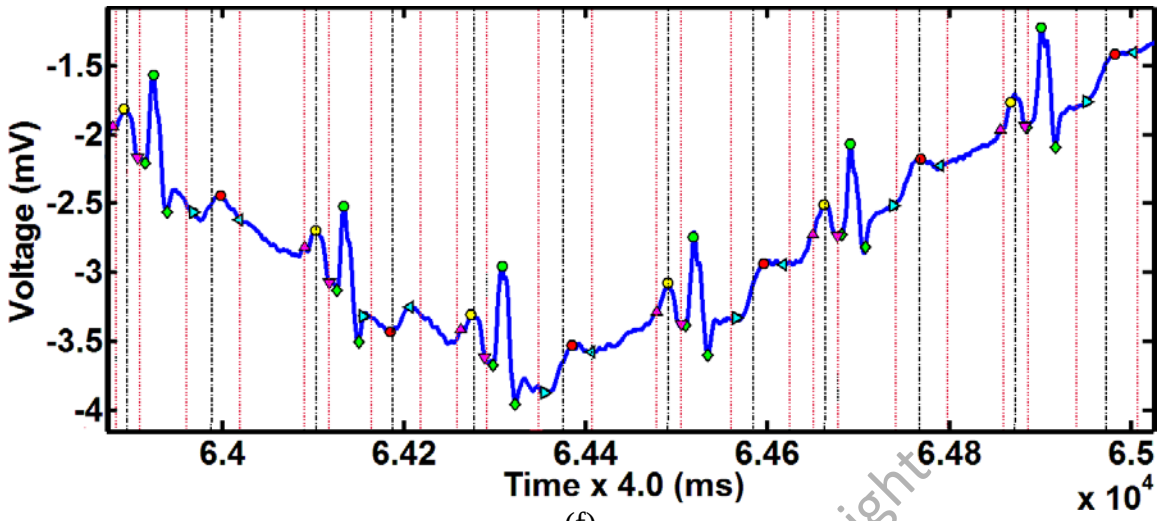

(f)

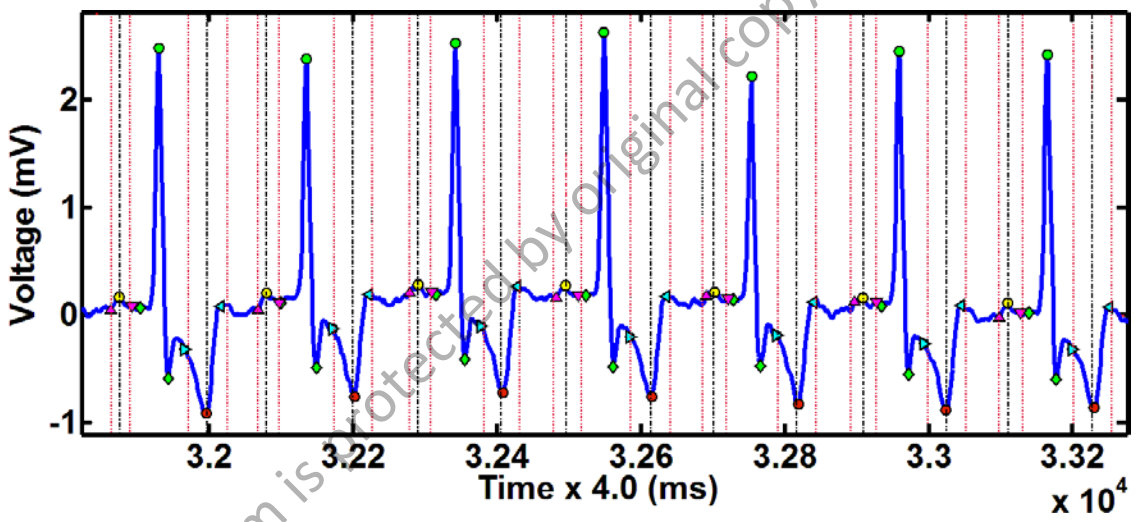

(g)

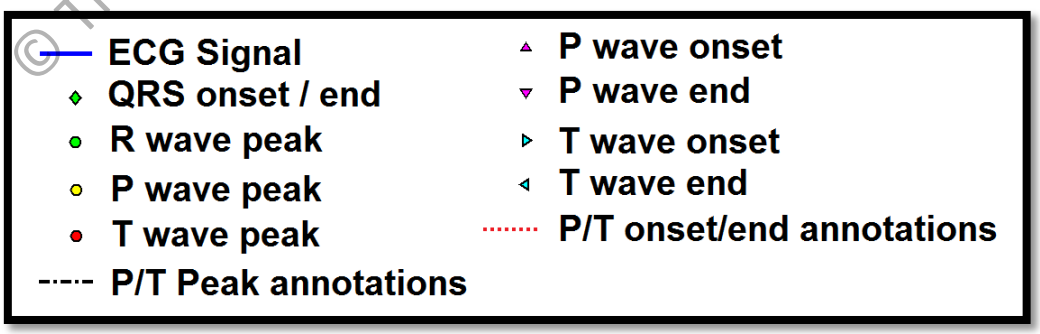

Figure 4.8 Delineation Results of (Onset, Peak, and End) Time Locations of P and T waves in Seven QTDB Records: (a) "SEL-232" Arrhythmia DB, (b) "SEL-307" ST Change DB, (c) "SEL-808" Super Ventricular DB, (d) "SEL-16483" Normal Sinus Rhythm DB, (e) "SEL-122" European ST-T DB, (f) "SEL-39" Sudden Death DB and (g) "SEL-14157" Long-Term DB.

4.3.2.3 Analytical Results of Delineating Time Characteristics in P and T waves

In this section, twenty eight ECG records were processed through the proposed delineation HSDPTW approach, and all delineated (onset, peak, and end) of P and T wave time locations were then evaluated by calculating the statistical metrics mentioned in Section 4.3.2.1 to prove the ability of this approach to perform accurate delineation for all these time characteristics. The selected ECG records were collected from QTDB as four random records from each of the seven categories in QTDB described in Chapter 2 Section 2.3.2.2. The delineation results of the onset, peak, and end) time locations for all twenty eight ECG records are illustrated in Table 4.5.

Table 4.5: Analytical Results of Statistical Metrics (Sensitivity, Specificity, Mean, and Standard Deviation) Obtained by Applying Proposed HSDPTW Delineation Approach on 28 ECG Records From QTDB

D.B	Record	Parameters	P_{ON}	P_{PEAK}	P_{OFF}	T_{ON}	T_{PEAK}	T_{OFF}
MIT-BIH Arrhythmia	SEL 100	Stored Beats	1129			1122		
		FN , FP	0 , 4			0 , 7		
		Se(%) , P+(%)	100 , 99.65			100 , 99.37		
		$m \pm s$ (ms)	-0.8 ± 2.4	-0.8 ± 2.5	-1.9 ± 4.4	-1.2 ± 4.1	0.6 ± 12.7	-6.8 ± 9.9
		P.T (s)	3.35					
	SEL 116	Stored Beats	1019			1183		
		(FN) , (FP)	0 , 3			0 , 2		
		Se(%) , P+(%)	100 , 99.71			100 , 99.83		
		$m \pm s$ (ms)	-4.7 ± 3.6	1.1 ± 3.4	0.5 ± 2.5	-1.6 ± 9.0	1.0 ± 6.1	4.9 ± 8.9
		P.T (s)	3.64					
	SEL 213	Stored Beats	1573			1631		
		(FN) , (FP)	0 , 7			0 , 4		
		Se(%) , P+(%)	100 , 99.56			100 , 99.76		
		$m \pm s$ (ms)	-1.1 ± 2.8	0.1 ± 6.5	4.4 ± 3.2	-0.8 ± 6.2	-0.5 ± 10.3	-1.6 ± 7.5
		P.T (s)	3.48					
	SEL 232	Stored Beats	784			847		
		(FN) , (FP)	0 , 3			0 , 5		
		Se(%) , P+(%)	100 , 99.62			100 , 99.41		
		$m \pm s$ (ms)	-2.2 ± 7.0	-1.8± 9.2	4.2 ± 8.5	-7.8 ± 4.8	1.1 ± 11.0	-4.6 ± 7.3
		P.T (s)	2.24					

Table 4.5: Continued

D.B	Record	Parameters	P_{ON}	P_{PEAK}	P_{OFF}	T_{ON}	T_{PEAK}	T_{OFF}
MIT-BIH ST Change	SEL 301	Stored Beats	1282			1347		
		(FN) , (FP)	0 , 8			0 , 0		
		Se(%) , P+(%)	100 , 99.38			100 , 100		
		m ± *s* (ms)	-6.6 ± 4.5	-1.5 ± 3.4	-3.9 ± 4.2	-4.7 ± 8.3	-0.8 ± 6.5	-0.8 ± 6.8
		P.T (s)	3.35					
	SEL 302	Stored Beats	1497			1499		
		(FN) , (FP)	0 , 0			0 , 0		
		Se(%) , P+(%)	100 , 100			100 , 100		
		m ± *s* (ms)	-3.6 ± 1.9	-2.1 ± 1.5	-0.8 ± 2.1	-2.3 ± 3.6	-1.3 ± 5.5	2.2 ± 3.8
		P.T (s)	3.44					
	SEL 306	Stored Beats	1036			1039		
		(FN) , (FP)	0 , 0			0 , 0		
		Se(%) , P+(%)	100 , 100			100 , 100		
		m ± *s* (ms)	-4.2 ± 2.7	-1.7 ± 1.9	-3.7 ± 2.6	-4.6 ± 1.6	-0.2 ± 1.1	1.9 ± 1.2
		P.T (s)	3.27					
	SEL 308	Stored Beats	1202			1289		
		(FN) , (FP)	0 , 15			0 , 14		
		Se(%) , P+(%)	100 , 98.77			100 , 98.93		
		m ± *s* (ms)	-4.5 ± 7.2	-4.1 ± 6.8	-1.9 ± 5.8	-2.4 ± 5.1	-0.5 ± 7.0	-1.6 ± 5.0
		P.T (s)	3.26					
MIT-BIH Super ventricular Arrhythmia	SEL 803	Stored Beats	953			1025		
		(FN) , (FP)	4 , 8			0 , 9		
		Se(%) , P+(%)	99.58 , 99.16			100 , 99.12		
		m ± *s* (ms)	-4.7 ± 3.1	1.1 ± 2.3	2.2 ± 1.3	-2.1± 3.7	0.7 ± 5.6	-0.2 ± 3.4
		P.T (s)	3.39					
	SEL 811	Stored Beats	747			755		
		(FN) , (FP)	0 , 15			0 , 14		
		Se(%) , P+(%)	100 , 98.77			100 , 98.93		
		P.T (s)	-2.5 ± 3.1	1.5 ± 2.6	1.5 ± 2.3	-0.6 ± 1.9	-1.3 ± 2.9	-1.0 ± 2.3
		P.T (s)	2.13					
	SEL 821	Stored Beats	1447			1550		
		(FN) , (FP)	0 , 12			0 , 15		
		Se(%) , P+(%)	100 , 99.17			100 , 99.04		
		m ± *s* (ms)	-3.8 ± 9.2	-1.1 ± 7.4	5.4 ± 7.7	-3.2 ± 7.3	2.5 ± 4.8	4.7 ± 2.8
		P.T (s)	2.28					
	SEL 853	Stored Beats	988			1110		
		(FN) , (FP)	0 , 4			0 , 2		
		Se(%) , P+(%)	100 , 99.59			100 , 99.82		
		m ± *s* (ms)	-2.0 ± 5.3	0.8 ± 3.8	1.9 ± 6.9	-8.9 ± 6.8	-0.4 ± 2.0	-1.6 ± 6.1
		P.T (s)	2.22					

Table 4.5: Continued

D.B	Record	Parameters	P_{ON}	P_{PEAK}	P_{OFF}	T_{ON}	T_{PEAK}	T_{OFF}
MIT-BIH Normal Sinus Rhythm	SEL 16265	Stored Beats	712			1030		
		(FN) , (FP)	0 , 0			0 , 0		
		Se(%) , P+(%)	100 , 100			100 , 100		
		m ± *s* (ms)	0.5 ± 1.0	0.7 ± 0.8	0.8 ± 3.5	-0.6 ± 6.4	0.2 ± 0.9	-0.7 ± 1.3
		P.T (s)	2.17					
	SEL 16273	Stored Beats	818			1110		
		(FN) , (FP)	0 , 0			0 , 0		
		Se(%) , P+(%)	100 , 100			100 , 100		
		m ± *s* (ms)	-0.03 ± 1.3	0.5 ± 0.7	1.3 ± 1.4	-4.2 ± 1.9	-0.2± 0.7	0.8 ± 1.9
		P.T (s)	2.06					
	SEL 16483	Stored Beats	1085			1084		
		(FN) , (FP)	0 , 6			0 , 7		
		Se(%) , P+(%)	100 , 99.45			100 , 99.35		
		m ± *s* (ms)	3.9 ± 1.4	-2.7 ± 1.5	1.2 ± 0.3	-0.9 ± 1.2	0.3 ± 0.5	-0.1 ± 0.7
		P.T (s)	3.5					
	SEL 16795	Stored Beats	759			759		
		(FN) , (FP)	0 , 0			0 , 0		
		Se(%) , P+(%)	100 , 100			100 , 100		
		m ± s (ms)	-12.3 ± 2.5	-7.7 ± 2.3	-6.7 ± 2.4	-4.8 ± 1.3	0.3 ± 0.5	-1.9 ± 0.8
		P.T (s)	3.44					
European ST-T	SEL 0106	Stored Beats	894			858		
		FN , FP	0 , 3			0 , 4		
		Se(%) , P+(%)	100 , 99.33			100 , 99.53		
		m ± *s* (ms)	-7.1 ± 1.2	4.2 ± 1.3	9.9 ± 2.2	-3.8 ± 4.4	7.1 ± 5.6	6.0 ± 4.5
		P.T (s)	3.25					
	SEL 0122	Stored Beats			1412			1412
		(FN) , (FP)	0 , 12			0 , 10		
		Se(%) , P+(%)	100 , 99.15			100 , 99.29		
		m ± *s* (ms)	5.4 ± 1.1	3.4 ±1.0	14.2 ±1.0	3.8 ± 10.7	13.9 ± 16.6	13.8 ± 12.3
		P.T (s)	3.6					
	SEL 0509	Stored Beats	1001			1025		
		(FN) , (FP)	0 , 10			0 , 10		
		Se(%) , P+(%)	100 , 99.01			100 , 99.03		
		m ± *s* (ms)	-1.9 ± 7.1	-3.0 ± 8.2	3.3 ± 7.2	-0.7 ± 3.1	2.5 ± 1.6	4.3 ± 1.8
		P.T (s)	3.43					
	SEL 0612	Stored Beats	749			749		
		(FN) , (FP)	0 , 9			0 , 10		
		Se(%) , P+(%)	100 , 98.81			100 , 98,68		
		m ± *s* (ms)	-0.7 ± 4.2	-0.4 ± 6.5	4.8 ± 6.2	-0.1 ± 3.4	0.7 ± 3.2	-0.8 ± 3.4
		P.T (s)	3.47					

Table 4.5: Continued

D.B	Record	Parameters	P_{ON}	P_{PEAK}	P_{OFF}	T_{ON}	T_{PEAK}	T_{OFF}
BIH Sudden Death Patients	SEL 34	Stored Beats	582			896		
		(FN) , (FP)	0 , 2			0 , 12		
		Se(%) , P+(%)	100 , 99.65			100 , 98.67		
		m ± *s* (ms)	-3.0 ± 2.9	-2.2 ± 2.4	2.9 ± 2.5	-0.4 ±10.5	0.2 ± 6.4	1.03 ± 9.5
		P.T (s)	2.21					
	SEL 39	Stored Beats	1147			1162		
		(FN) , (FP)	0 , 8			0 , 11		
		Se(%) , P+(%)	100 , 99.30			100 , 99.06		
		m ± *s* (ms)	-2.1 ± 4.5	-1.3 ± 3.7	0. 8 ± 2.7	4.8 ± 10.6	4.4 ± 10.8	-5.9 ± 8.3
		P.T (s)	2.43					
	SEL 48	Stored Beats	1335			1394		
		(FN) , (FP)	0 , 0			0 , 0		
		Se(%) , P+(%)	100 , 100			100 , 100		
		m ± *s* (ms)	1.3 ± 3.3	-1.5 ± 2.8	0.7 ± 3.1	7.2 ± 10.7	0.8 ± 6.8	1.6 ± 7.9
		P.T (s)	2.38					
	SEL 17152	Stored Beats	1625			1615		
		(FN) , (FP)	4 , 10			6 , 11		
		Se(%) , P+(%)	99.75 , 99.35			99.62 , 99.32		
		m ± *s (ms)*	-9.6 ± 5.5	-5.7 ± 5.8	0.5 ± 5.4	1.9 ± 8.4	11.7 ±11.3	13.6 ±10.9
		P.T (s)	2.39					
MIT-BIH Long Term ECG	SEL 14046	Stored Beats	1230			1256		
		(FN) , (FP)	0 , 11			0 , 25		
		Se(%) , P+(%)	100 , 99.11			100 , 98.04		
		m ± *s* (ms)	-2.7 ± 2.6	-0.9 ± 1.9	-0.7 ± 2.2	-4.2 ± 6.5	1.4 ± 5.5	11.8 ± 7.7
		P.T (s)	2.19					
	SEL 14157	Stored Beats	910			1079		
		(FN) , (FP)	0 , 12			0 , 21		
		Se(%) , P+(%)	100 , 98.69			100 , 98.08		
		m ± *s* (ms)	-2.1 ± 3.01	-1.9 ± 3.03	-4.06 ± 5.3	-0.1 ± 5.3	0.9 ± 4.6	8.9 ± 9.9
		P.T (s)	2.13					
	SEL 14172	Stored Beats	659			637		
		(FN) , (FP)	0 , 12			0 , 15		
		Se(%) , P+(%)	100 , 98.21			100 , 97.69		
		m ± *s* (ms)	-4.3 ± 1.6	-2.4 ± 1.1	-11.1 ± 2.1	0.7 ± 3.8	-5.4 ± 8.7	-0.9 ± 5.8
		P.T (s)	2.12					
	SEL 15814	Stored Beats	1006			1024		
		(FN) , (FP)	0 , 10			0 , 15		
		Se(%) , P+(%)	100 , 99.01			100 , 98.55		
		m ± *s (ms)*	-2.2 ± 1.7	-0.9 ± 1.1	-0.3 ± 1. 8	1.4 ± 5.5	-0.2 ± 1.8	-3.4 ± 3.5
		P.T (s)	2.17					
Average Se, P+ (%)			99.97 , 99.36			99.98 , 99.26		
Average *m* ± *s* (ms)			-3.0 ± 2.9	-0.7 ± 4.4	0. 7 ± 4.6	-3.3 ± 4.9	0.2 ± 5.4	-0.4 ± 5.7
Average Processing Time (s)			2.745					

As mentioned in Chapter 3 Section 3.3.2, the proposed HSDPTW approach to delineate time characteristics of P and T waves requires previous delineating of the QRS complex time locations, thus certain QRS detection method must be applied first. The proposed QRS detection RFEM approach mentioned in Chapter 3 Section 3.2 with an overall detection result of $Se = 99.95\%$ and $P^{+} = 99.97\%$ is considered for the QRS subject detection. The validation results presented in Table 4.5 prove that the proposed HSDPTW approach performs significant average Se (99.97% and 99.98%) for P and T wave, respectively which proves the ability of HSDPTW to minimize the probability of detecting false negatives waves. Moreover, at a high degree, the proposed HSDPTW approach has a good average P^{+} (99.36 % and 99.26%) for P and T wave detection, respectively. This relative decline comes from missing some P and T waves in the QTDB annotated data file in spite of the existence of these waves in the tested ECG signal and confirmation by site cardiologists. Therefore, these missing waves were detected as false positive waves (FP) which leads to a decreasing percentage of P^{+}. Continuously, the robustness of HSDPTW to delineate accurate time locations of peak and boundaries that are closest to those annotated manually by cardiologists can be proved through the average time deviation expressed by m which does not exceed one ECG sample (4 ms) as well as the average s (5 ms) for the P wave (6 ms) for the T wave. The resulting s and m values are satisfactory due to the huge size of the ECG signals with different categories.

The instantaneous processing based technique followed by the detection algorithms in HSDPTW to delineate the time characteristics of P and T wave and the simple mathematical calculations were implemented inside these algorithms. As a result, the average processing time required to perform the complete delineation of peak and boundary time locations in the P and T wave is about 2.745 s for a 15 minute

recording (about 225,000 ECG beats) as illustrated in Table 4.5. Furthermore, the processing time (P.T) required by HSDPTW to perform a complete delineation of the P and T wave in each of the 28 ECG records used to validate the proposed approach is presented in the same table. The processing time in all ECG records was obtained by a MATLAB implementation on a 2.1-GHz Core-i3 of (4GB RAM).

4.3.2.4 Validation of Proposed HSDPTW Approach

In this section, the performance of the proposed HSDPTW approach is evaluated by comparing the statistical evaluation metrics (Se, P+, m, and s) of the onset, peak, and end time locations in the P and T wave obtained by the proposed approach using the ECG records from QTDB with the corresponding metrics obtained from five PT detection methods (Ghaffari et al., 2009; C. Lin et al., 2010; Madeiro et al., 2013; A. Martínez et al., 2010; J. P. Martínez et al., 2004) proposed in literature using the same ECG database. The validation results presented in Table 4.6 demonstrate the effectiveness of the HSDPTW to delineate onset, peak and end time locations of the P and T waves with significant accuracy through a higher percentage of Se and P^+ with respect to the other detection methods considered for validation.

Through the average values of m and s illustrated in Table 4.6, the time deviations determined by the peak time locations in P and T wave are more accurate than those for the boundary (onset and end) time locations. In other words, the proposed delineation approach successfully performs exact computations of the peak time location, while for the onset and end time locations; it provides an approximation in some cases due the various shapes of the end points in ECG waves for different categories. However, the average values for m and s are higher than 4 with respect to the up-to-date detection methods considered for validation.

Table 4.6: Comparison the Statistical Metrics (Se, P^+, m, and s) of the Delineated Onset, Peak, and End Time Locations in P and T wave Obtained by the Proposed HSDPTW Approach and Other Five Detection Methods Using ECG Records From QTDB, (N/A: not applicable, N/R: not reported)

Method	Statistical Metrics	P_{ON}	P_{PEAK}	P_{OFF}	T_{ON}	T_{PEAK}	T_{OFF}
HSDPTW *(Proposed work)*	*Se(%)*	99.97	99.97	99.97	99.98	99.98	99.98
	P^+(%)	99.36	99.36	99.36	99.26	99.26	99.26
	m ± s	-3.0 ± 2.9	-0.7 ± 4.4	0. 7 ± 4.6	-3.3 ± 4.9	0.2 ±5.4	-0.4 ± 5.7
Automatic Delineation by PT (A. Martínez et al., 2010)	*Se(%)*	98.65	98.65	98.65	N/A	99.20	99.20
	P^+(%)	97.52	97.52	97.52	N/A	99.01	99.01
	m ± s	2.6 ± 14.5	32 ± 25.7	0.7 ±14.7	N/A	5.3 ±12.9	5.8 ± 22.7
ECG waves detection by Bayesian Approach and PCGS (C. Lin et al., 2010)	*Se(%)*	98.93	98.93	98.93	99.01	99.81	99.81
	P^+(%)	97.40	97.40	97.40	96.07	98.97	98.97
	m ± s	3.7 ± 17.3	4.1 ± 8.6	4.1 ± 8.6	7.1±18.5	1.3 ±10.5	4.3± 20.8
T wave Detection by skewed Gaussian function(Madeiro et al., 2013)	*Se(%)*	N/R	N/R	N/R	N/R	99.32	99.32
	P^+(%)	N/R	N/R	N/R	N/R	99.47	99.47
	m ± s	N/R	N/R	N/R	N/R	1.4 ± 9.0	2.8 ±15.3
Detection of P and T wave in Multi-ECG Lead using DWT (Ghaffari et al., 2009)	*Se(%)*	99.46	99.46	99.46	99.87	99.87	99.87
	P^+(%)	98.83	98.83	98.83	99.80	99.80	99.80
	m ± s	-1.2 ± 6.3	4.1±10.5	0.7 ± 6.8	-1.4 ± 5.7	0.3±4.1	0.8 ± 10.9
A Wavelet-Based ECG Delineator (J. P. Martínez et al., 2004)	*Se(%)*	98.87	98.87	98.87	N/A	99.77	99.77
	P^+(%)	91.03	91.03	91.03	N/A	97.79	97.79
	m ± s	2.0 ±14.8	3.6 ±13.2	1.9 ±13.8	N/A	0.2 ±13.9	-1.6 ±18.1

4.4 Performance Evaluation of LVH Cardiac Disease Diagnosis

In this section, the performance of proposed approach presented in Chapter 3 Section 3.4.1.4 of the diagnosis of LVH cardiac disease is evaluated by applying this approach on 50 ECG records which were pre-diagnosed by cardiologists. The ability of this approach to provide accurate diagnosis results is evaluated by calculating three statistical metrics (sensitivity, specificity, and accuracy). Additionally, the simulation

results of these metrics are validated with the corresponding results obtained by well-known LVH diagnostic criteria proposed in literature.

4.4.1 Selection of Tested ECG Data for Diagnosing LVH Cardiac Disease

The process of selecting suitable ECG data for the proposed diagnosis system is a more difficult issue due to the limited resources of 12-lead ECG data with specific cardiac disease especially high risk cardiac diseases like LVH. Thus, only 50 12-lead ECG records were selected to validate performance of the proposed diagnosing approach. The first group of tested data includes 34 ECG records which were collected from the INCART database, whereas most ECG records in this database were diagnosed manually by cardiologists as mentioned in Chapter 2 Section 2.3.2.3. The selected records include 11 patients that suffered from LVH cardiac disease and other patients with different cardiac diseases such as Acute Myocardial Infarction (AcMI), Transient Ischemic Attack (TIA), Ventricular Bigeminy (VBG), Atrioventricular nodal block (AVNB), Sinus Node Dysfunction (SND), Atrial Fibrillation (AF), Premature Ventricular Contractions (PVCs), Earlier Myocardial Infarction (EarMI), WPW, and ST elevation (STele). The second group of tested data includes 26 ECG records which were reconstructed using the proposed digital recovery approach presented in Chapter 3 Section 3.2.2.1; the printed charts of these records were collected from three cardiology references (Azeem et al., 2005; Hampton, 2013; Jenkins & Gerred, 2011). The reconstructed ECG data includes 10 records with LVH cardiac disease and 11 records of normal patients.

4.4.2 Quantitative Evaluation of Diagnosing Process

The quantitative evaluation of the proposed diagnosis approach can be performed by computing three statistical metrics which are mostly used to evaluate the performance of different approaches of diagnosing cardiac diseases based on ECG analysis using various computerized intelligent systems (Chang et al., 2012; Han & Kamber, 2006; Jager, Moody, Taddei, & Mark, 1991). The first metric is sensitivity which is also used to evaluate ECG wave detection as mentioned in Section 4.3.1.3. The same mathematical relation defined in Equation 4.7 is used to determine diagnosis sensitivity but the computed parameters for this relation have different concepts. Where, TP denotes the total number of true positive diagnosis (LVH was present and was diagnosed), and FN stands for false negative diagnosis (LVH was present but was not diagnosed).

The second metric is specificity which is defined by Equation 4.12, where TN denotes the total number of true negative diagnosis (LVH was not present and was not diagnosed), and FP stands for the false positive diagnosing (LVH was not present but was diagnosed).

$$Specificity = \frac{TN}{TN + FP} \times 100\% \tag{4.12}$$

The last considered metric for this evaluation is the accuracy of the diagnosis which is defined in Equation 4.13. The computed accuracy describes the overall performance of the diagnosis approach because it considers the positive (true and false) as well as negative (true and false) events.

$$Accuracy = \frac{TN + TP}{TP + FP + FN + TN} \times 100\% \quad (4.13)$$

4.4.3 Analytical Results of Proposed LVH Diagnosing Approach

In this section, the proposed approach of diagnosing LVH cardiac disease is applied on the 50 ECG records mentioned in the previous section. Each of these records includes standard 12 leads of ECG signal.

The first step of this implementation process is to determine eleven ECG voltage parameters required to compute (MDV, Expr1 and Expr2) that are mentioned in Chapter 3 Section 3.4.1.4. As, all these parameters are related to QRS complex characteristics, either voltage amplitude of the R or S wave, a certain method of QRS detection is needed to delineate these characteristics. The proposed RFEM approach of QRS detection mentioned in Chapter 3 Section 3.3.1 is considered to delineate time locations of R and S waves, and then to determine the required voltage parameters for three diagnostic expressions (MDV, Expr1 and Expr2). The simulation results of eleven voltage parameters as well as the corresponding proposed decision values obtained by MDV expression for the 50 ECG records which were selected previously as the tested data for the proposed diagnosis process are illustrated in Table 4.7.

The final decision related to the diagnosis of LVH cardiac disease is obtained by a logical value defined in Chapter 3 Section 3.4.1.2 Equation 3.22. This relation represents the proposed diagnostic criterion of diagnosing LVH cardiac disease which is integrated using the proposed FIS shown in Chapter 3 Section 3.4.1.4 Figure 3.13. The results of diagnosing LVH cardiac disease obtained by the proposed approach and nine

traditional diagnostic criteria (Sokolow, Cornell voltage, REC-CRT, and CRTA1 ... CRTA6) described in Chapter 3 Section 3.4.1.1 are illustrated in Table 4.8.

Table 4.7: The ECG Voltage Parameters of the LVH Diagnostic Criteria and MDV values of the Proposed Diagnostic Criterion

#	Record	Gender	Pre-Diagnosed Cardiac Disease	Voltage Parameters											MDV
				R(I)	S(III)	S(aVR)	R(aVL)	R(aVF)	S(V1)	S(V2)	S(V3)	R(V4)	R(V5)	R(V6)	
1	I01	F	AHT	10.1	12.3	9.4	5.7	12.2	5.1	7.2	11.9	13.6	11.1	11.1	59.4
2	I02	F	AHT	12.7	9.8	8.7	6.6	9.7	6.8	8.1	11.7	14.9	10.5	N.A	45.8
3	I05	M	AcMI	2.6	4.9	1.8	2.8	2.4	7.9	9.0	9.0	15.3	15.7	9.6	52.1
4	I10	F	AVNB	12.2	2.7	9.4	9.1	4.6	10.7	11.6	10.6	5.1	10.3	12.6	46.9
5	I11	M	AVNB	8.9	5.4	8.7	5.7	6.5	9.6	7.9	8.3	5.4	9.5	10.4	44.1
6	I15	M	TIA	4.6	12.9	10.5	6.9	16.9	11.5	12.0	14.7	3.2	15.9	18.9	76.9
7	I17	M	TIA	3.4	4.7	5.2	1.2	3.4	11.7	13.0	16.9	14.9	5.6	6.5	46.6
8	I20	F	LVH	4.7	15.8	12.0	6.8	17.8	10.6	9.1	13.4	10.2	17.6	15.4	79.3
9	I21	F	LVH	2.0	17.6	10.3	8.9	18.8	9.2	8.9	11.3	11.9	16.5	14.0	78.2
10	I22	F	LVH	4.3	13.3	18.2	17.1	33.9	13.0	23.0	39.2	27.9	26.3	20.2	128.0
11	I24	M	EarMI	1.9	8.0	7.8	3.7	8.2	5.3	23.8	16.7	16.8	5.0	3.0	51.4
12	I26	F	SND	4.3	5.1	5.7	1.6	6.3	9.0	7.8	11.0	7.1	15.5	14.2	55.3
13	I28	M	PVCs	1.2	15.9	8.7	7.2	14.8	7.8	16.1	13.3	16.0	35.5	17.0	102.4
14	I32	F	VBG	1.1	6.6	4.1	1.3	4.1	5.1	4.8	5.7	1.9	7.1	10.8	35.32
15	I33	M	PVCs	4.3	10.7	8.6	4.1	12.4	11.9	23.8	20.9	9.7	12.0	12.0	73.95
16	I35	F	LVH	8.6	50.4	25.4	24.5	47.2	18.9	26.0	64.9	39.9	40.1	76.6	265.4
17	I36	F	LVH	8.5	27.8	18.9	10.9	26.1	19.1	18.3	34.8	17.8	29.3	49.9	165.1
18	I37	F	LVH	8.8	43.9	24.2	21.0	39.2	14.5	25.3	55.3	39.8	33.5	61.9	226.3
19	I40	M	TIA	5.9	4.2	7.2	4.2	3.6	5.2	8.3	9.7	12.1	15.9	12.1	51.74
20	I41	M	TIA	3.5	5.5	4.7	3.5	1.1	3.7	6.2	14.2	16.8	28.1	19.7	74.38
21	I44	F	LVH	6.8	44.3	23.3	23.7	43.5	12.8	20.4	25.4	31.7	28.6	19.8	159.6
22	I45	F	LVH	5.1	42.4	21.4	19.8	38.6	12.8	14.7	21.8	32.3	26.9	17.8	147.1
23	I46	F	LVH	5.3	39.4	19.3	18.9	35.4	10.9	13.6	24.7	28.9	23.5	15.2	134.9
24	I50	M	AF	8.8	6.7	11.7	3.0	9.8	10.9	16.2	13.5	10.0	12.4	10.5	59.7
25	I55	M	EarMI	12.0	23.3	6.0	16.7	14.9	12.0	7.6	18.0	13.4	8.6	6.2	71.1
26	I56	M	EarMI	5.9	14.0	3.8	10.1	10.9	7.7	4.2	12.7	13.3	5.2	3.8	47.5
27	I58	F	AHT	6.7	5.2	7.9	1.5	8.2	7.1	5.0	4.5	N.A	9.2	10.2	36.9
28	I60	F	STelv	7.9	15.5	14.6	5.3	11.8	6.3	4.9	8.3	8.7	16.6	16.7	68.7

Table 4.7: Continued

#	Record	Gender	Pre-Diagnosed Cardiac Disease	Voltage Parameters											MDV
				R(I)	S(III)	S(aVR)	R(aVL)	R(aVF)	S(V1)	S(V2)	S(V3)	R(V4)	R(V5)	R(V6)	
29	I68	M	WPW	9.8	15.7	4.9	12.4	2.0	8.4	11.7	15.1	10.4	10.6	6.2	56.3
30	I69	M	PVCs	5.9	20.5	12.5	6.6	7.9	6.1	8.7	18.0	16.7	21.2	13.7	84.0
31	I70	M	WPW	8.5	8.4	11.7	3.5	11.8	13.7	27.5	7.9	11.4	17.2	16.8	78.4
32	I71	M	WPW	7.3	8.2	10.1	1.6	10.8	13.7	11.7	8.7	8.6	15.2	16.7	66.8
33	I72	M	LVH	7.7	66.0	41.9	10.3	31.1	35.3	22.7	42.4	12.7	31.2	22.5	191.9
34	I73	M	LVH	5.8	41.9	17.1	21.5	37.3	4.7	8.2	26.0	22.0	11.9	46.0	148.8
35	H1	M	LVH	10.7	17.0	17.1	9.1	22.9	9.6	27.1	28.6	21.4	34.3	29.8	135.9
36	P72	M	LVH	35.0	22.2	24.0	25.0	7.5	22.5	9.0	24.5	24.2	23.5	22.0	111.6
37	P73	M	LVH	27.0	11.5	18.0	19.0	31.0	21.5	25.4	31.3	16.0	42.0	43.0	159.1
38	P74	M	Normal	11.3	4.5	11.3	7.5	3.5	12.3	22.5	13.1	21.0	22.5	20.0	83.18
39	P75	F	Normal	7.3	4.5	8.8	2.1	8.0	11.0	9.5	10.5	13.3	12.5	9.5	52.63
40	R40	F	LVH	8.8	12.8	14.6	2.8	19.3	28.8	36.1	31.4	18.5	23.4	14.4	117.6
41	R85	M	LVH	17.1	3.2	14.7	12.3	9.9	23.6	27.9	25.1	29.4	36.1	35.2	132.6
42	W1	F	Normal	6.5	2.2	5.7	4.2	2.8	9.8	23.3	16.5	3.8	6.7	7.3	44.33
43	W2	M	LVH	15.3	15.8	16.9	14.7	7.9	18.5	19.6	14.8	16.1	31.9	23.3	109.5
44	W3	F	LVH	7.5	6.2	6.6	6.6	6.3	19.1	22.4	16.8	23.1	32.1	15.2	97.25
45	W4	F	LVH	12.3	3.5	9.5	9.0	3.9	13.8	29.8	31.6	6.9	18.8	16.4	81.67
46	W5	M	LVH	15.5	14.6	11.3	15.8	13.5	11.9	14.9	11.9	18.8	28.9	27.3	106.4
47	W6	F	LVH	13.5	3.7	13.3	5.5	9.5	13.9	14.3	14.2	16.9	27.2	23.3	88.56
48	W7	F	Normal	4.8	3.6	4.7	2.1	4.3	6.5	14.3	17.6	7.1	13.4	10.7	52.5
49	W8	M	Normal	10.8	13.6	5.6	12.3	2.4	10.3	25.3	25.8	13.9	10.3	6.4	69.08
50	W9	F	Normal	11.4	6.8	7.6	8.9	3.2	14.8	24.8	24.3	9.3	11.1	12.8	68.87

The validation results of diagnosing LVH cardiac disease illustrated in Table 4.8 show that some ECG records are diagnosed manually with LVH cardiac disease. However, the determined diagnosis about LVH cardiac disease is not verified (i.e. false negative diagnosing), for example Record I20, I21 are not diagnosed with LVH by seven traditional criteria (Skolow, CRTA1 to CRTA6), while these records are annotated manually with LVH cardiac disease. Additionally, other ECG records in the same table are normal or pre diagnosed manually with other cardiac diseases (non LVH

cardiac disease), but the determined diagnosis is LVH cardiac disease (i.e. false positive diagnosing), for example Record I55 is diagnosed wrongly with LVH according to four traditional criteria (Cornel, REC-CRTA, CRTA1, and CRTA2), while this record is annotated manually with Earlier MI cardiac disease. On the other hand, the diagnosis results obtained by the proposed system prove that all LVH samples are recognized successfully and all non-LVH samples are excluded. Furthermore, these results prove the significant ability of proposed approach to provide an accurate diagnosis without any interference with other cardiac diseases.

Table 4.8: Comparison Between the LVH Diagnosis Results Obtained by the Proposed Approach and Nine traditional Diagnostic Criteria Using 50 ECG Patients Suffering From Different Cardiac Diseases. (■: LVH, □: Other Cardiac Diseases or Normal Patient)

#	Record	Gender	Pre Diagnosed Cardiac Disease	**Proposed Criterion**	**Skolow**	**Cornell**	**REC-CRTA**	**CRTA1**	**CRTA2**	**CRTA3**	**CRTA4**	**CRTA5**	**CRTA6**
1	I01	F	AHT	□	□	□	□	□	□	□	□	□	□
2	I02	F	AHT	□	□	□	□	□	□	□	□	□	□
3	I05	M	AcMI	□	□	□	□	□	□	□	□	□	□
4	I10	F	AVNB	□	□	□	□	□	□	□	□	□	□
5	I11	M	AVNB	□	□	□	□	□	□	□	□	□	□
6	I15	M	TIA	□	□	□	■	□	□	□	□	□	□
7	I17	M	TIA	□	□	□	□	□	□	□	□	□	□
8	I20	F	LVH	■	□	■	■	□	□	□	□	□	□
9	I21	F	LVH	■	□	■	■	□	□	□	□	□	□
10	I22	F	LVH	■	■	■	■	■	□	■	■	■	■
11	I24	M	EarMI	□	□	□	■	□	□	□	□	□	□
12	I26	F	SND	□	□	□	□	□	□	□	□	□	□
13	I28	M	PVCs	□	■	□	■	□	□	□	□	■	■
14	I32	F	VBG	□	□	□	□	□	□	□	□	□	□
15	I33	M	PVCs	□	□	□	■	□	□	□	□	□	■
16	I35	F	LVH	■	■	■	■	■	■	■	■	■	■
17	I36	F	LVH	■	■	■	■	□	■	■	■	■	■
18	I37	F	LVH	■	■	■	■	■	■	■	■	■	■

Table 4.8: Continued

#	Record	Gender	Pre-Diagnosed Cardiac Disease	**Proposed Criterion**	**Skolow**	**Cornell**	**REC-CRTA**	**CRTA1**	**CRTA2**	**CRTA3**	**CRTA4**	**CRTA5**	**CRTA6**
19	I40	M	TIA	□	□	□	□	□	□	□	□	□	□
20	I41	M	TIA	□	□	□	■	□	□	□	□	■	□
21	I44	F	LVH	■	■	■	■	■	■	■	■	■	■
22	I45	F	LVH	■	■	■	■	■	■	■	■	■	■
23	I46	F	LVH	■	□	■	■	■	■	■	■	■	■
24	I50	M	AF	□	□	□	□	□	□	□	□	□	□
25	I55	M	EarMI	□	□	■	■	■	■	□	□	□	□
26	I56	M	EarMI	□	□	□	□	□	□	□	□	□	□
27	I58	F	AHT	□	□	□	□	□	□	□	□	□	□
28	I60	F	STelv	□	□	□	■	□	□	□	■	□	□
29	I68	M	WPW	□	□	□	■	□	■	□	□	□	□
30	I69	M	PVCs	□	□	□	■	□	■	□	□	□	□
31	I70	M	WPW	□	□	□	■	□	□	□	□	□	■
32	I71	M	WPW	□	□	□	□	□	□	□	□	□	□
33	I72	M	LVH	■	■	■	■	□	■	■	■	■	■
34	I73	M	LVH	■	■	■	■	■	■	■	■	■	■
35	Oteh	M	LVH	■	■	■	■	□	■	■	■	■	■
36	P72	M	LVH	■	■	■	■	■	■	□	■	□	■
37	P73	M	LVH	■	■	■	■	■	■	■	■	■	■
38	P74	M	Normal	□	□	□	□	□	□	□	□	□	■
39	P75	F	Normal	□	□	□	□	□	□	□	□	□	□
40	R40	F	LVH	■	■	■	■	□	□	□	■	□	■
41	R85	M	LVH	■	■	■	■	□	□	□	■	■	■
42	W1	F	Normal	□	□	■	□	□	□	□	□	□	□
43	W2	M	LVH	■	■	■	■	■	■	□	■	■	■
44	W3	F	LVH	■	■	■	■	□	□	□	□	□	■
45	W4	F	LVH	■	□	■	■	□	□	□	□	□	■
46	W5	M	LVH	■	■	□	■	■	■	□	□	■	■
47	W6	F	LVH	■	■	□	■	□	□	□	□	■	■
48	W7	F	Normal	□	□	□	□	□	□	□	□	□	□
49	W8	M	Normal	□	□	■	■	□	□	□	□	□	■
50	W9	F	Normal	□	□	■	■	□	□	□	□	□	■

4.4.4 LVH Diagnosis Results Using Proposed FIS

In this section, the results of LVH cardiac disease diagnosis which are obtained by the proposed FIS for some ECG records are presented. The structure design of the proposed FIS illustrated in Chapter 3 Section 3.4.1.4 Figure 3.12 is implemented using fuzzy graphical user interface (GUI) editor by a MATLAB environment. Six ECG records from the tested data mentioned in Section 4.4.1 were selected as the validation data in this implementation. Three ECG records (I28, I50, and I73) were selected from male patients and pre diagnosed with PVCs, LVH, AF cardiac diseases, respectively. Another three ECG records (I10, I21, and I36) were selected from female patients and pre-diagnosed with AVNB, LVH, and LVH, respectively. The final diagnosis in the proposed FIS takes the form of activating one or more output MFs mentioned in Chapter 3 Section 3.4.1.4 Figure 3.15 based on the conditional results of fuzzy rules that are considered in the proposed FIS. Moreover, the results of these rules are varied according to the desired entry values by input ECG record.

Through the implementation of the proposed FIS approach on six ECG records presented above, the three cases (I21, I36, and I73) are classified successfully as LVH patients; and other cases (I10, I28, and I50) are classified as non LVH patients. However the behaviour of the proposed FIS approach to prepare the final classification decision is different in all six cases. Therefore the implementation of each case is highlighted in more details with the rules viewer diagram which is generated automatically by the fuzzy GUI editor. This diagram views all input and output MFs in the proposed FIS.

Three output MFs are considered in the proposed FIS, the first is Expr1, which denotes the decision of Cornell or REC_CRTA diagnostic criterion; the second is Expr2, which denotes the decision of Cornell and Skolow and successive occurrences in

CRTA1-6 diagnostic criteria; the third is MDV, which denotes the decision of the proposed diagnostic criterion through three MFs (MDV-Fe-LVH, MDV-Normal, and MDV-Ma-LVH). These MFs reflect a diagnosis for LVH female patients, non LVH patients, and LVH male patients, respectively.

In the 1st ECG record (I21), the MDV-Fe-LVH and Expr1 MFs are activated, while Expr2 MF is not activated as shown in the rule viewer diagram in Figure 4.9. According to these output MFs results, the final diagnosis is LVH based on the main diagnosis decision rule defined in Chapter 3 Section 3.4.1.2 Equation 3.22.

In the 2nd ECG record (I36), the diagnosis of LVH cardiac disease is not decided by MDV criterion because both MDV-Fe-LVH and MDV-Normal MFs are activated. At the same time, both Expr1 and Expr2 MFs are activated as shown in Figure 4.10. Thus, the final diagnosis due to the main diagnosis decision rule is LVH. The diagnosis in this case views clearly the reason behind using some LVH traditional criteria in the main diagnosis decision rule.

In the 3rd ECG record (I73), the diagnosis of LVH cardiac disease is prepared smoothly because all successive output MFs (MDV-Ma-LVH, Expr1, and Expr2) are activated as shown in Figure 4.11.

In other ECG records which are pre diagnosed with other cardiac diseases. The MDV-Normal MF is activated and both Expr1 and Expr2 are not activated in the 4th and 5th ECG records (I10 and I50) as shown in Figure 4.12 and Figure 4.13, respectively. Thus the diagnosis in both cases is prepared smoothly as non LVH patients. In the 6th ECG record (I28), the Expr1 is activated, but both the Expr2 and MDV MFs are not activated as shown in Figure 4.14. Thus, the final diagnosis is non LVH according to the logical value obtained by the main diagnosis decision rule.

Figure 4.9: The Generated Rule Viewer Diagram by Proposed FIS on I21 Patient

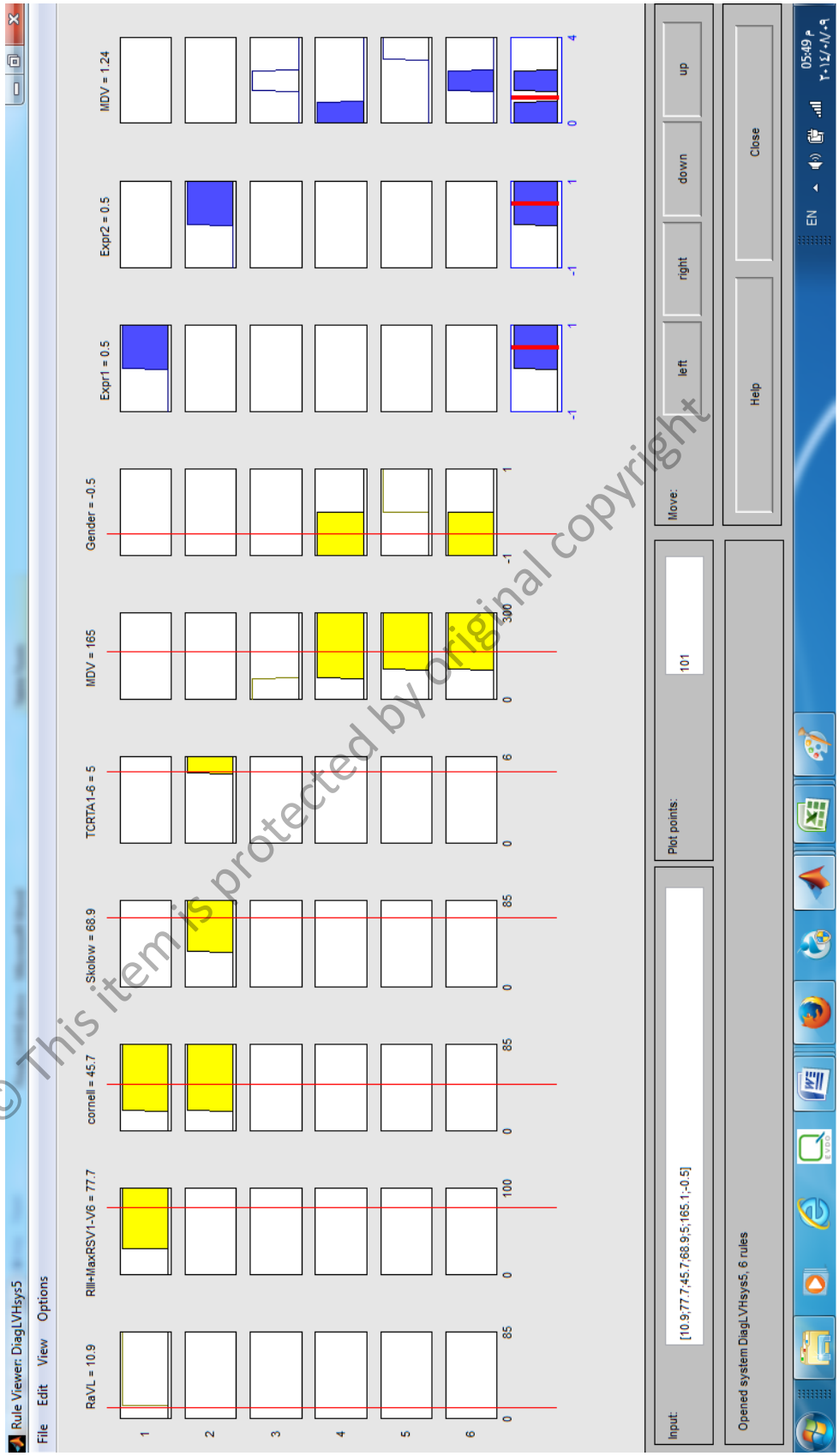

Figure 4.10: The Generated Rule Viewer Diagram by Proposed FIS on I36 Patient

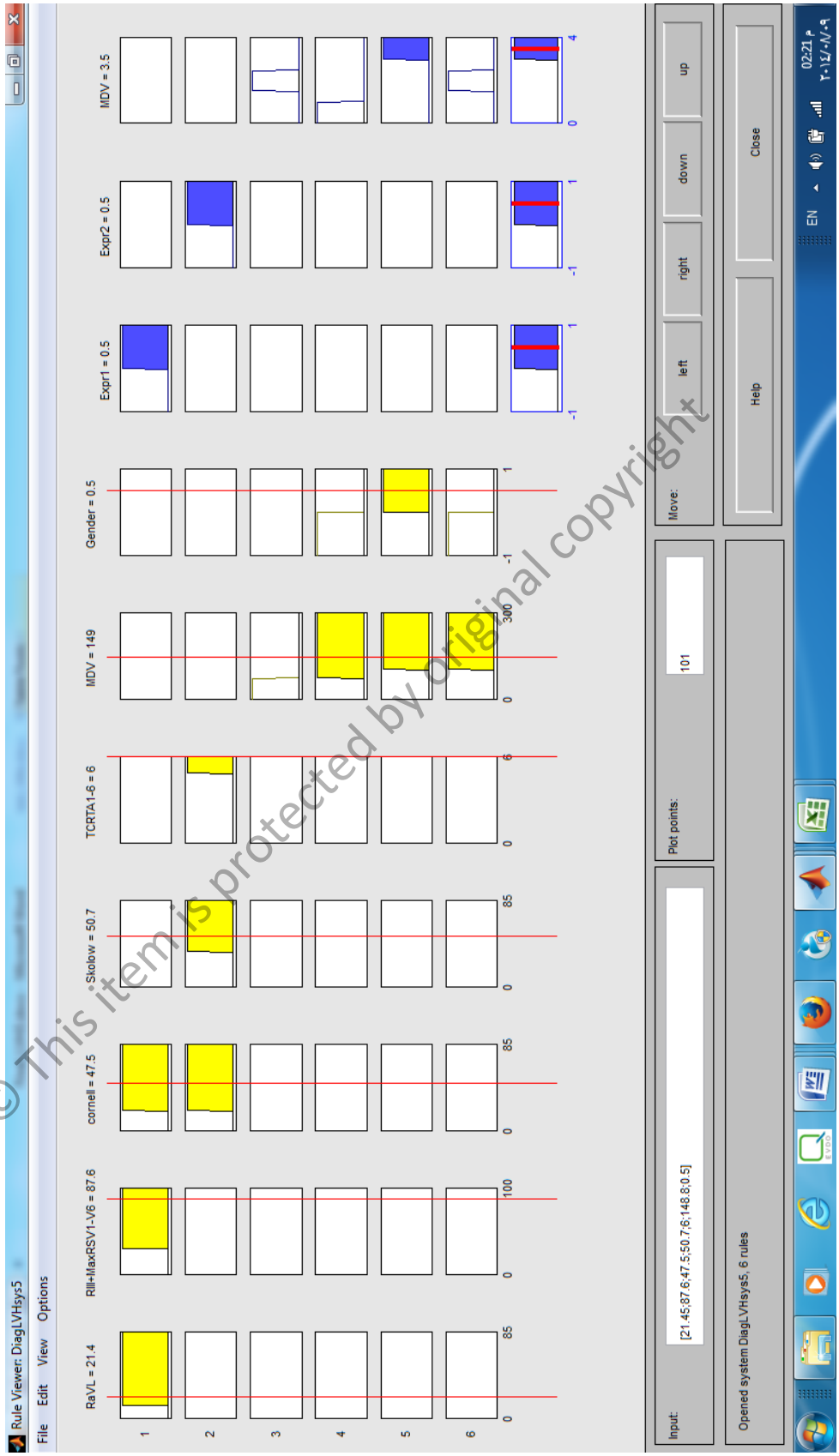

Figure 4.11: The Generated Rule Viewer Diagram by Proposed FIS on I73 Patient

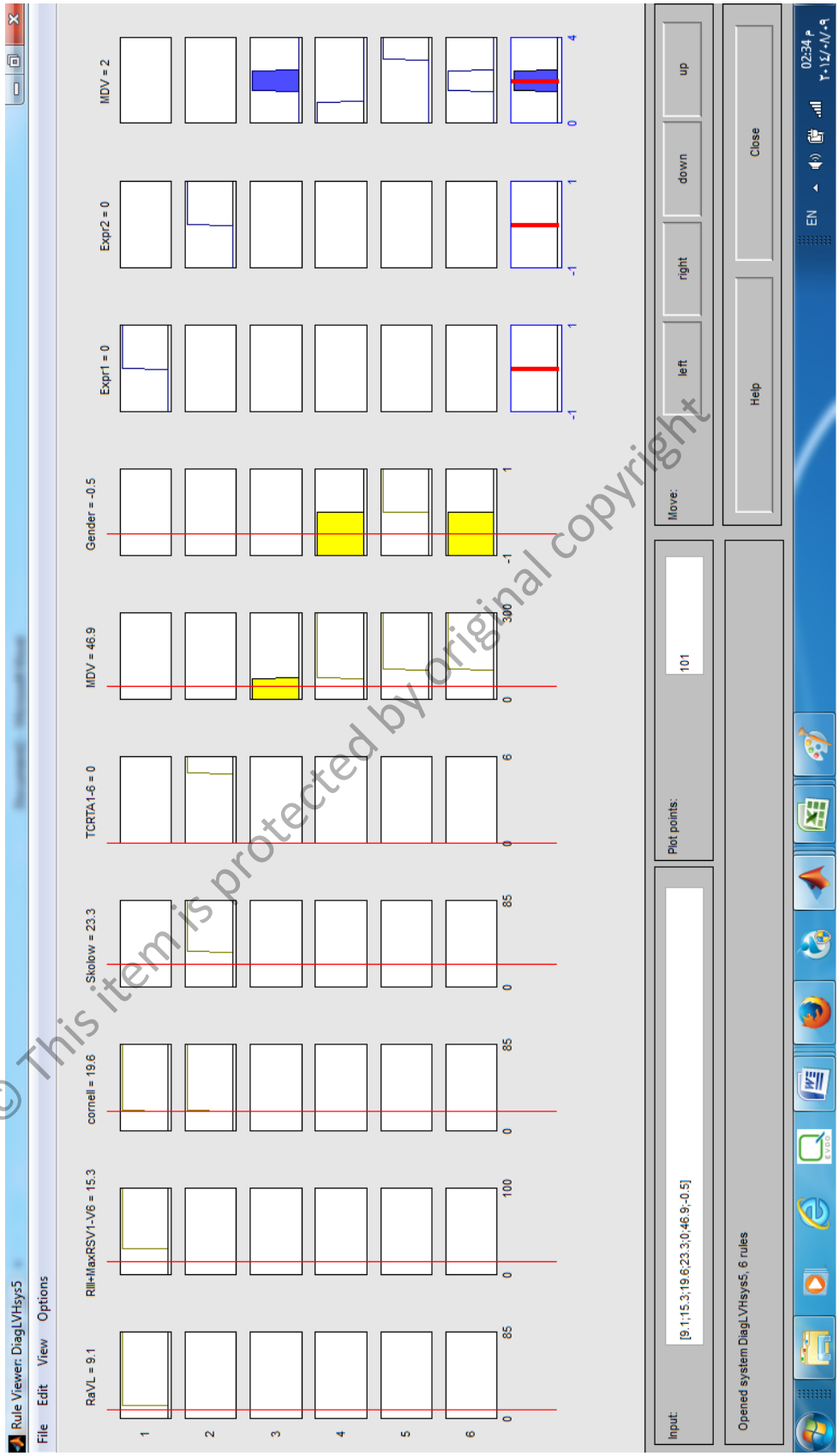

Figure 4.12: The Generated Rule Viewer Diagram by Proposed FIS on I10 Patient

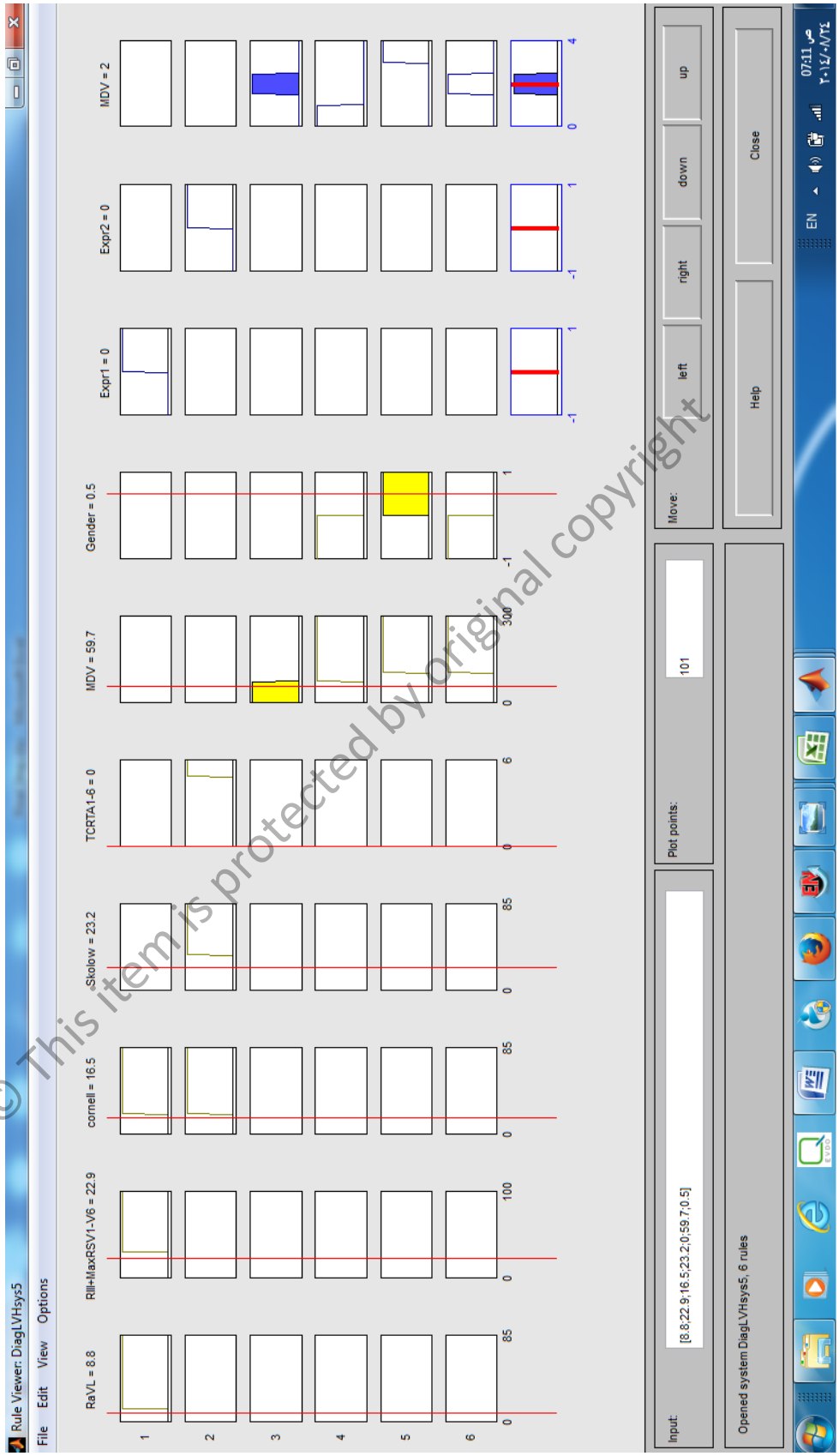

Figure 4.13: The Generated Rule Viewer Diagram by Proposed FIS on I50 Patient

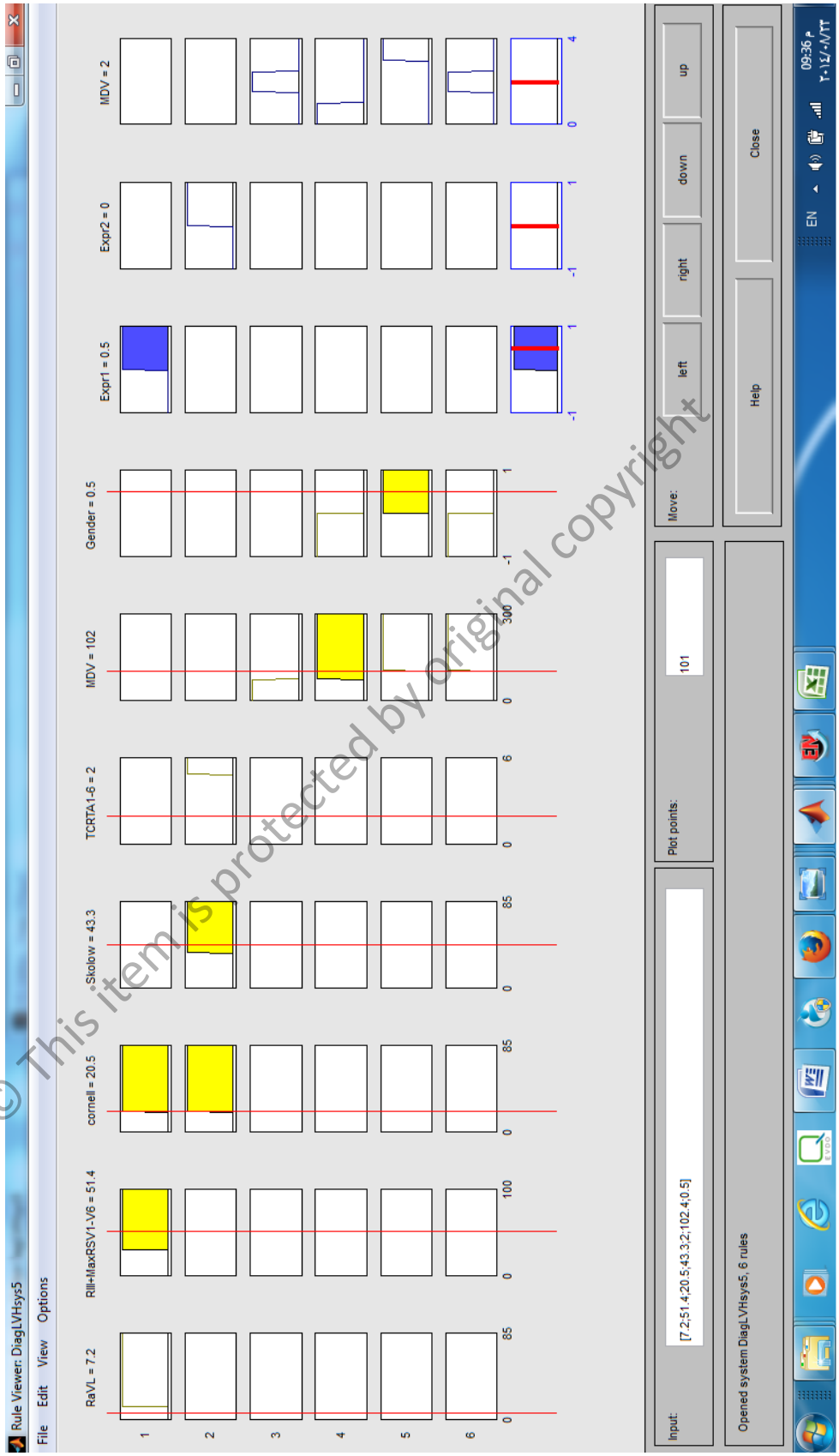

Figure 4.14: The Generated Rule Viewer Diagram by Proposed FIS on I28 Patient

4.4.5 Validation of Proposed Diagnostic Approach

In this section, the performance of the proposed approach for diagnosing LVH cardiac disease is evaluated by comparing the statistical evaluation metrics (sensitivity, specificity, and accuracy) mentioned in section 4.4.2, which were obtained by the proposed approach using the tested ECG records mentioned in section 4.4.1, with the corresponding metrics which are obtained by nine LVH diagnostic criteria using the same set of ECG records. The validation results presented in Table 4.9 show that only one metric from the sensitivity or the specificity is high, and other is low or limited, except for the proposed criterion which performed perfectly for both metrics.

Table 4.9: Comparison of Evaluation Parameters for Diagnosing LVH Cardiac Disease Using Proposed Criterion and Other Nine Diagnostic Criteria

#	Criterion Name	Description of ECG Patients	True Diagnosis (TP)	False Negative (FN)	False Positive (FP)	True Negative (TN)	Sensitivity (%)	Specificity (%)	Accuracy (%)
1	Proposed Criterion	Total No. of tested Patients: 50	21	0	0	29	100	100	100
2	Skolow		17	4	1	28	80.95	96.55	90.00
3	Cornell		19	2	4	25	90.48	86.21	88.00
4	REC-CRTA		21	0	12	17	100	58.62	76.00
5	CRTA1	21 LVH Patients	11	10	1	28	52.38	96.55	78.00
6	CRTA2		13	8	3	26	61.90	89.66	78.00
7	CRTA3		11	10	0	29	52.38	100	80.00
8	CRTA4	29 Patients with other Cardiac Diseases	15	6	1	28	71.43	96.55	86.00
9	CRTA5		16	5	2	27	76.19	93.10	86.00
10	CRTA6		19	2	6	23	90.48	79.31	84.00

Additionally, the results of diagnostic accuracy for all traditional diagnostic criteria take the same limits of precision (not exceeding 90%), whereas a perfect percentage of diagnostic accuracy (100%) is occurred by using the proposed diagnosis criterion. The perfect results of statistical metrics (sensitivity, specificity, and accuracy) obtained by the proposed approach demonstrate the robustness of this approach in performing a correct LVH diagnosis among various cardiac diseases in the ECG tested data.

4.5 Summary

In this chapter, many evaluation scenarios have been conducted to validate the performance of the proposed approaches. The selection of suitable evaluation scenarios for each approach depends mainly on the types of ECG data used for validation, the availability of this data in various rhythms/morphologies, and the availability of pre-defined information for each patient like (cardiac disease, gender, etc), and the standard metrics that were adopted for this evaluation.

For the first approach of digital recovery, two evaluations are presented to validate the robustness of this approach to generate highly precise 12 lead raw ECG data. The first evaluation is performed to calibrate the graphical behavior of the reconstructed data with respect to the baseline detected by the same approach. The second is analytical evaluation that takes two forms; a qualitative evaluation that computes the similarity between the printed ECG chart and the reconstructed ECG signal using a single lead of three ECG charts, and a quantitative evaluation that determines the accuracy of the generated raw data by calculating five standard parameters for reconstructed data and comparing them with the corresponding

parameters which are computed by the ECG machine itself. The same three ECG charts were used in this evaluation and final average accuracy exceeded 98%.

Regarding the RFEM approach which is proposed to detect the QRS complex in the ECG signal and delineate its time characteristics, two graphical evaluations are performed to compute accuracy of the delineated results. The first is applied to evaluate R_{PEAK} time locations using 48 ECG records from the MIT-BIH arrhythmia database, which is mostly used by related QRS detection methods. However, the second is performed to evaluate all time characteristics of the QRS complex (Q_{ONSET}, Q_{END}, R_{PEAK}, S_{ONSET}, and S_{END}) using five ECG records from the QT database which includes manual annotations by cardiologists for all these characteristics. Additionally, the detection results obtained by the RFEM approach are validated with eight QRS detection methods in literature using three statistical metrics (Fd, Se, and P^+), and the average processing time to implement this approach is validated with the corresponding processing time of three methods in literature.

Regarding the HSDPTW approach which is proposed to detect the P and T waves in the ECG signal and delineate boundary and peak time locations of these waves, the delineation results of seven ECG records from QTDB are evaluated graphically with the manual annotation characteristics in this database. The ECG records were selected randomly from seven QTDB categories in order to prove the ability of this approach to process different ECG morphologies. The analytic results of the delineated time characteristics in both P and T waves and four statistical evaluation metrics (Se, P^+, m, and s), which are obtained by applying the HSDPTW approach on 28 ECG records from QTDB are presented in a single table mentioned in Section 4.3.2.3 Table 4.5. Additionally, these results are validated with corresponding ones reported by five P and T detection methods proposed in literature.

Regarding The FIS approach which is proposed to diagnose LVH high risk cardiac disease using proposed diagnosis criterion. It is applied on the ECG records of 50 patients, only 21 patients suffered from LVH, while the others suffered from other cardiac disease or normal patients. Three statistical evaluation metrics (S, P^{+}, and accuracy) are used to evaluate the performance of this approach. The analytic results prove that the proposed FIS approach provides perfect percentages (100%) of diagnostic accuracy, while the greatest accuracy occurred by the traditional LVH diagnostic criteria not exceeding 90%.

CHAPTER 5

CONCLUSIONS AND FUTURE WORK

5.1 Conclusion

As mentioned in Chapter 3 Section 3.1, a new system with three main stages has been proposed for analyzing a 12 lead ECG signal, detecting ECG waves (P, QRS complex, and T), delineating the time characteristics of ECG waves, and diagnosing a specific high risk cardiac disease called LVH. Through the new ECG system, four approaches have been proposed based on new processing algorithms to improve the performance of different subjects considered in this system with respect to existing methods or to automate those using computerized intelligent techniques with respect to other subjects that were performed manually by cardiologists like diagnosing high risk cardiac diseases.

The first proposed approach in the new ECG system performs an operation of digital recovery to reconstruct 12 lead raw ECG data from colored paper printout recordings. In other words, an open bank of 12 lead ECG data can be generated by this approach which can assist the researcher to do more work in terms of analyzing and interpreting the ECG signal. This approach was characterized by low-cost computing, low mathematical complexity, independent of any previous readings, high accuracy of the resulting raw ECG data, independent of ECG frequency recording, and ability to recover raw ECG data with different morphologies, size of paper printout and pen size of printing. Furthermore, it was able to detect the ECG baseline using simple calculations. Moreover, the resulting raw ECG data were smoothed and free from the

printed text and handwriting inside the paper printout. As mentioned in Chapter 4 Section 4.2, the recovered 12 lead ECG data was evaluated graphically with respect to the baseline detection, as well as two forms of analytical evaluation being performed for a single lead in three ECG recordings with different morphologies. The validation results prove the robustness of the proposed approach in reconstructing the ECG data in the printed chart with all deviations of finite precision. In addition, high precision matching exceeding than 98% was verified between the original and recovered ECG data. Furthermore, the proposed digital recovery approach applies simple and fast computing for processing a color scanned image of paper printout containing an ECG chart. Therefore, it can be easily integrated into a portable smart hardware system which can be developed later to do more real time ECG signal analysis and cardiac diseases diagnosis.

The second part of new ECG system includes the process of detecting ECG waves and then delineating time characteristics of these waves to compute different diagnostic parameters/features related to the ECG signal. Two approaches have been proposed in this subject. The first approach named RFEM was designed to detect the QRS complex and delineate peak and boundary time locations of their components (Q, R, and S) waves. As the RFEM approach is based on a straight forward algorithm to perform QRS detection without the need for any mathematical transformation or estimation, it is characterized by high-speed processing time. The same instantaneous strategy to detect the QRS complex was considered by another approach named HSDPTW to detect P and T waves, and then delineate the boundaries and peak time locations of these waves (P_{on}, P_{peak}, P_{off}, T_{on}, T_{peak}, and P_{off}). Two algorithms were applied by the HSDPTW approach to perform the detection of P and T waves within the

fixed length search intervals which identified by previous time characteristics of the QRS complex.

The delineated time characteristics determined by the RFEM and the HSDPTW approaches were used to calculate significant diagnostic criteria for different cardiac diseases. The highest detection accuracy verified by these approaches led to excellent diagnosis results for different cardiac diseases. Additionally, the high processing speed attained by these approaches enables these approaches to be applied as the smart hardware integrated chips inside ECG machine for real time processing ECG signal and to perform detailed delineation of all ECG waves instead of a general ECG wave description which is performed by modern ECG machine.

The third part in the new ECG system focuses on diagnosing cardiac diseases using computerized intelligent techniques. A new FIS for diagnosing the LVH cardiac disease has been proposed based on new diagnostic criterion. All the input voltage parameters and the output of the logical expressions related to the proposed diagnostic criterion were expressed as the MFs in the proposed FIS. In contrast to the traditional LVH diagnostic criteria, the decision of the proposed criterion was obtained by three logical expressions. Two of them were a combination of some traditional diagnostic criteria, whereas the other expression (MDV) was obtained by the eight voltages from the 12-lead ECG with a different level for each gender. The proposed diagnostic system was validated successfully with 50 ECG samples from both genders with differing ages. However, 29 samples from the total validated samples did not suffer from LVH; the proposed diagnostic system achieved perfect results (100%) in terms of sensitivity, specificity, and accuracy.

According the process of integrating the proposed LVH diagnosing system in a single FIS intelligent model, the simplicity of conditioning statements for all input and

output MFs in the proposed FIS, the perfect diagnosis accuracy, and the simplicity and the highly processing speed of the based technique followed by the RFEM approach to delineate the time characteristics of QRS complex and generate diagnostic parameters for the proposed diagnosis system. The idea of implementing the proposed diagnosis system on an intelligent hardware unit (which can be added to the ECG machine) to perform actual diagnosis of LVH cardiac disease became more realistic.

5.2 Future Works

Based on the proposed approaches in this thesis, some future works can be suggested:

1- Implement the proposed digital recovery approach on a portable embedded system with high resolution vision system and huge storage media. As the system performs entire reconstructing raw ECG data in a single device, also facilities the process of capture and storage inside general hospitals or clinical centres.

2- Implement the proposed detection RFEM and HSDPTW approaches in a single programmable micro chip unit to process the ECG output signal from the ECG machine and provide detailed parameters and features that can be beneficial for future diagnosis.

3- Develop more computerized intelligent systems for diagnosing other high risk cardiac diseases like HOCM, WPW, LQTcS, ARVC, etc based on detailed analysis of the 12 lead ECG signal.

4- Design a computerized intelligent system for predicating SCD based on the diagnostic results of high risk cardiac diseases, standard tests of HH, and other hereditary issues.

REFERENCES

Addison, Paul S, Watson, James N, Clegg, Gareth R, Holzer, Michael, Sterz, Fritz, & Robertson, Colin E. (2000). Evaluating arrhythmias in ECG signals using wavelet transforms. *Engineering in Medicine and Biology Magazine, IEEE, 19*(5), 104-109.

Aehlert, Barbara J. (2012). *Pocket reference for ecgs made easy*: Elsevier Health Sciences.

Alfaouri, Mikhled, & Daqrouq, Khaled. (2008). ECG signal denoising by wavelet transform thresholding. *American Journal of Applied Sciences, 5*(3), 276.

Assadi, Ramin, Motabar, Ali, & Lange, Richard A. (2011). Conduction System of the Heart *http://emedicine.medscape.com/article/1922987-overview*: MedScape.

Azeem, Tariq, Vassallo, Michael, & Samani, Nilesh J. (2005). *Rapid Review of ECG Interpretation*: Manson Publishing.

Bazett, HC. (1997). AN ANALYSIS OF THE TIME-RELATIONS OF ELECTROCARDIOGRAMS. *Annals of Noninvasive Electrocardiology, 2*(2), 177-194.

Bowbrick, Steven, & Borg, Alex N. (2006). *ECG complete*: Elsevier Health Sciences.

Casale, PAUL N, Devereux, RICHARD B, Alonso, DANIEL R, Campo, E, & Kligfield, P_. (1987). Improved sex-specific criteria of left ventricular hypertrophy for clinical and computer interpretation of electrocardiograms: validation with autopsy findings. *Circulation, 75*(3), 565-572.

Casale, Paul N, Devereux, Richard B, Kligfield, Paul, Eisenberg, Richard R, Miller, David H, Chaudhary, Banvir S, & Phillips, Malcolm C. (1985). Electrocardiographic detection of left ventricular hypertrophy: development and prospective validation of improved criteria. *Journal of the American College of Cardiology, 6*(3), 572-580.

Chang, Pei-Chann, Lin, Jyun-Jie, Hsieh, Jui-Chien, & Weng, Julia. (2012). Myocardial infarction classification with multi-lead ECG using hidden Markov models and Gaussian mixture models. *Applied Soft Computing, 12*(10), 3165-3175.

Chebil, Jalel, Al-Nabulsi, Jamal, & Al-Maitah, Mohammed. (2008). *A novel method for digitizing standard ECG papers.* Paper presented at the International Conference on Computer and Communication Engineering, 2008. ICCCE 2008. , Kuala Lumpur, Malaysia.

Chesnokov, YC, Nerukh, D, & Glen, RC. (2006). *Individually adaptable automatic QT detector.* Paper presented at the Computers in Cardiology, 2006.

Choi, Samjin. (2008). Detection of valvular heart disorders using wavelet packet decomposition and support vector machine. *Expert Systems with Applications, 35*(4), 1679-1687.

Christov, Ivaylo I. (2004). Real time electrocardiogram QRS detection using combined adaptive threshold. *BioMedical Engineering OnLine, 3*(1), 28.

Daubechies, Ingrid. (1990). The wavelet transform, time-frequency localization and signal analysis. *Information Theory, IEEE Transactions on, 36*(5), 961-1005.

Devereux, Richard B, Casale, Paul N, Eisenberg, Richard R, Miller, David H, & Kligfield, Paul. (1984). Electrocardiographic detection of left ventricular hypertrophy using echocardiographic determination of left ventricular mass as the reference standardComparison of standard criteria, computer diagnosis and physician interpretation. *Journal of the American College of Cardiology, 3*(1), 82-87.

Doğan, Berat, & Korürek, Mehmet. (2012). A new ECG beat clustering method based on kernelized fuzzy c-means and hybrid ant colony optimization for continuous domains. *Applied soft computing, 12*(11), 3442-3451.

Dokur, Zümray, & Ölmez, Tamer. (2001). ECG beat classification by a novel hybrid neural network. *Computer methods and programs in biomedicine, 66*(2), 167-181.

Drazen, Erica, Mann, Nancy, Borun, Raymond, Laks, Michael, & Bersen, Alan. (1988). Survey of computer-assisted electrocardiography in the United States. *Journal of electrocardiology, 21*, S98-S104.

e Silva, AR Gomes, de Oliveira, Hélio Magalhães, & Lins, Rafael Dueire. (2008). Converting ECG and other paper legated biomedical maps into digital signals *Graphics Recognition. Recent Advances and New Opportunities* (pp. 21-28): Springer.

Ebrahimzadeh, A, Shakiba, B, & Khazaee, A. (2014). Detection of electrocardiogram signals using an efficient method. *Applied Soft Computing, 22*, 108-117.

Ebrahimzadeh, Elias, & Pooyan, Mohammad. (2011). Early detection of sudden cardiac death by using classical linear techniques and time-frequency methods on electrocardiogram signals. *Journal of Biomedical Science & Engineering, 4*(11).

Espiritu-Santo-Rincon, Antonio, & Carbajal-Fernandez, Cuauhtemoc. (2010). *ECG feature extraction via waveform segmentation.* Paper presented at the Electrical Engineering Computing Science and Automatic Control (CCE), 2010 7th International Conference on.

Fishbein, Michael C. (2010). Cardiac disease and risk of sudden death in the young: the burden of the phenomenon. *Cardiovascular Pathology, 19*(6), 326-328.

Foster, D Bruce. (2007). *Twelve-lead electrocardiography: Theory and interpretation*: Springer.

Gacek, Adam, & Pedrycz, Witold. (2012). ECG Signal Analysis, Classification, and Interpretation: A Framework of Computational Intelligence *ECG Signal Processing, Classification and Interpretation* (pp. 47-77): Springer.

Ghaffari, A, Homaeinezhad, MR, Akraminia, M, Atarod, M, & Daevaeiha, M. (2009). A robust wavelet-based multi-lead electrocardiogram delineation algorithm. *Medical engineering & physics, 31*(10), 1219-1227.

Ghongade, Rajesh, & Ghatol, AA. (2007). *A brief performance evaluation of ECG feature extraction techniques for artificial neural network based classification.* Paper presented at the TENCON 2007-2007 IEEE Region 10 Conference.

Goldberger, Ary L, Amaral, Luis AN, Glass, Leon, Hausdorff, Jeffrey M, Ivanov, Plamen Ch, Mark, Roger G, . . . Stanley, H Eugene. (2000). Physiobank, physiotoolkit, and physionet components of a new research resource for complex physiologic signals. *Circulation, 101*(23), e215-e220.

Graham, TP, Driscoll, DJ, Gersony, WM, Newburger, JW, Rocchini, A, & Towbin, A. (2005). 36th Bethesda Conference: Eligibility recommendations for competitive athletes with cardiovascular abnormalities. Task Force 2: Congenital heart disease. *J Am Coll Cardiol, 45*, 1326-1333.

GUBNER, RICHARD, & UNGERLEIDER, HARRY E. (1943). Electrocardiographic criteria of left ventricular hypertrophy: factors determining the evolution of the

electrocardiographic patterns in hypertrophy and bundle branch block. *Archives of Internal Medicine, 72*(2), 196.

Güler, İnan. (2005). ECG beat classifier designed by combined neural network model. *Pattern recognition, 38*(2), 199-208.

Gupta, Rajarshi, Mitra, Madhuchhanda, & Bera, Jitendranath. (2013). *ECG Acquisition and Automated Remote Processing*: Springer.

Hadj Slimane, Zine-Eddine, & Naït-Ali, Amine. (2010). QRS complex detection using Empirical Mode Decomposition. *Digital Signal Processing, 20*(4), 1221-1228.

Hampton, John R. (2008). *The ECG made easy*: Elsevier Health Sciences.

Hampton, John R. (2013). *The ECG in practice*: Elsevier Health Sciences.

Han, Jiawei, & Kamber, Micheline. (2006). *Data Mining, Southeast Asia Edition: Concepts and Techniques*: Morgan kaufmann.

Hanss, Michael. (2005). *Applied fuzzy arithmetic*: Springer.

Jager, Franc, Moody, George B, Taddei, Alessandro, & Mark, Roger G. (1991). *Performance measures for algorithms to detect transient ischemic ST segment changes.* Paper presented at the Computers in Cardiology 1991, Proceedings.

Jenkins, Dean, & Gerred, Stephen. (2009). ECG Library *http://www.ecglibrary.com/*.

Jenkins, Dean, & Gerred, Stephen John. (2011). *ECGs by example*: Elsevier Health Sciences.

Kabir, Md Ashfanoor, & Shahnaz, Celia. (2012). Denoising of ECG signals based on noise reduction algorithms in EMD and wavelet domains. *Biomedical Signal Processing and Control, 7*(5), 481-489.

Kasturiwale, HP, & Deshmukh, CN. (2009). *Quality assessment of ICA for ECG signal analysis.* Paper presented at the Emerging Trends in Engineering and Technology (ICETET), 2009 2nd International Conference on.

Kelly, Rory, & Galvin, Joseph. (2010). Sudden cardiac death in the young: causes and prevention. *Royal College of Surgeons in Ireland Student Medical*(2009-2010), 42-46.

Korürek, Mehmet, & Doğan, Berat. (2010). ECG beat classification using particle swarm optimization and radial basis function neural network. *Expert systems with Applications, 37*(12), 7563-7569.

Kundu, Mahantapas, Nasipuri, Mita, & Kumar Basu, Dipak. (2000). Knowledge-based ECG interpretation: a critical review. *Pattern Recognition, 33*(3), 351-373.

Kutlu, Yakup, & Kuntalp, Damla. (2011). A multi-stage automatic arrhythmia recognition and classification system. *Computers in biology and medicine, 41*(1), 37-45.

Kutlu, Yakup, & Kuntalp, Damla. (2012). Feature extraction for ECG heartbeats using higher order statistics of WPD coefficients. *Computer methods and programs in biomedicine, 105*(3), 257-267.

Laguna, Pablo, Mark, Roger G, Goldberg, A, & Moody, George B. (1997). *A database for evaluation of algorithms for measurement of QT and other waveform intervals in the ECG.* Paper presented at the Computers in Cardiology 1997.

Levy, Daniel, Labib, Sherif B, Anderson, Keaven M, Christiansen, Jane C, Kannel, William B, & Castelli, William P. (1990). Determinants of sensitivity and specificity of electrocardiographic criteria for left ventricular hypertrophy. *Circulation, 81*(3), 815-820.

Li, Cuiwei, Zheng, Chongxun, & Tai, Changfeng. (1995). Detection of ECG characteristic points using wavelet transforms. *Biomedical Engineering, IEEE Transactions on, 42*(1), 21-28.

Lin, Chao, Mailhes, Corinne, & Tourneret, J-Y. (2010). P-and T-wave delineation in ECG signals using a Bayesian approach and a partially collapsed Gibbs sampler. *Biomedical Engineering, IEEE Transactions on, 57*(12), 2840-2849.

Lin, Tao, & Tian, Shuang. (2012). An ECG Signal Processing System Based on MATLAB and MIT-BIH *Recent Advances in Computer Science and Information Engineering* (pp. 787-792): Springer.

Llamedo, M, Khawaja, A, & Martínez, JP. (2010). *Analysis of 12-lead classification models for ECG classification.* Paper presented at the Computing in Cardiology, 2010.

Llamedo, Mariano, & Martínez, Juan Pablo. (2011). Heartbeat classification using feature selection driven by database generalization criteria. *Biomedical Engineering, IEEE Transactions on, 58*(3), 616-625.

Luthra, Atul. (2011). *ECG made easy*: JP Medical Ltd.

Madeiro, João PV, Nicolson, William B, Cortez, Paulo C, Marques, João AL, Vázquez-Seisdedos, Carlos R, Elangovan, Narmadha, . . . Schlindwein, Fernando S. (2013). New approach for T-wave peak detection and T-wave end location in 12-lead paced ECG signals based on a mathematical model. *Medical engineering & physics, 35*(8), 1105-1115.

Maglaveras, Nicos, Stamkopoulos, Telemachos, Diamantaras, Konstantinos, Pappas, Costas, & Strintzis, Michael. (1998). ECG pattern recognition and classification using non-linear transformations and neural networks: a review. *International journal of medical informatics, 52*(1), 191-208.

Malmivuo, Jaakko, & Plonsey, Robert. (1995). *Bioelectromagnetism: principles and applications of bioelectric and biomagnetic fields*: Oxford University Press.

Manikandan, M Sabarimalai, & Soman, KP. (2012). A novel method for detecting R-peaks in electrocardiogram (ECG) signal. *Biomedical Signal Processing and Control, 7*(2), 118-128.

Maron, Barry J. (2009). Sudden death in hypertrophic cardiomyopathy. *Journal of cardiovascular translational research, 2*(4), 368-380.

Maron, Barry J, Doerer, Joseph J, Haas, Tammy S, Tierney, David M, & Mueller, Frederick O. (2009). Sudden deaths in young competitive athletes analysis of 1866 Deaths in the United States, 1980–2006. *Circulation, 119*(8), 1085-1092.

Martínez, Arturo, Alcaraz, Raúl, & Rieta, José Joaquín. (2010). Application of the phasor transform for automatic delineation of single-lead ECG fiducial points. *Physiological measurement, 31*(11), 1467.

Martínez, JP, Almeida, R, Olmos, S, Rocha, AP, & Laguna, P. (2006). *stability of QT measurements in the PTB database depending on the selected lead.* Paper presented at the Computers in Cardiology, 2006.

Martínez, Juan Pablo, Almeida, Rute, Olmos, Salvador, Rocha, Ana Paula, & Laguna, Pablo. (2004). A wavelet-based ECG delineator: evaluation on standard databases. *Biomedical Engineering, IEEE Transactions on, 51*(4), 570-581.

Mehta, SS, & Lingayat, NS. (2008). Development of SVM based classification techniques for the delineation of wave components in 12-lead electrocardiogram. *Biomedical Signal Processing and Control, 3*(4), 341-349.

Minhas, Afsar, & Arif, Muhammad. (2008). Robust electrocardiogram (ECG) beat classification using discrete wavelet transform. *Physiological Measurement, 29*, 555-570.

Mitra, Sucharita, & Mitra, Mandar. (2003). An automated data extraction system from 12 lead ECG images. *Computer methods and programs in biomedicine, 71*(1), 33-38.

Mneimneh, MA, Povinelli, RJ, & Johnson, M. (2006). *Integrative technique for the determination of QT interval.* Paper presented at the Computers in Cardiology, 2006.

Molloy, Thomas J, Okin, Peter M, Devereux, Richard B, & Kligfield, Paul. (1992). Electrocardiographic detection of left ventricular hypertrophy by the simple QRS voltage-duration product. *Journal of the American College of Cardiology, 20*(5), 1180-1186.

Moody, GB. (2008). *The physionet/computers in cardiology challenge 2008: T-wave alternans.* Paper presented at the Computers in Cardiology, 2008.

Moody, George B, Koch, Hans, & Steinhoff, Uwe. (2006). *The physionet/computers in cardiology challenge 2006: Qt interval measurement.* Paper presented at the Computers in Cardiology, 2006.

Moody, George B, & Mark, Roger G. (1990). *The MIT-BIH arrhythmia database on CD-ROM and software for use with it.* Paper presented at the Computers in Cardiology 1990, Proceedings.

Moody, George B, & Mark, Roger G. (2001). The impact of the MIT-BIH arrhythmia database. *Engineering in Medicine and Biology Magazine, IEEE, 20*(3), 45-50.

Morris, Francis, Brady, William J, & Camm, John. (2009). *ABC of clinical electrocardiography* (Vol. 93): John Wiley & Sons.

Murukesan, L, Murugappan, M, & Iqbal, M. (2013). *Sudden cardiac death prediction using ECG signal derivative (Heart Rate Variability): A review.* Paper presented at the Signal Processing and its Applications (CSPA), 2013 IEEE 9th International Colloquium on.

Nasiri, Jalal A, Naghibzadeh, Mahmoud, Yazdi, Hadi Sadoghi, & Naghibzadeh, Bahram. (2009). *ECG arrhythmia classification with support vector machines and genetic algorithm.* Paper presented at the Third UKSim European Symposium on Computer Modeling and Simulation, 2009. EMS'09. .

Nazmy, TM, El-Messiry, H, & Al-Bokhity, B. (2010). *Adaptive neuro-fuzzy inference system for classification of ECG signals.* Paper presented at the The 7th International Conference on Informatics and Systems (INFOS), 2010

Noseworthy, Peter A, & Newton-Cheh, Christopher. (2008). Genetic determinants of sudden cardiac death. *Circulation, 118*(18), 1854-1863.

Nugent, Chris Desmond, Webb, JAC, Black, Norman D., Wright, GTH, & McIntyre, M. (1999). An intelligent framework for the classification of the 12-lead ECG. *Artificial Intelligence in Medicine, 16*(3), 205-222.

Özbay, Yüksel, & Tezel, Gülay. (2010). A new method for classification of ECG arrhythmias using neural network with adaptive activation function. *Digital Signal Processing, 20*(4), 1040-1049.

Pan, Jiapu, & Tompkins, Willis J. (1985). A real-time QRS detection algorithm. *Biomedical Engineering, IEEE Transactions on*(3), 230-236.

Paterni, M, Belardinelli, A, Benassi, A, Carpeggiani, C, & Demi, M. (2002). *An automatic procedure to convert ECGs from graph paper to digital signals.* Paper presented at the Computers in Cardiology, 2002.

Pelliccia, Antonio, Fagard, Robert, Bjørnstad, Hans Halvor, Anastassakis, Aris, Arbustini, Eloisa, Assanelli, Deodato, . . . Corrado, Domenico. (2005). Recommendations for competitive sports participation in athletes with cardiovascular disease A consensus document from the Study Group of Sports Cardiology of the Working Group of Cardiac Rehabilitation and Exercise Physiology and the Working Group of Myocardial and Pericardial Diseases of the European Society of Cardiology. *European Heart Journal, 26*(14), 1422-1445.

Petrou, Maria, & Petrou, Costas. (2010). *Image processing: the fundamentals*: John Wiley & Sons Ltd.

Petrutiu, Simona, Ng, Jason, Nijm, Grace M, Al-Angari, Haitham, Swiryn, Steven, & Sahakian, Alan V. (2006). Atrial fibrillation and waveform characterization. *Engineering in Medicine and Biology Magazine, IEEE, 25*(6), 24-30.

Pewsner, Daniel, Jüni, Peter, Egger, Matthias, Battaglia, Markus, Sundström, Johan, & Bachmann, Lucas M. (2007). Accuracy of electrocardiography in diagnosis of left ventricular hypertrophy in arterial hypertension: systematic review. *Bmj, 335*(7622), 711.

PTB Diagnostic ECG Database. Retrieved from: http://physionet.org/physiobank/database/ptbdb/

Rai, Hari Mohan, Trivedi, Anurag, & Shukla, Shailja. (2013). ECG signal processing for abnormalities detection using multi-resolution wavelet transform and Artificial Neural Network classifier. *Measurement, 46*(9), 3238-3246.

Rajendra Acharya, U, Subbanna Bhat, P, Iyengar, S Sitharama, Rao, Ashok, & Dua, Sumeet. (2003). Classification of heart rate data using artificial neural network and fuzzy equivalence relation. *Pattern Recognition, 36*(1), 61-68.

Reichek, Nathaniel, & Devereux, Richard B. (1981). Left ventricular hypertrophy: relationship of anatomic, echocardiographic and electrocardiographic findings. *Circulation, 63*(6), 1391-1398.

Romhilt, Donald W, & Estes Jr, E Harvey. (1968). A point-score system for the ECG diagnosis of left ventricular hypertrophy. *American heart journal, 75*(6), 752-758.

Saini, Indu, Singh, Dilbag, & Khosla, Arun. (2013). QRS detection using K-Nearest Neighbor algorithm (KNN) and evaluation on standard ECG databases. *Journal of Advanced Research, 4*(4), 331-344.

Sanromán-Junquera, M, Mora-Jiménez, Inmaculada, Caamaño, Antonio J, Almendral, J, Atienza, F, Castilla, L, . . . Rojo-Álvarez, José Luis. (2012). Digital recovery of biomedical signals from binary images. *Signal Processing, 92*(1), 43-53.

Saxena, SC, Kumar, Vinod, & Hamde, ST. (2002). Feature extraction from ECG signals using wavelet transforms for disease diagnostics. *International Journal of Systems Science, 33*(13), 1073-1085.

Shen, Tsu-Wang, Shen, Hsiao-Ping, Lin, Ching-Heng, & Ou, Yi-Ling. (2007). *Detection and prediction of Sudden Cardiac Death (SCD) for personal healthcare.* Paper presented at the 29th Annual International Conference of the IEEE Engineering in Medicine and Biology Society, 2007. EMBS 2007. , Lyon, France.

Shen, TW, & Laio, TF. (2009). *Image processing on ECG chart for ECG signal recovery.* Paper presented at the Computers in Cardiology, 2009.

Sivanandam, SN, Sumathi, Sai, & Deepa, SN. (2007). *Introduction to fuzzy logic using MATLAB* (Vol. 1): Springer.

Sokolow, Maurice, & Lyon, Thomas P. (1949). The ventricular complex in left ventricular hypertrophy as obtained by unipolar precordial and limb leads. *American heart journal, 37*(2), 161-186.

Sörnmo, Leif, & Laguna, Pablo. (2005). ECG Signal Processing *Bioelectrical Signal Processing in Cardiac and Neurological Applications* (pp. 453-566): Academic Press.

Sörnmo, Leif, & Laguna, Pablo. (2006). Electrocardiogram (ECG) signal processing. *Wiley Encyclopedia of Biomedical Engineering*.

Sternickel, Karsten. (2002). Automatic pattern recognition in ECG time series. *Computer methods and programs in biomedicine, 68*(2), 109-115.

Sumathi, Sai, & Paneerselvam, Surekha. (2010). *Computational intelligence paradigms: theory & applications using MATLAB*: CRC Press.

Suri, Jasjit S, & Spaan, Jos AE. (2007). *Advances in cardiac signal processing*: Springer.

Swamy, Prashanth, Jayaraman, Srinivasan, & Chandra, M Girish. (2010). *An improved method for digital time series signal generation from scanned ECG records.* Paper presented at the International Conference on Bioinformatics and Biomedical Technology (ICBBT 2010).

Taddei, A, Distante, G, Emdin, M, Pisani, P, Moody, GB, Zeelenberg, C, & Marchesi, C. (1992). The European ST-T database: standard for evaluating systems for the analysis of ST-T changes in ambulatory electrocardiography. *European heart journal, 13*(9), 1164-1172.

Tan, KF, Chan, KL, & Choi, K. (2000). Detection of the QRS complex, P wave and T wave in electrocardiogram. *Advances in Medical Signal and Information Processing*, 41-47.

Tang, Guodong, & Qin, Aina. (2008). *ECG de-noising based on empirical mode decomposition.* Paper presented at the The 9th International Conference for Young Computer Scientists. ICYCS 2008. .

Unser, Michael, & Aldroubi, Akram. (1996). A review of wavelets in biomedical applications. *Proceedings of the IEEE, 84*(4), 626-638.

Vasiliadis, I, Kolovou, G, Mavrogeni, S, Nair, DR, & Mikhailidis, DP. (2014). Sudden cardiac death and diabetes mellitus. *Journal of diabetes and its complications, 28*(4), 573-579.

Wagner, Galen S. (2008). *Marriott's Practical Electrocardiography*: Lippincott Williams & Wilkins.

Willems, Jos L, Arnaud, Pierre, Van Bemmel, Jan H, Bourdillon, Peter J, Degani, Rosanna, Denis, Bernard, . . . Mazzocca, Gianfranco. (1987). A reference data base for multilead electrocardiographic computer measurement programs. *Journal of the American College of Cardiology, 10*(6), 1313-1321.

Wu, CY, & Chiu, HW. (2006). *A semi-automatic QT interval measurement based on digital filters.* Paper presented at the Computers in Cardiology, 2006.

Yeh, Yun-Chi, & Wang, Wen-June. (2008). QRS complexes detection for ECG signal: The Difference Operation Method. *Computer methods and programs in biomedicine, 91*(3), 245-254.

Yeh, Yun-Chi, Wang, Wen-June, & Chiou, Che Wun. (2010). Feature selection algorithm for ECG signals using Range-Overlaps Method. *Expert Systems with Applications, 37*(4), 3499-3512.

Zidelmal, Z, Amirou, A, Ould-Abdeslam, D, Moukadem, A, & Dieterlen, A. (2014). QRS detection using S-Transform and Shannon Energy. *Computer Methods and Programs in Biomedicine, 116*(1), 1-9.

Zidelmal, Zahia, Amirou, Ahmed, Adnane, Mourad, & Belouchrani, Adel. (2012). QRS detection based on wavelet coefficients. *Computer methods and programs in biomedicine, 107*(3), 490-496.

Zigel, Yaniv, Cohen, Arnon, & Katz, Amos. (2000). The weighted diagnostic distortion (WDD) measure for ECG signal compression. *Biomedical Engineering, IEEE Transactions on, 47*(11), 1422-1430.

Zipes, Douglas P. (2005). Epidemiology and mechanisms of sudden cardiac death. *Can J Cardiol, 21*(Suppl A), 37A-40A.

Appendix A

The 12-lead ECG chart shown in Figure A-1 is scanned with 600 dpi from the original ECG printout paper. The distribution of ECG leads in this chart are different from that shown in Figure 4.1, also the size of paper is different. The scanned image of this chart is processed by the proposed digital recovery approach that is mentioned in Chapter 3 Section 3.2.2.1 to recover the 12 lead raw ECG data in a digitally form. The recovered 12 lead ECG data are plotted separately with the same scale for all graphs, also the ECG base line which is pre detected in the same approach is plotted in each graph with a dashed red line as shown in Figure A-2.

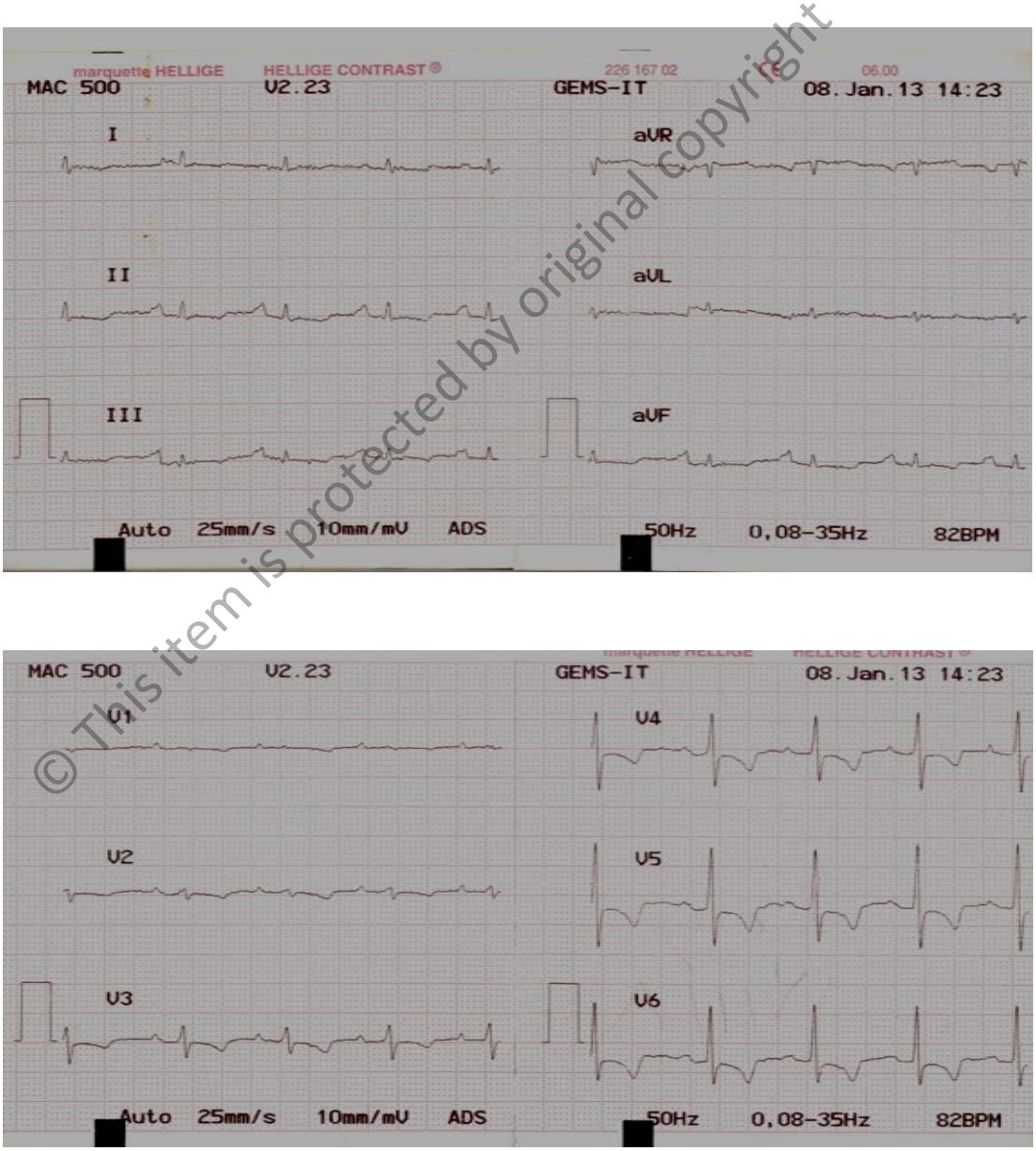

Figure A-1: The Scanned Image (with 600 dpi) of 12-Lead ECG Chart.

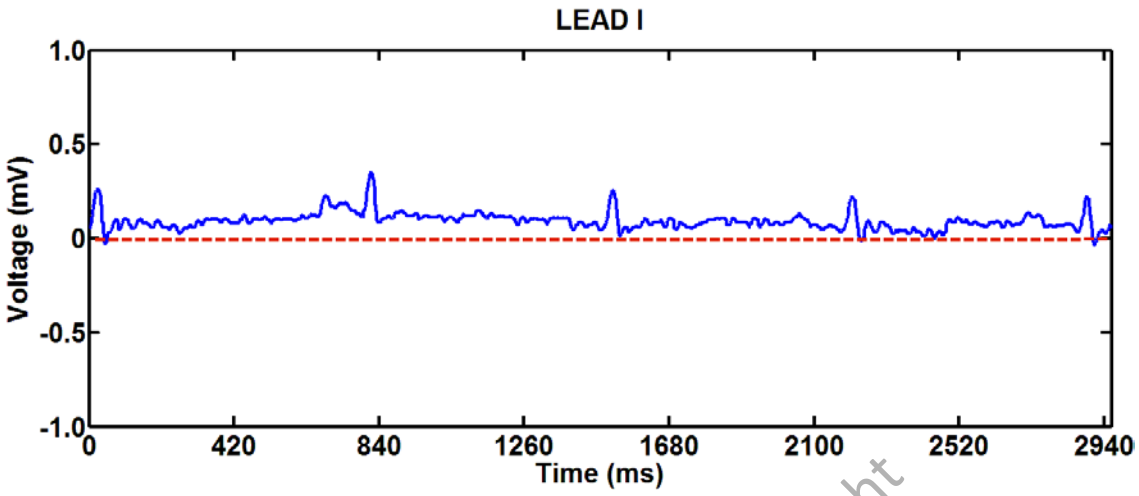

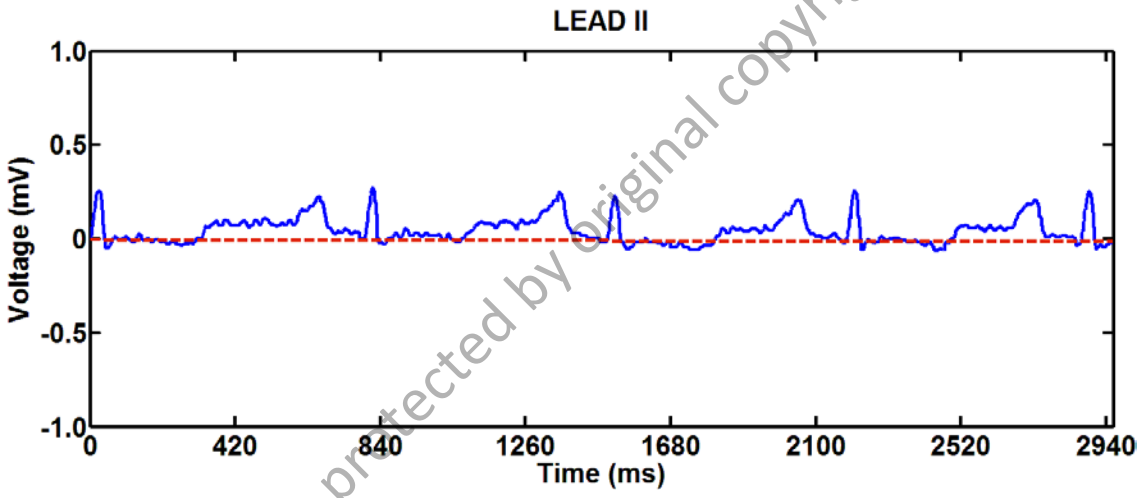

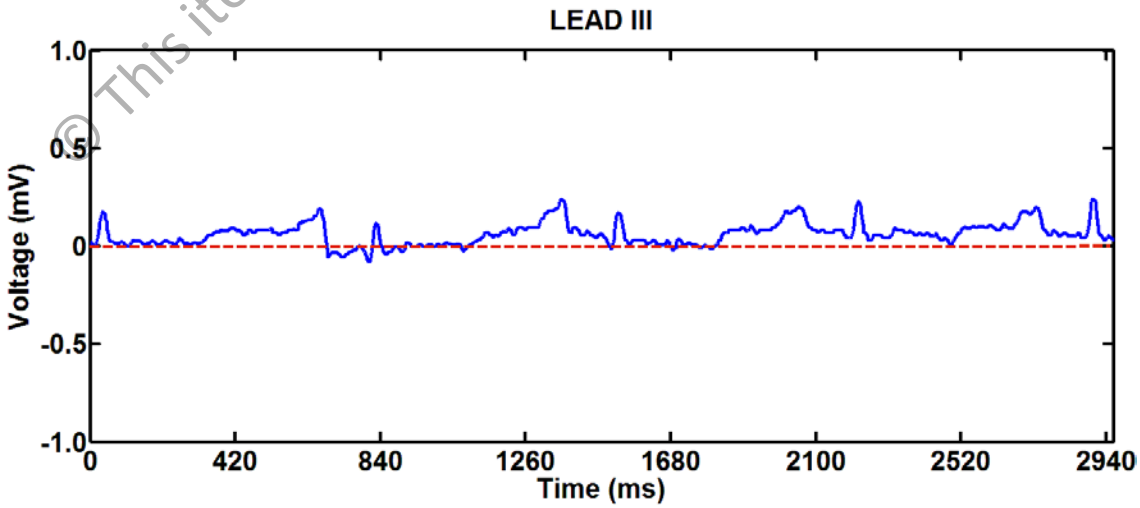

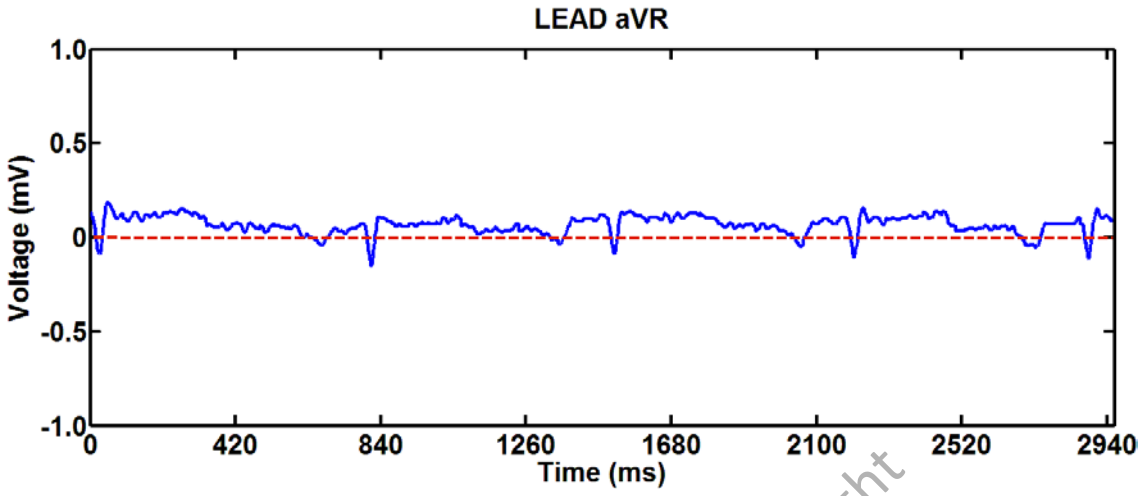

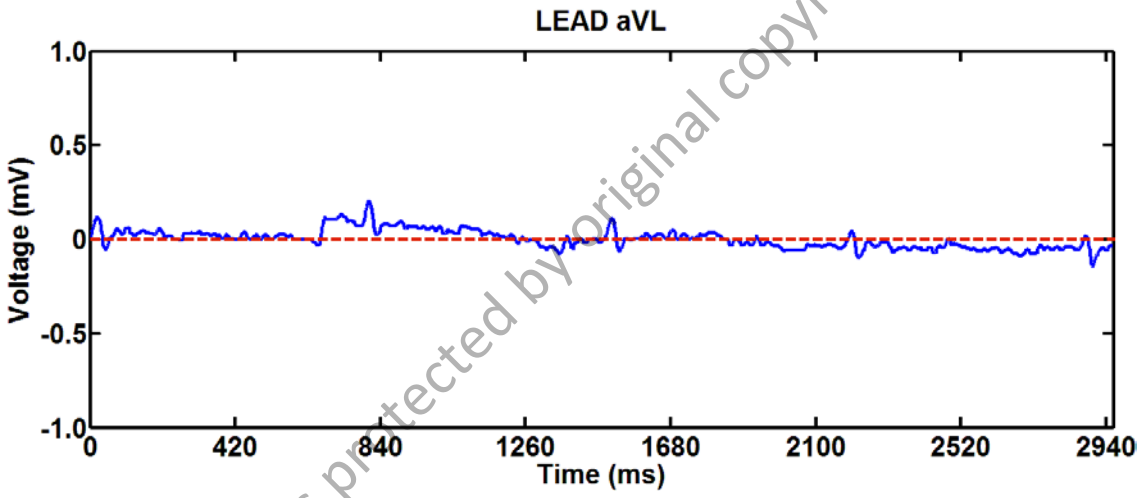

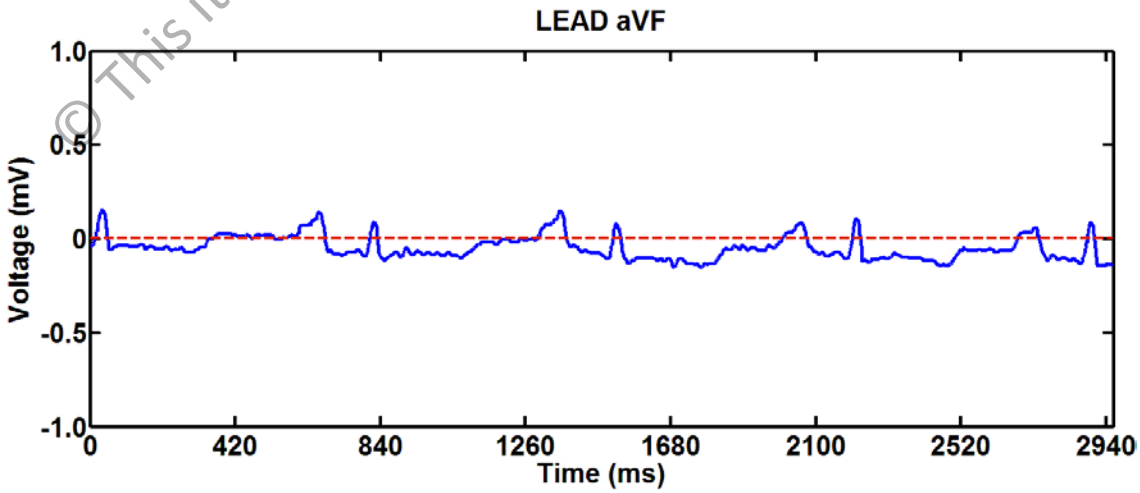

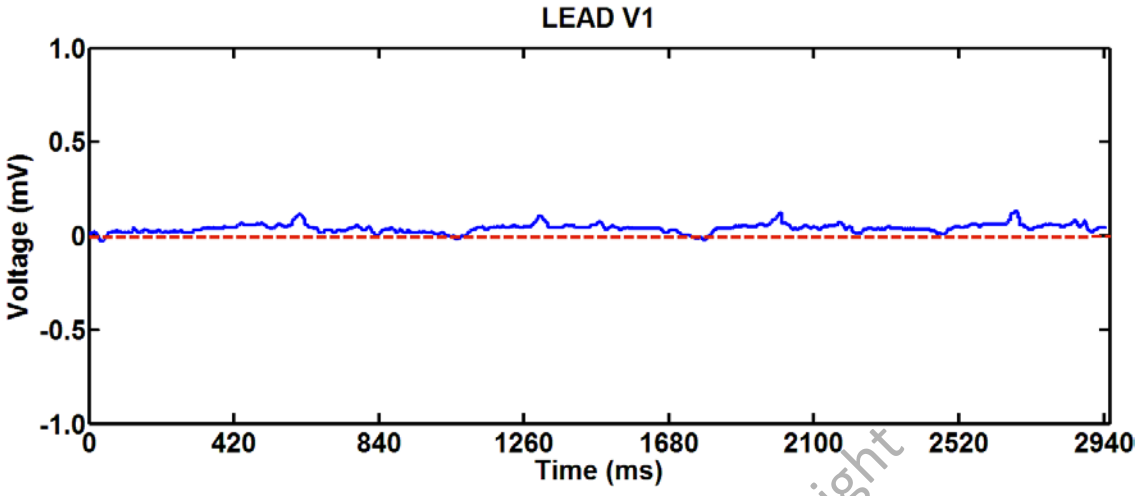

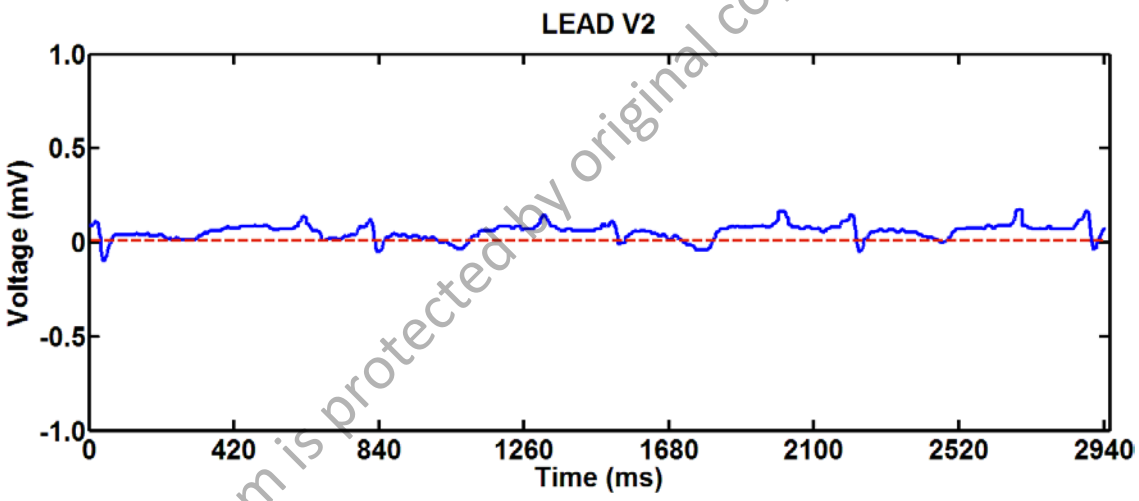

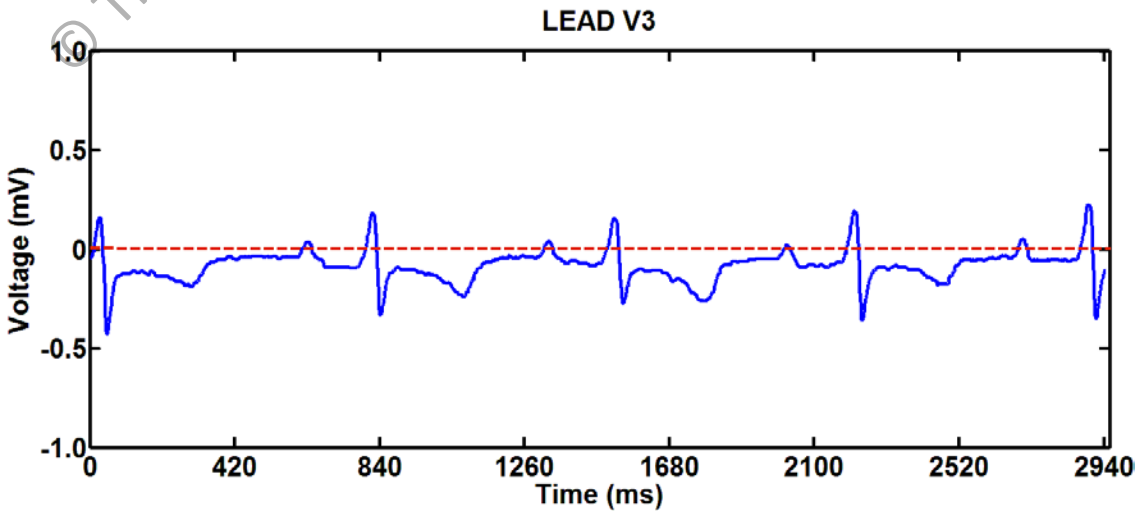

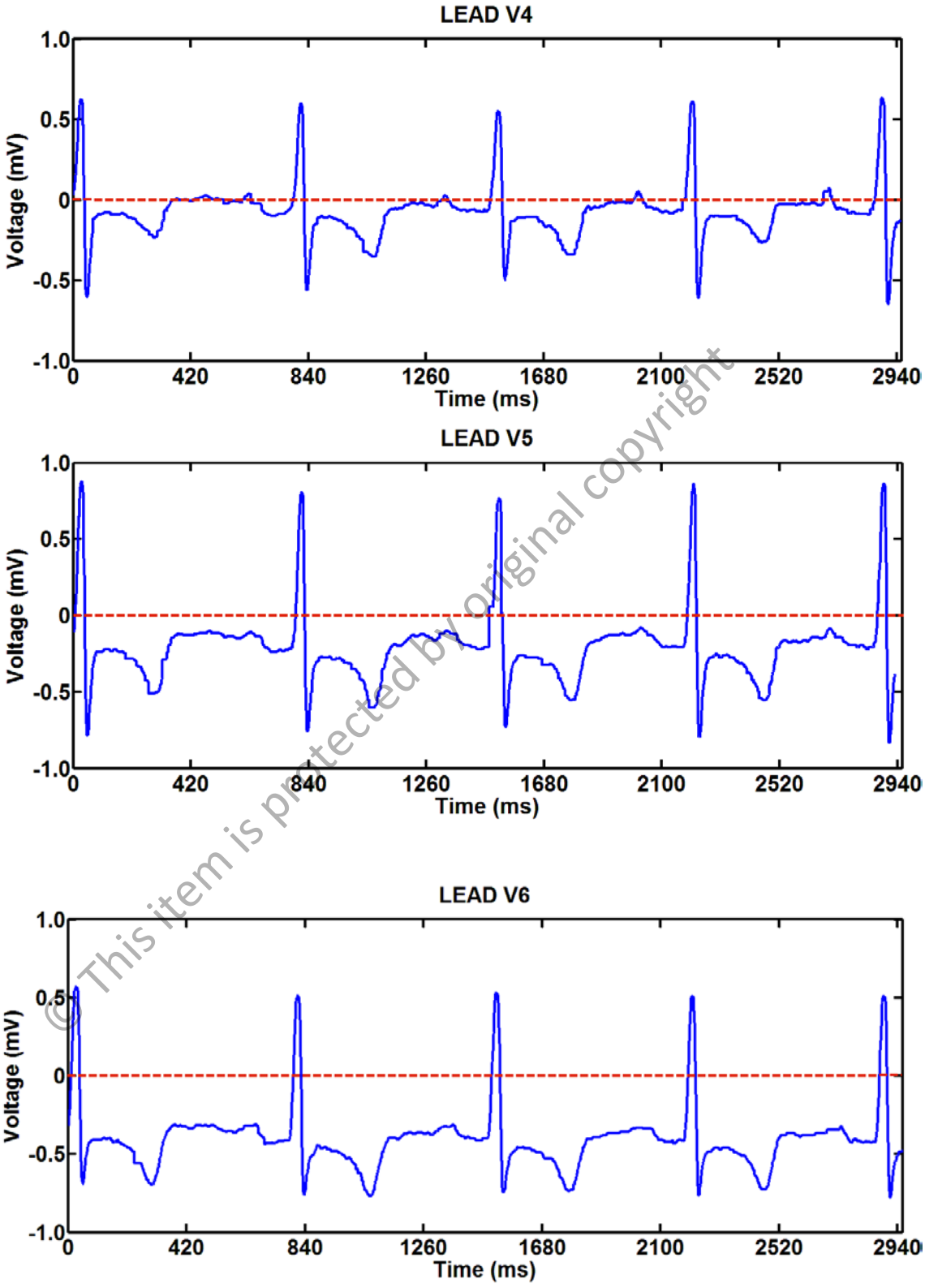

Figure A.2: The Reconstructed 12-Lead Raw ECG Data of the ECG chart shown in Figure A-1.

Appendix B

The scanned images of the ECG records which were used in the analytic evaluation of digital recovery approach mentioned in Chapter 4 Section 4.2.2 are shown in Figure B.1, B.2, and B.3, respectively. In these figures, the partition that is rounded by dashed red circle in the header part in each record contains the ECG parameters that are computed automatically by the ECG machine itself and used for quantitative evaluation. The colour grid part in each record contains the detail drawing charts of 12 lead ECG. These charts are used for qualitative evaluation. All images of ECG records are scanned in 600 dpi.

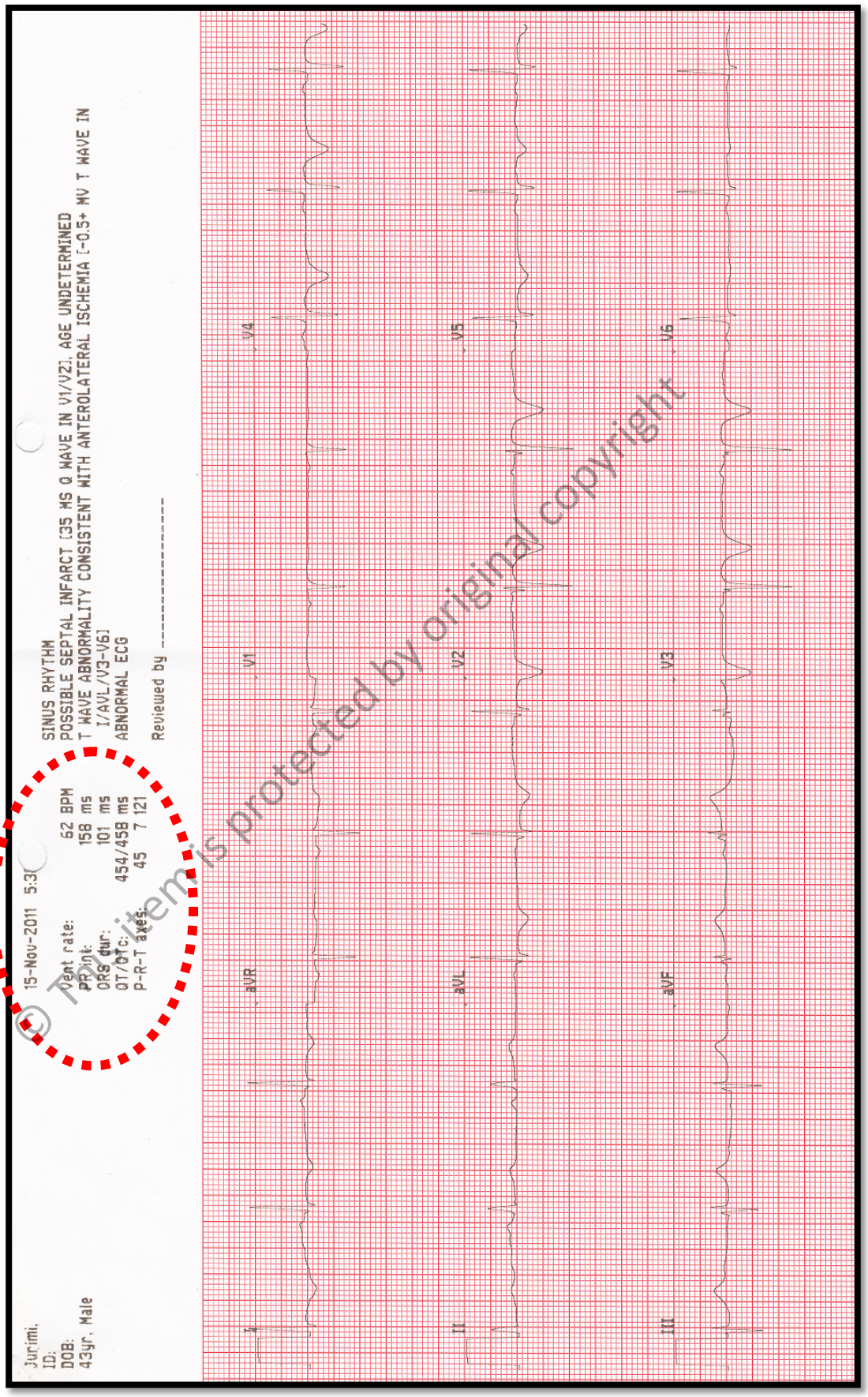

Figure B.1: Scanned Image of 12 lead ECG Record for First Patient (P1)

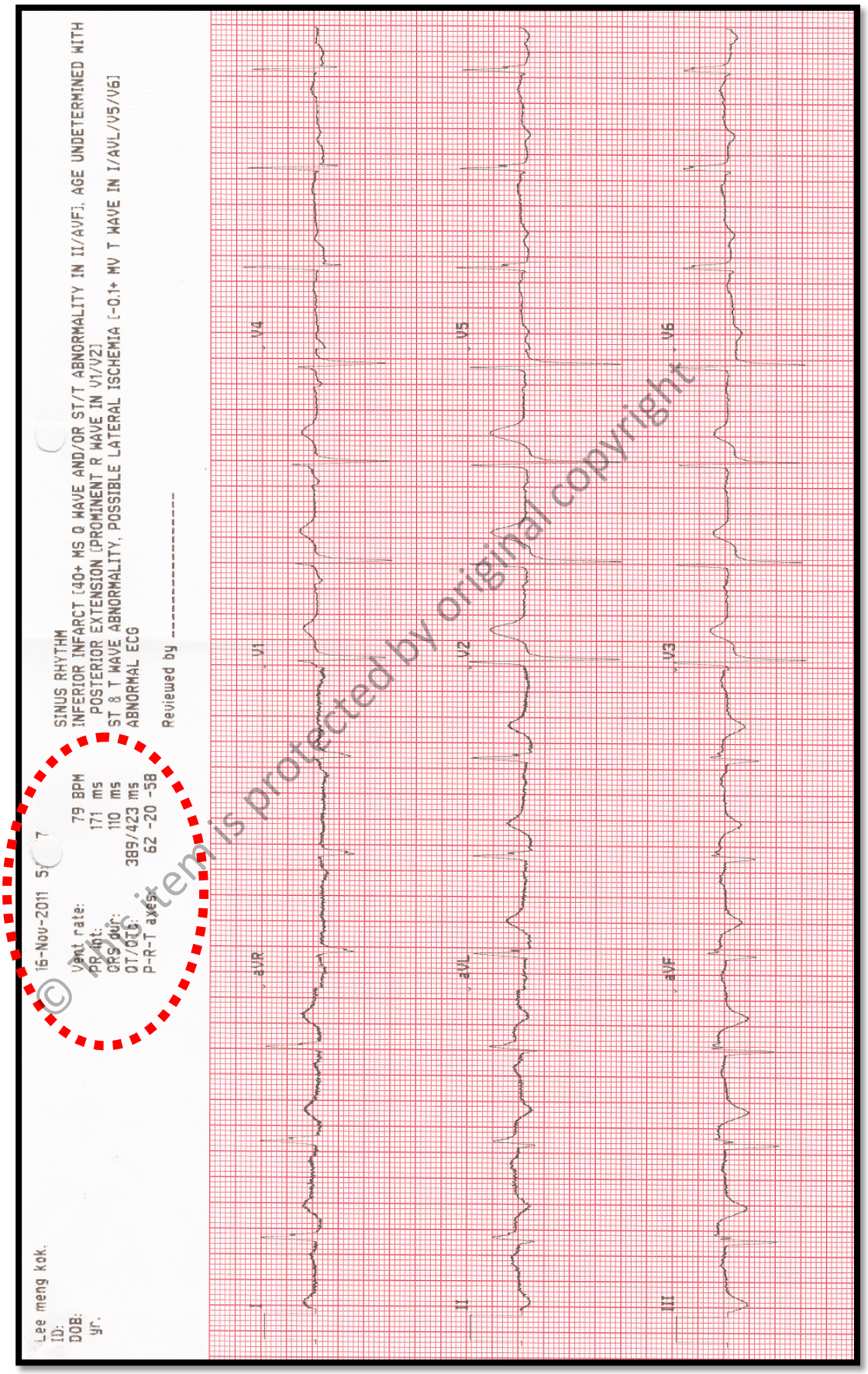

Figure B.2: Scanned Image of 12 lead ECG Record for Second Patient (P2)

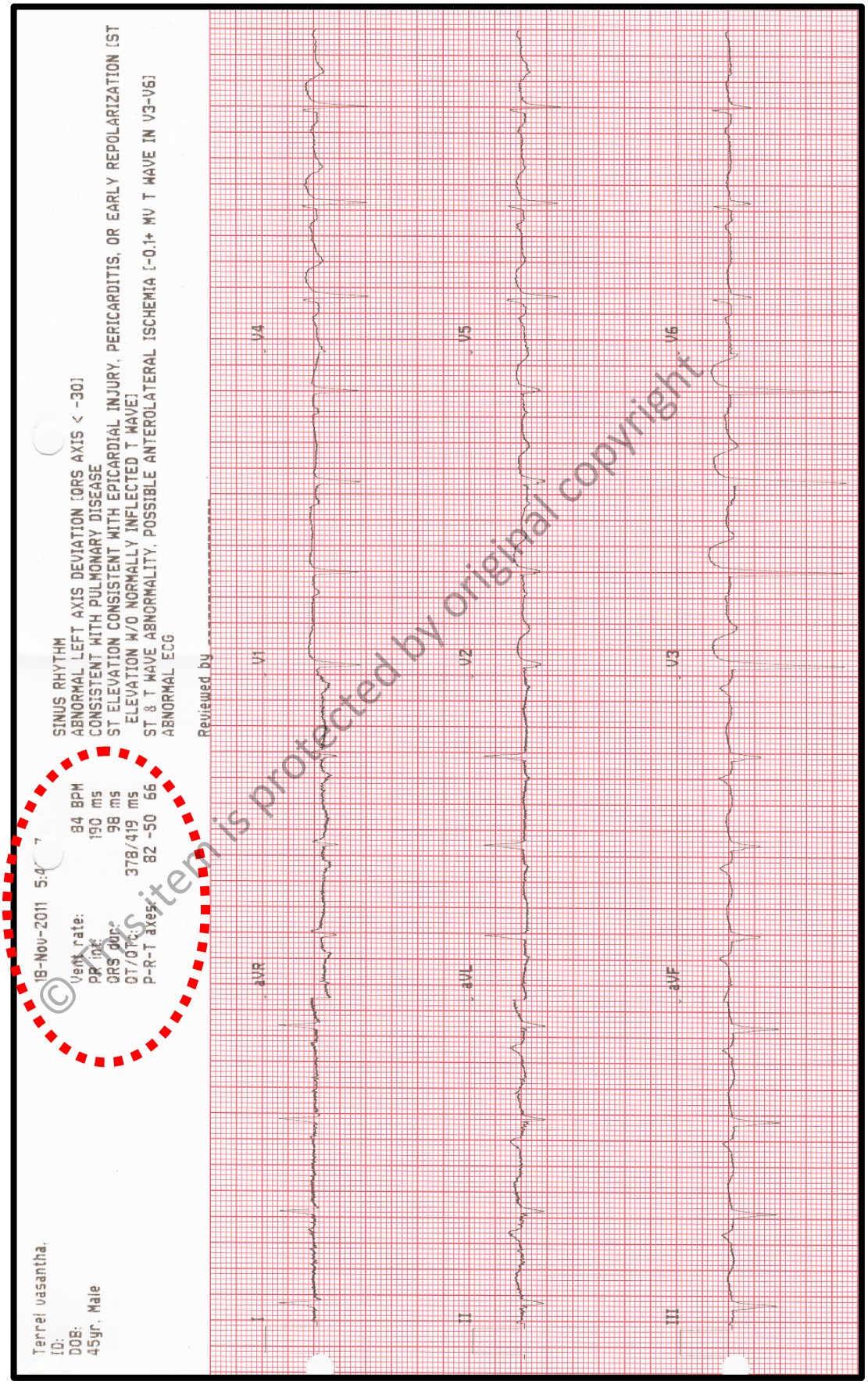

Figure B.3: Scanned Image of 12 lead ECG Record for Third Patient (P3)

LIST OF PUBLICATIONS

International Journals

1- **SAMEER K. SALIH *,** S. A. ALJUNID, SYED M. ALJUNID,OTEH MASKON, and ABID YAHYA, " HIGH-SPEED APPROACH FOR DELINEATING P AND T WAVES CHARACTERISTICS IN ELECTROCARDIOGRAM SIGNAL", Journal of Mechanics in Medicine and Biology, Vol. 14, No. 2 (2014), DOI: 10.1142/S0219519414300038,**World Scientific** Publisher, Indexed by **SCOPUS**, (**Impact Factor 0.790**).

2- **Sameer K. Salih *,** S. A. Aljunid, Syed M. Aljunid, and Oteh Maskon, "New Approach for Diagnosing Left Ventricular Hypertrophy Cardiac Disease using Fuzzy Inference System ", Journal of Medical Imaging and Health Informatics, **American Scientific** Publishers, Indexed by **SCOPUS** , (**Impact Factor 0.642**).

3- **Sameer K. Salih** *, S. A. Aljunid, Syed M. Aljunid, and Oteh Maskon, "Adaptive Filtering Approach for Denoising Electrocardiogram Signal Using Moving Average Filter", Journal of Medical Imaging and Health Informatics, **American Scientific** Publishers, Indexed by **SCOPUS** , (**Impact Factor 0.642**).

4- **Sameer K. Salih ***, S. A. Aljunid, Abid Yahya, and Khalid Ghailan, "A Novel Approach for Detecting QRS Complex of ECG signal ", International Journal of Computer Science Issues (IJCSI), Vol. 9, Issue 6, No 3, November 2012. Indexed by **Elsevier's Compendex,** (**Impact Factor 0.242**).

5- **Sameer K. Salih ***, S. A. Aljunid, Syed M. Aljunid, Oteh Maskon, Abid Yahya, "A Robust Approach for Detecting QRS Complexes of Electrocardiogram Signal with Different Morphologies", Key Engineering Materials Vols. 594-595 (2014) pp 972-979, DOI:10.4028/KEM.594-595.972, , Indexed by **SCOPUS.**

6- **Sameer K. Salih ***, S. A. Aljunid, Syed M. Aljunid, and Oteh Maskon, "New Digital Recovery Approach of Reconstructing 12-lead Raw ECG Data from Coloured Scanned Image of Paper Printout Recording", Image Vision and Computing, **Elsevier Publisher**, Indexed by **SCOPUS,** (**Impact Factor 1.581**), (Under Review).

International Conferences

1- Sameer K. Salih *, S. A. Aljunid, Syed M. Aljunid, Oteh Maskon, Abid Yahya, "High Speed Approach for Detecting QRS Complex Characteristics in Single Lead Electrocardiogram Signal", IEEE International Conference on Control System, Computing and Engineering (ICCSCE2013), pp 391-396, Indexed by **SCOPUS.**

2- Sameer K. Salih *, S. A. Aljunid, Syed M. Aljunid, and Oteh Maskon," Robust Approach of De-noising ECG signal using Multi-resolution Wavelet Transform", International Postgraduate Conference on Engineering and Management 2014 (IPCEM2014),